Dissertation

submitted to the

Combined Faculties for the Natural Sciences and for Mathematics

of the Ruperto-Carola University of Heidelberg, Germany

for the degree of

Doctor of Natural Sciences

presented by

Dipl.-Chem. Tim Kersebohm

born in Dortmund

Oral Examination: February 23rd, 2005

PNA-Ligand Bioconjugates as Potential Building Blocks for Sequence-Specific, Metal-Mediated DNA-/RNA-Cleavage

Referees: **Prof. Dr. Nils Metzler-Nolte**

Prof. Dr. Andres Jäschke

This work was carried out between December 2000 and November 2004 at the Institute of Pharmacy and Molecular Biotechnology, Department of Chemistry Ruperto-Carola University of Heidelberg, Germany

Where is the Wisdom, We lost in Knowledge
Where is the Knowledge, We lost in Information
Where is the Information, We lost in Data
T.S. Eliot (1888-1965)

Acknowledgements

I am very grateful to everybody who supported me during my work and life, no matter if professionally or personally.
My gratitude especially concentrates on the following people:

Prof. Dr. Nils Metzler-Nolte for luring me to Heidelberg and giving me the opportunity to face all challenges we had to overcome together while building up research and teaching in our department – the students will nevertheless appreciate that one day, I am sure…

Prof. Dr. Reinhard Brossmer for his patriarchal and inspiring spirit.

Dr. Ulrich Hoffmanns for attending me for the last 10 years, being my friend and buddy and staying solid as a rock in a world of strange adversities. Without you, dear Uli, I wouldn't have made it at all.

Dr. Sreçko Kirin, Thomas Happ and Andrea Maurer for the cooperation with the PNA monomer synthesis, for checking out the solid phase and melting curve stuff, introducing these techniques to our group and for fruitful discussions about science and life. Special thanks to Dr. Sreçko Kirin for providing me with the bpa know-how, many creative controversies and several hints and for reviewing this thesis.

Xavier deHatten for being French.

Dina Pavlovic Rosman, Fozia Noor, Dr. Janine Chantson, Dr. Judy Caddy, Dr. Daniel Milani for their collegiality and their support.

Richard Wombacher for introducing the terms "krasse knowledge", "krasse Ansage" "pang" and "difficile" and everybody else from The Jäschke Group.

Dr. Walter Kramer for technical and theoretical assistance and for “keeping the educational level”.

Heiko Rudy for being one of the best technical employees one could imagine by anticipating one’s every wish. Keep on like this, and everybody will value your work.

Ute Hertle and Tobias Timmermann for measuring numerous NMR spectra.
Angelika Seith, Bianca Flock and Dr. Ulrich Schatzschneider for the measurement of MALDI-TOF and ESI spectra.

Viola Funk for her helpfulness, her trustability and her commitment in so many cases.
Karin Weiß for being a real natural wonder of cheerfulness – somebody should write a PhD thesis about *this* phenomenon. Karin, I’d like you to be my personal lifetime-assistant !

The students of Pharmacy and Molecular Biotechnology for playing the counterpart to life in the lab and for providing new friends.

My parents for their love, security, admiration, support, respect and my spiritual and social home.

Abstract

Kersebohm, Tim Dipl.-Chem. February 23rd, 2005

"PNA-Ligand Bioconjugates as Potential Building Blocks for Sequence-Specific, Metal-Mediated DNA-/RNA-Cleavage"

Referees: Prof. Dr. Nils Metzler-Nolte
Prof. Dr. Andres Jäschke

In this Thesis, the development of new nuclease mimics on the basis of PNA-metal bioconjugates is described. The design of artificial enzymes for sequence-specific DNA and RNA cleavage is one of the most challenging problems in modern biotechnology, since the commercially available biotools are restricted to a limited number of promoter sequences. Possible nuclease mimics consist of a recognition- and a cleavage domain, with the latter one in this case being chosen to be a metal complex. Complexes of several chelating nitrogen ligands are proved to catalyze the phosphodiester cleavage of oligonucleotides. In the course of this Thesis, functionalized nitrogen ligands (terpyridine, bis-picolylamine and phenanthroline) were synthesized, and their metal binding behaviour in unsubstituted form and as pseudoneurotensin conjugates were investigated, revealing different binding modes depending on the type of ligand and its substitution. As a recognition domain, PNA (peptide nucleic acid), a DNA mimic with a pseudopeptide backbone was chosen, and the synthesis of monomer building blocks was optimized. PNA oligomers with terminal ligand substitution were developed, and their DNA hybridization behaviour was examined by UV melting experiments, revealing the intercalating effect of a terminal terpyridine ligand. A new criterion for the significance of PNA•DNA melting curves was introduced. The influence of the replacement of one internal PNA monomer with two unsubstituted amino acids on hybridization is described. Presumably, a bulge structure is formed by the modified PNA, involving the insight that the substituted PNA nucleotide does not have to be omitted for optimum attraction. A new and versatile method for the internal derivatization of PNA oligomers was developed by the introduction of a *p*-nitro-phenylalanine residue which is reduced on resin and is accessible for peptide bond formation. A large variety of ligands, organometallic moieties or fluorescent markers can thus be coupled to PNA oligomers at any position.

Zusammenfassung

Kersebohm, Tim Dipl.-Chem. 23. Februar 2005

„PNA-Ligand-Biokonjugate als Potentielle Bausteine für die Sequenzspezifische, Metallvermittelte DNA-/RNA-Spaltung“

Gutachter: Prof. Dr. Nils Metzler-Nolte
Prof. Dr. Andres Jäschke

Im Rahmen der vorliegenden Arbeit wurde die Entwicklung neuer künstlicher Nucleasen, basierend auf PNA-Metall-Biokonjugaten beschrieben. Das Design künstlicher Enzyme für die sequenzspezifische DNA- und RNA-Spaltung ist eine der größten Herausforderungen der modernen Biotechnologie, da die kommerziell erhältlichen Werkzeuge auf einige wenige Promotersequenzen beschränkt sind. Mögliche Nucleasen bestehen aus einer Erkennungs- und einem Spaltungsdomäne, wobei die Letztere in diesem Fall ein Metallkomplex sein sollte. Komplexe vieler verschiedener stickstoffhaltiger Chelatliganden sind in der Lage, die Spaltung von Phosphodiesterbindungen in Oligonucleotiden zu katalysieren. In dieser Arbeit wurden funktionalisierte Stickstoffliganden (Terpyridin, Bis-Picolylamin and Phenanthrolin) synthetisiert, und ihr Metallbindungsverhalten in unsubstituiertem Zustand und in Form von Pseudoneurotensin-Konjugaten wurde untersucht. Die Wahl einer Erkennungsdomäne fiel auf PNA (Peptide Nucleic Acid), einem DNA-Analogon mit einem Pseudopeptid-Rückgrat, und die Synthese der Monomerbausteine wurde optimiert. PNA-Oligomere mit endständiger Ligandsubstitution wurden entwickelt, und ihr Hybridisierungsverhalten mit komplementärer DNA wurde mittels UV-Schmelzexperimenten untersucht. Hierbei zeigte sich ein interkalierender Effekt des endständigen Terpyridin-Liganden. Ein neues Kriterium für die Signifikanz von PNA • DNA-Schmelzkurven wurde eingeführt. Der Einfluß einer internen Substitution eines PNA-Monomers durch ein Dipeptid auf die Hybridisierung wurde beschrieben und führte zu dem Ergebnis, daß die modifizierte PNA aller Wahrscheinlichkeit nach eine Schleifenstruktur ausbildet, so daß für eine optimale attraktive Wechselwirkung kein PNA-Monomer ersetzt, sondern das Dipeptid eingeschoben werden sollte. Desweiteren wurde eine interne Derivatisierung von PNA-Oligomeren durch den Einbau eines *p*-Nitro-Phenylalanin-Bausteins erreicht, der am Harz reduziert wird und dadurch für eine Peptidbindung zur Verfügung steht. Mit Hilfe dieser Methode ist es möglich, eine vielfältige Anzahl von Liganden, Organometallverbingungen oder Fluoreszenzmarkern an jeder beliebigen Stelle des PNA-Oligomers einzuführen.

For Andrea, the love of my life

Table of Contents

Abbreviations

Å	angström
Ar	aryl group
B	nucleobase
br	broad
bp	base pairs
cm	centimeter
CT	charge transfer
d	doublet
dd	double doublet
ds	double strand
δ	chemical shift, isomer shift
EI	electron impact
ESI	electro-spray interface
Et	ethyl
ε	molar extinction coefficient
FAB	fast atom bombardment
h	hour
HPLC	high performance liquid chromatography
Hz	hertz
IR	infrared
J	coupling constant
K	kelvin
λ	wavelength
m	multiplet, meter, milli-, medium (intensity)
M	molar, mega-
MALDI-TOF	matrix-assisted laser desorption/ionisation – time of flight
max	maximum
Me	methyl

min	minute, minimum
m/z	mass per charge ratio
n.o.	not observed
n.m.	not measured
NMR	nuclear magnetic resonance
ν	stretching vibration
PG	protection group
ppb	parts per billion
ppm	parts per million
q	quartet
RT	room temperature
s	singlet, second, strong (intensity)
sm	self-melting (of PNA)
ss	single strand
σ	standard deviation
SPPS	solid phase peptide synthesis
SPS	solid phase synthesis
T	tesla, temperature
T_M	melting temperature
t	triplet
tert	tertiary
UV	ultra violet
Vis	visible
vs.	versus
w	weak (intensity)

Abbreviations for chemicals and solvents

A, Ad, a	adenine
AA	amino acid
Ac	acetyl-
Ada-OH	adipic acid
Aeg	N-(2-aminoethyl)glycine
Ahx-OH	amino-hexanoic acid (deprotonated)
BB	PNA backbone (aminoethyl glycine)
Bzl	benzyl
bpa	*N*,*N'*-bis(2-picolyl)amine
bpa*-OH	bpa-Bzl
bpa'	bpa*-Ahx- / bpa-Bzl-Ahx-
Bhoc	benzhydryloxycarbonyl
Boc	*tert*-butyloxycarbonyl
C, Cy, c	cytosine
Cys	cysteine
DCC	*N*,*N'*-dicylohexyl-carbodiimide
DCM	dichloromethane
DIPEA	di-isopropyl-ethylamine
DMAc	*N*,*N'*-dimethylacetamide
DMF	dimethylformamide
DMSO	dimethylsulfoxide
EDC	*N*-(3-dimethylaminopropyl)-*N'*-ethylcarbodiimide hydrochloride
EtOAc	ethyl acetate
EtOH	ethanol
Fmoc	fluorenyl-9-methoxycarbonyl
G, Gu, g	guanine
GF	glycine-phenylalanine
Gly	glycine
HATU	2-(1H-7-azabenzotriazole-1-yl)-1,1,3,3-tetramethyluronium hexafluorophosphate

HBTU	2-(1H-benzotriazole-1-yl)-1,1,3,3-tetramethyluronium hexafluorophosphate
HOBt	*N*-hydroxybenzotriazole
Hex-OH	hexanoic acid
HOBt	1-hydroxy-1H-benzotriazole
Ile	isoleucine
ivDde	(*N*-α-Fmoc-*N*-ε-1-(4,4-dimethyl-2,6-dioxocyclohex-1-ylidene)-3-methylbutyl-L-lysine)
K	lysine
Leu	leucine
Lys	lysine
MeCN	acetonitrile
MeOH	methanol
PG	protecting group (in all cases: Bhoc)
Phe	phenylalanine
phen	1,10-phenanthroline
phen*-H	5-amino-1,10-phenanthroline
PNA	peptide nucleic acid
pnt	pseudo-neurotensin
Pro	proline
T, Th, t	thymine
TBTU	2-(1H-benzotriazole-1-yl)-1,1,3,3-tetramethyluronium tetrafluoroborate
tpy	2,2':6',2''-terpyridine
tpy*-OH	4-[4'-oxa-(2,2':6',2''-terpyridinyl)]hexanoic acid
TFA	trifluoro-acetic acid
THF	tetrahydrofuran
TIS	tri-isopropylsilane
Tyr	tyrosine

General Remarks

Whenever terms like „standard SPPS chemistry" are used, it refers to the Fmoc-strategy described in the Experimental Part.

Peptides in this Thesis are written according to the IUPAC Peptide Nomenclature (http://www.chem.qmul.ac.uk/iupac/AminoAcid), specifying the atoms at both sides of the amino acid which can be exchanged. For example, the free amino acid phenylalanine is written "H-Phe-OH"; in a peptide chain, only "-Phe-" is left. Protection and substitution is handled correspondingly (Fmoc-Phe-OH, H-Phe-OMe). Side chain substituents are written in brackets (Fmoc-Phe(NO_2)-OMe).
Exception: The term "Lys" stands for as Lys-NH_2 except as indicated
The synonym "tpy*-OH" refers to the carboxyl ligand 4-[4'-oxa-(2,2':6',2''-terpyridinyl)]hexanoic acid **3.5** in its free form, whereas "tpy*" refers to **3.5** as a substituent. Similarly, "bpa*" stands for "bpa-Bzl-", and phen* for phen-NH-.

DNA sequences are always displayed in capital letters, PNA sequences in lower case letters. PNA sequences are written with the N-terminus at the left side.

For convenience, the numbering of compounds was conceived as follows:
Each chapter was given a numbering of its own; the number is indicated "**x.y**" with **x** indicating the particular chapter.

The melting curves displayed in this thesis only show the heating process; initial cooling and final re-annealing data are left out. Whenever melting curves occur, representative examples are shown. The values written in tables are averages of four melting experiments after cancelling mavericks. In literature, the melting temperature often is referred to as "T_m", in this Thesis indicated "T_M" – both are meaning the same. Because of their high quantity, some of the tables in Chapter 6 were not labelled, but embedded in the text.

1 Introduction

1.1 Bioinorganic Chemistry

In former times, science and philosophy were seen as exactly the same topic.[a]
With the increasing amount of knowledge earned by mankind during the ages and the human brain by nature being subject to various restrictions, the traditional sciences more and more started to divide. New specialized fields were built up such as organic chemistry, which did not represent an issue of its own until the important role of carbon became obvious. During the last two to three decades, the natural sciences started to develop into the opposite direction. Certain branches merged again, establishing new scientific (inter-)disciplines, one of which is bioinorganic chemistry, combining aspects both of biology and inorganic chemistry. Nearly 80% of the elements are metals, and their deposit in earth's crust cannot be denied, so that a biological role of metal atoms is obvious. In fact, more than 2% of the human body consist of metals with alkaline and earth alkaline elements representing the main part; the rest is known as trace elements (0.1%).[1] Recent investigations actually revealed that inorganic elements even played an essential role in the creation and evolution of living cells.[2]

The broad range of studies on the synthesis and applications of metal conjugates with biomolecules (sugars, amino acids, nucleic acids, steroids etc.) has been widely reviewed.[3, 4] Applications of bioinorganic chemistry extend over a wide scale including important medical breakthroughs such as labelling,[5, 6] radiodiagnostics[7] and cancer treatment.[8, 9] In contrast to the relatively new field of bioorganometallic chemistry,[10] most of the bound metals in nature are not covalently attached to a biomolecule[b], but fixed by coordinative forces.

---

[a] gr. φίλος = friend; σοφία = wisdom
[b] organometallic compounds: compounds with at least one metal-carbon bond

1.2 Metals in Biological Systems

The important role of metal atoms in flora and fauna is not only restricted to the presence of alkaline and earth alkaline metals which are mainly responsible for buffer systems in blood and cells, charge carriers, osmotic and electrochemical gradients across cell membranes,[11] signal transduction in neurons and structural constitution of bones and teeth.[c] When the investigation of biochemical systems became more detailed, scientists learned that many biomolecules, such as enzymes,[12, 13] transport proteins[14] and structural cell molecules would not work without the presence of transition metal atoms. Vitamin B_{12}[15] and haemoglobin[16] (binding dioxygen in its heme group)[17] contain cobalt[18] and iron, respectively, coordinated by a porphyrinoid ring system. In most of the cases, the catalytic properties of the transition metal center are significantly involved.
Metalloenzymes are biocatalysts bearing at least one metal atom or ion in their active site.[19] They are involved in important biocatalytic processes such as fixation of nitrogen, methane biogenesis and oxidation, oxygen storage and utilization in higher organisms, and oxidative or reductive degradation of metabolites or xenobiotics. Often supported by metal centers, enzymes are able to act in a highly specific way called lock-key principle, which was primarily expressed by Emil Fischer.[20]
Well-known and important examples of metalloenzymes are superoxide dismutases (Cu, Zn), oxygenases (Fe, Cu) and hydrolases (Mg, Zn).[d]

The most interesting metal-containing biomolecules are from the group of DNA-binding proteins, which take over several different functions such as gene regulation and polymerase activity. Some of them contain the so-called zinc-finger domain,[21] a protein loop motif with two histidines and two cysteines binding to a zinc ion,[22] saturating the coordination sphere of the metal.

[c] Some earth alkaline metals such as Mg^{2+} and Ca^{2+} also act as enzyme activators, structure promoters and Lewis acids
[d] Particular metalloenzymes will be described in the course of this Thesis

Thus, the role of zinc must be not catalytical but structural, maintaining the conformation of proteins that bind to DNA to activate and deactivate genes (Fig. 1.1). Zinc-finger proteins are found in nucleic acid polymerases and transcription factors.[23]

Although the zinc atoms in zinc fingers do not participate in chemical reactions, there are metalloenzymes from the group of DNA cleaving molecules, called nucleases, where the zinc finger takes over the role of the binding domain, and also examples of non-structural, but catalytical zinc ions in nucleases are known.

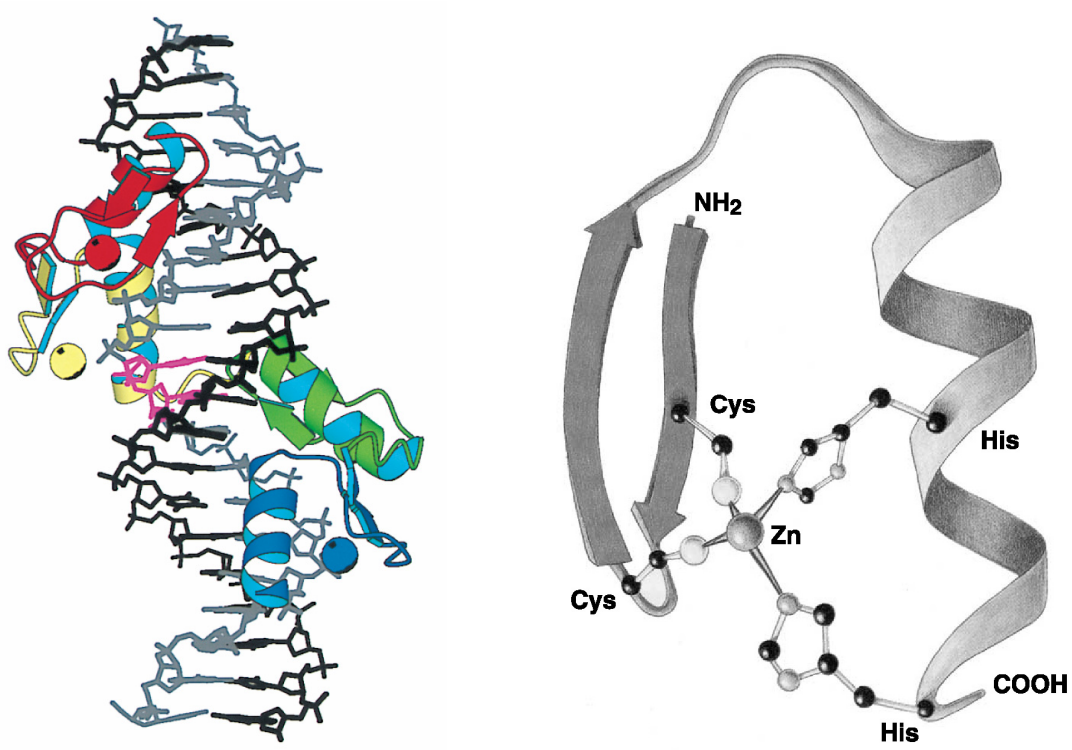

Fig. 1.1: *left: Crystal Structure of Two Zinc Finger Proteins, Binding on the Major Groove of a DNA Double Helix[24] (The Zinc Ions are Shown as Spheres); right: The Binding Domain of a Zinc Finger, Consisting of two Histidines and two Cysteines[25, 26]*

1.3 Nucleases

1.3.1 Natural Nucleases

Natural nucleases are enzymes which are able to cleave phosphodiester bonds in oligonucleotides (see Chapter 1.5.1) in a hydrolytic way. At physiological pH, the phosphate groups are negatively charged, complicating the attack of anionic nucleophiles.[27] Phosphodiester bonds are even more resistant to hydrolytic cleavage than amide or ester bonds.[28] Out of this reason, a hydrolytic cleavage mechanism strongly affords the presence of electron acceptors. The cleavage mechanism in Ribonuclease A shows the involvement of two histidines in the primary structure of this protein whose imidazoles act as Brønsted acids and bases, respectively (Fig. 1.2).[29]

Nucleases can be divided into different groups:

- *Exonucleases* (digest nucleic acids starting from one terminus)
- *Endonucleases* (acting within the sequence and recognizing specific sites)
- *Ribonucleases* (degrade RNA)
- *Deoxyribonucleases* (degrade DNA)

In contrast to most of the nucleases, restriction endonucleases[30] are able to cleave DNA sequence-specifically. They were first discovered in bacteria[31] which defend themselves against phages by digesting the alien DNA, protecting their own genetic material by methylation.[32] Restriction endonucleases are able to recognize palindromic sequences of 4-8bp. They consist of two independent proteins: The restriction enzyme and a methylase, protecting hemimethylated DNA against degradation.

Ribonucleases[33] are often metalloenzymes containing Zn^{2+} or Mg^{2+} ions in their active sites.[34, 35] The half-life of nonactivated phosphodiesters is approximately $2 \cdot 10^{11}$a for DNA and $1 \cdot 10^{2}$a for RNA; metal cofactors are able to increase the rate of hydrolysis by the factor 10^{10}-10^{15}.[36] Bleomycin, a product of *streptomyces* fermentation, cleaves DNA via an iron-oxo intermediate[37] and therefore via a redox mechanism (the difference between a hydrolytic and an oxidative mechanism will be discussed in Chapter 1.3.3).

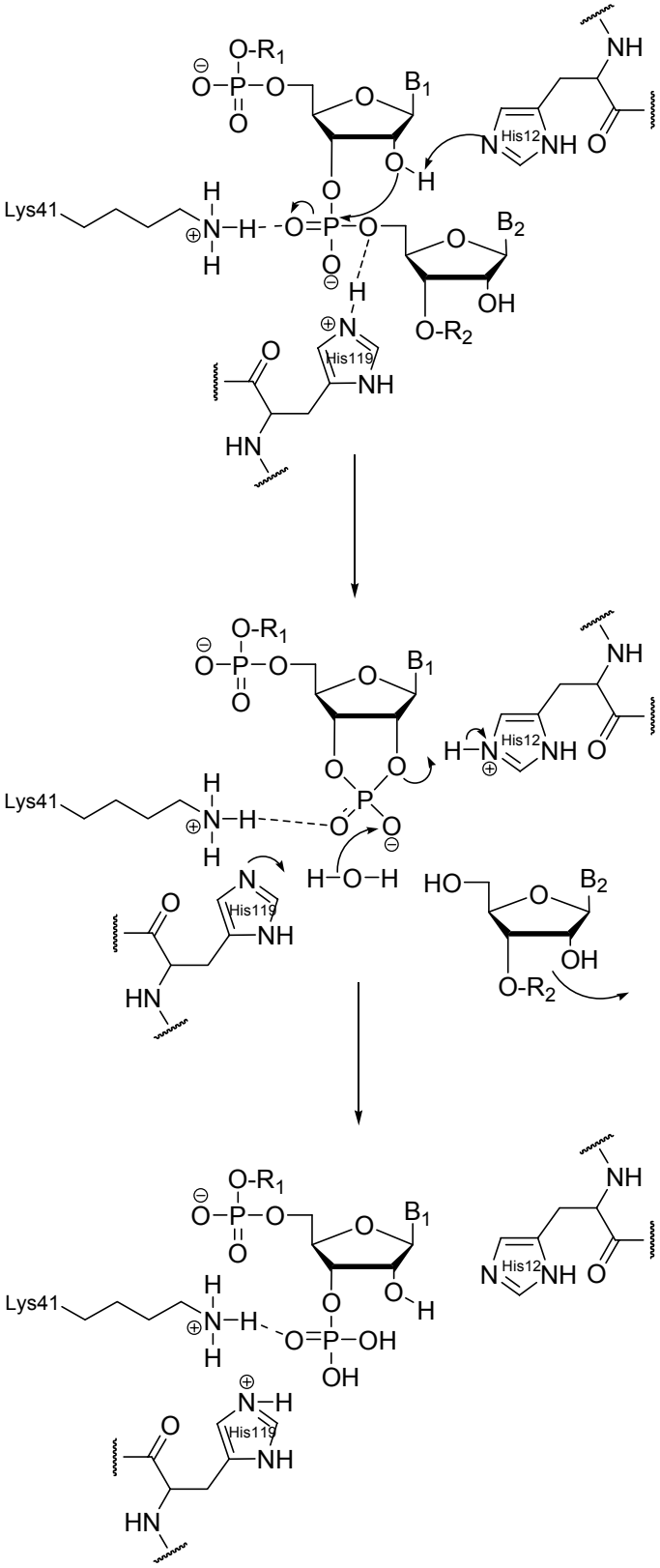

Fig. 1.2: *Mechanism of Hydrolytic Phosphodiester Cleavage by RNase A*

It is well established that phosphate ester hydrolysis (and phosphoryl transfer) are strongly metal-ion dependent and responsible for the observed rate-acceleration at neutral pH when compared to metal-free conditions. The role of the metal ion or ions is to provide the nucleophile (coordinated hydroxide) for attack of the phosphorus atom, to act as a Lewis acid by polarizing P-O bonds and making the P more susceptible to attack, and to stabilize the leaving group.[38, 39]

The proposed mechanism is shown in Fig. 1.3.[40]

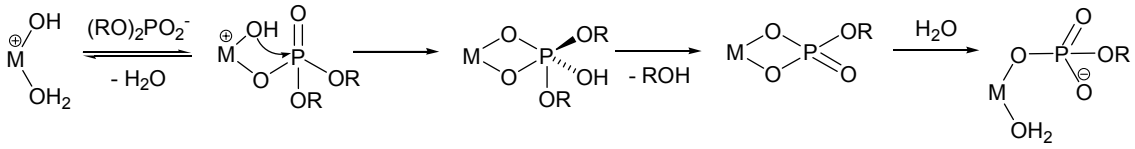

Fig. 1.3: *Metal-Mediated Phosphodiester Cleavage Mechanism*

An example of a non-specific phosphomonoesterase with two catalytic metal centers is purple acid phosphatase (PAP), in mammals with a dinuclear Fe^{3+}/Fe^{2+} active site (Fig. 1.4).[41, 42] Their intense purple colour is caused by tyrosine-Fe(III) charge transfer. Other phosphatases contain Mn or Zn ions.[43]

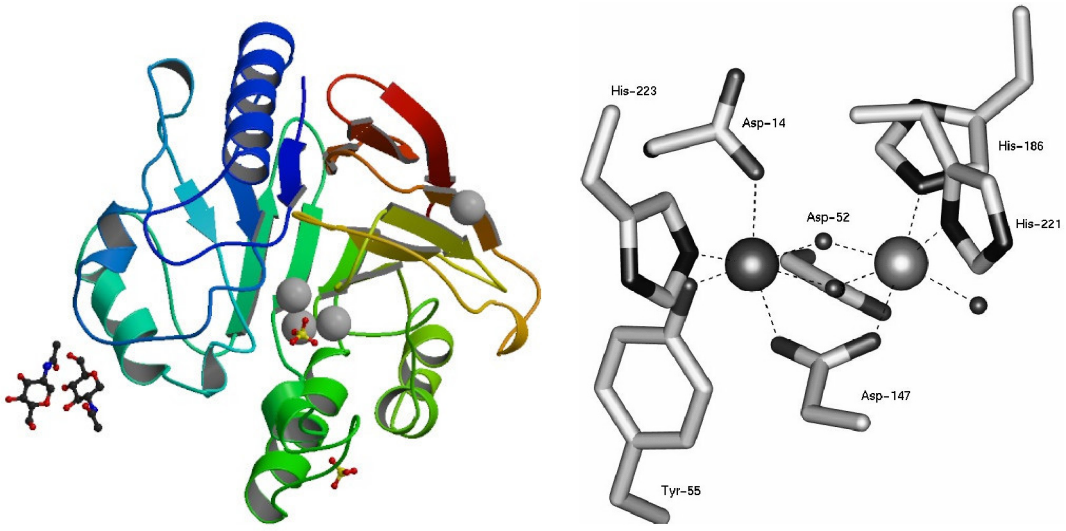

Fig. 1.4: *left: Crystal Structure of a Purple Acid Phosphatase from* rattus norvegicus *with a μ-(Hydr)oxo Bridged Di-Iron Center.*[44] *right: Active Center of PAP from* Ipomoea batatas[45]

The sequence-specific hydrolysis of phosphodiester bonds in polymerase I is catalyzed by the Klenow fragment,[46] one of three domains in this enzyme which is responsible for the removal of mismatched base pairs. The Klenow fragment is a 3'-5'-exonuclease with a binuclear active center bearing Mg^{2+} and Zn^{2+} (Fig. 1.5).[47, 48]

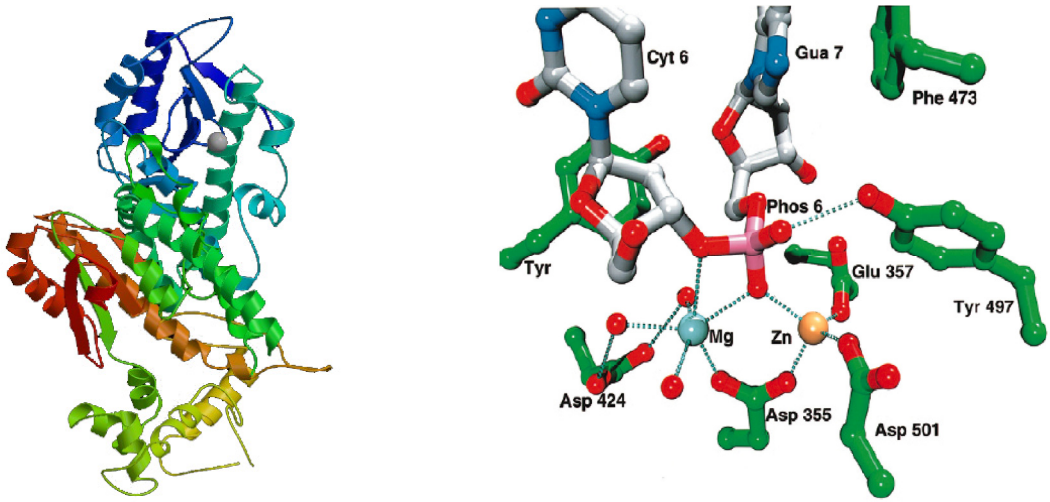

Fig. 1.5: *left: Crystal Structure of the Klenow Fragment from* Escherichia Coli *DNA Polymerase I right: Active Center of a 3'-5'-Exonuclease*

1.3.2 Nucleases in Biotechnology

The most common use of nucleases in the context of genetic engineering is the fragmentation of DNA in order to isolate certain areas from the genome. Applications of this technique are sequencing, cloning, foot- and fingerprinting.

Nucleases used in molecular biology are mostly isolated from bacteria in the form of restriction endonucleases and are quite specific. They are divided into three main categories:

- *Type I*: specific sequence recognition, but random cleavage
- *Type II*: specific sequence recognition, specific cleavage
- *Type III*: specific sequence recognition, cleavage at a distance of 20-25bp

2750 different enzymes of Type II nucleases are known up to date, and 211 different specifications have been isolated. The vast number of possible cleavage sites demanded

by the scientist reveals the limited use of these biotools. Type II nucleases are able to identify only some defined promoter sequences and only possess very short recognition sites which results in a huge number of different fragments after cleavage. Therefore, one of the major challenges for biotechnological and medical purposes is to develop artificial nucleases which are able to cleave nucleic acids *at any favoured position* within the sequence.

1.3.3 Artificial Nucleases

Biomimetic (hydrolytic or oxidative; see below) cleavage of oligonucleotides is of increasing importance in biotechnology and medicine,[49-52] because natural restriction enzymes are lacking selectivity.[53, 54] A number of relevant enzymes have been studied extensively and model compounds for the same kind of chemistry have been developed.[49, 55-58]

Natural restriction enzymes recognize the target cleavage site by a short sequence of four to eight nucleobases.[59] This strongly limits the specificity of an enzyme, because the statistical frequency of such a recognition sequence leads to an uncontrollable fragmentation. For the uniqueness of a sequence in the human genome, a number of more than 12 nucleobases is statistically necessary.[60] The development of artificial nucleases, being able to recognize longer and therefore rarer sequences is thus one of the major challenges in modern biotechnology. Such a tool should consist of a recognition domain (an antisense oligonucleotide) and a cleavage domain (the catalytic center). Further specifications comprise feasible cellular uptake properties[61, 62] and resistance towards enzymatic degradation. The metabolism of natural nucleases limits their availability to cleave; artificial nuclease mimics therefore should be stable in biological environment.

One major approach for the design of artificial nucleases are conjugates that are hybrid molecules between oligonucleotides and nucleases or nuclease fragments.[63-65]
For example, attempts have been made to recruit the ubiquitous mammalian enzyme Topoisomerase I (TopoI) to cleave DNA by tethering a TopoI inhibitor, camptothecin,

to the third strand and "attracting" TopoI to cleave one strand of the double-stranded DNA, at the site determined by the oligonucleotide sequence.[66]

Another concept of designing artificial nucleases is the covalent attachment of metal complexes to oligonucleotides.[40, 67] Among the best investigated compounds are iron and copper complexes. In particular, single-stranded DNA[67] but also RNA[68-70] were cleaved by such conjugates at specific sites in a metal-dependent redox reaction. The metal ion generates oxygen or peroxide radicals which diffuse to the DNA target and initialize a radical-mediated hydrogen abstraction.[53, 54] The disadvantage is that a co-reactant such as H_2O_2 is afforded to provide the cleaving species. Many artificial restriction enzymes were designed executing oxidative scission.[71, 72]

Another feasible mechanism is the hydrolytic cleavage, induced by redox-inactive metal complexes showing Lewis-acidity.[49, 50] Polydentate ligands are strongly favoured for this, because they are chelating the metal atom, therefore increase the binding force and not reducing the Lewis acidity of the metal ions.[50]

In contrast to the products of oxidative cleavage, the hydrolytic mechanism leads to fragments bearing hydroxyl groups both at the 3' and 5' ends which enables them to be recognized by religation enzymes.[49, 50, 53, 54] The religation allows it to reinsert the nucleic acid into a strand, whereas an oxidative cleavage causes an irreversible strand break.[73] As a consequence, only the hydrolytic mode of operation makes artificial nucleases usable as real restriction enzyme mimics.

The question whether a hydrolytic or oxidative pathway is preferred led to several investigations concerning various metal complexes.[53, 54, 57, 74, 75]

As a result, transition metal and lanthanide complexes were proven to most effectively degrade RNA[27, 76-78] substrates, favouring non-redox active metal ions such as Zr(IV)[79], Mg(II), Pb(II),[80] Zn(II),[81] Th(IV)[82], Co(III)[83, 84] and the lanthanides[85, 86] for hydrolytic cleavage and redox active metal ions such as Fe(II)[87, 88] and Mn[57] for an oxidative mechanism. Ce(IV),[79, 89-92] Rh(III)[93] and Cu(II)[94] ions turned out to behave depending on the reaction conditions. For the sequence-selective, hydrolytic[95] and oxidative[96] cleavage of double-stranded DNA, only some examples are known up to the present.

Most of the artificial nucleases and also nucleases in nature cleave in the single-stranded region after their hybridization with the target strand. In the case of an internal positioning of the cleavage moiety within the recognition sequence, cleavage takes place in the double-stranded area, leading to a significant decrease of stability. The basic idea behind this concept is the fact that a duplex of n base pairs will dehybridize again after cleavage because of the number of adjacent base pairs also being cut into halves. As a consequence, the artificial nuclease acts in a catalytic way (Fig. 1.6). This idea will be revisited in the course of this Thesis.

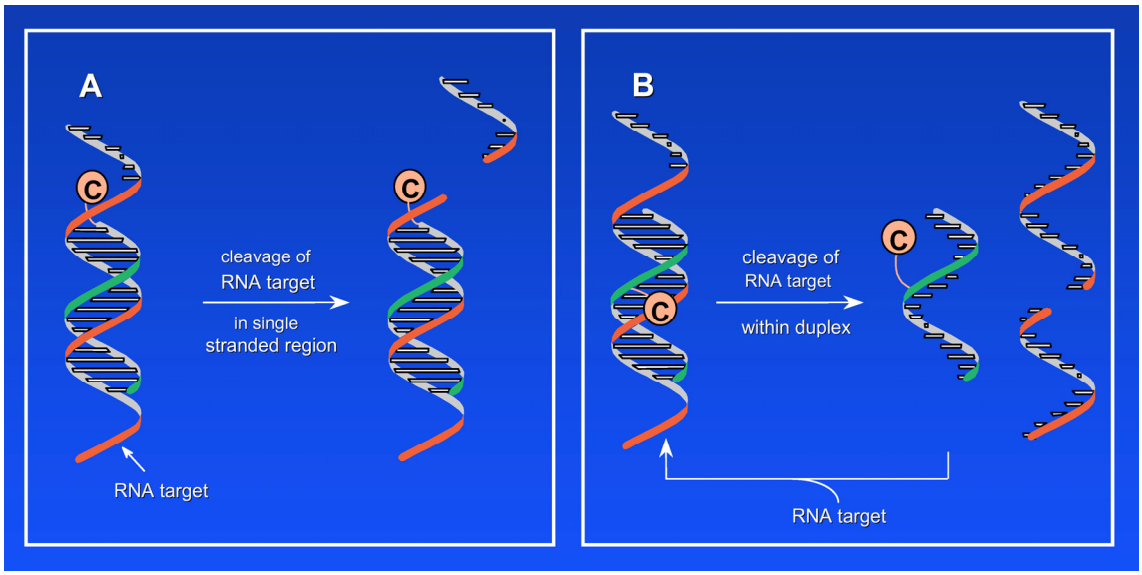

Fig. 1.6: *Sequence-Specific RNA Cleavage in Single (A) and Double Strand Region (B)*

Chemical nucleases

"Chemical nucleases" are defined as redox-active coordination complexes that nick nucleic acids under physiological conditions by oxidative attack on the ribose or deoxyribose moiety.[67, 97, 98] The 1,10-phenanthroline copper complex was the first synthetic coordination complex demonstrated to have an efficient nucleolytic activity.[99, 100]
Other complexes showing oxidative nuclease activity are ferrous-EDTA,[101, 102] metalloporphyrins[103, 104] and uranyl acetate.[105]

Besides its known ability to hydrolytically cleave oligonucleotides, preliminary investigations on our group suggested copper for its use in artificial nucleases.[106]

1.4 The Bioinorganic Chemistry of Copper

1.4.1 Copper in Nature

Apart from its questionable use in anti-aging cosmetics containing "Active Copper®" in the form of "peptide-copper complexes",[107] Cu is an essential element in any living organism, forming a large number of metalloproteins bearing copper ions in their prosthetic group – the recommended dietary intake of copper for adults is 1.0-1.5mg/d.[108, 109] The importance of copper as a cofactor is proven by the fact that copper enzymatic defects cause various metabolic deficiency syndromes. For example, albinism is the direct after-effect of an underproduction of tyrosinase[110, 111] being responsible for the synthesis of pigments (Fig. 1.7, Fig. 1.8). A genetically caused lack of ceruloplasmin (Fig. 1.9), a copper transport protein,[112] is the reason for *Morbus Wilson*, a lethal factor causing an increased accumulation of copper compounds in brain, liver, eye and other tissues leading to death without treatment.[113] In 2001, the essential role of another copper transporter, CTR1, in embryonic development was discovered.[114, 115]

Among the functions of the copper proteins are:

- *Electron Transfer* with either an outer-sphere mechanism, or functioning as an inner-sphere reductase, both involving the Cu(I)/Cu(II) couple
- *Superoxide Degradation* to form dioxygen and peroxide
- *Dioxygen Transport*
- *Oxygenases*, which incorporate an oxygen atom into a substrate
- *Oxidases*, which reduce primary alcohols to the corresponding aldehydes and thereby form either water or hydrogen peroxide from dioxygen

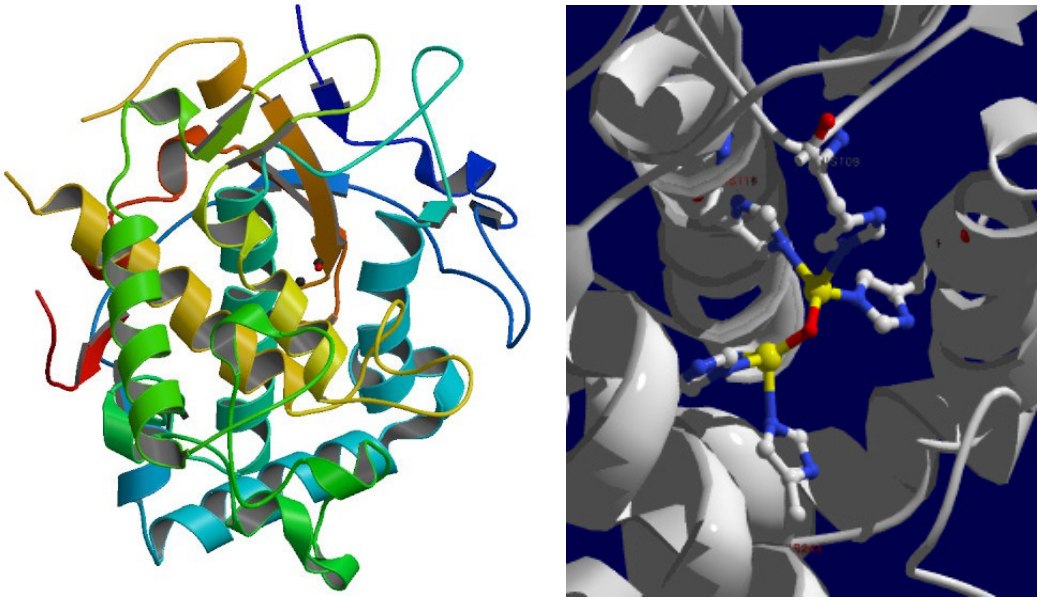

Fig. 1.7: *X-Ray Structure of Catechol Oxidase, a Tyrosinase-Related Protein[116] from Sweet Potatoes and an Enlarged Rendering of its Active Center (yellow: copper atoms, red: oxygen atoms). The amino acid sequence of tyrosinase was already revealed in the late seventies,[117] and the structure of the binuclear copper active site has been studied intensively,[118-120] whereas attempts to obtain diffraction quality crystals from tyrosinase have been failing up to the present.[121]*

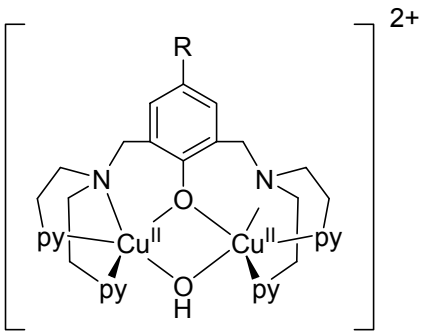

Fig. 1.8: *A Tyrosinase Model Compound for Kinetic Study of Reversible Oxygenation.[122] Pay attention to the binding pocket, allocated by two pyridines and one additional nitrogen atom*

Fig. 1.9: *Molecular Structure of Human Serum Ceruloplasmin, Containing 8 Cu Centers (green)*[123]

Examples of important copper enzymes are:

- *Cu/Zn Superoxide Dismutase* (SOD)
  involved in antioxidant defense
- *Galactose Oxidase* (see Chapter 3.5.2)
  catalyzing the oxidation of primary alcohols to aldehydes
- *Cytochrome C Oxidase* (Fig. 1.10)
  terminal enzyme in the electron transport chain

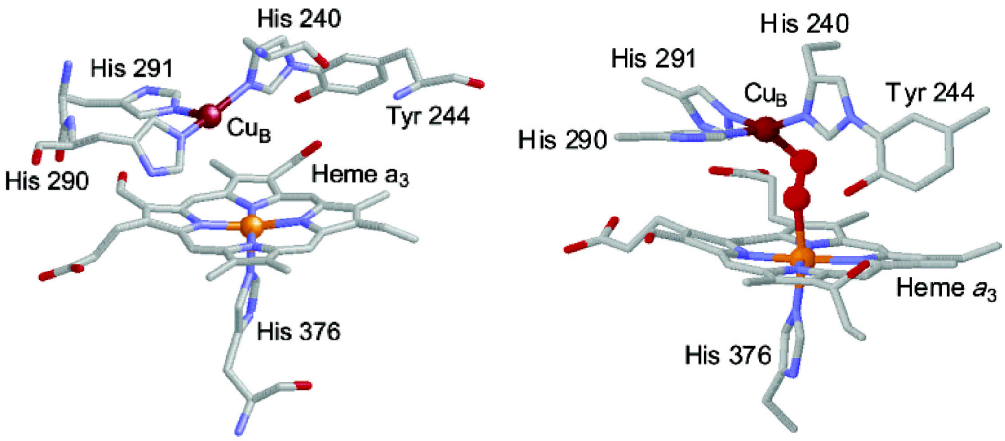

Fig. 1.10: *Crystal Structures of the Heme a_3-Cu_B Site of Fully Reduced (left) and Fully Oxidized (right) ($Fe^{II}\cdots Cu^{I}$) Bovine Cytochrome C Oxidase*[124]

From a structural and spectroscopic point of view, the three main types of biologically active copper centres in copper proteins may be distinguished according to a generally accepted convention deriving mainly from their electron paramagnetic resonance (EPR) spectra.[125]

Type 1, (T1), have 'blue' copper centers, with the copper normally coordinated to two nitrogen and two sulphur atoms

Type 2, (T2), have 'non-blue' copper centers, with the copper coordinated to two or three nitrogen and oxygen atoms

Type 3, (T3), have copper dimers. The nitrogen atoms come from histidine groups, the sulphur atoms from methionine and cysteine, the oxygen atoms from a carboxylic acid in the protein. Water, hydroxide and alkoxide oxygen atoms are also used.

In most of the copper enzymes found in nature, the metal center is bound to the imidazole of histidines. Those structural motifs of copper enzymes directly result in the idea of mimicking their active centers by the use of nitrogen ligands. In consideration of the design of artificial nucleases, copper is predestined because its offers both possibilities to either cleave in an oxidative or a hydrolytic way.

1.4.2 Cleavage of Nucleotides by Copper

In nature, no nucleases are known which work with the help of copper ions in their active site. Nevertheless, the redox activity and therefore cleavage ability of mono-,[126] di-[127] and trinuclear[128] copper(II) complexes have been extensively studied.[129]
Many of these compounds have similar structures to the dinuclear active site of tyrosinase shown in Fig. 1.8. For example, *Karlin et al.* isolated a copper-dioxygen complex with two tmpa ligands (Fig. 1.11).

Meunier et al. developed a ligand system comprising two phenanthroline ligands in one molecule (Fig. 1.12),[130] retaining an advantageous copper-ligand ratio of 1:2. Up to the present, no sequence-selective cleavage with this oxidative system could be achieved except the conjugation of 3-Clip-Phen with a DNA minor groove binder (a distamycin analogue) which decreased its ability to perform C1′ oxidation as well as the initial rate of the reaction.[131]

Cu(II) complexes containing *N*,*N*-donor ligands and dipeptides[132] and copper-histidine systems[133] were shown to act as hydrolytic DNA-cleavage agents, as well.

However, an all-purpose site-specific cleavage of oligonucleotide targets is still far from being commercially exploited and *a fortiori* far from working at satisfactory rates.

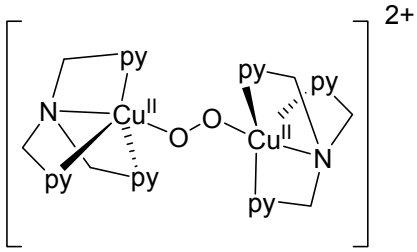

Fig. 1.11: *$[\{(tmpy)Cu\}_2(O_2)]^{2+}$*

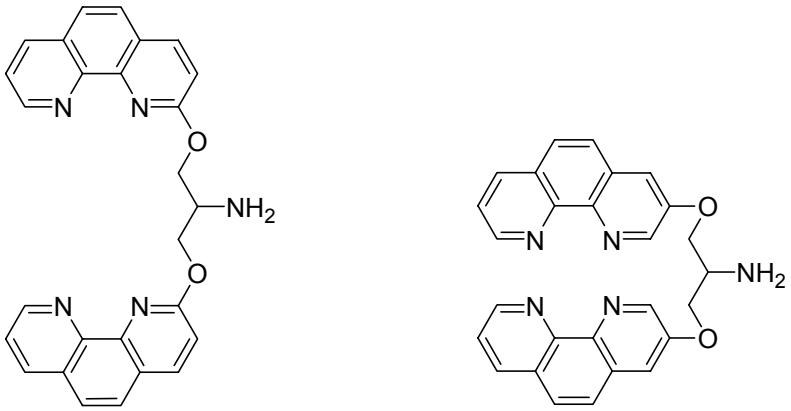

Fig. 1.12: *2-Clip-Phen (left) and 3-Clip-Phen (right)*

1.5 DNA and PNA

As shown before, many compounds are able to cleave phosphodiester bonds in oligonucleotides, but in order to do this in a sequence specific way, a recognition domain has to be implemented into the artificial nuclease, which was chosen to be, in this case, PNA, whose features and those of DNA will be described in the following.

1.5.1 Desoxyribonucleic Acid (DNA)

In every living organism, the genetic information is retained in the DNA, determined by the sequence of nucleobases serving as a template. The human genome consists of more than $3 \cdot 10^9$ nucleobases. During the transcription of this template, ribonucleic acid (RNA) is formed which is transported out of the nucleus. Ribosomes translate this information into the amino acid sequence of a protein (Fig. 1.13).

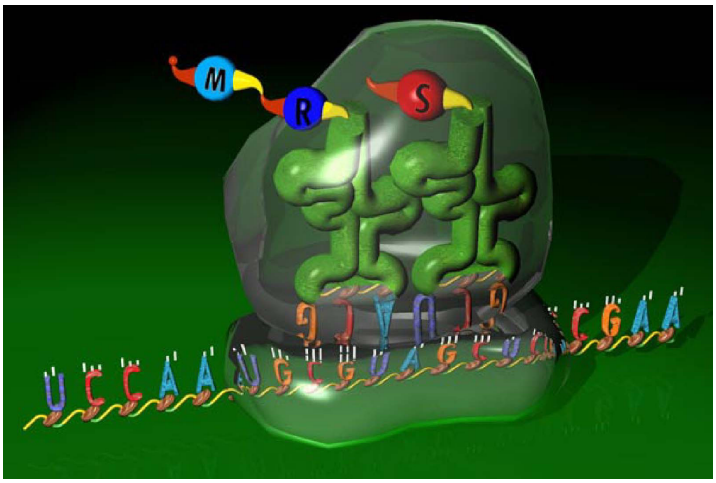

Fig. 1.13: *A Ribosome Translating the Genetic Code into a Protein Sequence*[134]

DNA consists of two antiparallel strands forming a right-handed double helix.[135]
Each single strand is made up of single nucleotides being composed of a 2'-desoxyribose, a phosphate group, a purine base (adenine A or guanine G) and a pyrimidine base (thymine T or cytosine C), respectively. The nucleotides are connected via phosphodiester bonds between the 5'-hydroxy and 3'-hydroxy groups of the 2'-desoxyribose units (Fig. 1.14). The sugar phosphates serve as structural factors, rep-

resenting the backbone of the DNA, whereas the nucleobases are pointing towards the center of the helix, bearing the genetic information in their sequence.

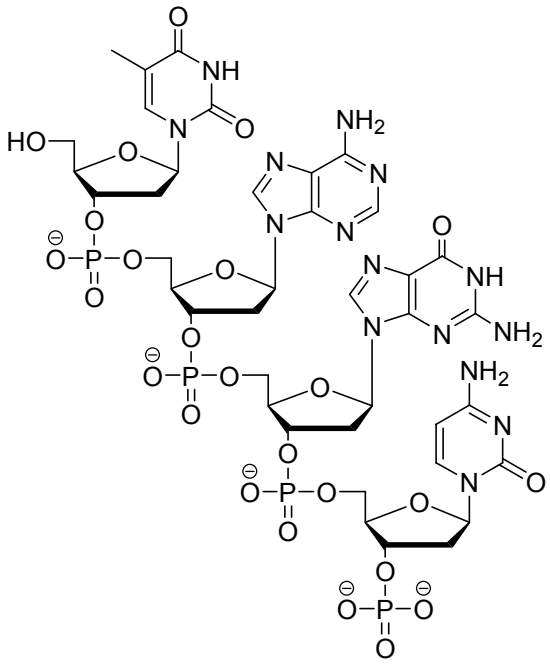

Fig. 1.14: *Structure of a DNA Single Strand*

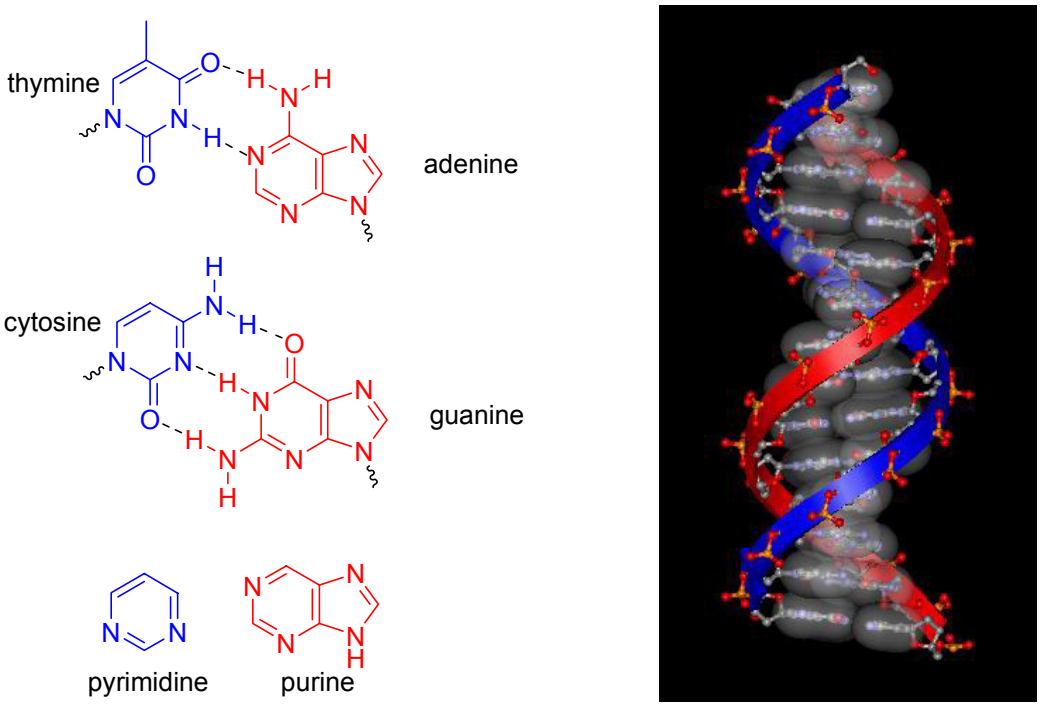

Fig. 1.15: *The Watson-Crick Base Pairing between Nucleobases Leads to a Double Helical Structure*

The DNA is self-complementary, so that every single strand contains the information of its counterpart. Within the helix, each adenine is linked to a corresponding thymine by two hydrogen bonds, whereas each guanine is related to a cytosine by three hydrogen bonds (Fig. 1.15). In RNA, the desoxyribose is replaced by a ribose, containing a 2'-hydroxy group. Besides that, in RNA uracil is used instead of thymine.

The idea to regulate gene expression by the use of deoxyoligonucleotides as chemotherapeutic agents[136] lead to a number of related concepts – antisense strategy (preventing translation by hybridizing single-strand oligonucleotides with an mRNA target),[60, 137, 138] antigene approach (preventing transcription by the inhibiting formation of a DNA triplex),[139] ribozyme targeting[140] or aptamer binding to proteins[141] – presently being investigated and in clinical testing. The principle of antisense- and antigene oligonucleotides is displayed in Fig. 1.16.

It is generally assumed that an oligonucleotide containing 12-15 nucleobases is sufficient to target a unique sequence of an mRNA, because the number of unique sequences being a combination of the four bases ($4^{12}=1.7\cdot10^{7}$) exceeds the number of bases representing potential targets.

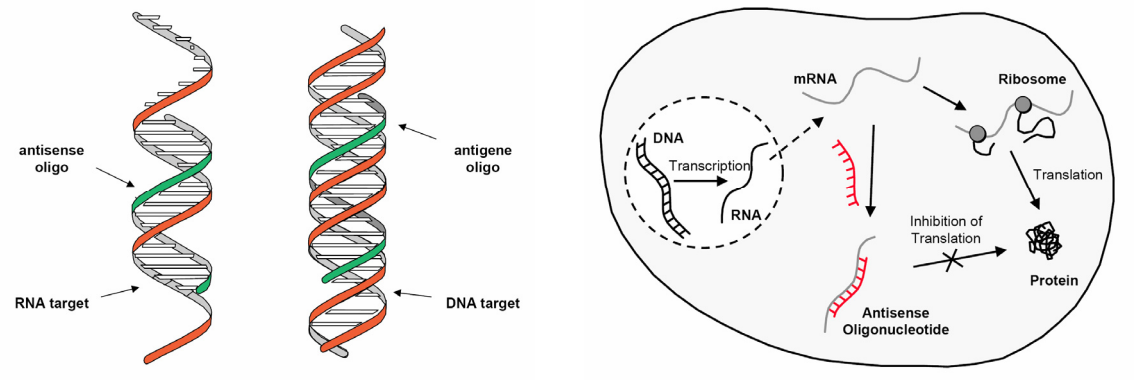

Fig. 1.16: *Antisense and Antigene Technology*[134]

The use of DNA as gene suppressors underlying several constraints resulted in various attempts to develop DNA analogues[142] in order to overcome those restrictions (Tab. 1.1), one of those being PNA.

Tab. 1.1: *DNA Modifications*

sugar modifications	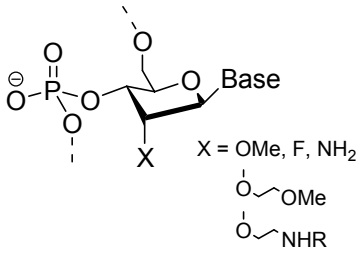 2'-substitutions	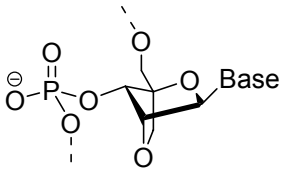 locked nucleic acid (LNA)
backbone modifications	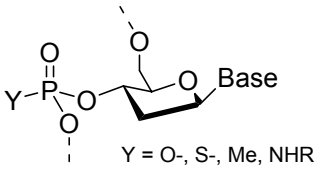 phosphate modifications	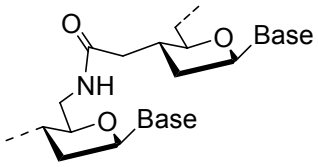 amide derived backbone

1.5.2 Peptide Nucleic Acid (PNA)

In 1991, *Nielsen et al.* developed a DNA analogue with the phosphate-sugar backbone being replaced by an uncharged *N*-(2-aminoethyl)glycine peptide backbone (Fig. 1.17).[143-146]

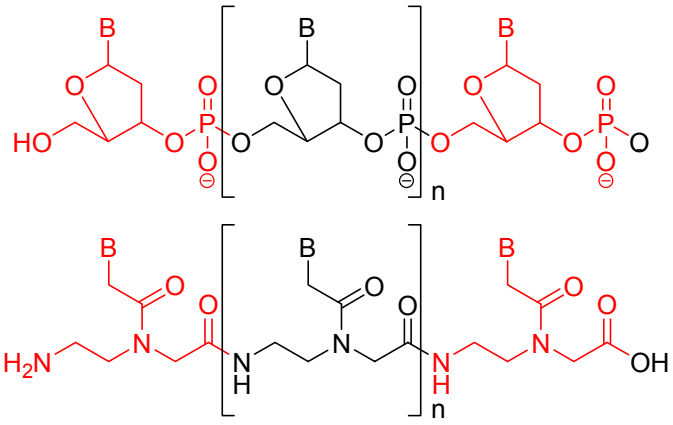

Fig. 1.17: *DNA and PNA*

This invention turned out to be one of the most revolutionary discoveries in chemistry in the last decade, providing a versatile tool for mimicking DNA including many advantages: In comparison to DNA, PNA is stable in biological environment[147] because of its resistance to enzymatic degradation[148, 149] and shows a high binding specificity and increased thermal stability to a complementary DNA strand.[150] Duplexes of PNA and DNA (Fig. 1.18) show a higher melting temperature than the corresponding DNA-DNA duplexes due to the lack of charge repulsion of the uncharged PNA backbone.[149] This has the effect that triplex formation and strand displacement can be observed.[151-153] The binding affinity is independent on salt concentration,[154-157] and even the presence of Mg^{2+} does not have any inhibiting influence.

Unfortunately, these facts lead to the disadvantage that PNAs show a reduced water solubility and tend to aggregate which can be compensated by including one ore more lysine units into the PNA sequence.[158]

The pseudopeptide backbone of PNA is resistant even towards strong acids, so that well-established synthetic strategies such as solid phase peptide synthesis (SPPS; see Chapter 1.6) can be applied. Furthermore, many possibilities of functionalizing PNA in order to attach reactive centers, proteins or functional groups are established by the use of SPPS which made PNA the right choice for our idea of sequence-specific targeting of metal complexes.

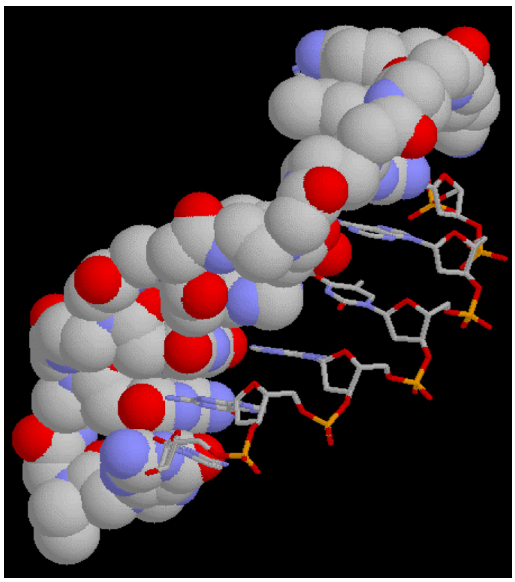

Fig. 1.18: *Solution Structure of a PNA-DNA Duplex*[150]

The therapeutic use of PNA is limited by insufficient cell delivery[148] leading to attempts to enhance cellular uptake by chemical modifications (see also Chapter 5.5).
Biotinylated PNA was successfully delivered into human mitochondria *in vitro*,[159] and connecting PNA to a lactose moiety enables it to be taken up by liver cells.[160]
However, unmodified PNA is able to enter neuronal cells in vivo[161] and to cross the blood-brain barrier, which has been shown by targeting it to the neurotensin receptor.[162]

Other important applications of PNA are

- activation of transcription[163]
- antigene[164] and antisense[165-167] applications
- restriction enzyme blocking[168]
- screening for genetic mutations[169]
- nucleic acid capture enhancement of the selectivity of PCR[170]
- probes in molecular biotechnology, diagnostics and mutation research
- gene therapy and microbiology

PNA-like molecules have been proposed as candidates for a prebiotic genetic material preceding RNA and DNA, which was recently shown by Miller,[171] who was the first one to demonstrate how easily nucleobases and amino acids are obtained under conditions thought to imitate the primitive earth.[172, 173]

In addition to the fact that PNA cannot be digested by nucleases itself, its hybridization properties suggest its use for targeting DNA and RNA in order to cleave oligonucleotides in a sequence-specific way.
In 1993, *Nielsen et al.* targeted a DNA double strand with a PNA sequence, and single strand specific nuclease S1 was shown to digest the target at the occupied PNA strand displacement binding site.[153]
The lack of specificity of oligonucleotide cleaving agents leads to the development of recognition domains, connected to a metal-ligand moiety.
In our group, PNA thymine monomers were labelled with organometallic moieties,[174] and transition metal derivatives of PNA were shown to bind to complementary DNA oligomers.[175, 176]

PNA-metal conjugates already have been used for the sequence-specific cleavage of RNA[81, 177] and for oxidative cleavage of DNA.[178]

A PNA-metal conjugate which was able to cleave dsDNA in a hydrolytic way was developed by *Krämer et al.*[179] (Fig. 1.19). This conjugate cleaves DNA in its single strand region, hybridizing with the full length of the PNA sequence.

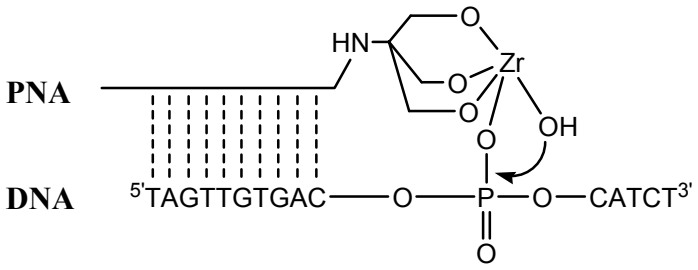

Fig. 1.19: *A Proposed Model for Hydrolytic DNA Scission by a PNA-Zr(IV) Conjugate*

One of the major advantages of PNA is its facile assembly by solid phase peptide synthesis.

1.6 Solid Phase Synthesis

The use of bifunctional precursors in chemistry (in this case PNA monomers; see Chapters 4 and 5) faces one major problem. Since each molecule is bearing two reactive sites, every possible combination of building blocks can be thought of forming products. The most common example of this is the use of amino acids for the synthesis of oligopeptides. Peptides are poly-amino acids linked via amide (peptide) bonds (Fig. 1.20).

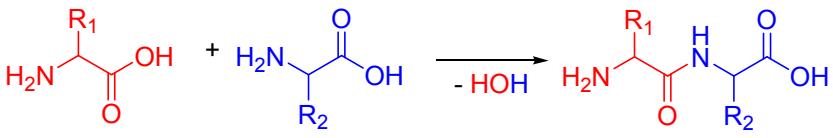

Fig. 1.20: *Condensation of two Amino Acids Forming a Dipeptide*

The problem can be schematized as follows.

Presuming two different amino acids forming only dimers, one can imagine four different products:

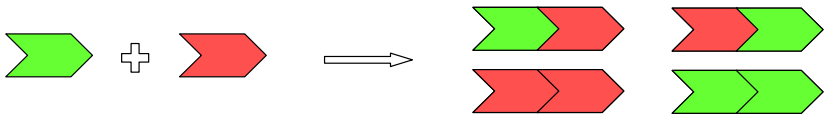

If trimers are allowed, the number of products raises up to eight:

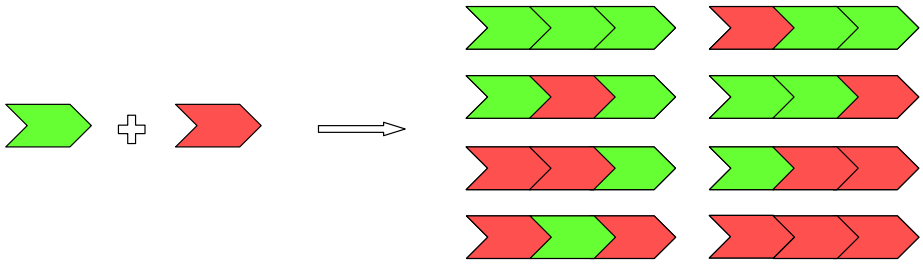

In general: If m different amino acids react with each other, m^n different n-mer species are possible (2^2=4, 2^3=8 etc.). In an uncontrolled solution-phase reaction, this increases the number of unintentional side-products over the limits. With only two different amino acids forming oligomers up to n=10, 2046 different species will be potentially present in the reaction mixture. With 10 different amino acids, this number will go up to 10^{11}, and with 100 amino acids forming 100mers, this number (10^{202}) will exceed by far the number of atoms in our universe (10^{78}).

R.B. Merrifield (Nobel Price 1984) developed a technique which allows to overcome those limitations[180] and became known as solid phase peptide synthesis (SPPS).

In contrast to the peptide synthesis carried out by nature,[181] Merrifield's concept builds up the chain from the *C*-terminus to the *N*-terminus.

The amino acids are protected at one function (usually *N*-protection, Fig. 1.22, Fig. 1.23) and immobilized on a solid support, namely a polymer resin (Fig. 1.21). The carboxyl function of the second protected amino acid is activated (Fig. 1.24, Fig. 1.25), and after deprotection of the resin-bound amino group, coupling is performed. The polymer chain is built up step by step, thus avoiding by-products (Tab. 1.2).

Tab. 1.2: *Solid Phase Synthesis – Schematic Course of Action*

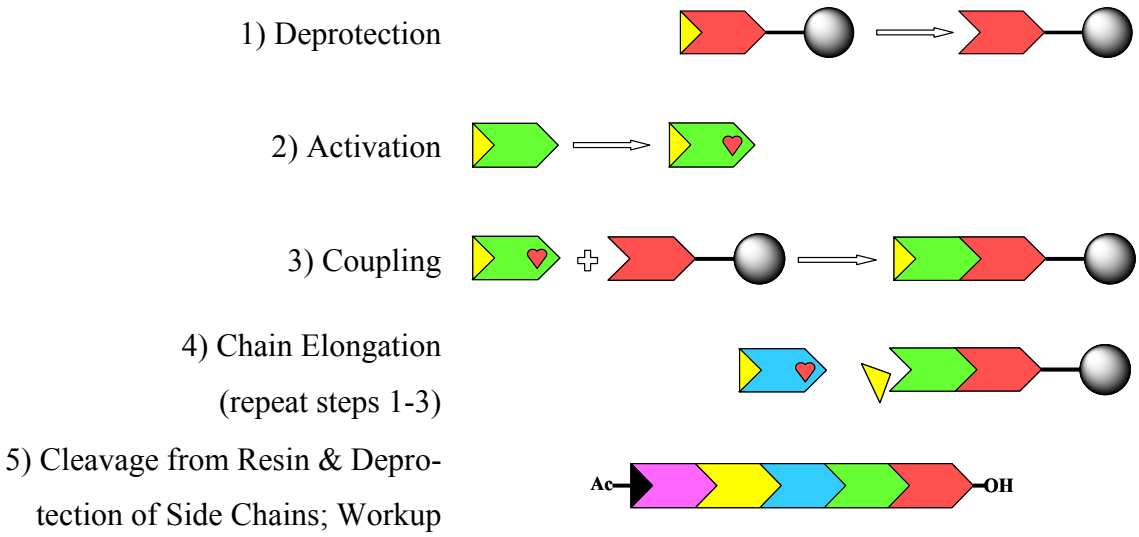

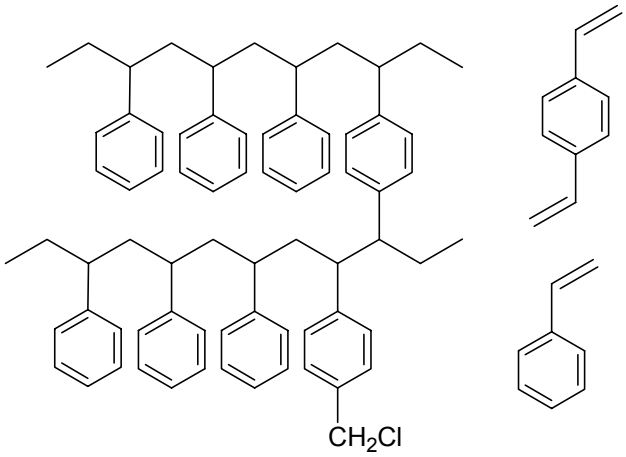

Fig. 1.21: *Merrifield Resin, Consisting of Cross-Linked Polystyrene Chains and a Linker for "Semi-Permanent" Binding*

For the two major strategies of modern, *N*-terminal protected SPPS, the most common protecting groups are Fmoc and Boc (Fig. 1.22). During SPPS, Boc is removed by TFA/DCM or HBr/HOAc, and the resin linker is chosen to be base or HF labile. The deprotection of Fmoc is carried out with 20% piperidine in DMF, shown in Fig. 1.23, and the resin is cleaved with TFA.

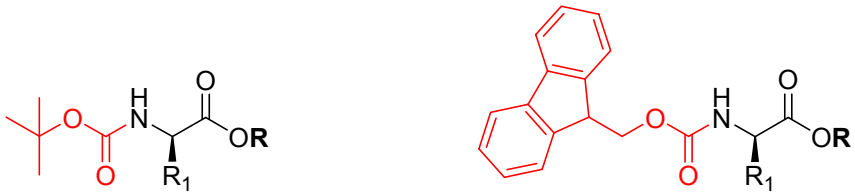

Fig. 1.22: *Boc and Fmoc Protecting Groups*

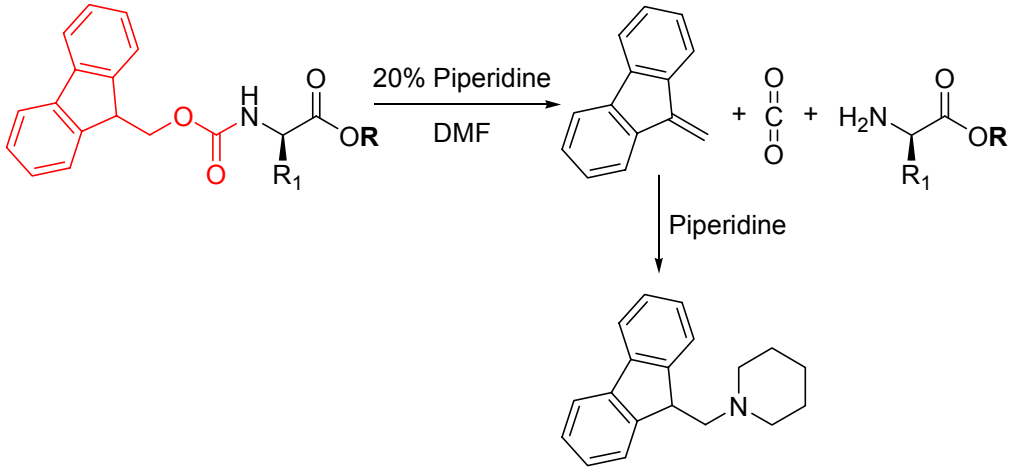

Fig. 1.23: *Removal of an N-terminal Fmoc Protecting Group*

If amino acids with reactive side chains are incorporated (Lys, Cys, Tyr etc.), they also have to be prevented from coupling ("orthogonal protection"). Usually, protecting groups are chosen which are resistant to *N*-terminal deprotection and are removed in the context of the final cleavage from the resin.

The assembly of amino acids is performed by preceding activation of their carboxyl group, because harsh reaction conditions could have an effect on the protection groups. This activation can be achieved by various coupling reagents, forming a more reactive acid derivative, for example an acid halide (using $SOCl_2$), *O*-acylisourea (using carbodiimides such as DCC and EDC; Fig. 1.24) or activated esters (using benzotriazoles like HOBt, HBTU, TBTU and HATU; Fig. 1.25).

Fig. 1.24: *DCC (left) and EDC (right) Act as Coupling Reagents*

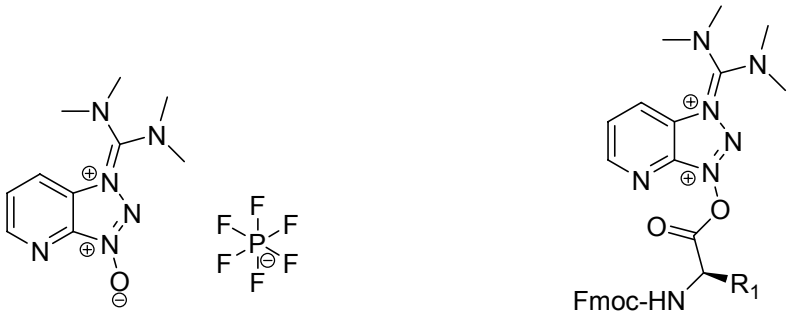

Fig. 1.25: *HATU in its Commercially Available Form (left) and as an Activated Amino Acid (right)*

The innovative advantages of SPPS are:

- Easy Removal of Byproducts by Washing
- Quick Work Steps
- High Yields by Use of Excess and Repeated Coupling (>99%)
  → longer chains are possible
- Good Reproducibility
- Automation Possible

For PNA synthesis, the strategy in Fig. 1.26 turned out to be optimum. Fig. 1.27 shows the coupling of an adenine monomer to a PNA chain and the final cleavage of the oligomer from the solid support. As an amine side chain protection, the acid labile Bhoc protecting group (written as "PG") was chosen.

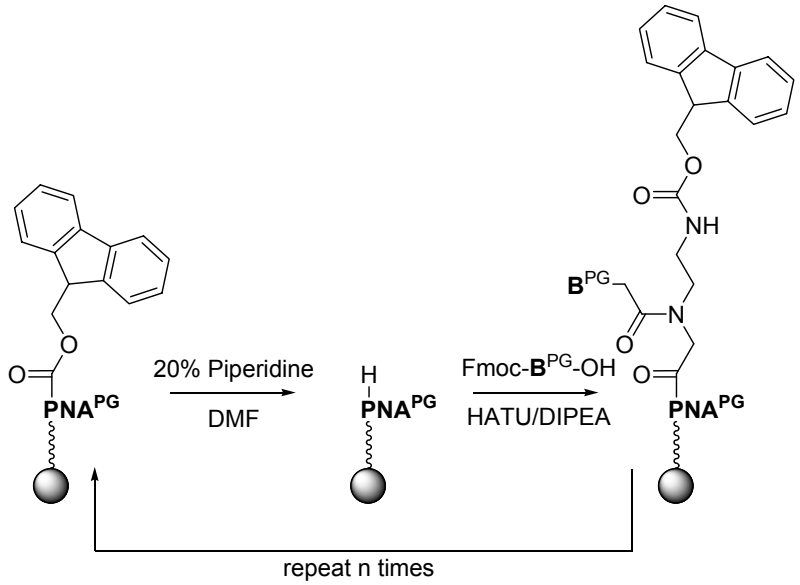

Fig. 1.26: *PNA SPS Cycle – Acid Labile Strategy (**B**=A, T, G, C)*

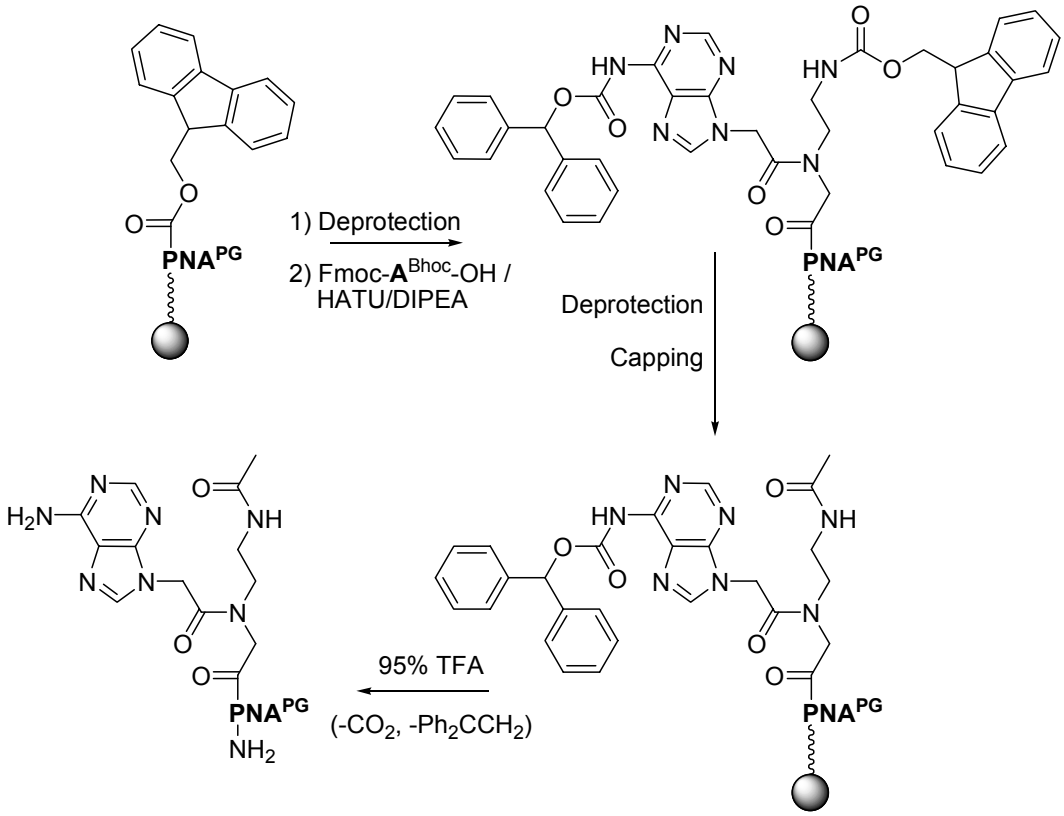

Fig. 1.27: *Coupling of a Final Adenine PNA Monomer to a Growing Chain and Final Deprotection*

2 Objectives and Outline of This Thesis

The cleavage of oligonucleotide phosphodiester bonds in biological systems is often catalyzed by metalloenzymes the mimicking of which is the aim of this project. A versatile artificial nuclease should be able to perform its action at any desired sequence within a genome.

Based on the known abilities of copper complexes with chelating nitrogen ligands such as terpyridine, phenanthroline and bis-picolylamine to catalyze the backbone cleavage of RNA and DNA, this work aims at combining both the cleavage activity of metal complexes and the selectivity / specificity of PNA (peptide nucleic acid). In addition to that, PNA comprises several advantages in contrast to DNA/RNA, predominantly the resistance towards enzymatic degradation preventing self-cleavage of the artificial nuclease as well as a higher affinity to a complementary oligonucleotide strand.

In the first part of this thesis, nitrogen ligands will be functionalized in order to enable them to be incorporated into standard solid phase peptide synthesis (SPPS). Those ligands and their copper complexes will be characterized by mass spectrometry and by UV-Vis titration in their free form and as peptide bioconjugates in order to illustrate their ability to bind metal ions and fix them at the desired position.
Furthermore, the synthesis of PNA monomers with base labile protecting groups is aspired. Terminal PNA-ligand conjugates are to be assembled by SPPS and characterized, including the investigation of their hybridization behaviour with complementary DNA strands in comparison to non-substituted sequences.
The most important challenge is the introduction of ligands into the center of a PNA sequence in order to obtain a bioconjugate being able to cleave oligonucleotides in a catalytic way and thus being a nuclease mimic.

3 Ligands

3.1 Introduction

As mentioned above, the most versatile nuclease mimic should consist of a recognition domain (PNA) and a cleavage domain, namely a metal complex. The feasibility of nitrogen-containing, pyridine-derived ligands for oligonucleotide cleavage has been shown by numerous investigations.[182]

1,10-phenanthroline (phen) is a well-known motif to prepare a large range of strong chelating ligands for various metal ions.[183]

In 1977, *Sigman et al.* investigated the DNA binding properties of the phenanthroline copper complex $Cu^{+}(phen)_2$[184, 185] which was able to cleave DNA instead of just intercalating.[100] The cleavage turned out to be oxygen-dependent and was thoroughly investigated in the aftermath.[67, 186] This complex was the first reagent oxidatively attacking ribose moieties in the presence of hydrogen peroxide. DNA conjugates of phenanthroline were obtained by linking 5-glycylamido-1,10-phenanthroline to a 5'-phosphorimidazolide of DNA (Fig. 3.1a).[187]

In order to turn DNA binding proteins into site specific scission reagents, *Sigman* converted amino acid residues adjacent to the DNA to cysteines which were then alkylated by 5-iodoacetamido-1,10-phenanthroline (Fig. 3.1b).[188] The involvement of cysteine may cause complications; therefore, the ligand conjugates in this project were designed based on peptide bonds.

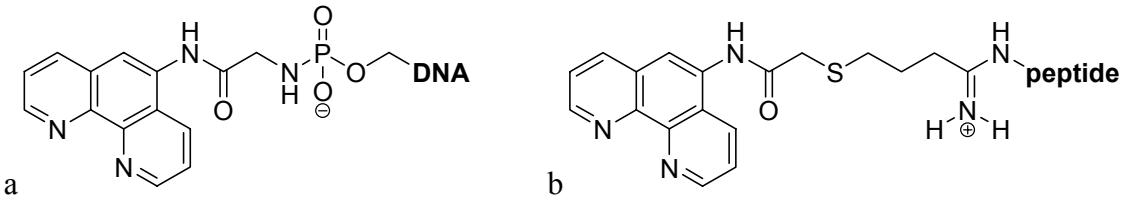

Fig. 3.1: *DNA- and Peptide Conjugates of Phenanthroline*

2,2':6',2''-terpyridine (tpy)

In contrast to the oxidative $Cu^{+}(phen)_2$, requiring the presence of H_2O_2, another copper complex was developed by *Bashkin et al.*, comprising tpy as a ligand and cleaving in a hydrolytic way.[189]

Bashkin managed to successfully synthesize tpy-DNA conjugates (by connecting the ligand to a thymine monomer; Fig. 3.2)[190] which were shown to sequence-specifically cleave HIV mRNA.[191] Another tpy-oligonucleotide with nuclease activity was presented by *Ohtsuka et al.*[192-194] However, PNA conjugates of terpyridine are not known yet.

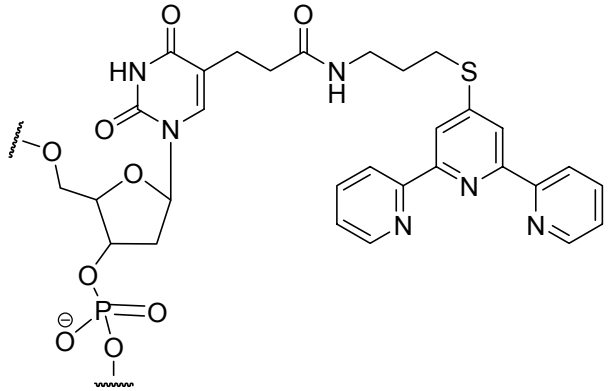

Fig. 3.2: *A Terpyridine Unit as Part of a Ribozyme Mimic*

N,*N*-bis(2-picolyl)amine (bpa)

The cleavage abilities of several bpa complexes already were extensively studied in our group,[106] so that an incorporation of bpa (Fig. 3.3) into a PNA sequence appeared to be reasonable.

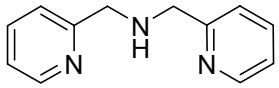

Fig. 3.3: *N,N-bis(2-picolyl)amine*

The basic concept behind the choice, functionalization and coupling of ligands was to build up the ligand coupling via amide bonds, exclusively in order to make them compatible with standard solid phase synthesis.

Because of peptide chains in the majority of cases being assembled from the *C*-terminus to the *N*-terminus, a carboxylic acid functionalization of ligands was aimed at.

In the following Chapter, synthesis and characterization of the three ligands tpy*-OH **3.5**, bpa*-OH **3.6** and phen*-H **3.8** are described.

3.2 Synthesis of Ligands

3.2.1 Terpyridine

Carboxylic acid derivatives of 2,2':6',2''-terpyridine with various chain lengths were obtained from 4'-chloro-2,2':6',2''-terpyridine and the corresponding lactones via a base catalyzed nucleophilic substitution (Fig. 3.4).

The lactones were suspended with an excess of KOH in dry DMSO, and equimolar amounts of 4'-chloro-2,2':6',2''-terpyridine and H_2O were added, followed by refluxing the mixture for 7-10d at 60°C. Aqueous workup and precipitation at neutral pH yielded the ligand derivates as white solids (Tab. 3.1).

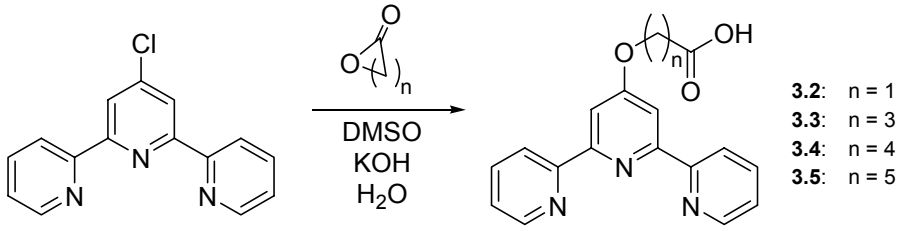

Fig. 3.4: *Synthesis of Carboxylic Acid Derivatives of 2,2':6',2''-Terpyridine*

Tab. 3.1: *Carboxylic Acid Derivatives of 2,2':6',2''-Terpyridine – Overview*

	n	reactant	Yield
3.2	1	glycolic acid	50%
3.3	3	γ-Butyrolactone	57%
3.4	4	δ-Valerolactone	69%
3.5	5	ε-Caprolactone	78%

The progress of the reaction could be easily monitored by ^{1}H-NMR spectroscopy, examining the chemical shift of the 3'- and 5'-protons (Fig. 3.7) which is exemplified by the hexanoic acid derivative **3.5** (n=5; also referred to as "tpy*-OH"). The side reaction of 4-chloro-2,2':6',2''-terpyridine ("tpy-Cl") with water giving 4-hydroxy-2,2':6',2''-terpyridine **3.1** ("tpy-OH") also was observed in single cases.

Tab. 3.2: *^{1}H-NMR Chemical Shift of the Protons Adjacent to Substitution*

δ (ppm)	tpy-Cl	tpy-OH **3.1**	tpy*-OH **3.5**
$H^{3'}_{tpy}$ & $H^{5'}_{tpy}$	8.42	7.88	7.95

The concurring side reaction to the hydroxyl derivative obviously is slower the longer the chain is and hence negligible for the synthesis of **3.5**.

Therefore, the use of the hexanoic acid derivative **3.5** (n=5; "tpy*-OH") for all further investigations turned out to be the most feasible in terms of yield and handling. Furthermore, the enhanced flexibility of its extended alkyl chain is presumably advantageous for catalytic attack of the oligonucleotide phosphate ester.[81]

In addition to ^{1}H-NMR, ^{13}C-NMR, HPLC and ESI-MS showed pure products in all cases. The $[tpy\text{-}OH]^{+}$ peak in Fig. 3.6 must be a product fragment and not tpy-OH **3.1**, because the corresponding ^{1}H-NMR spectrum of **3.5** (Fig. 3.7c) does not show this impurity.

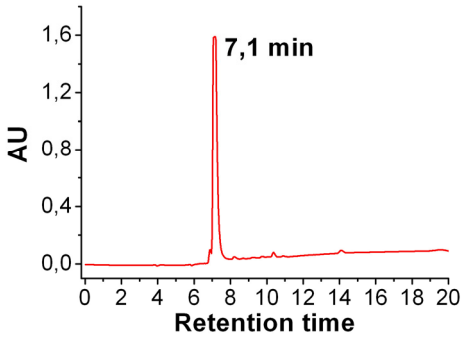

Fig. 3.5: *HPLC Chromatogram of tpy*-OH **3.5** at 254nm*

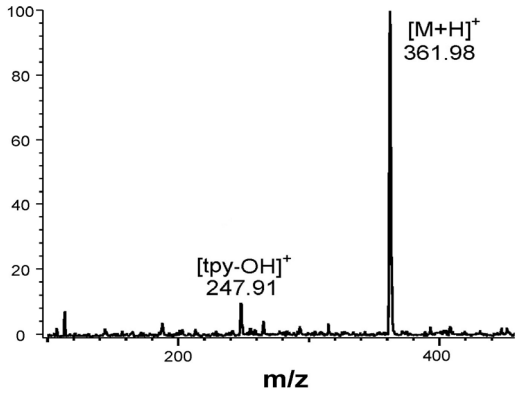

Fig. 3.6: *ESI-MS Spectrum of tpy*-OH **3.5** (M_{calc}=363.16)*

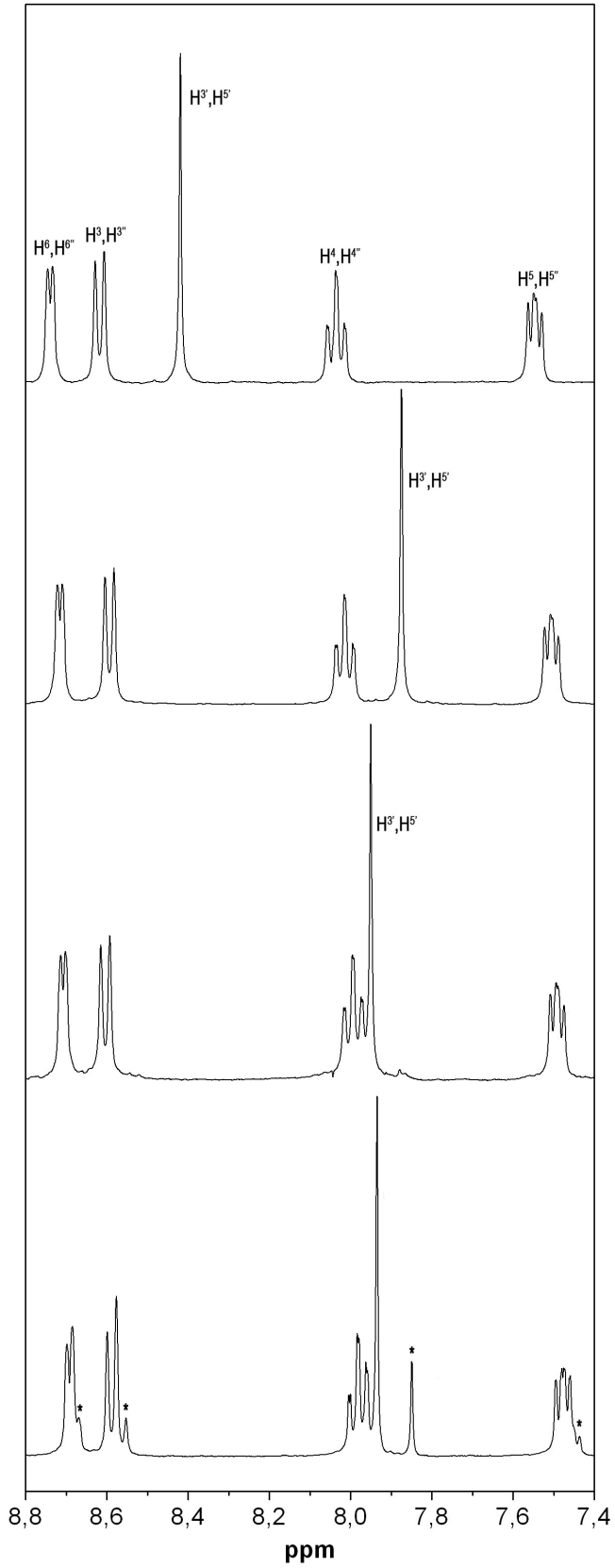

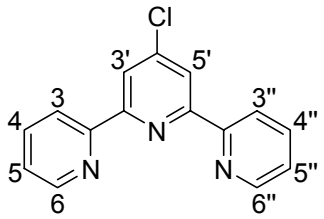

a

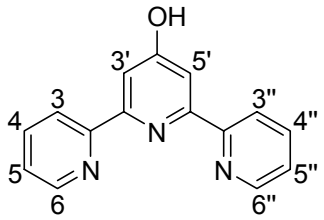

b **3.1**

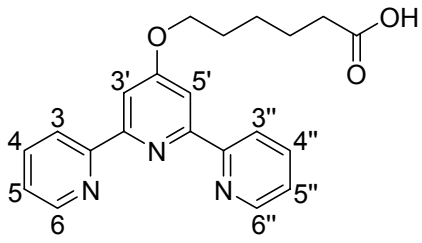

c **3.5**

Spectrum of **3.5** with impurities of **3.1** (*)

d

Fig. 3.7: *^{1}H-NMR Spectra of Terpyridine Derivatives*

3.2.2 Bis-Picolylamine

The aromatically substituted ligand *N*-(4-carboxymethyl)benzyl-*N*,*N*-bis(2-picolyl)amine **3.6** was synthesized by refluxing *N*,*N*-bis(2-picolyl)amine and methyl-*p*-(bromomethyl)benzoate in THF together with DIPEA as a base.[195] After column chromatography, the methyl ester of **3.6** was obtained in 81% yield. It was saponified with 1M NaOH and, and **3.6** was crystallized in 71% yield. ^{1}H-NMR, ^{13}C-NMR, HPLC and ESI-MS showed a pure product. **3.6** will be referred to as "bpa*-OH" in the following.

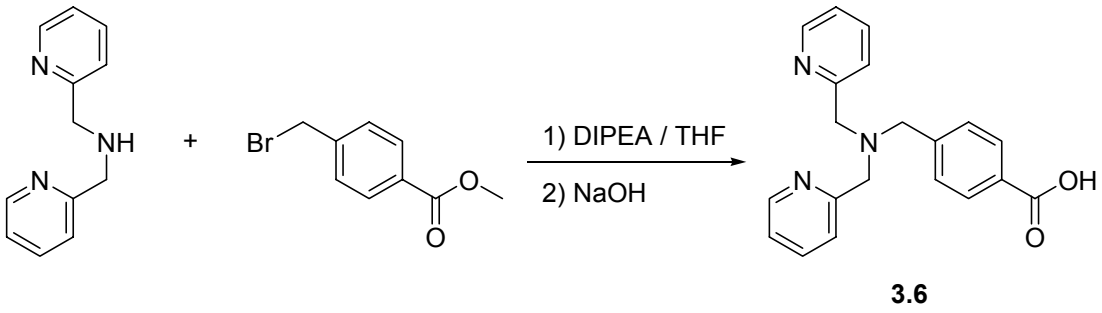

Fig. 3.8: *Synthesis of bpa* **3.6***

3.2.3 Phenanthroline

The functionalization of 1,10-phenanthroline was carried out by nitrating the ligand in 5-position, followed by reduction of the nitro group with ammonium sulphide (Fig. 3.9). Each reaction step could easily verified by ^{1}H-NMR (Fig. 3.11).

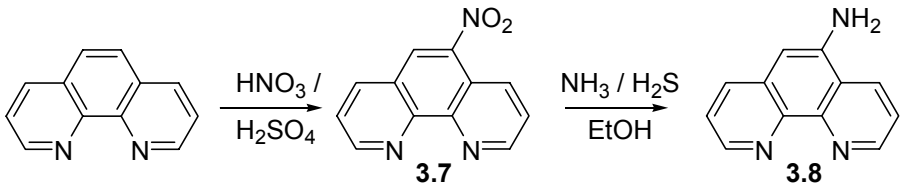

Fig. 3.9: *Synthesis of phen*-H* ***3.8***

Attempts to turn aminophenthroline (phen*-H) **3.8** into carboxylic acid derivatives applicable for SPPS were carried out by reaction with bromo-toluic acid bromide, cyclic anhydrides, bromoacetic acid methylester, dicarboxylic acid monoesters and its acid halides (Fig. 3.10). Those reactions either failed or the products were hard to purify, so that the main attention of further research was concentrated on the ligands tpy*-OH **3.5** and bpa*-OH **3.6**.

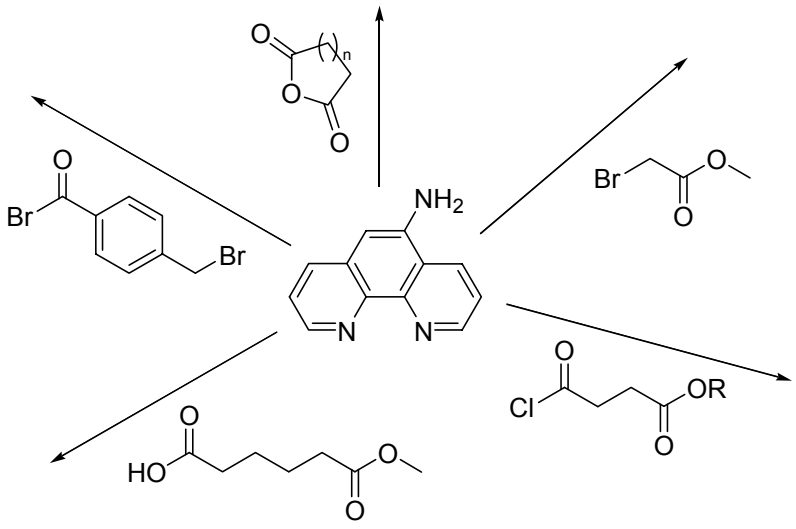

Fig. 3.10: *Attempts to Convert* ***3.8*** *into a Carboxylic Acid*

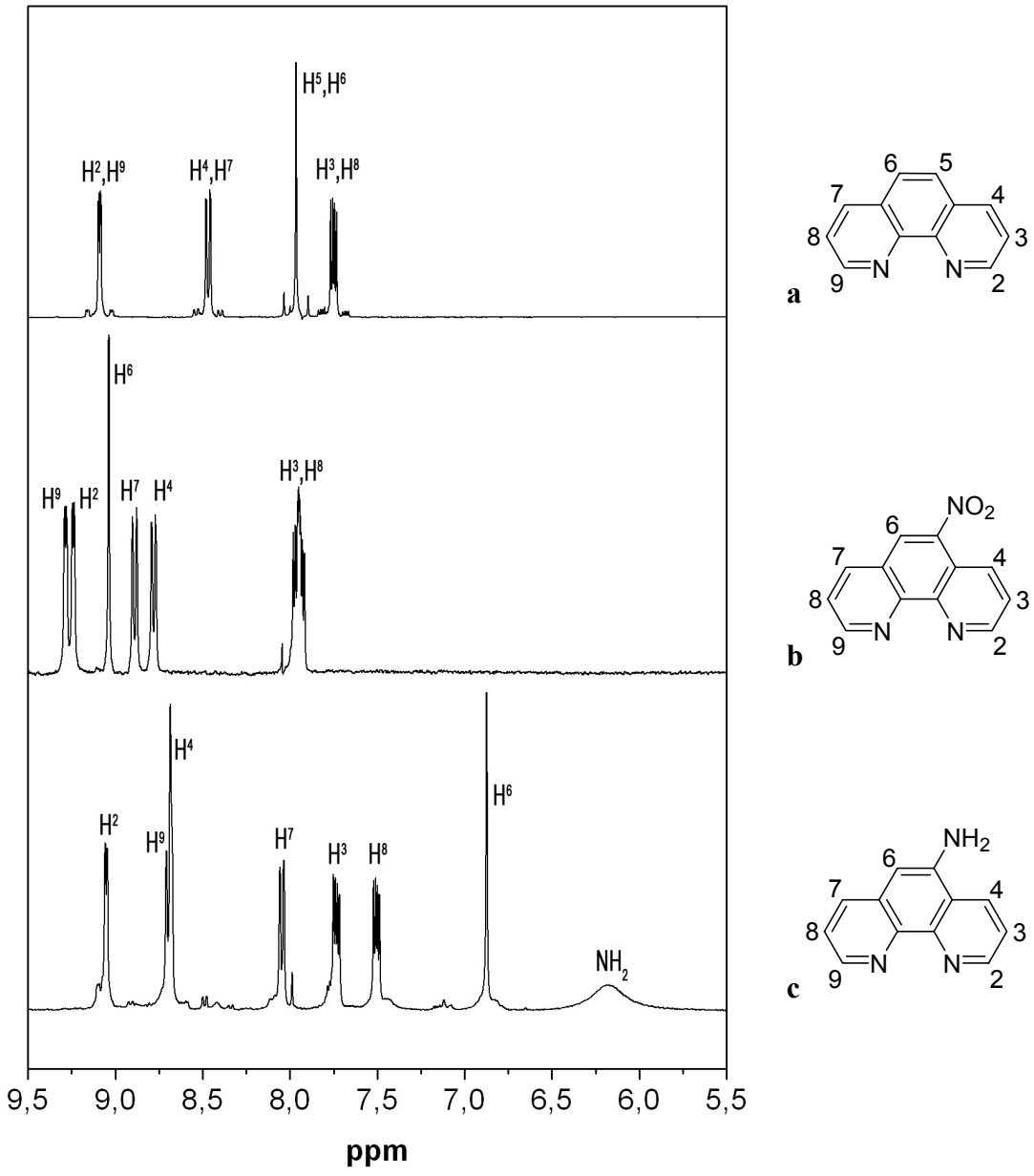

Fig. 3.11: *^{1}H-NMR Spectra of Phenanthroline Derivatives*

3.3 Phenylalanine Conjugates

In order to prove the usability of **3.5** and **3.6** for SPPS, the ligands were coupled to phenylalanine methyl ester (Fig. 3.12, Fig. 3.13).

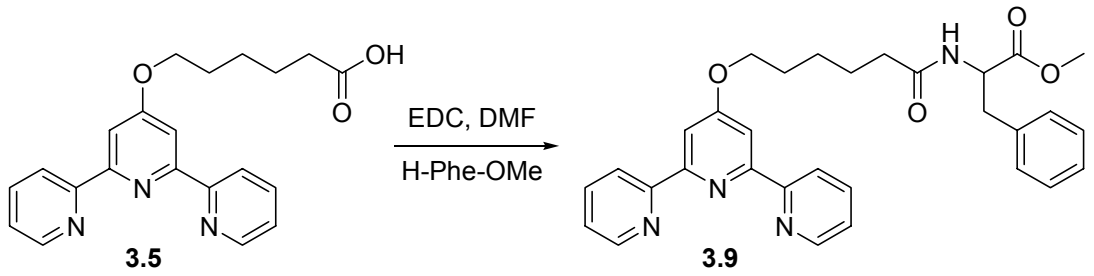

Fig. 3.12: *Synthesis of tpy*-Phe-OMe **3.9***

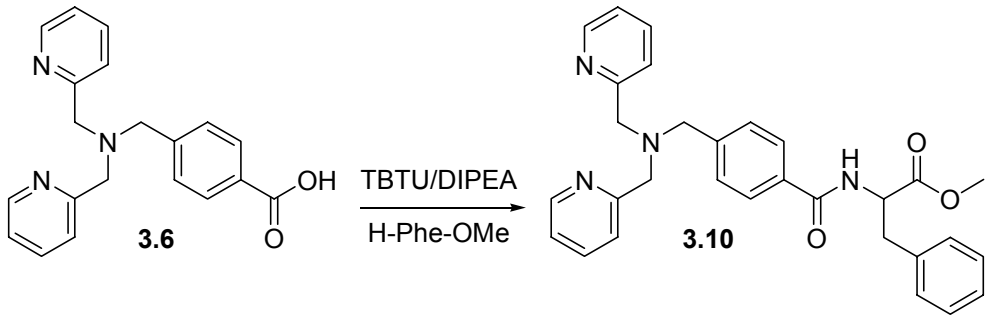

Fig. 3.13: *Synthesis of bpa*-Phe-OMe **3.10***

3.5 and H-Phe-OMe were condensated with EDC in DMF. After reaction of the mixture overnight at ambient temperature and evaporation of the solvent, a pink oil was obtained and coevaporated with MeOH. The residue was stirred with water overnight yielding a white solid which was separated from the pink supernatant by filtration and dried *in vacuo*. For the synthesis of **3.9**, bpa*-OH **3.6** was activated using TBTU/DIPEA in acetonitrile.[195] After removal of the volatiles, the residue was triturated with DCM, which was after filtration dried over Na_2SO_4 and evaporated. The resulting white product was purified by column chromatography.

^{1}H-NMR, ^{13}C-NMR and EI-MS revealed the ligands **3.5** and **3.6** being suitable for peptide coupling in good yield.

3.4 Pseudoneurotensin Conjugates

Neurotensin is a biologically active tridecapeptide isolated from the hypothalamus:[196]
pGlu[1]-Leu[2]-Tyr[3]-Gly[4]-Asn[5]-Lys[6]-Pro[7]-Arg[8]-Arg[9]-Pro[10]-Tyr[11]-Ile[12]-Leu[13]-OH
It has been shown to induce hypotension and hypothermia in the rat brain,[197] to stimulate contraction of guinea pig ileum and rat uterus, and to cause relaxation of rat duodenum. There is also evidence that it acts as both a peripheral and a central nervous system neurotransmitter.[198]
Actual findings suggest that in brains of Alzheimer's disease patients there are deficits in this peptide in certain regions involved with memory function.[199] Neurotensin may also be implicated in the pathophysiology of Parkinson's disease[200] and schizophrenia.[201] Therefore, metal-neurotensin conjugates could represent important markers for the localization of those receptors and potential novel therapeutic agents for these neuropsychiatric diseases, stimulating neurotensin receptors in the brain.
Recently, *Bläuenstein et al.* presented a ^{99m}Tc-labelled neurotensin analogue showing enhanced tumor uptake (Fig. 3.14).[202, 203]

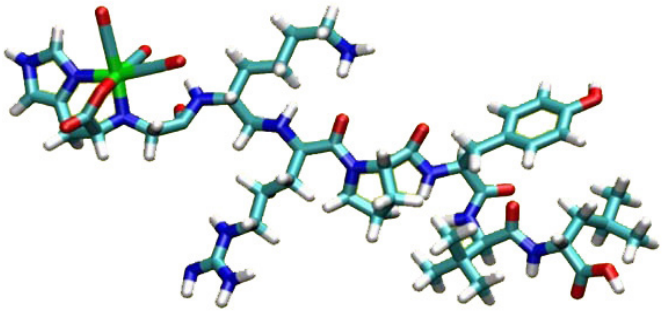

Fig. 3.14: *Model structure of [^{99m}Tc(CO)$_3$](NαHis)Ac-Lys-(ψCH$_2$-NH)-Arg-Pro-Tyr-Tle-Leu-OH*

Copper complexes of tpy-neurotensin conjugates could be promising anti-tumor agents by accumulating in tumor cells and cutting DNA.

The peptide model compounds were also synthesized in order to examine the copper binding behaviour of the ligands and their bioconjugates in solution and to show that side chains like amine groups within the sequence do not influence coordination chemistry. Peptides are known to be able to bind several metal ions. Metalloenzymes are based on a metal center, surrounded by amino acid ligands as mentioned in the Introduction.

Richelson et al. have clearly shown that the last six amino acids of this peptide are all that is needed to activate potently neurotensin receptors.[204, 205] Therefore, in this work the neuropeptide pseudoneurotensin H-Lys-Lys-Pro-Tyr-Ile-Leu-OH (pnt) was chosen to be part of metal-ligand bioconjugates.
Pnt also can be written as [Lys^8, Lys^9]-neurotensin(8-13), indicating the modifications and the section related to the original peptide.

For all pnt conjugates in this Thesis, standard SPPS chemistry with Fmoc protection (Fig. 3.15; for details and procedures, see Experimental Part) was performed, using Lys(Boc), Tyr(*t*Bu) and a preloaded Fmoc-Leu-Wang resin (0.68mmol/g) which leads to the free acid after cleavage with TFA. Capping with hexanoic acid as a comparison and *N*-terminal derivatization of pnt with tpy*-OH **3.5** and bpa*-OH **3.6** was carried out by this means, as well (Fig. 3.15). Each substance was purified by HPLC and characterized with ESI mass spectrometry.

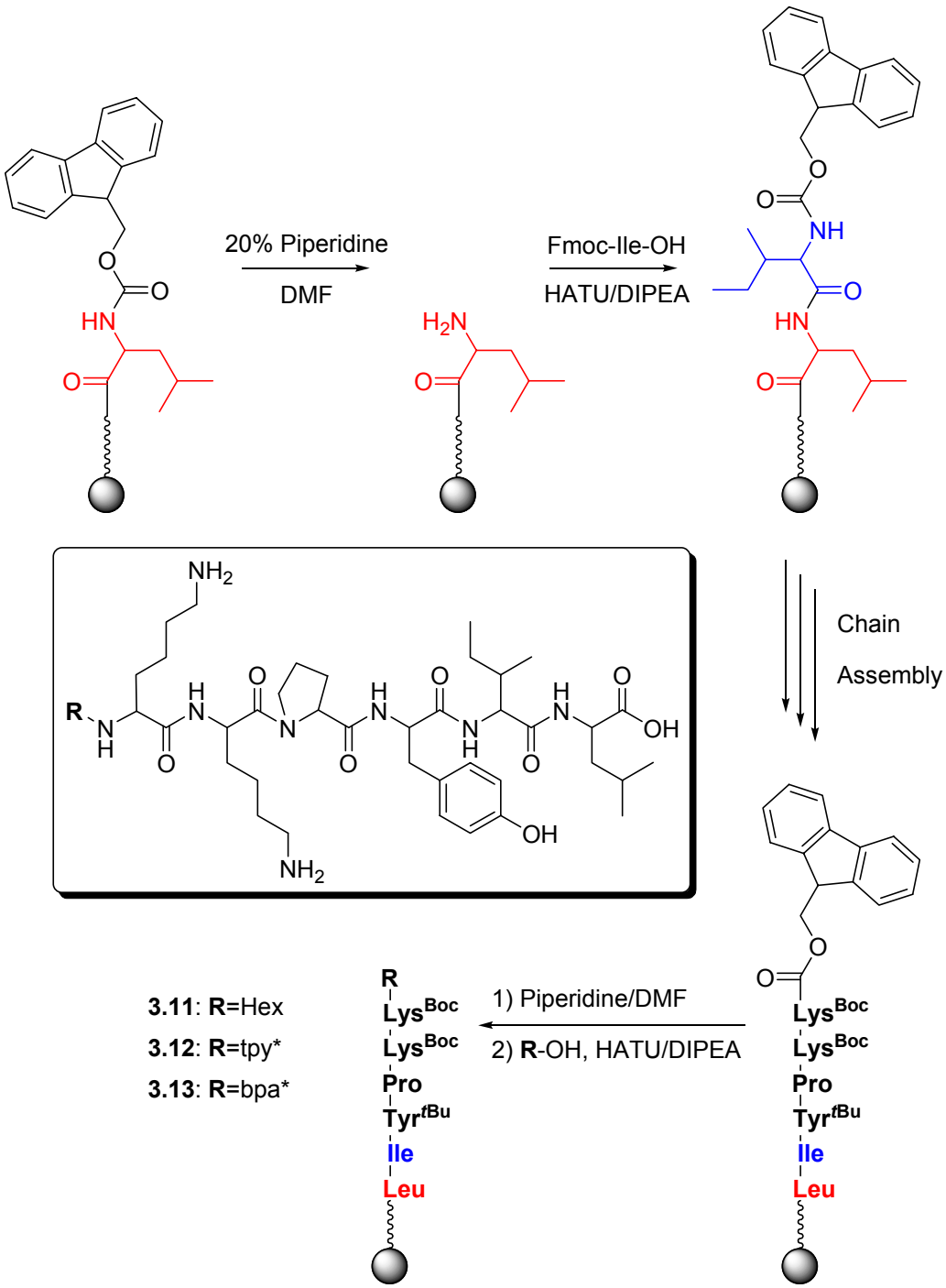

Fig. 3.15: *Synthesis of Pseudoneurotensin Conjugates – Overview and Synthesis Scheme*

For comparison, pseudoneurotensin was synthesized without ligand, but with a hexanoic acid capping group (Hex-Lys-Lys-Pro-Tyr-Ile-Leu-OH **3.11**). After HPLC-purification, ESI-MS showed a very pure product (Fig. **3.16**).

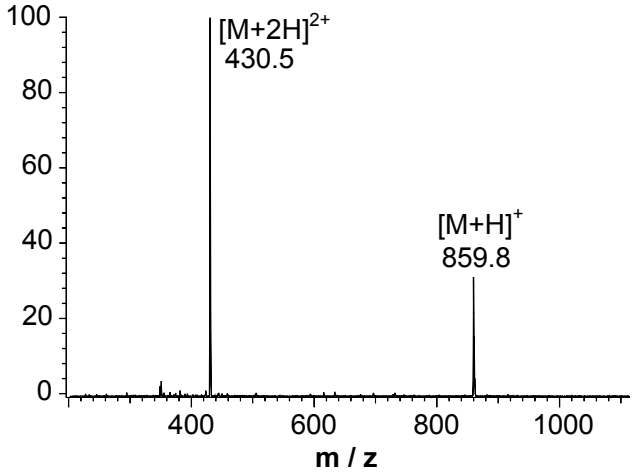

Fig. 3.16: *ESI spectrum of Hex-Lys-Lys-Pro-Tyr-Ile-Leu-OH* ***3.11*** *after HPLC purification (M_{calc}=858.7)*

With the help of HH-correlation, all ^{1}H-NMR signals could be identified. The HH-COSY spectrum of **3.11** is shown in Fig. 3.17.

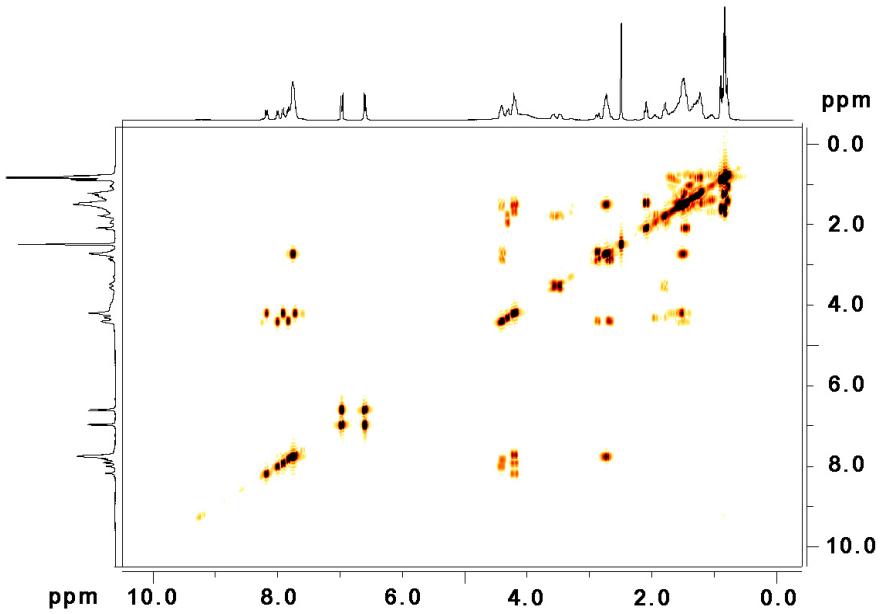

Fig. 3.17: *HH-COSY 2D NMR Spectrum of Hex-pnt* ***3.11****, measured in DMSO-d_6 at 300.16MHz*

The crude product of the tpy*-substituted pnt derivative (tpy*-Lys-Lys-Pro-Tyr-Ile-Leu-OH **3.12**) was of conspicuous pink colour. It was purified by HPLC, and besides the obtainment of the pure and colourless bioconjugate, the pink coloured peak could be separated (Fig. 3.19, Fig. 3.20). ESI-MS of this peak revealed that the observed colour comes from the iron complex of **3.12**. It was supposed that the iron originates from the TFA which is used for the cleavage from the resin. In fact, the addition of Fe(II) salts to any compound containing tpy leads to a pink solution, and **3.5**, dissolved in Millipore® water, turns pink if TFA (purchased from Acros) is added (Fig. 3.18). This observation will be taken a rain check on in the course of this Thesis. An overview of UV-Vis spectra of these compounds with and without iron is given in Fig. 3.25.

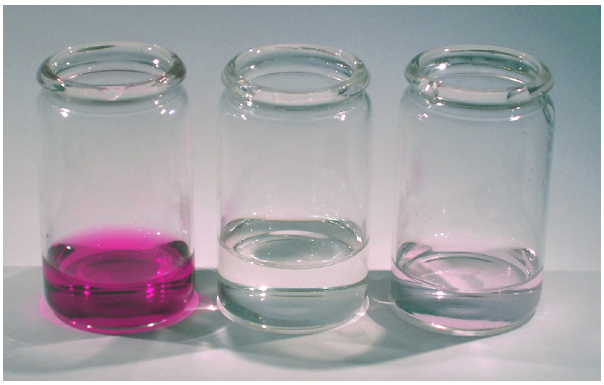

Fig. 3.18: *Aqueous Solutions (Millipore®) of*
left: ***3.12*** *and* $FeCl_2$*; middle:* ***3.12*** *alone; right:* ***3.12*** *and TFA*

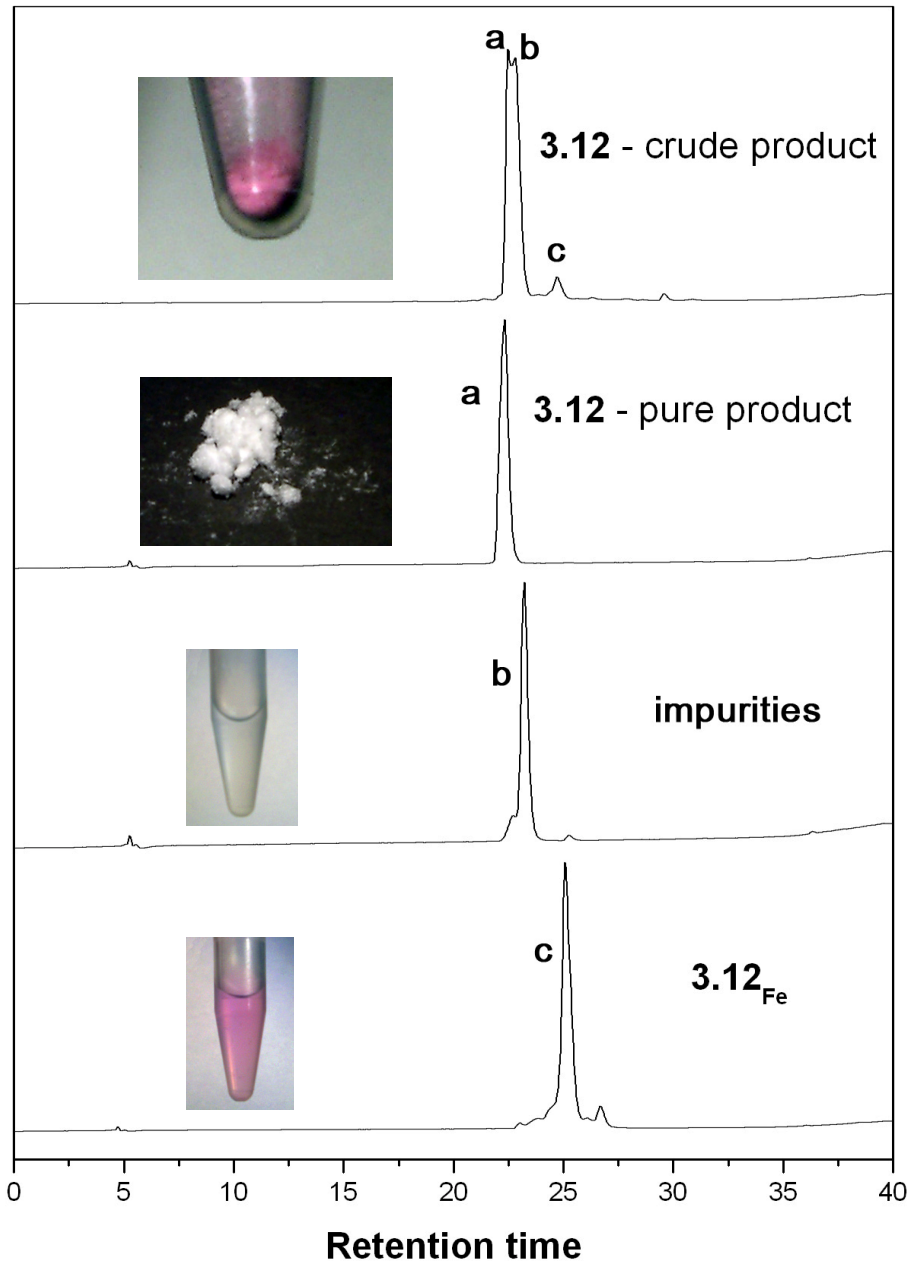

Fig. 3.19: *HPLC Purification of tpy*-pnt* ***3.12***
The pictures and chromatograms show (from top to bottom): the dry crude product, a) the lyophilized, purified product, b) and c) the two HPLC fractions of the particular by-products. Note the intense colour in comparison to the low iron compound peak height in the crude product.

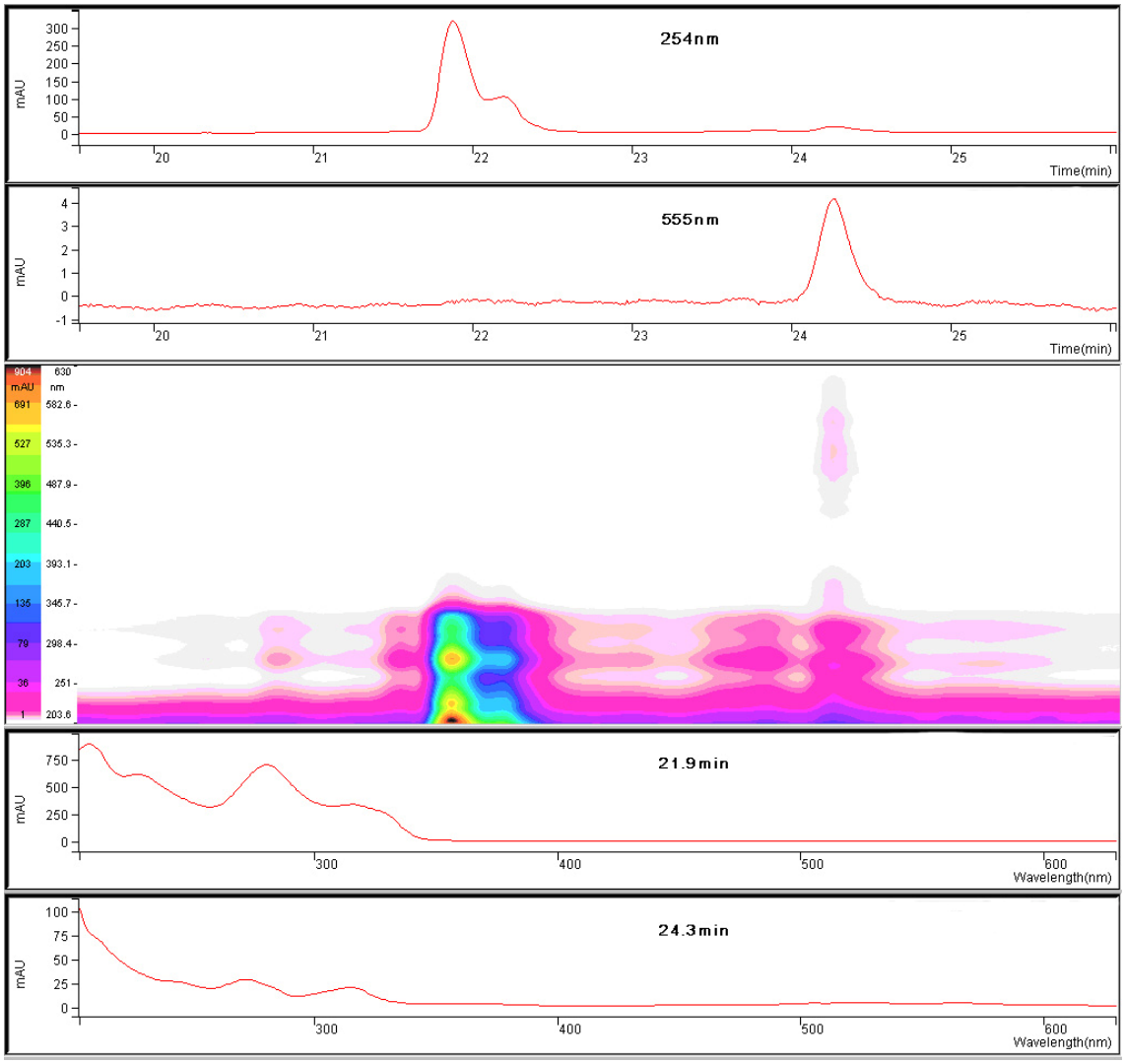

Fig. 3.20: *Three-Dimensional HPLC Spectrum of the Crude Product of* ***3.12****, Showing the Iron Peak at 555nm.*

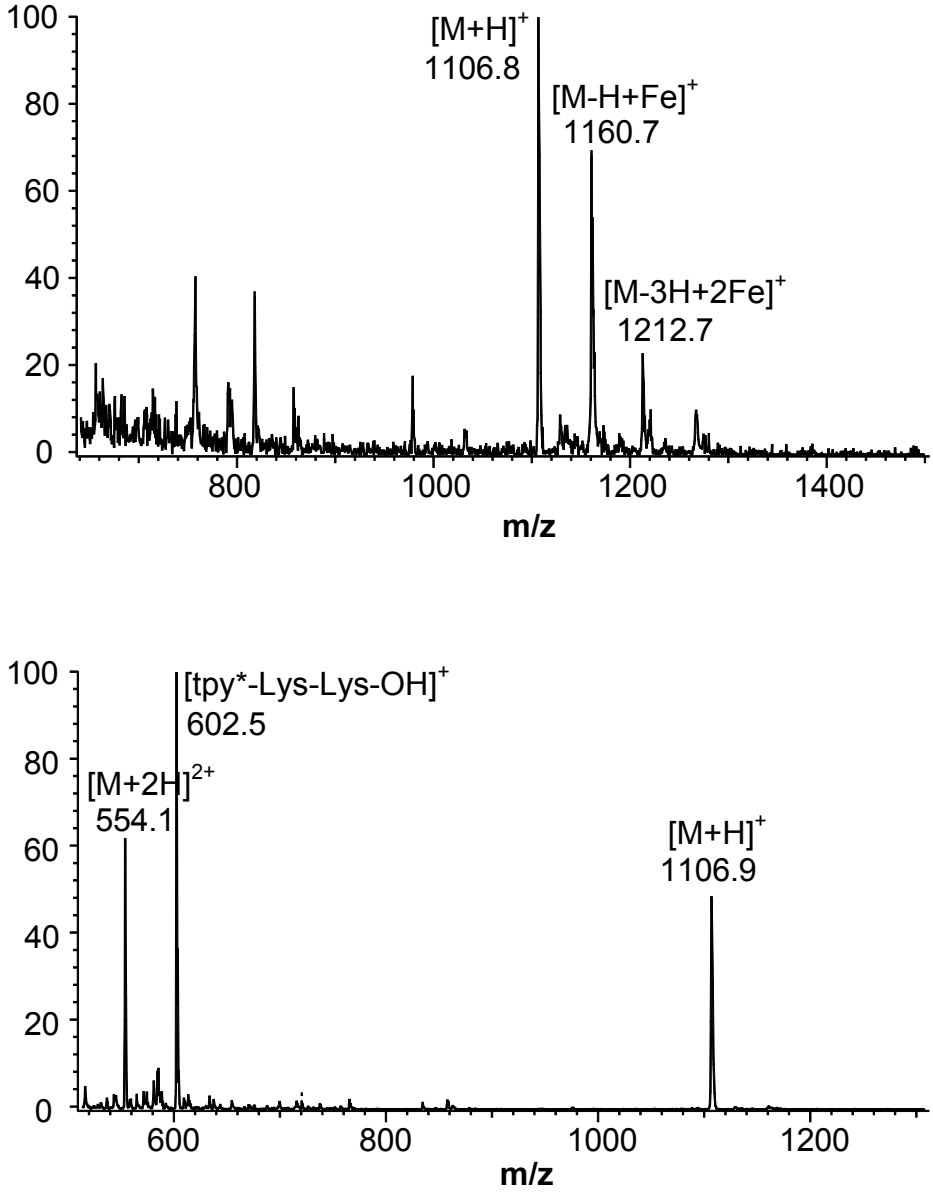

Fig. 3.21: *ESI-MS Spectra of **3.12** before (top) and after (bottom) HPLC Purification (M_{calc}=1106.6)*

In the case of bpa-substitution of pnt (bpa*-Lys-Lys-Pro-Tyr-Ile-Leu-OH **3.13**), no iron peak was observed, and the product could be obtained in high purity after HPLC-purification, which was again proved by ESI-MS (M_{calc}= 1075.6; M_{found}=1075.8).

An overview of all mass spectra will be given in the next Chapter.

3.5 Copper Complexes

3.5.1 Synthesis and Characterization

For the in situ preparation of Cu complexes, equimolar amounts of ligand / bioconjugate and copper solution as well as 2:1 ratios were mixed to obtain a 10mM dilution which was subjected to MS. The intense blue colour indicated the formation of the complex (Fig. 3.22; see Fig. 3.25 for UV-Vis spectra).

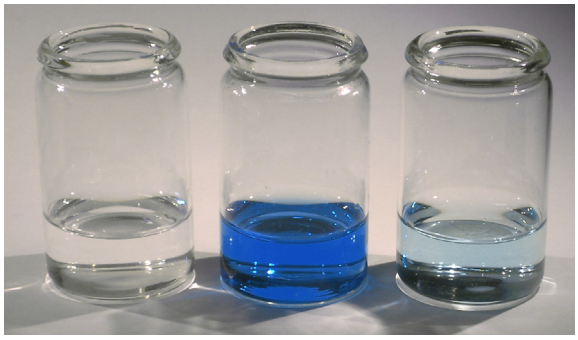

Fig. 3.22: *Equimolar Aqueous Solutions (Millipore®) of left:* ***3.12*** *alone; middle:* ***3.12*** *and $Cu(NO_3)_2 \cdot 3H_2O$; right: $Cu(NO_3)_2 \cdot 3H_2O$ alone*

In the case of bpa*, the complexes were crystallized and collected by filtration.

Mass spectra of the samples were taken in order to verify the complex formation (Tab. 3.3).

Tab. 3.3: *Overview of MS Data from tpy- and bpa-Derivatives and their Copper Complexes*

	MS	**M_{calc} (ML, ML_2)**	**M_{found} (ML, ML_2)**
Hex-pnt **3.11**	ESI+	858.6	859.8
tpy*-OH **3.5**	ESI	363.2	362.0 (-) 364.3 (+)
(tpy*-OH)Cu **3.5_{Cu}**	ESI+	426.1, 789.3	426.2, 788.3
tpy*-Phe-OMe **3.9**	EI	524.2	524.9
(tpy*-Phe-OMe)Cu **3.9_{Cu}**	FAB+	587.2, 1111.4	587.2, 1111.6
tpy*-pnt **3.12**	ESI+	1105.6	1106.9
(tpy*-pnt)Cu **3.12_{Cu}**	ESI-	1168.6, 2274.2	1167.6, ///
bpa*-OH **3.6**	EI	333.2	333.1
(bpa*-OH)Cu **3.6_{Cu}**	ESI+	396.1, 729.2	396.1
	FAB+	396.1, 729.2	396.4
bpa*-Phe-OMe **3.10**	EI	494.2	494.2
$(bpa^*\text{-Phe-OMe})_{Cu}$ **3.10_{Cu}**	ESI+	557.2, 1051.4	557.0
	FAB+	557.2, 1051.4	557.0
bpa*-pnt **3.13**	ESI+	1075.6	1075.8
$(bpa^*\text{-pnt})_{Cu}$ **3.13_{Cu}**	ESI-	1138.6, 2214.2	1137.6
	FAB+	1138.6, 2214.2	1138.7

As one can clearly see from the MS data displayed in Tab. 3.3, the formation of bivalent complexes is observed for tpy-derivatives with shorter chain length. For tpy*-pnt **3.12**, no peak was found at all in that area. This might be due to the length of the peptide chain, sterically preventing a second equivalent from binding to the copper center. In the case of most of the bpa derivatives, the measuring range was not extended to the masses of the ML_2 complexes, so that their existence is neither proved nor disproved.

Exemplarily, the ESI spectra of (tpy*-OH)Cu **3.5_{Cu}**, $(tpy^*\text{-OH})_2Cu$ **$(3.5)_{2Cu}$** and (tpy*-pnt)Cu **3.12_{Cu}** are displayed in Fig. 3.23.

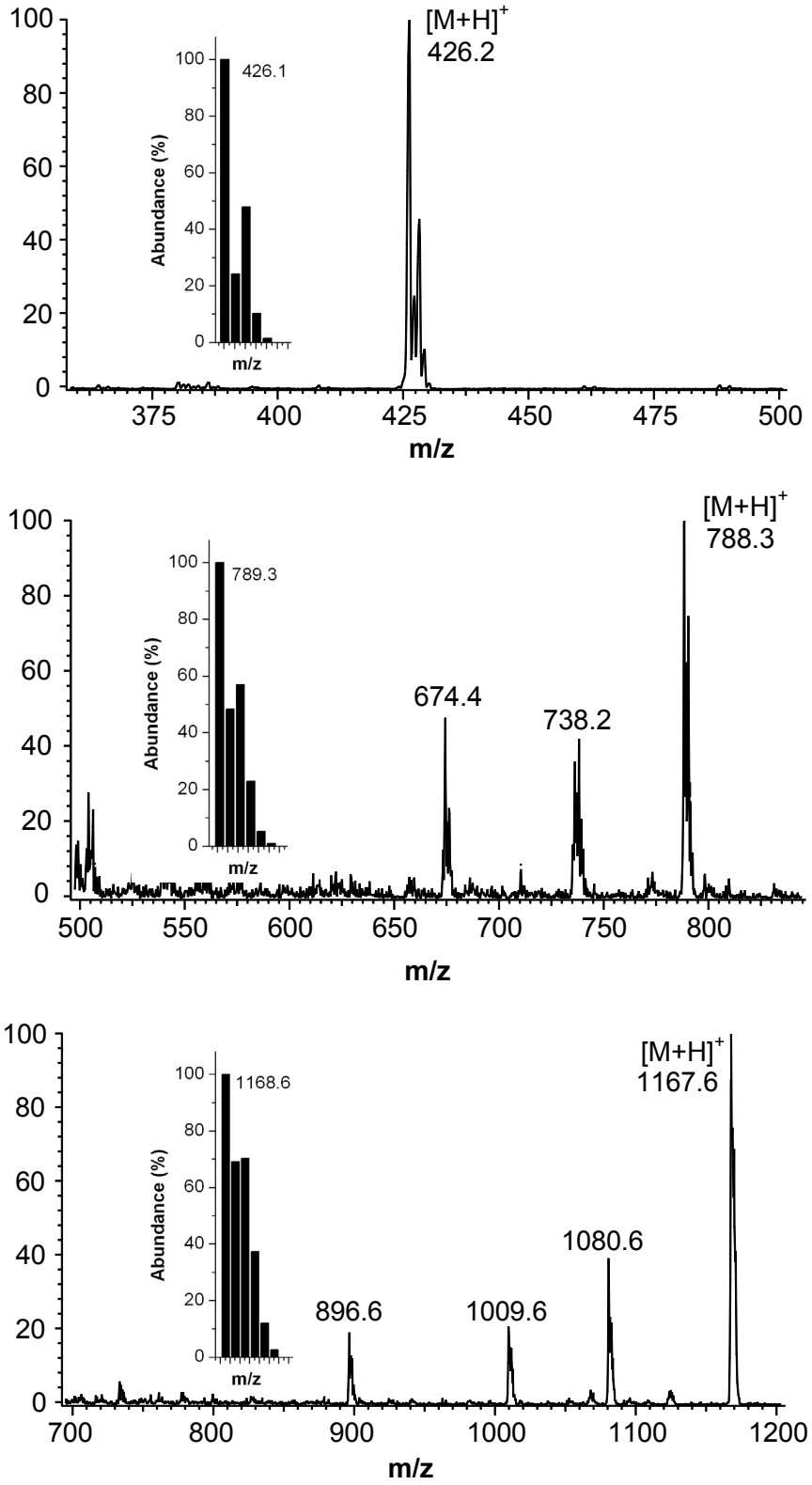

Fig. 3.23: *ESI Spectra and Isotopic Patterns of* $\mathbf{3.5}_{Cu}$, $\mathbf{(3.5)}_{2Cu}$ *and* $\mathbf{3.12}_{Cu}$ *(from top to bottom)*

3.5.2 UV-Vis Titration

In order to examine the copper complexation behaviour of the ligands and their bioconjugates and to verify the applicability of the conjugates for ligand-specific metal binding, UV-Vis titration was performed, showing the increase of absorbance (hyperchromic shift) at certain wavelengths depending on the metal/ligand ratio when preparing the complexes *in situ*. Advantage was taken of the fact that complexes of transition metals are usually coloured. This can be observed on the basis of the metal-to-ligand-charge-transfer band (MLCT) in UV-Vis spectra which is a result of the electronic constitution of aromatic π-electrons. The hypso- or bathochromic shift of the MLCT is a consequence of the change of ligand field energy caused by ligand exchange.

For all measurements, $Cu(NO_3)_2 \cdot 3H_2O$ was used as the copper salt, being stable on air and non-hygroscopic, so that exact concentrations could be ensured. 400µl of a 10mM solution of the particular analyte were titrated in 5µl steps with a 50mM solution of titrant, recording a spectrum from 900 to 500nm after each addition. All absorbance values were corrected according to the dilution effect by adding solvent during the titration. For the general procedure and practical details of UV-Vis titration, see Experimental Part.

In contrast to its pnt-conjugate **3.12**, the free terpyridine ligand **3.5** turned out to be completely insoluble in water and methanol, but readily dissolved in DMF, so that the experiments had to be carried out in that solvent. The solution of $Cu(NO_3)_2 \cdot 3H_2O$ in DMF turned from blue to green some minutes after preparation because of the ligand substitution by the solvent (Fig. 3.24). Nevertheless, this solution was used for the experiments, and this fact did not influence the measurements as long as equilibration time was maintained after each titration step. In the case of the free bpa ligand **3.6**, MeOH was used as a solvent for both the titrant and the analyte out of the same reason. All other compounds were dissolved in water. An overview of important UV-Vis spectra is displayed in Fig. 3.25.

Fig. 3.24: *Solution of $Cu(NO_3)_2 \cdot 3H_2O$ in Water (left) and DMF (right)*

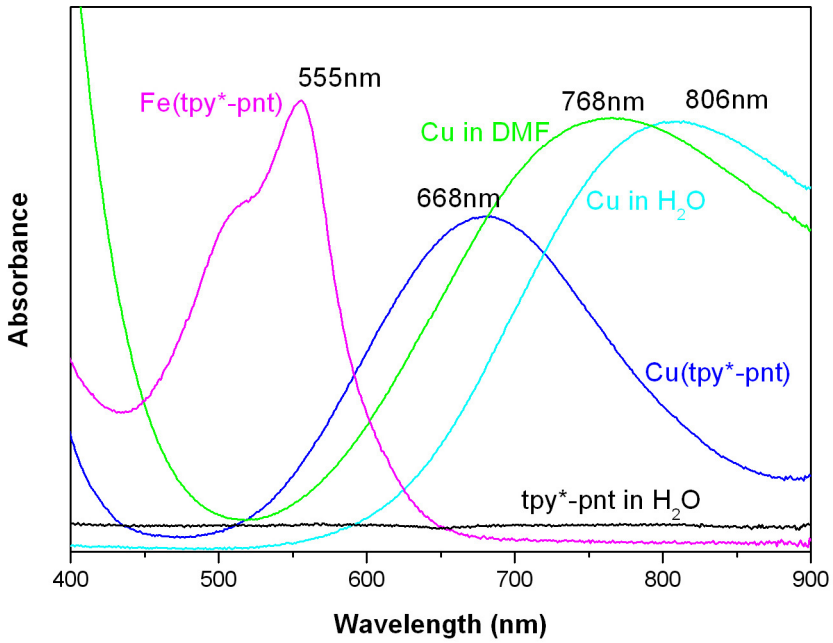

Fig. 3.25: *UV-Vis Spectra of Miscellaneous Compounds*

For comparison, hexanoic acid capped pseudo-neurotensin **3.11** was titrated with copper(II) in order to rule out coordinating influence of the peptide chain. This was important, because there are several examples for copper-binding proteins where the side chains of tyrosine or lysine are involved in metal binding. For example, galactose oxidase, a copper containing enzyme that catalyzes the oxidation of primary alcohols to the corresponding aldehydes, is bearing tyrosine in its active site[206, 207] (Fig. 3.26), and lysyl oxidase has been shown to oxidize lysyl side chains in structural proteins by binding them to its copper center.[208-210]

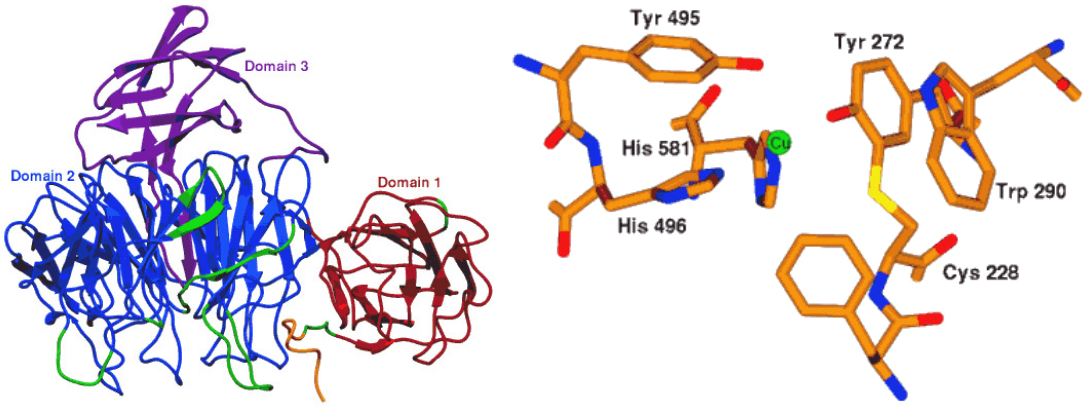

Fig. 3.26: *Crystal Structure of Galactose Oxidase with two Tyrosine Side Chains bound to the Copper Center*[211]

3.5.2.1 Experiments and Results

Titration of Hex-pnt **3.11** with Cu(II)

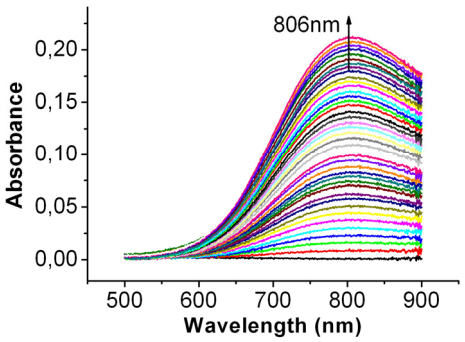

Fig. 3.27: *Absorbance Curves during the in situ-preparation of* ***3.11***$_{Cu}$

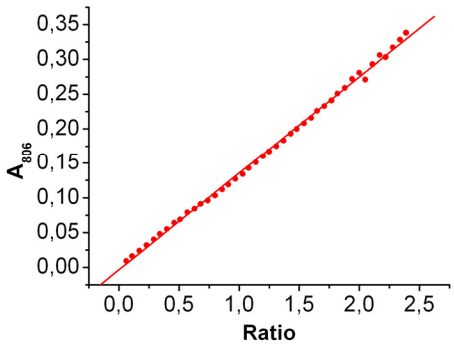

Fig. 3.28: *Plot of the Absorbance at 806nm against the Ratio* Cu^{2+}*:* ***3.11***

Each curve shows a maximum at 806nm with a linear increase of absorbance. The curve progression is similar to that of free copper salt at different concentrations, so that it can be concluded that the presence of the neuropeptide does not influence the absorbance and no reaction takes place at all.

Titration of tpy*-OH **3.5** with Cu(II)

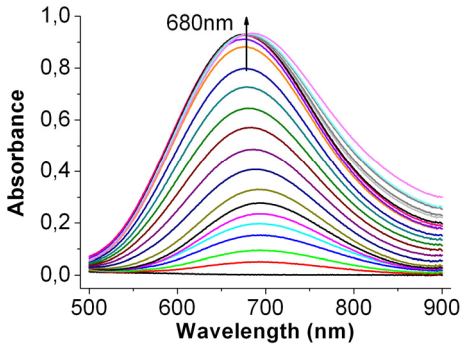

Fig. 3.29: *Absorbance Curves during the in situ-preparation of* ***3.5$_{Cu}$***

At the beginning of the experiment, the maxima of the curves have values of 694nm; after addition of 35µl of Cu(II) solution, they are hypsochromically shifted to 675nm, just to rise again for $\tau > 1$. For this reason, the particular values of absorbance were plotted against τ (Fig. 3.30) and compared with the plot of A_{max} against τ (Fig. 3.31).

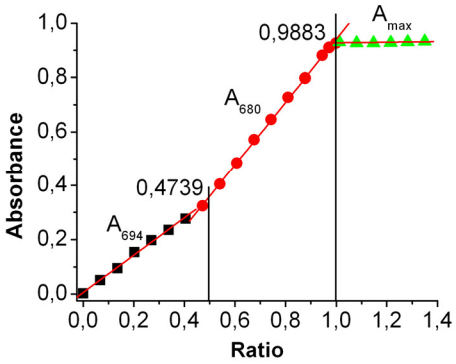

Fig. 3.30: *Plot of A at Misc. Wavelengths against the Ratio Cu^{2+}:**3.5***

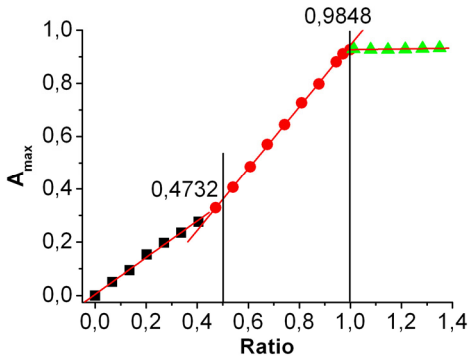

Fig. 3.31: *Plot of the Absorbance at Maximum against the Ratio Cu^{2+}:**3.5***

The two plots, not revealing a significant difference in shape, both show an increase of slope at $\tau = 0.47$ and stagnate after $\tau = 0.98$. In the accordant areas of the λ_{max} plot, the values change significantly.

This leads to the assumption that between a Cu/tpy ratio of 0.0 and 0.5, the bivalent complex $Cu(tpy)_2^{2+}$ is formed with a lower extinction coefficient and a different absorbance maximum than the monovalent complex. After exceeding this point, the $Cu(tpy)^{2+}$ complex starts to form at the expense of the $Cu(tpy)_2^{2+}$ compound. Further addition of Cu(II) does not have an effect on the absorbance, because there are no more free ligand molecules present in the solution.

Titration of Cu(II) with tpy*-OH **3.5**

In order to confirm this, the titration was repeated by adding equivalents of **3.5** to Cu(II). Minimization of inherent bias was done by the dividing the titration into two different experiments with the second one starting from $\tau = 1$.
For clarity, the two parts of this experiment are displayed separately.

The first part of the titration indicates an isosbestic point at 824nm, alluding to a proper direct reaction with no detectable intermediates (Fig. 3.32).

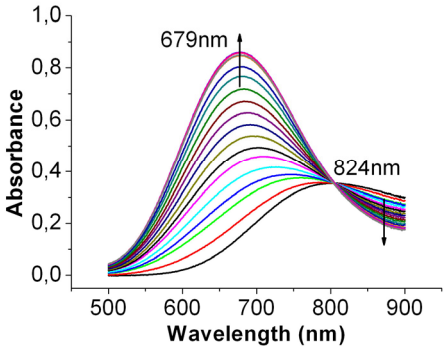

Fig. 3.32: *Absorbance Curves during the reverse in situ-preparation of* ***3.5$_{Cu}$***

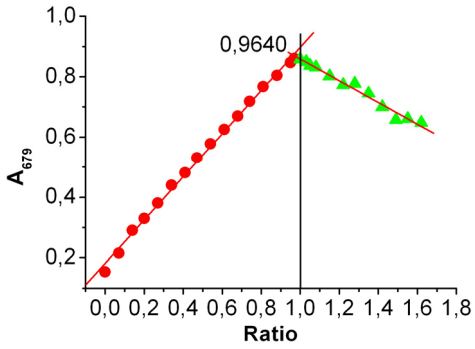

Fig. 3.33: *Plot of the Absorbance at 679nm against the Ratio Cu^{2+}:* ***3.5***

The maxima of the curves show a hypsochromic shift from $\lambda_{max} = 803nm$ ($\tau = 0$) to $\lambda_{max} = 679nm$ ($\tau = 1$) due to the fact that the broadness of the absorbance curve of the free copper and the curve of the complex overlap and therefore pass into each other. Thus, A_{679} was plotted against τ, showing a linear increase of absorption up to $\tau = 1$.

The second part of the titration shows decreasing absorbance values as supposed:

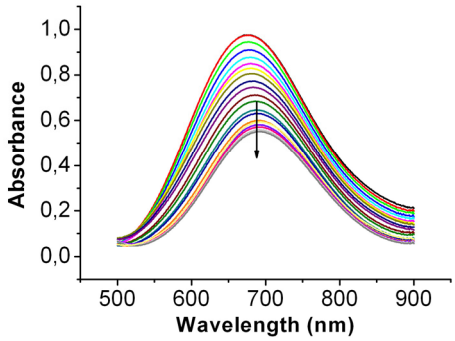

Fig. 3.34: *Absorbance Curves during the reverse in situ-preparation of* ***3.5***$_{Cu}$

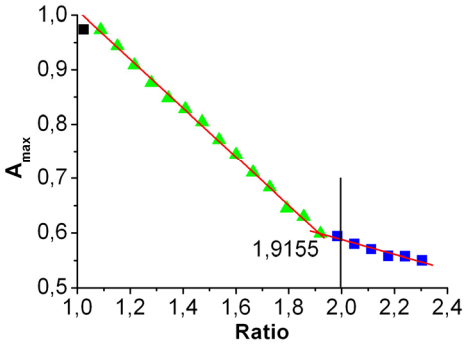

Fig. 3.35: *Plot of the Absorbance at Maximum against the Ratio* ***3.5***:Cu^{2+}

A bathochromic shift of the maxima was observed reaching from 676 to 692nm. Nevertheless, A_{max} was plotted indicating a point of equivalence at Cu:L = 1:1.92.

As it can be concluded from this experiment, the formation of the bivalent complex CuL_2 is very likely. This is confirmed by the observation that after the addition of one equivalent of ligand to the copper solution, the isosbestic point vanishes, which is a hint for a multi-component system (Fig. 3.37).

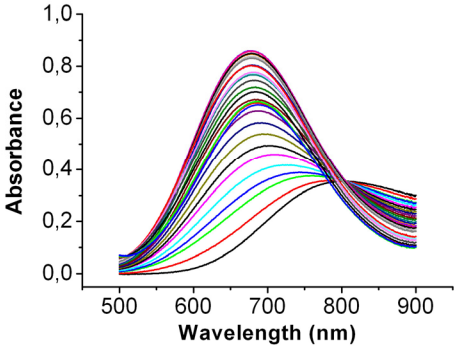

Fig. 3.36: *Absorbance Curves of the Whole Range of Titration*

Titration of tpy*-pnt **3.12** with Cu(II)

The fact that CuL_2 complexes are observed raises a problem concerning a possible oligonucleotide cleavage mechanism, because the formation of mononuclear PNA dimers would definitely affect the activity of the artificial nuclease.

In order to obtain knowledge about the influence of biomolecular moieties on the complexation behaviour, the tpy*-pnt conjugate **3.12** was titrated with copper as well and *vice versa*.

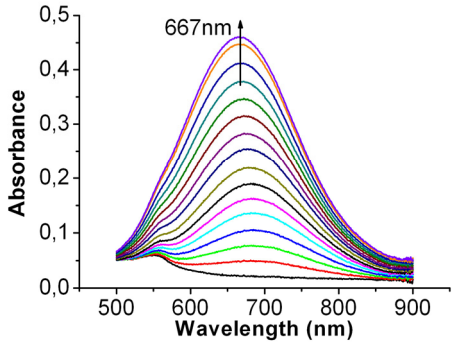

Fig. 3.37: *Absorbance Curves during the in situ-preparation of* ***3.12***$_{Cu}$

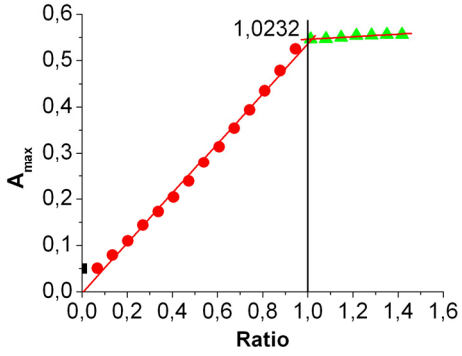

Fig. 3.38: *Plot of the Absorbance at Maximum against the Ratio* ***3.12***$:Cu^{2+}$

The spectra show a slight shoulder at ~550-560nm, originating from iron contamination of the bioconjugate (already mentioned in Chapter 3.4). This observation corresponds to the occurrence of an $[M+54]^+$ peak in all ESI and MALDI-TOF spectra measured of solid-phase made tpy* conjugates being worked up with TFA. These iron traces must originate from a different source than TFA, because the conjugate was HPLC purified. The iron is diluted with the proceeding experiment, so that the shoulder disappears. The resulting unavailability of some ligand molecules was neglected. The maxima demonstrate a hypsochromic shift from 685 to 667nm, which was ignored for the evaluation. Plotting A_{685} or A_{667} versus τ does not have a significant effect on the curve / the point of equivalence, so that for clarity, A_{max} was chosen to be plotted against τ. The curve shows a linear increase of absorbance without any change in slope until equal amounts of ligand and metal are present. Further addition of copper does not have any influence.

As a comparison, the converse experiment was carried out as well.

Titration of Cu(II) with tpy*-pnt **3.12**

As expected on the basis of the previous results, the absorbance maximum of the solution did not decrease significantly again after one equivalent of ligand being added.

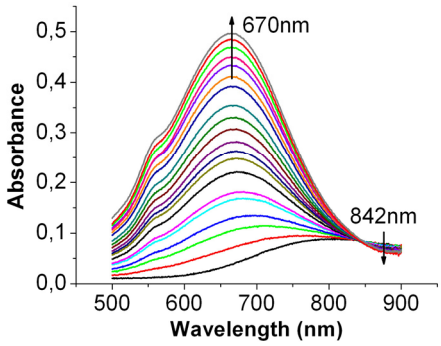

Fig. 3.39: *Absorbance Curves during the reverse in situ-preparation of* ***3.12***$_{Cu}$

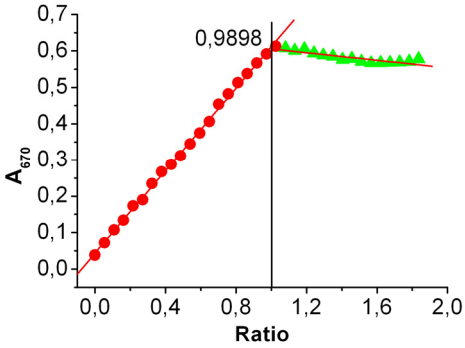

Fig. 3.40: *Plot of the Absorbance at 670nm against the Ratio* Cu^{2+}*:* ***3.12***

The maximum absorbance of the curves shifts from 803nm (pure copper) to 667nm at $\tau = 0.44$ till the end (670nm). For this reason, A_{670} was plotted against ratio. The appearance of an isosbestic point at 842nm proves the reaction being consistent. Again, a $Fe(tpy)^{2+}$ peak can be observed, but emerges because this time, the contaminated ligand is being added to the copper solution, thus accumulating iron in the cuvette. This contamination was hard to avoid because of the syringe used for titration consisting of steel and the very high complexation constant of iron and terpyridine.

The absorbance linearly increases during the progress of complex formation and remains nearly constant after equimolarity is reached.

The results indicate that the influence of the peptide chain attached to the ligand completely prevents the formation of a bivalent complex. As a result, the effect mentioned above should have no influence on the copper binding behaviour of PNA conjugates. This strongly favours the tpy*-OH ligand **3.5** for its incorporation into PNA oligomers.

Titration of bpa*-OH **3.6** with Cu(II)

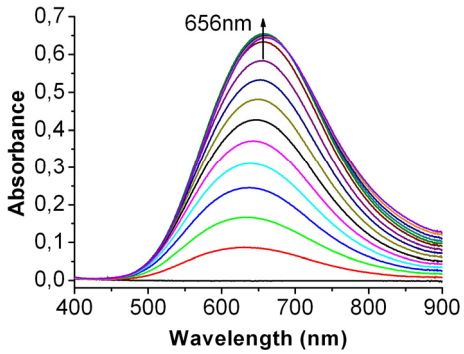

Fig. 3.41: *Absorbance Curves during the in situ-preparation of* ***3.6***$_{Cu}$

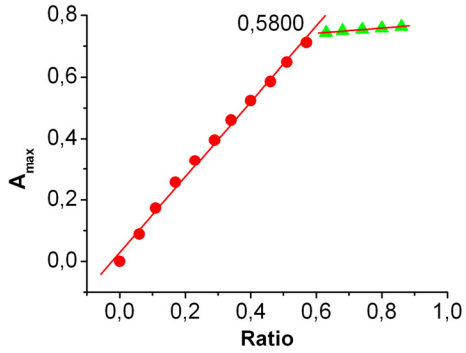

Fig. 3.42: *Plot of the Absorbance at Maximum against the Ratio Cu^{2+}:* ***3.6***

The curves show a bathochromic shift from 632nm at the beginning to 656nm at the point of equivalence (final maximum of the complex). Plotting A_{max} or A_{656} against τ does not make any difference. The absorbance linearly increases up to $\tau = 1$ and remains constant after that. Adding more equivalents of titrant to the solution (tested up to $\tau = 2$) did not reveal any changes. The formation of a bivalent complex $\mathbf{(3.6)_{2Cu}}$ seems to be obvious.

Titration of bpa*-pnt **3.13** with Cu(II)

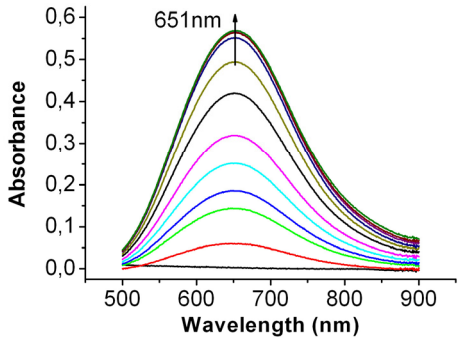

Fig. 3.43: *Absorbance Curves during the in situ-preparation of* ***3.13*** $_{Cu}$

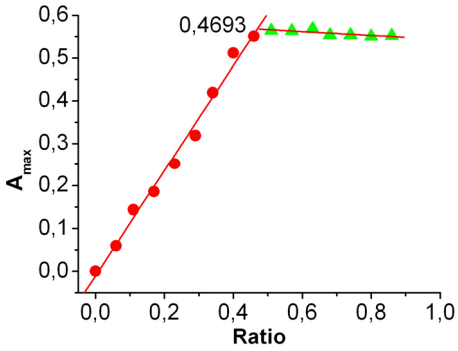

Fig. 3.44: *Plot of the Absorbance at Maximum against the Ratio* Cu^{2+}*:****3.13***

The maxima of the curves were determined to be at nearly the same wavelength; no significant shift was observed (average maximum: 651nm). As a consequence, A_{max} was plotted against τ (Fig. 3.44). Similar to the case of **3.6**, the increase of absorbance stops at a Cu^{2+}:**3.13** ratio of 0.5. Adding more equivalents of titrant to the solution (tested up to τ = 2) did not reveal any changes. Apparently, the peptide chain of the bioconjugate **3.13** does not prevent a second equivalent of ligand from binding to the metal center.

3.5.2.2 Discussion

The titration of the free ligands tpy*-OH **3.5** and bpa*-OH **3.6** exposed a dominant difference in their metal binding behaviour. An overview of the data obtained from the experiments is given in Tab. 1.1.

Tab. 3.4: *Points of Equivalence – Overview (Absorbance Maxima in Brackets)*

	Ratio Cu^{2+}/L (λ_{max}/nm)	**Ratio L/Cu^{2+} (λ_{max}/nm)**
Hex-pnt 3.11	not observed	not observed
tpy*-OH 3.5[e]	0.47 (694) / 0.98 (680)	0.96 (679) / 1.92 (692)
tpy*-pnt 3.12	1.02 (667)	0.99 (670)
bpa*-OH 3.6[f]	0.58 (656)	/
bpa*-pnt 3.13	0.47 (651)	/

The free terpyridine ligand **3.5** was suspected to form a 2:1 complex with copper which was broken up again with addition of further metal indicating reversible complexation equilibria. In the converse experiment (titration of Cu with added ligand), the $Cu(tpy)_2^{2+}$ complex did not start to build until every copper was bound monovalently.

The presence of two different species can be observed by a hypsochromic shift in the first case (694nm→680nm/-14nm) and a bathochromic shift in the second case (679nm→692nm/+13nm).

In the following, general insights into structural details of terpyridine will be presented and pulled together with the results obtained in this Chapter.

Terpyridine is typically depicted in the *cis*/*cis* conformation with regard to the dihedral angle of the N-C-C-N bonds in order to emphasize its ability to act as a chelating ligand (Fig. 3.45). However, it has to be kept in mind that the solid state conformation of the uncomplexed and unprotonated form is *trans*/*trans*, which is explained by the steric repulsion of the *ortho*-hydrogen atoms (3/3’ and 5’/3’’) in combination with an electro-

[e] Solvent: DMF
[f] Solvent: MeOH

static repulsion of the three nitrogen lone pairs. The steric effect can be seen in the space-filling model in Fig. 3.45.

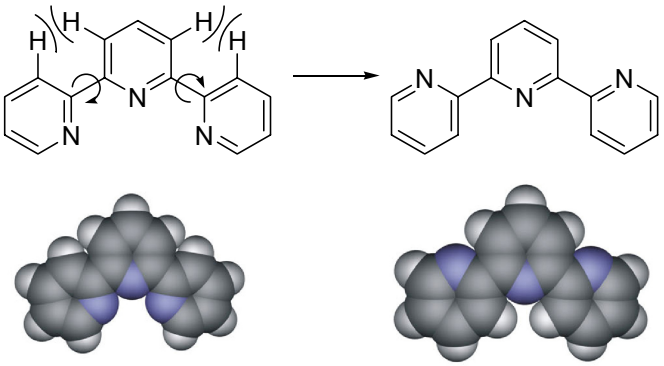

Fig. 3.45: *Scheme and Molecular Model of the tpy Ligand in the* cis/cis *(left) and the* trans/trans *(right) Conformation. Note the proximity of the 3/3' and 5'/5'' hydrogen atoms in the space-filled model of the* cis/cis *conformation*

Theoretical calculations[212] of different conformations also gave support for the *trans*/*trans* conformation as the energetically favoured one, and showed that the *cis*/*cis* conformation should be twisted with a dihedral angle of ca. 48°. The conformation of tpy in solution follows the same trend but is dependent on the hydrogen bonding properties of the solvent. In acidic media, stabilization of the *cis*/*cis* conformation can be achieved by protonation of one pyridine unit, which leads to a favourable hydrogen bonding between the proton and the lone pairs of the remaining free nitrogen atoms. The lowest energy structure is one with the central nitrogen protonated and the lateral pyridine units forming hydrogen bonds, which leads to the *cis*/*cis* conformation being energetically favoured (Fig. 3.46).[213]

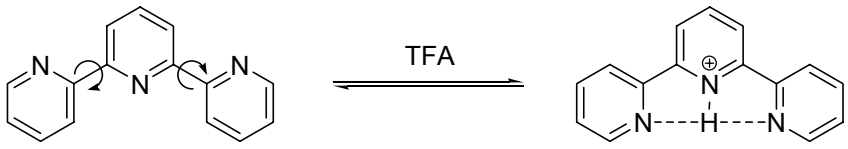

Fig. 3.46: *2,2':6',2''-Terpyridine in its Free and its Protonated Form*

In the decades after its discovery,[214, 215] tpy complexes with a large number of metal ions were studied.[216-219] Crystal structures revealed that there are two predominant complex types to be found, depending on the metal ion and on the stoichiometry applied in the crystallization process: a 2:1 complex showing a slightly distorted octahedral coordination with the two tpy units arranged perpendicular to each other, and a 1:1 complex with the metal ion coordinated in a distorted trigonal pyramidal way, the tpy coordinating the axial sites and one site in the trigonal plane, and the counter ions situated in the two residual planar positions. Fig. 3.47 shows both the 1:1 and the 2:1 complex. The distortion of the complex from its ideal structure can be seen clearly by the deviation of the axial N-M-N[g] bond from an ideal 180° angle.

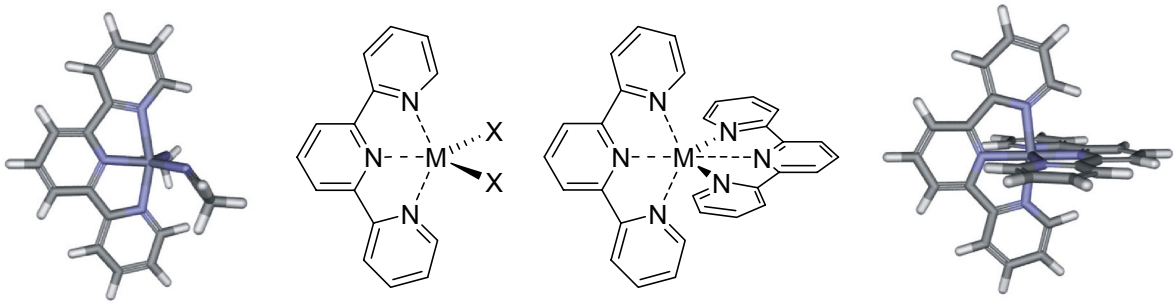

Fig. 3.47: *Schemes and Molecular Models of 1:1 (left) and 2:1 (right) tpy Complexes. The 1:1 complex is modelled with two acetonitrile molecules. X represents any counter ion or coordinating solvent molecule*

DMF, MeOH and H_2O were chosen as solvents for the titrations since they act as competitive ligands for the complexation which should lead to a decreased binding constant and additionally facilitate ligand exchange.

[g] Not to be mixed up with certain acronyms ! Characters, places and incidents in this thesis are fictitious. Any resemblance to actual events, locales or persons, living or dead, is entirely coincidental

The characteristic feature of the $Cu(tpy)_2^{2+}$ complex (Fig. 3.47) is the metal-ligand charge transfer (MLCT) band with a maximum at 694 nm, which is responsible for its blue to green colour, whereas the monovalent terpyridine complex shows an absorbance maximum at 680nm.

The plots of λ_{max} against τ show significant changes indicating the presence of these two different species. Due to the different ε values of the particular complexes, the absorbance of the solution changes during the progress of the titration, as well, signifying the re-detachment of the second ligand ($\tau > 0.5$; titration of **3.5** with Cu^{2+}) and its additional binding ($\tau > 1.0$; titration of Cu^{2+} with **3.5**), respectively. Possible mechanisms for this observation are shown in Fig. 3.48 and Fig. 3.49.

In the first case, the slope of the A vs. τ curve rapidly changes when the second half-equivalent of Cu is started to be added. This second process stops immediately when 1:1 stoichiometry is reached, indicating the smooth formation of a 1:1 complex.

$M(tpy)^{2+}$ and $M(tpy)_2^{2+}$ cannot be distinguished but based on the change of slope at a ratio of 0.5 it can be concluded that from that point on, all added metal ions and 1:2 complexes are directly converted to $M(tpy)^{2+}$ up to a ratio of 1.0.

During the titration of Cu(II) with **3.5**, the absorbance rises straight proportionally with the amount of added ligand **3.5**. All titrations show very clear isosbestic points suggesting that only two species (the uncomplexed **3.5** and $\mathbf{3.5_{Cu}}$) are present during the titration process. After equimolarity is reached, the absorbance decreases again with a concomitant bathochromic shift, indicating the formation of the bivalent complex.

The fact that the spectra of $Cu(tpy)_2^{2+}$ and $Cu(tpy)^{2+}$ are not identical suggests two different terpyridine coordination modes in the two species. In the case of a similar binding of the second ligand, the absorbance maximum should remain constant without any hypso- or bathochromic shift, whereas the extinction coefficient would be expected to change because of the doubled number of chromophores per metal center.

It can be concluded that the second ligand does not bind to copper as firmly as the first one, which might be explainable by the Jahn-Teller distortion caused by the first ligand which prevents the second one from binding as a tridentate. This leads to a *cis/trans* conformation for the second tpy, making it act as a bidentate ligand like 2,2'-bipyridine. In fact, *Merbach et al.*[220] substantiated this suggestion by kinetic measurements, which was confirmed by ΔH^0 determinations carried out by *Würthner et al.*[221] Furthermore, it is common knowledge since the early eighties (but only for coordination chemists) that especially Cu^{2+} can strike an unusual five-coordination caused by a second-order Jahn-Teller effect.[222, 223]

As a consequence, the complexation constant of the second tpy is significantly lower than that of the 1:1 complex which enables $Cu(tpy)_2^{2+}$ to break up again (Fig. 3.48) in favour of the formation of $Cu(tpy)^{2+}$. In the case of a reverse titration, a second ligand is able to bind additionally, causing a spectral change at higher ligand/metal ratios than 1:1 (Fig. 3.49).

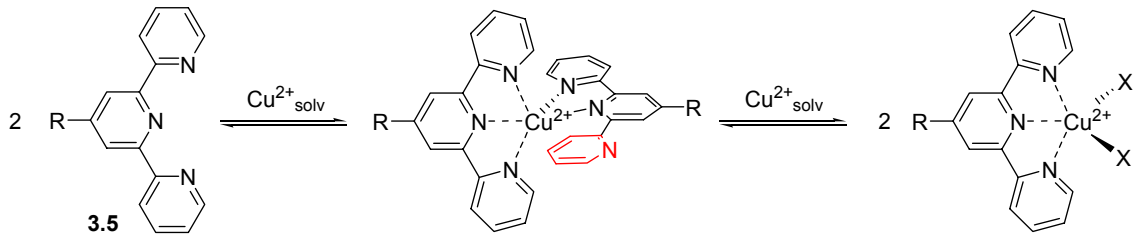

Fig. 3.48: *Supposed Mechanism for the Titration of* ***3.5*** *with* Cu^{2+}

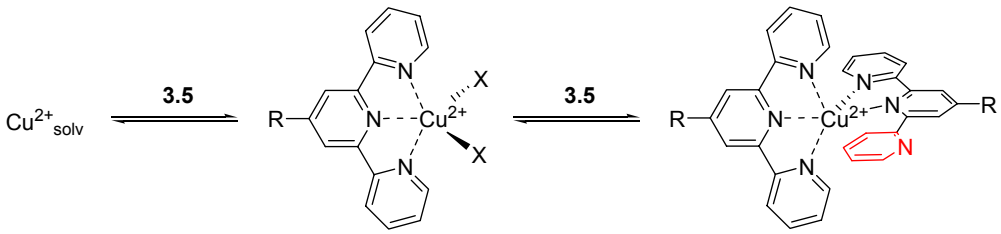

Fig. 3.49: *Supposed Mechanism for the Titration of* Cu^{2+} *with* ***3.5***

These results were not observed with the tpy*-pnt conjugate **3.12**, indicating a proper 1:1 complexation during the progress of the titration which did not show any species present except a monovalent complex. The presence of an isosbestic point even after exceeding equimolarity substantiates this observation, so it can be concluded that the peptide chain is bulky enough to prevent a second ligand from binding to the metal center. In the case of a PNA-conjugate, it can be expected that the similar effect will take place, so that no dimer formation during hybridization has to be worried about.

In contrast to that, bpa*-OH **3.6** as a free ligand as well as a bioconjugate formed a 2:1 complex with copper which was not able to break up again.

All curves showed the formation of a stable complex at a metal/ligand ratio of 0.5.

Those results were shown to be reproducible by repeating the experiments with fresh stock solutions and disagree with X-ray structures obtained in our group from the free ligand copper complexes.[106] In the solid state, Cu is obviously complexed by only one ligand molecule, maybe due to the coordinating assistance of nitrates or solvent molecules. Mass spectra, as mentioned in the previous chapter, show the monovalent complex, but the existence of ML_2 species was not investigated for bpa. The formation of dimers also can be taken into consideration.

A valid explanation for the different behaviour of bpa could be its flexibility in contrast to tpy which allows it to adapt to the distorted ligand field caused by a primarily bound ligand. Thus, the second binding constant is high enough to prevent further copper ions from displacing the second ligand (Fig. 3.50) and even high enough to rule out the sterical influence of the peptide chain. In fact, the octahedral conformation of bivalent $Cu(bpa)_2^{2+}$ complexes is known from literature.[224, 225]

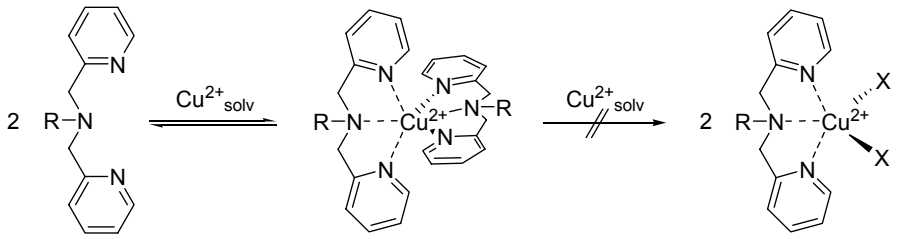

Fig. 3.50: *The Complexation of Cu^{2+} with bpa*-OH **3.6** Stops at a Ratio of 1:2*

3.6 Summary

In this Chapter, several functionalized ligands were synthesized and characterized.
The hexanoic acid derivative of terpyridine **3.5** and the bpa ligand **3.6** were successfully coupled to phenylalanine methyl ester and therefore shown to be suitable for SPPS. All ligands and their phenylalanine conjugates were obtained in good yield and high purity, which was confirmed by NMR and MS methods. Aminophenanthroline turned out to defy functionalization and therefore was decided not to be useful for a peptide-based artificial nuclease design. Nevertheless, an attempt to couple aminophenanthroline **3.8** to a PNA chain will be described in Chapter 5.5.3.

Conjugates of the ligands with the peptide pseudoneurotensin (pnt) were synthesized and characterized.

In order to examine the copper binding ability of the synthesized ligands and their conjugates, the particular complexes were either prepared in solution or isolated by crystallization. The complexes were characterized by ESI and FAB mass spectra

UV-Vis-titration with Cu(II) was performed on the free ligands and on the corresponding conjugates. The experiment with a ligand-free pnt derivative revealed that the side chains of the neuropeptide are not involved into metal binding, and the copper ion is expected to be bound by the chelating ligands, exclusively. In the case of tpy*-OH **3.5**, the formation of a bivalent complex, comprising two ligand molecules and one copper center, was observed. The attachment of this ligand to pnt prevented the binding of a second ligand because of the bulky peptide chain. bpa ligands turned out to form bivalent complexes, exclusively, in their free form as well as in the form of peptide conjugates.

The results presented in this chapter lead to the conclusion that terpyridine is the most favoured ligand to be incorporated into a PNA SPS.

4 Peptide Nucleic Acids – Monomer Synthesis

4.1 Introduction

The assembly of PNA oligomers by solid phase synthesis, as explained in the Introduction, normally is conceived with acid labile side chain protecting groups. In the context of the final deprotection from the solid support with TFA, this orthogonal protection is abolished. Fmoc deprotection during the synthesis is performed with piperidine.
The major motivation for designing a base labile side chain protection concept was the challenge of attaching acid labile moieties to PNA, such as ferrocene, which are not resistant to TFA. Only PNA monomers with acid labile side chain protection are commercially available, so that the monomers for this purpose have to be synthesized.

Another difference between the basic cleavage strategy in contrast to the TFA method is that the hydrazide of the oligomer is obtained, whereas the acidic cleavage results in formation of the amide.

The first synthesis of PNA was described by *Nielsen et al.* using the Merrifield solid phase synthesis protocols and therefore a Boc/Z protection group scheme.[226, 227] Since then many different protection strategies have been introduced, basically to circumvent the harsh Merrifield conditions and to make the PNA synthesis compatible to oligonucleotide synthesis.[228-232] The improved monomer synthesis described here is based on the work of *Kovacs et al.*,[233] who uses an Fmoc/acyl protection scheme. For this reason, the particular steps will not be discussed in detail in this Chapter; details are to be found in the Experimental Part.

4.2 Synthesis of PNA Backbone

The synthesis of the PNA backbone **4.2** was carried out in two steps: ethylenediamine was substituted with *t*-butyl-bromo acetate, followed by *N*-terminal protection with Fmoc succinimide (Fig. 4.1). The resulting white and crystalline product was obtained as its hydrochloride salt and had to be deprotonated before the coupling of the particular nucleobases.

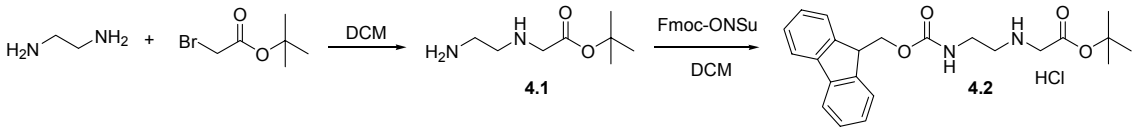

Fig. 4.1: *Synthesis of PNA Backbone* ***4.2***

4.3 Synthesis of Thymine Monomer

Because of thymine lacking reactive side chains, no orthogonal protection had to be performed, so that the acetic acid linker could be directly attached to the nucleobase, followed by coupling to the backbone **4.2** and cleavage of the *t*-butyl ester (Fig. 4.2). Dissolving in THF and precipitation from hexane:toluene yielded a very pure product.

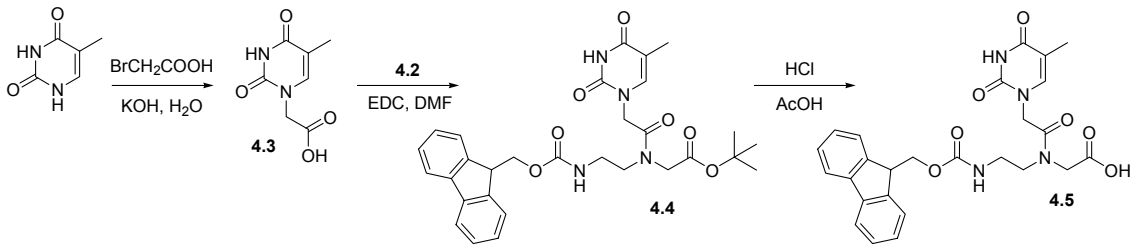

Fig. 4.2: *Synthesis of Thymine Monomer* ***4.5***

4.4 Synthesis of Cytosine Monomer

First attempts to protect the amino side chain of cytosine made use of anisoyl chloride (Fig. 4.3). The free acid **4.8** could be obtained in good yield and purity, but turned out to be very poorly soluble in DMF and therefore not suitable for its coupling to the backbone.

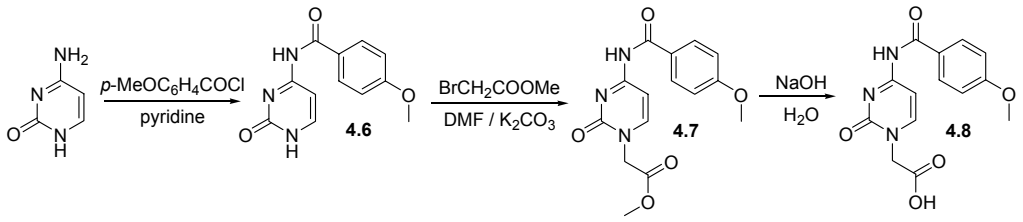

Fig. 4.3: *Synthesis of Cytosine Acetic Acid **4.8***

For that reason, a different protection strategy had to be established, comprising the 4-*t*-butylbenzoyl group as an amino substituent (Fig. 4.4).

After protection of the side chain, acetic acid methylester was attached to the aromatic amine, followed by saponification to yield the free acetic acid derivative **4.11**. Coupling to the backbone was carried out in DMF with TBTU/HOBt and DIPEA as a base, and the *t*-butylester of **4.12** was cleaved with TFA.

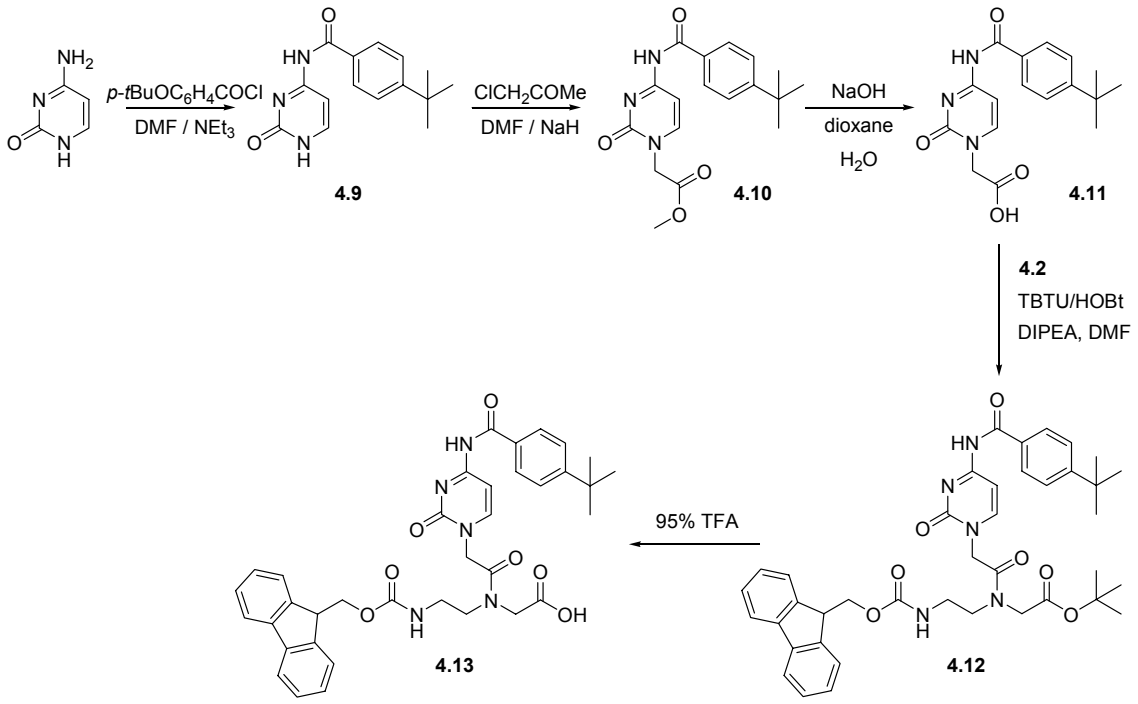

Fig. 4.4: *Synthesis of Cytosine Monomer **4.13***

4.5 Synthesis of Adenine Monomer

Early experiments for the synthesis of adenine PNA monomers comprised the protection of its side chain with anisoyl chloride and the coupling of acetic acid methylester (Fig. 4.5). The two emerging isomers **4.15a** and **4.15b** were separated by column chromatography, but resisted from being purified by recrystallization which is indispensable for providing satisfactory quantities.

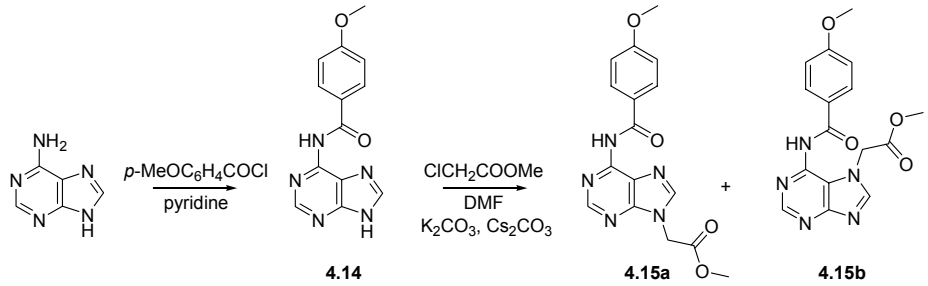

Fig. 4.5: *Synthesis of Adenine-Acetic Acid Methyl Ester* ***4.15a***

Because of that, the strategy was changed in favour of the use of acetic acid *t*-butyl ester instead of its methyl ester (Fig. 4.6). The resulting isomers **4.16a** and **4.16b** were separated by column chromatography, and dissolution experiments revealed that **4.16a** could be easily separated by recrystallization from ethyl acetate.

The *t*-butyl ester of **4.16a** was cleaved with TFA, followed by coupling to the backbone and saponification, yielding the adenine monomer **4.19** in quantitative yield.

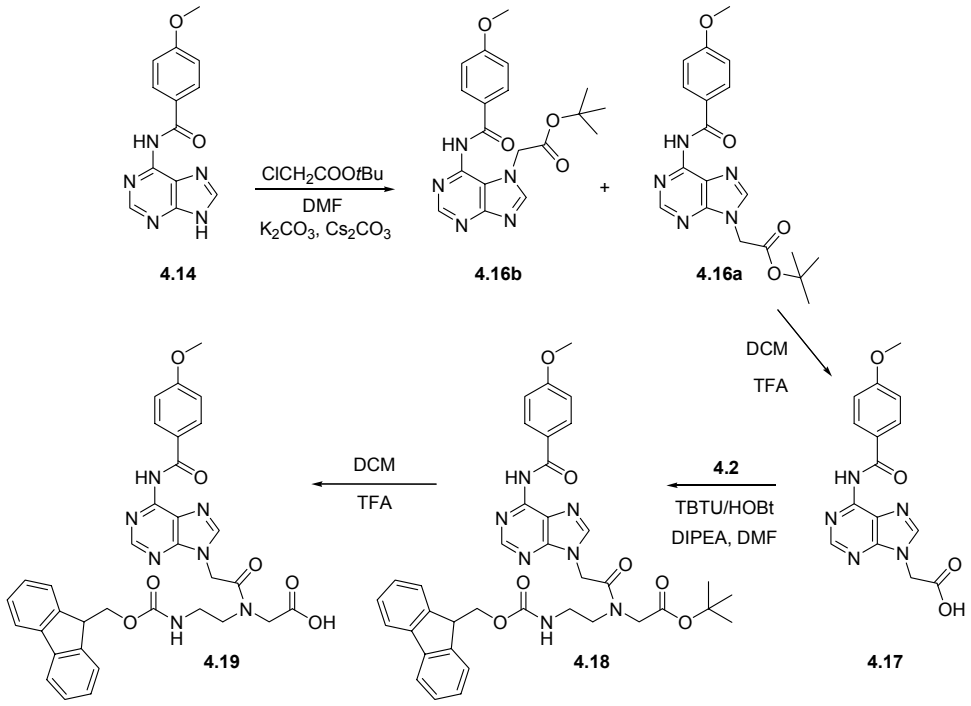

Fig. 4.6: *Synthesis of Adenine Monomer* ***4.19***

4.6 Synthesis of Guanine Monomer

The synthesis of guanine PNA turned out to be the most difficult one, because guanine possesses two reactive side chains. The exocyclic amino function of guanine was protected by an acetyl group. The diphenylcarbamoylation of the O^6 position ensures the regioselective coupling[234] of methyl bromoacetate in the next step. Both protection groups are readily removed under the basic conditions of the final oligomer cleavage from the resin. Acetylation with methyl bromoacetate, followed by the removal of the methyl ester, coupling to the backbone and *t*-Bu-ester cleavage yielded two products. This was revealed by FAB-MS, showing that the majority of the carbamoyl protecting groups must have been lost. This fact should not influence the oligomer synthesis, so that the monomer was used as it was without worry.

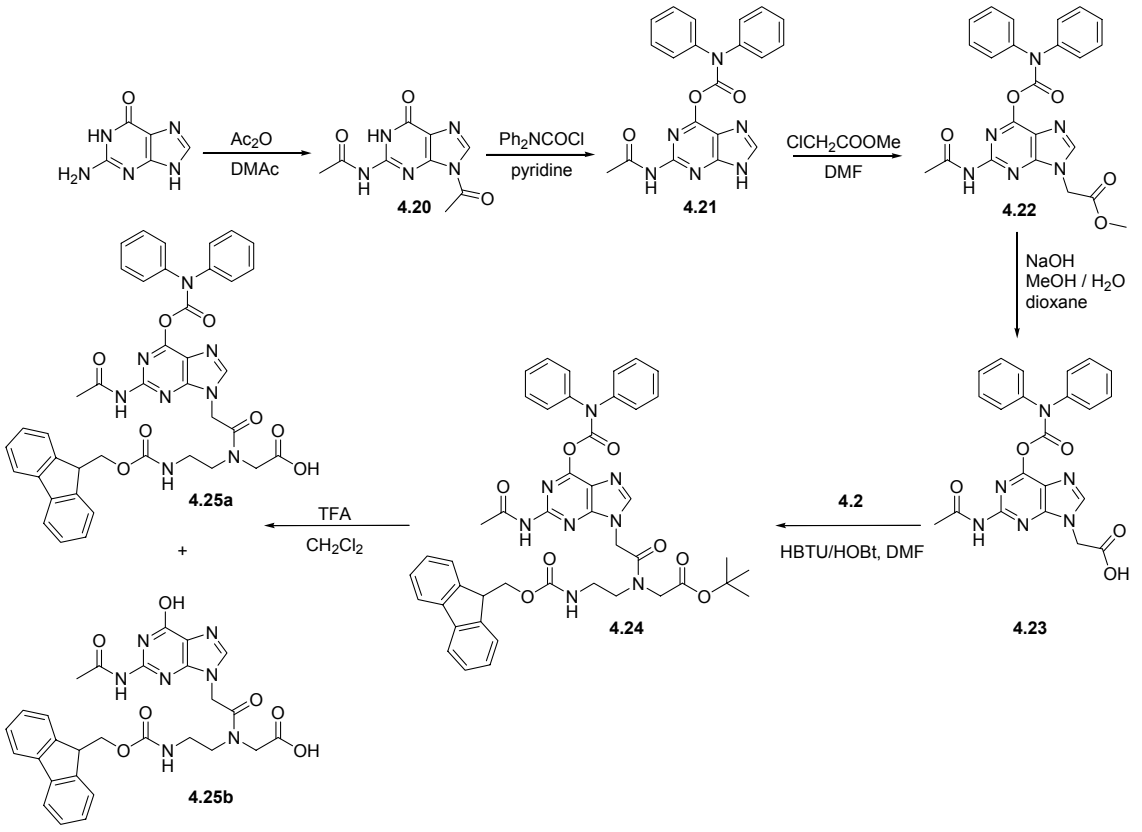

Fig. 4.7: *Synthesis of Guanine Monomer* ***4.25***

4.7 Synthesis of PNA Oligomers with Base Labile Protecting Groups

In order to prove the feasibility of the monomers for oligomer synthesis, the random sequence **4.26** was prepared by SPPS according to the standard procedure (see succeeding Chapter and Experimental Part), using TentaGel® S HMB-Lys(ivDde)Fmoc resin with a base labile resin linker (Fig. 4.8).[h] Cleavage was performed with 5% hydrazine in DMF for 1h, followed by filtration and removal of the volatiles. The workup was similar to the standard procedure.

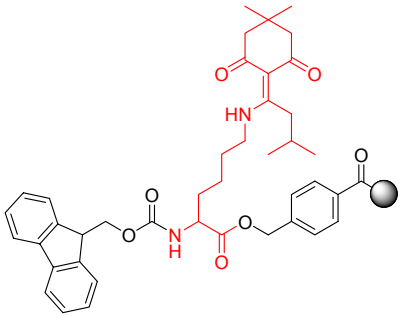

Fig. 4.8: *TentaGel® S HMB-Lys(ivDde)Fmoc*

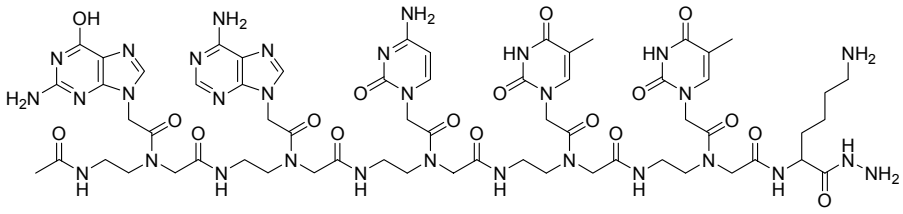

Fig. 4.9: *Ac-agctt-Lys-NHNH$_2$* ***4.26***

[h] ivDde (*N*-α-Fmoc-*N*-ε-1-(4,4-dimethyl-2,6-dioxocyclohex-1-ylidene)-3-methylbutyl-L-lysine) is more stable to piperidine than Dde and less prone to migrate from protected to unprotected lysine side chains

HPLC purification afforded the PNA oligomer as a white solid, and MALDI-TOF mass spectrometry showed a single product peak at m/z = 1553.2 (calc: 1552.7).

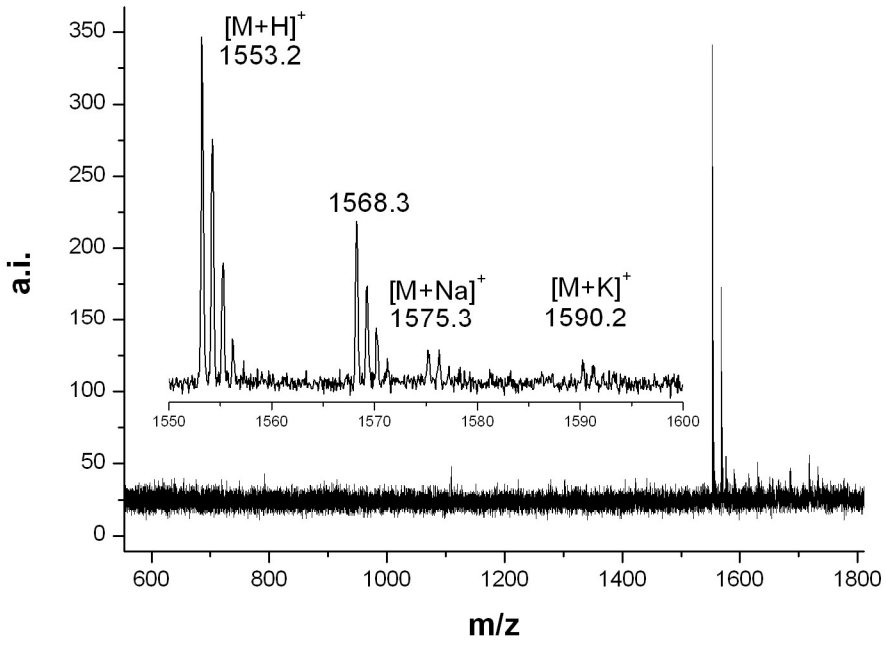

Fig. 4.10: *MALDI Spectrum of* ***4.26***

4.8 Summary

The synthesis of PNA monomers with base labile side-chain protecting groups was of importance in terms of establishing a system which allows the attachment of acid-sensitive moieties to PNA oligomers. Otherwise, those would be degraded during TFA cleavage from the resin. In this project, PNA monomers with all four nucleobases could be synthesized and fully characterized in high purity. The resistance of the side chain protecting groups towards Fmoc-deprotection with piperidine and their removal with hydrazine showed the usability of this system. An unfunctionalized PNA oligomer was assembled and characterized by MALDI-TOF spectrometry.

One major application of PNA monomers with base labile protecting groups was developed in our group by *Maurer et al.*,[235] who attached an acid labile ferrocene moiety to the N-terminus of a PNA chain consisting of the monomers described in this Chapter.

5 Peptide Nucleic Acids – Oligomer Synthesis

5.1 Introduction

In contrast to the base labile protected monomers presented in the previous Chapter, oligomer synthesis in this project was chosen to be based on commercially available PNA monomers with acid labile Bhoc side chain protection (Fig. 5.1). The thymine monomer was self-made and synthesized as described before, since it has no reactive side chains and therefore is suitable for both the base and the acid labile strategy.

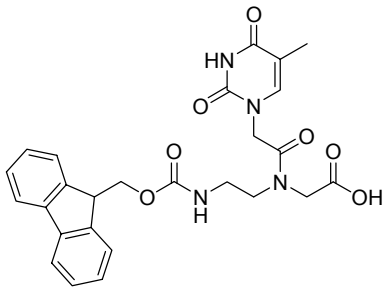

Thymine (Fmoc-T-OH)

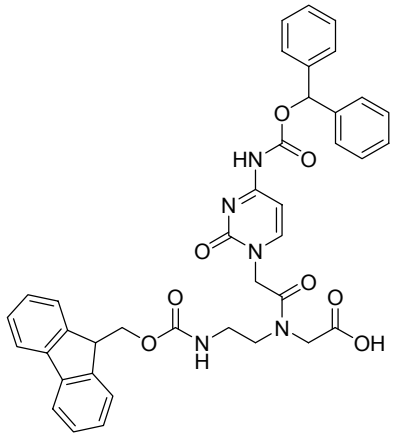

Cytosine (Fmoc-C(Bhoc)-OH)

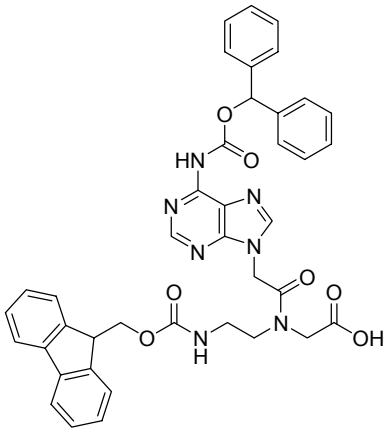

Adenine (Fmoc-A(Bhoc)-OH)

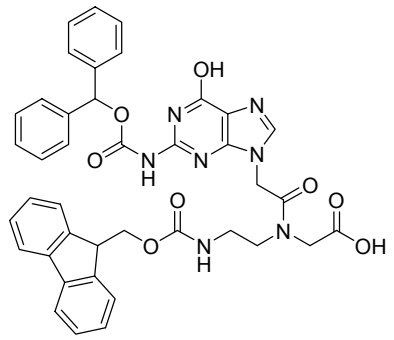

Guanine (Fmoc-G(Bhoc)-OH)

Fig. 5.1: *PNA Monomers with Acid Labile Side Chain Protecting Groups*

Solid Phase Synthesis was carried out in DMF, comprising HATU / DIPEA as coupling reagents. This procedure is described in detail in the Experimental Part.

The resin of choice was a TentaGel® R RAM-Lys(Boc)Fmoc resin provided by Rapp Polymers, Inc., preloaded with a Boc-protected lysine residue (0.17mmol/g), finalizing each PNA oligomer at the *C*-terminus for enhanced solubility. TentaGel® R is a resin designed for difficult sequences and long peptides showing an increased swelling volume. The RAM linker requires acidic cleavage with 95% TFA yielding the oligomer as its *C*-terminal amide. Fig. 5.3 shows the RAM linker immobilized on a resin bead, preloaded with orthogonally (Boc-/Fmoc-) protected lysine.

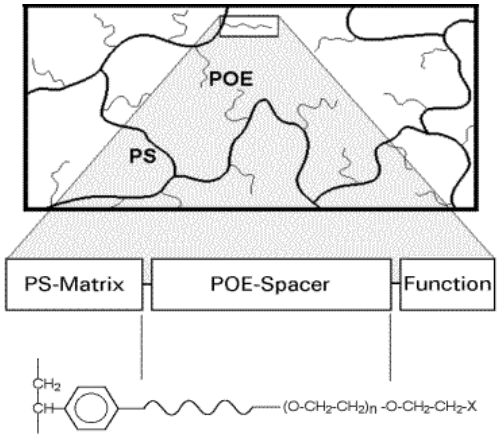

Fig. 5.2: *Chemical Architecture of TentaGel® Resins (PS=Polystyrene; POE=Poly(ortho)ester)*[236]

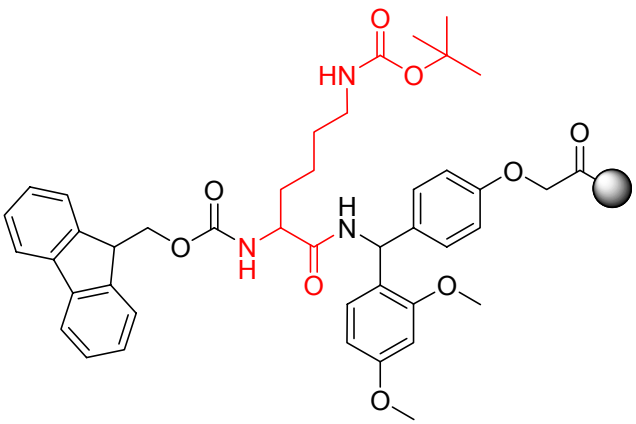

Fig. 5.3: *TentaGel® R RAM-Lys(Boc)Fmoc Resin (The "X" from Fig. 5.2 is shown here)*

The synthesis cycle performed in this Chapter is illustrated in Fig. 5.4.

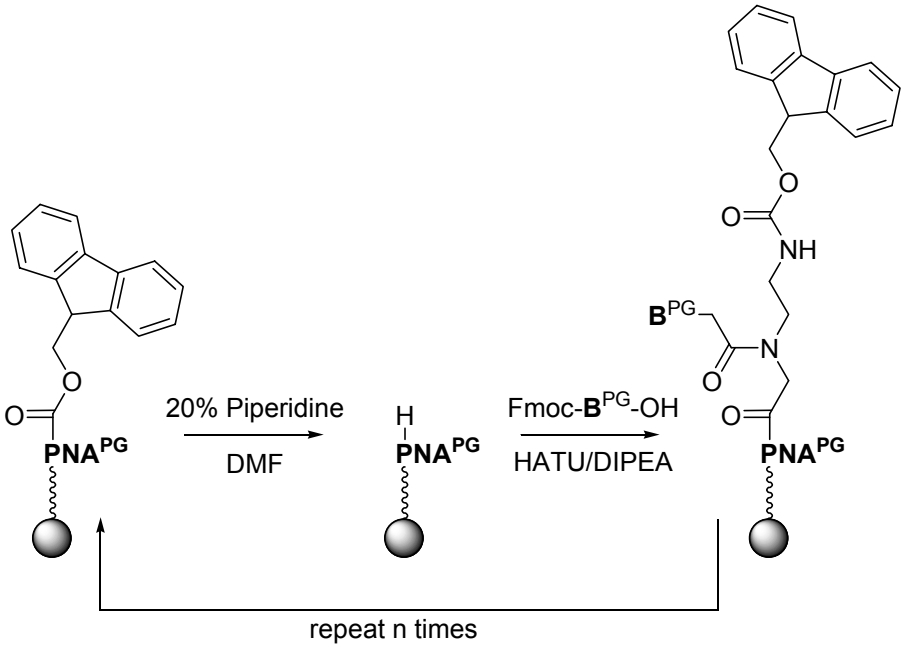

Fig. 5.4: *Elongation of a PNA chain (**B** = A, C, G, T)*

After *N*-terminal deprotection and acetylation (capping), the oligomers were both deprotected and freed from the solid support by treatment with TFA containing 2.5% water and 2.5% TIS. The use of TIS is required because the removal of the Bhoc protection produces benzhydryl cations (Ph_2CH^+), which are scavenged and otherwise would alkylate the electron rich aromatic rings of the nucleobases. All PNA oligomers were purified by reverse phase HPLC[237] and characterized by MALDI-TOF spectrometry.[238]

5.2 Choice of Sequences

As a model sequence for the investigation of the duplex binding of modified and unmodified PNAs, an 18bp sequence was chosen that is originally recognized by the site-specific homing endonuclease I-Sce I, encoded by a mitochondrial intron of *Saccharomyces cerevisiae*.[239, 240] Homing endonucleases allow the introduction of a single or several double-strand breaks into complex genomes.[241-243] They recognize long, 14-40bp sequences and are, therefore, extremely rare-cutting restriction enzymes.[244, 245] Statistically, an 18bp recognition site will occur once in $6.9 \cdot 10^{10}$bp, or once in every 20th human genome.[246] The investigation of this sequence originally was derived from a project of our group together with C. Happel and C. Klein, Hannover. This sequence is applicable for PNA synthesis, because no self-complementarity with more than 2 bases in a row and no hairpin formation are expected.
In order to mimic the sequence-specific cleavage carried out by I-Sce I, PNA oligomers with the same sequence recognized by this endonuclease were synthesized in the context of this Thesis.

I-Sce I recognition sequence:

5'- T A G G G A T A A | C A G G G T A A T -3'
3'- A T C C C | T A T T G T C C C A T T A -5'

For both the terminal and the central strategy of ligand attachment (Fig. 1.6), the cleavage moiety of the particular PNA scissors was intended to cleave at the same position. For that reason, different sections of the original sequence were chosen for synthesis (DNA sequences are always displayed in capital letters, PNA sequences in lower case letters; the cleavage / modification site is red-coloured):

5'- T A G G G A T A A C A G G G T A A T -3'
5'- T A G G G A T A A C A G G G T A A T -3'
C/3'- a t c c c t a t t g t c c c a t t a -N/5'
C/3'- a t c c c t a t t g t c c c a t t a -N/5'

As a convention, all PNA sequences in this thesis from now on will be written from the *N*- to the *C*-terminus, according to their peptide character. Because of the *C*-terminus for the PNA being equivalent to the 3'-terminus of the DNA (anti-parallel hybridisation can be observed, but is not favoured),[149] the corresponding complementary PNA oligomers will all be part of the following sequence:

N/5'- a t t a c c c t g t t a t c c c t a -C/3'

In order to compare the influence of different chain lengths on the melting behaviour (i.e. hybridisation properties), each main type of sequence was prepared in three variations of length containing an acetyl capping group at the *N*-terminus and a lysine residue at the *C*-terminus in order to enhance solubility.[247]

The acidic cleavage from the TentaGel R RAM Lys resin yields the PNA oligomer as its *C*-terminal amide. For clarity, "Lys" is written in this chapter, actually standing for "Lys-NH_2" (i.e. lysine carboxamide) in correct notation.

terminal:

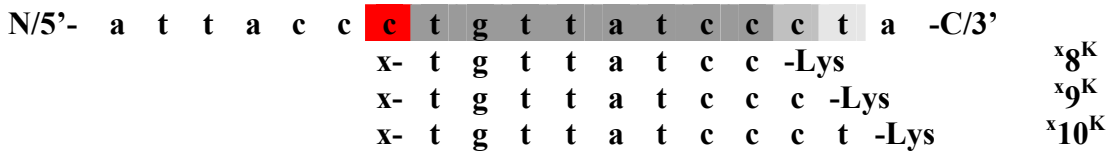

central:

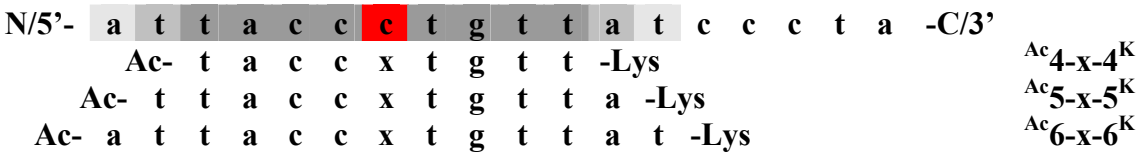

Another series of sequences was synthesized in order to obtain evidence about the influence of omitted monomers within the sequence on its melting behaviour compared to non-match, mismatch and amino acid-replaced sequences:

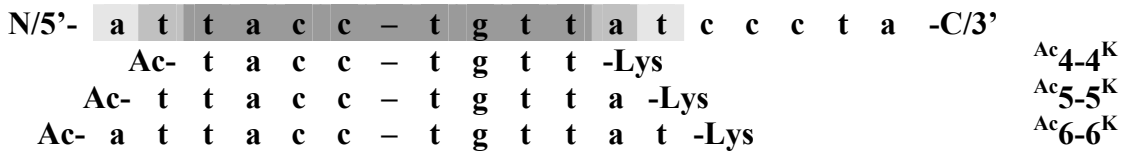

All other sequences and special modifications will be explained in the particular chapters.

5.3 Nomenclature

The naming of PNA oligomers is normally based on the standard peptide nomenclature. In this Thesis, abbreviations had to be found in order to obtain short oligomer names. The disadvantage of a mere numbering of compounds is the complete lack of information which would have to be looked up each time in order to know which sequence is talked about. This could be cinfusing especially for the discussion of melting curve data (Chapter 6).

In order to provide a short and definite naming of the compounds in this Chapter, the following conventions were made:

- Every sequence or part of a sequence contains will be represented by the number of nucleobases it consists of. Because of the use of only two main sequence types in this Thesis (see preceding Chapter), the numbers will be unambiguous.

- *N*- and *C*-termini of the sequences will be indexed by their substituent, so that confusion and mixing up with compounds in other Chapters can be excluded.

- Besides that, the substituents are written similar to peptide nomenclature, ignoring their special functionalization which is clear from the context. bpa' is written for bpa*-Ahx.

- Lysine residues at the *C*-terminus of the PNA oligomer are obtained as amides after cleavage. Nevertheless, "Lys" or simply "K" is written for that.

The DNA nomenclature (introduced in Chapter 6.3) will be analogous.

See Appendix for a complete list of sequences.

5.4 PNA Oligomers without Ligand

Unsubstituted PNA oligomers were synthesized in order to be able to compare their hybridisation behaviour with that of the PNA-ligand conjugates.

All sequences were prepared following the standard procedure described in the Experimental Part and finally acetylated at the *N*-terminus. The final cycle of SPPS is displayed in Fig. 5.5.

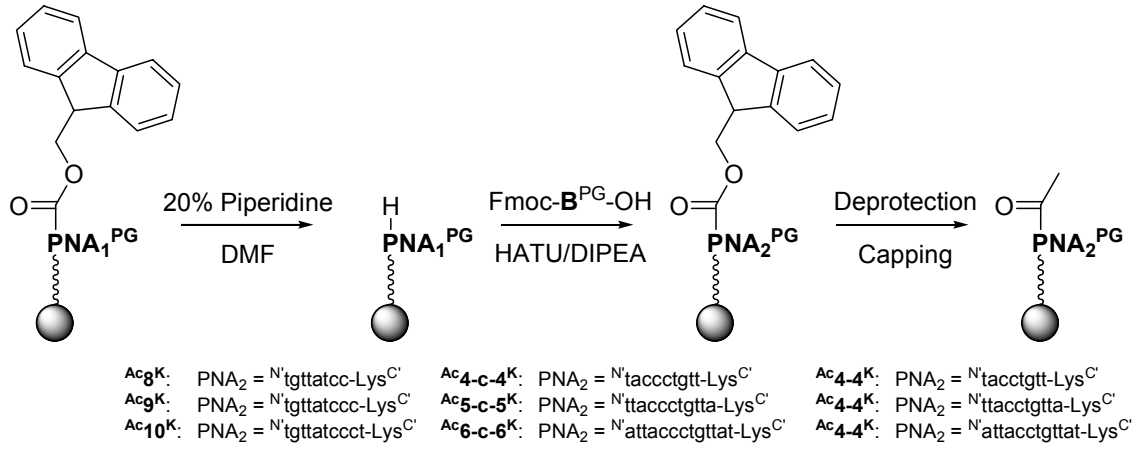

Fig. 5.5: *Elongation of a PNA Chain – Final Cycle*

The consecutive steps of the solid phase synthesis were monitored by MALDI-TOF spectrometry, which is shown exemplarily, considering spectra of the last two steps in the synthesis of compound $^{Ac}\mathbf{8}^{K}$ (Fig. 5.6, Fig. 5.7). The MALDI spectrum of the Fmoc-protected oligomer $^{Fmoc}\mathbf{8}^{K}$ shows many impurities. In most of the cases, this are capping products of intermediate steps, which was ignored when only monitoring was aimed at, as long as the final product was successfully purified by HPLC (Fig. 5.8).

An overview of all sequences is given at the end of this subchapter.

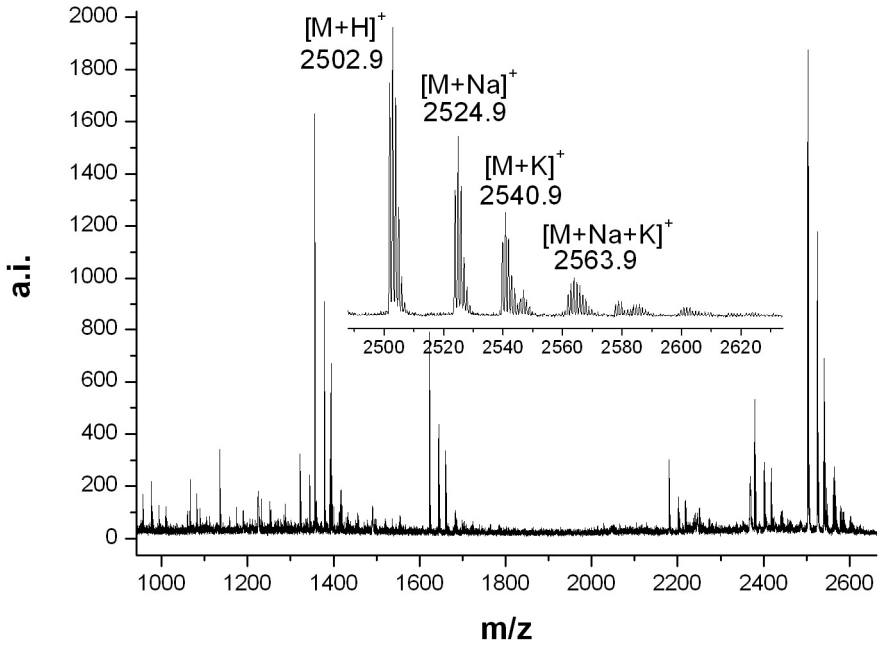

Fig. 5.6: *MALDI Spectrum of* $^{Fmoc}\mathbf{8}^{K}$ *(*M_{calc}*=2501.0)*

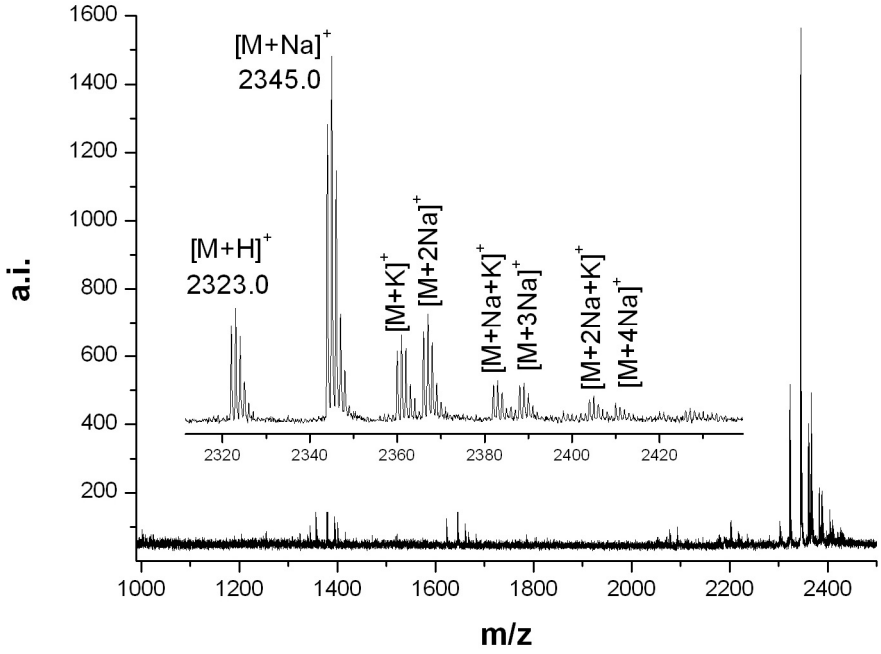

Fig. 5.7: *MALDI Spectrum of* $^{Ac}\mathbf{8}^{K}$ *after HPLC Purification*

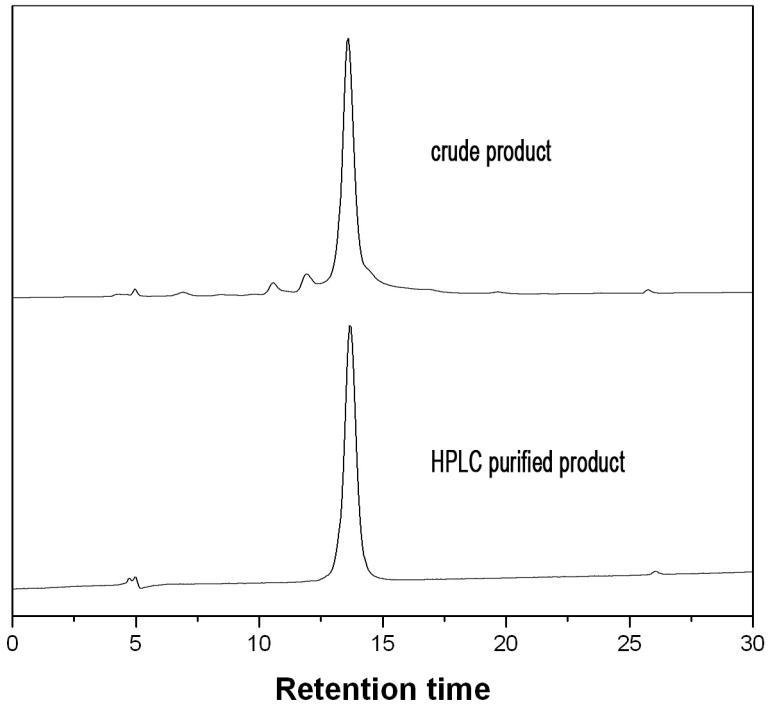

Fig. 5.8: *HPLC Chromatograms of* $^{Ac}8^{K}$***, the Crude Product Showing Capping Residues***

Tab. 5.1: *Sequences for Terminal Attachment of Ligands*

terminal		M_{calc}	M_{found}
Ac-tgttatcc-Lys	^{Ac}**8**^{K}	2321.0	2323.0
Ac-tgttatccc-Lys	^{Ac}**9**^{K}	2572.1	2573.2
Ac-tgttatccct-Lys	^{Ac}**10**^{K}	2838.2	2839.7

Tab. 5.2: *Sequences for Central Attachment of Ligands*

central		M_{calc}	M_{found}
Ac-taccctgtt-Lys	^{Ac}**4-c-4**^{K}	2572.1	2573.1
Ac-ttaccctgtta-Lys	^{Ac}**5-c-5**^{K}	3113.3	3115.1
Ac-attaccctgttat-Lys	^{Ac}**6-c-6**^{K}	3655.5	3654.9

Tab. 5.3: *Central Sequences with Cytosine Omitted*

central		M_{calc}	M_{found}
Ac-tacctgtt-Lys	^{Ac}**4-4**^{K}	2321.0	3221.7
Ac-ttacctgtta-Lys	^{Ac}**5-5**^{K}	2862.2	2863.1
Ac-attacctgttat-Lys	^{Ac}**6-6**^{K}	3404.4	3404.5

All oligomers were purified by semi-preparative reverse-phase HPLC and characterized by MALDI-TOF mass spectrometry.

5.5 PNA Oligomers with Terminal Ligand

The metal labelling of PNA is a very promising goal for the development of sequence-specific markers and biomolecular tools in general.

In our group, a transition metal complex was successfully coupled to the *N*-terminus of a thymine monomer (Fig. 5.9).[174, 248]

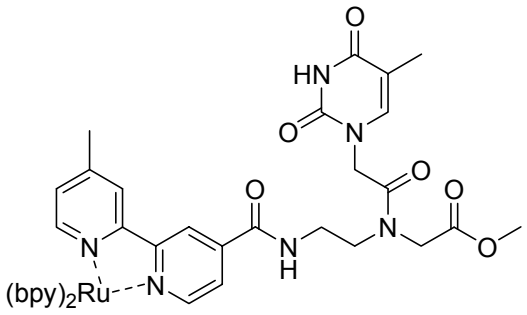

Fig. 5.9: *Ruthenium-Labelled Thymine PNA Monomer*

In this subchapter, the coupling of the ligands synthesized in Chapter 3 is described.

5.5.1 Terpyridine

The terpyridine ligand **3.5** was attached to the *N*-terminus of PNA oligomers by standard HATU/DIPEA coupling, but under slightly modified conditions (see Experimental Part). Fig. 5.10 illustrates this last step.

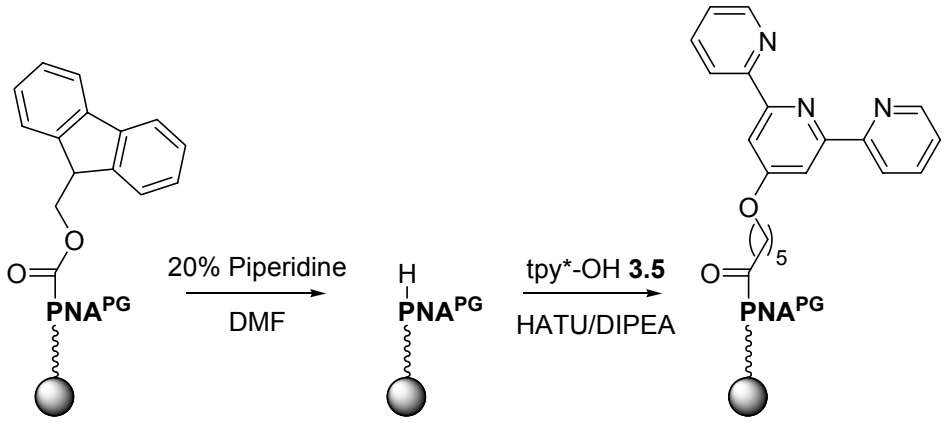

Fig. 5.10: *Final Attachment of **3.5** to the PNA Chain*

The coupling of **3.5** turned out to be quantitative under the optimized procedure. As an example, the MALDI spectrum of $^{tpy}\mathbf{8}^{K}$ is shown in Fig. 5.11.

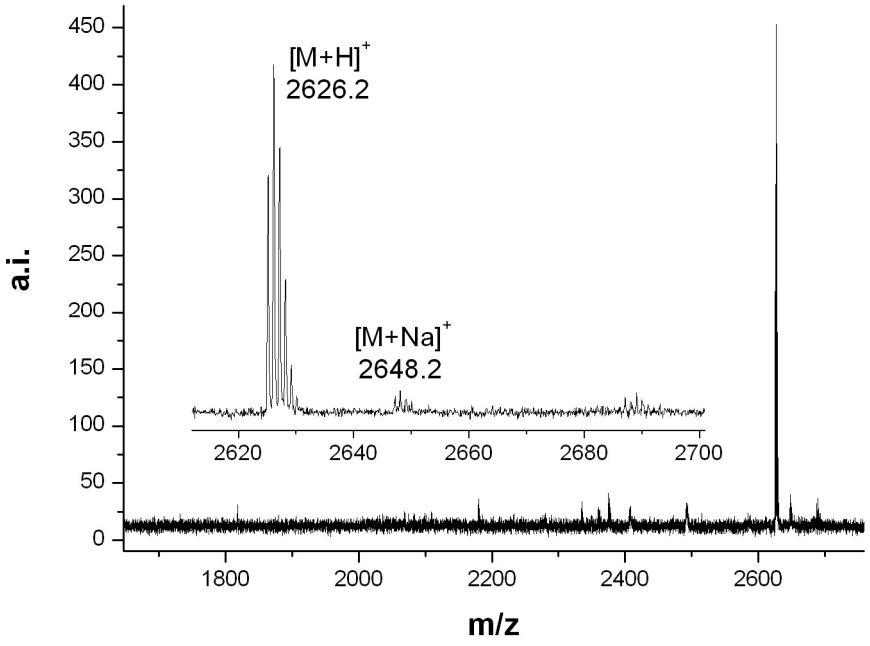

Fig. 5.11: *MALDI Spectrum of* $^{tpy}\mathbf{8}^{K}$

Similar to all other tpy-conjugates mentioned in this Thesis, iron peaks could be observed in every single case, but the contamination was completely removed after HPLC purification. Three different chain lengths with *N*-terminal terpyridine were prepared, as shown in Tab. 5.4.

Tab. 5.4: *Sequences for Terminal Attachment of tpy* **3.5***

terminal		$\mathbf{M_{calc}}$	$\mathbf{M_{found}}$
tpy*-tgttatcc-Lys	$^{tpy}\mathbf{8}^{K}$	2624.1	2626.2
tpy*-tgttatccc-Lys	$^{tpy}\mathbf{9}^{K}$	2875.2	2876.3
tpy*-tgttatccct-Lys	$^{tpy}\mathbf{10}^{K}$	3141.3	3143.5

5.5.2 Bis-Picolylamine

For a better comparison of the terminal bpa oligomer to the tpy derivative, an amino-hexanoic acid linker (Ahx) was introduced in order to adjust the chain length between PNA and ligand to that of the terpyridine compounds (Fig. 5.12).

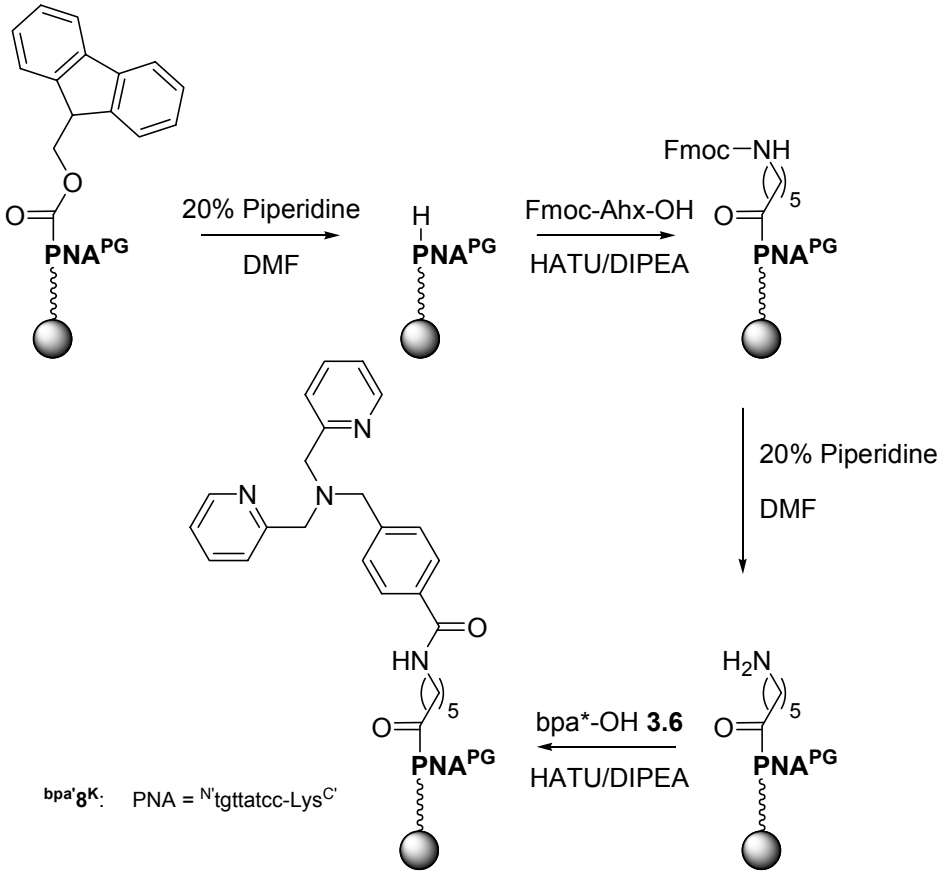

Fig. 5.12: *Attachment of the bpa-Ligand **3.6** to PNA via an Aminohexanoic Acid Linker (Ahx)*

Tab. 5.5: *Sequence for Terminal Attachment of bpa* **3.6***

terminal		M_{calc}	M_{found}
bpa*-Ahx-tgttatcc-Lys	$^{bpa'}\mathbf{8}^{K}$	2707.2	2709.0

5.5.3 Phenanthroline

In order to be able to attach amino-phenanthroline **3.8** to the *N*-terminus of the PNA chain, the latter one had to be converted into a C-terminus.

This was achieved by coupling adipic acid monomethylester (MeO-Ada-OH) to the amino end and subsequent saponification with 0.5% LiOH in DMF/dioxane. As a consequence, the activation had to occur on resin instead of in solution (Fig. 5.13).

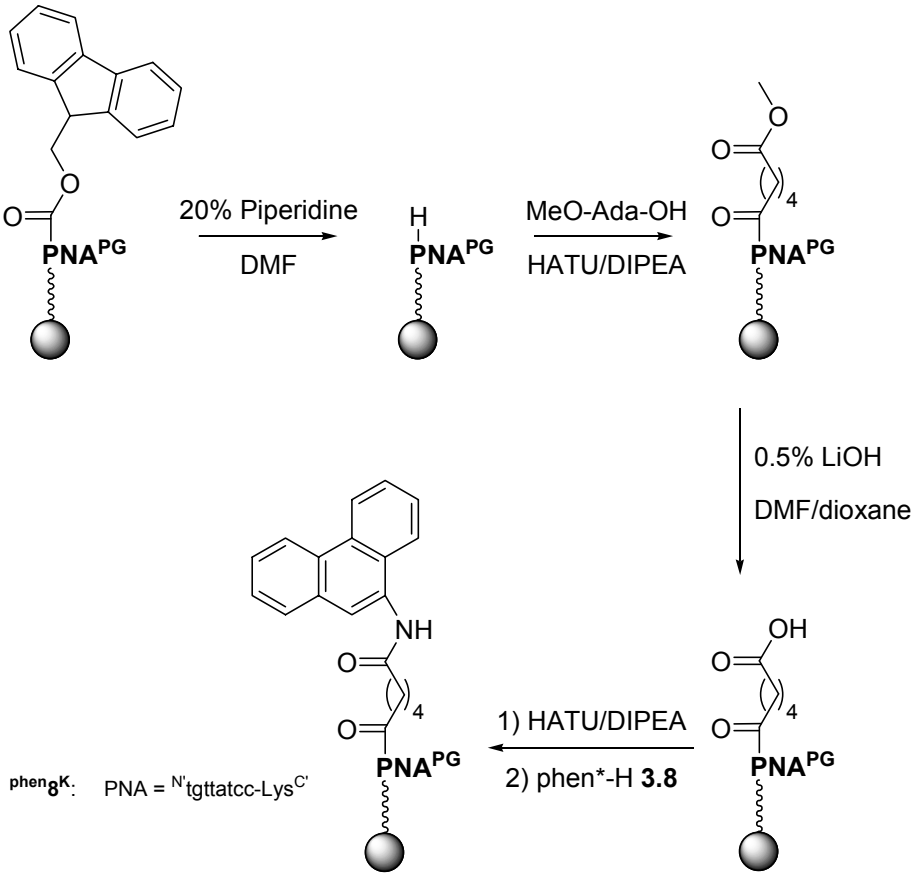

Fig. 5.13: *Attachment of phen*-H **3.8** to PNA via an Adipic Acid Linker (Ada)*

Both the linker coupling and its saponification were shown to be quantitative by MALDI spectroscopy (Fig. 5.14, Fig. 5.15).

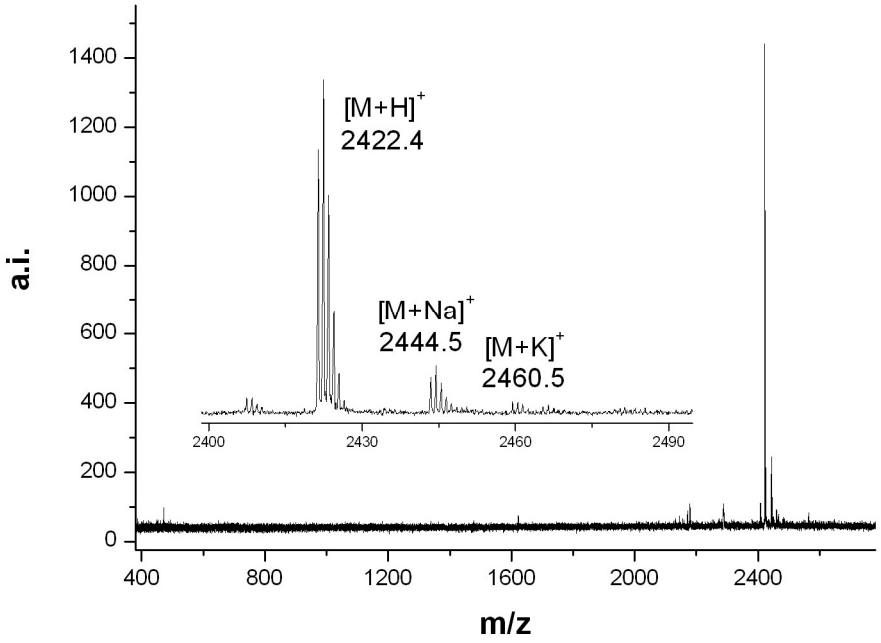

Fig. 5.14: *MALDI Spectrum of MeO-Ada-tgttatcc-Lys* $^{MeOAda}8^{K}$

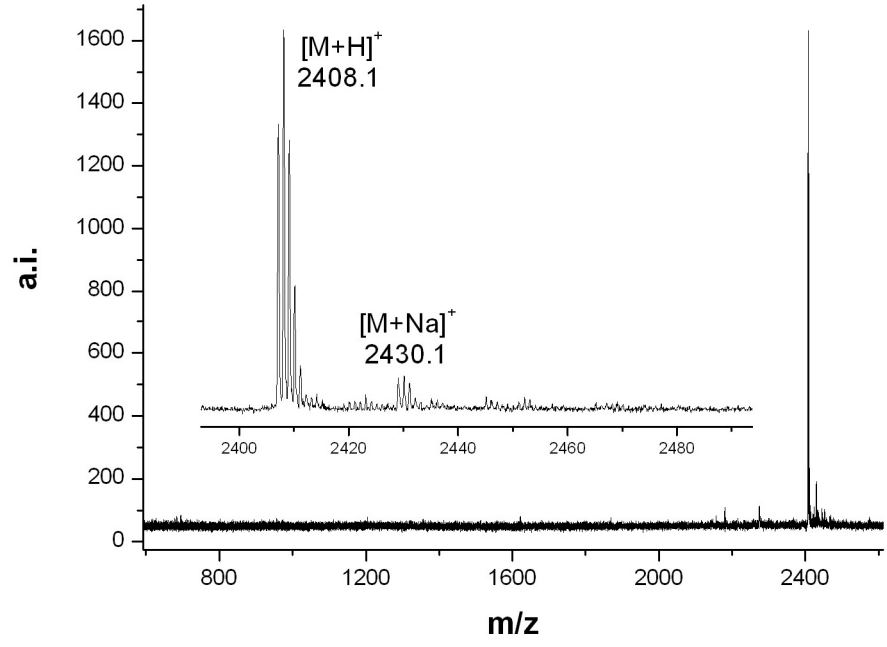

Fig. 5.15: *MALDI Spectrum of HO-Ada-tgttatcc-Lys* $^{HOAda}8^{K}$

The succeeding on-resin activation with HATU/DIPEA and the ligand coupling both were carried out overnight.

The MALDI spectrum of the expected phen*-conjugate only showed unreacted $^{HOAda}\mathbf{8}^{K}$.

Tab. 5.6: *Overview of Intermediates of the PNA Synthesis with Terminal phen*-Attachment*

terminal		$\mathbf{M}_{calc}$	$\mathbf{M}_{found}$
MeO-Ada-tgttatcc-Lys	$^{MeOAda}\mathbf{8}^{K}$	2421.0	2422.4
HO-Ada-tgttatcc-Lys	$^{HOAda}\mathbf{8}^{K}$	2407.0	2408.1
phen*-Ada-tgttatcc-Lys	$^{phen'}\mathbf{8}^{K}$	2485.1	/

These results lead to the conclusion that an on-resin activation of carboxyl residues on PNA is more difficult than expected. A change of activation / coupling time and/or the use of a different coupling reagent could remedy those deficiencies.

Nevertheless, a versatile method for converting the PNA amino terminus into a free carboxyl group was established, disclosing various possibilities for further derivatization.

5.6 PNA Oligomers with Central Ligand

As already mentioned in the Introduction, the development of artificial ribonucleases with their cleavage site being located in the center of the recognition sequence is very promising due to their assumed catalytic functionality. After cleavage, the PNA•Oligonucleotide duplex should reopen again, being ready for further turnovers (Fig. 5.16).[249]

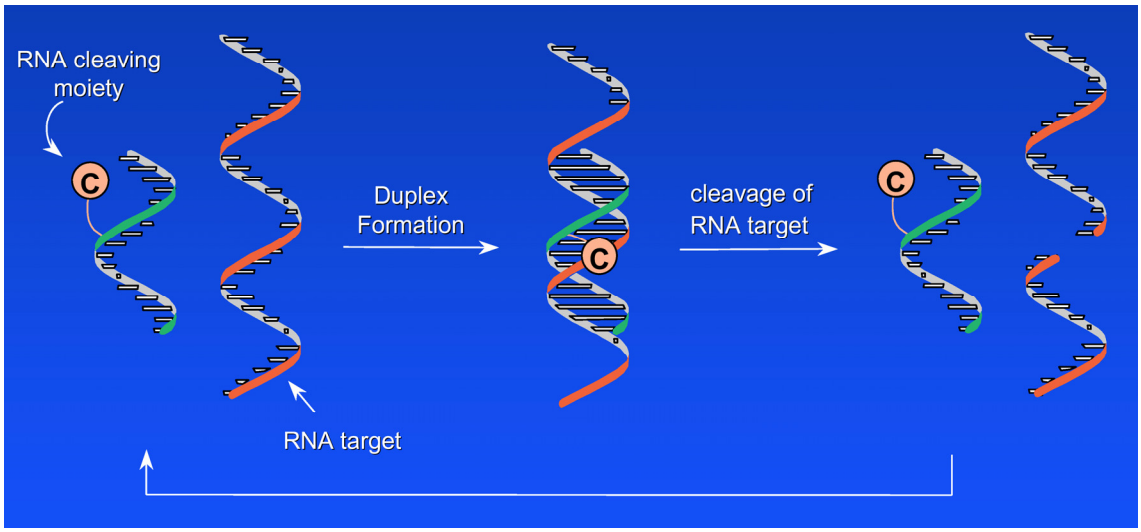

Fig. 5.16: *Catalytic Operation of an Artificial Nuclease with Central Cleaving Moiety*

Double-stranded RNA is considerably more resistant to metal ion promoted transesterification than its single-stranded counterpart.[250]

Häner et al. developed modified DNA oligonucleotides with a central europium complex (Fig. 5.17) which were able to cleave in the double strand region formed by the artificial nuclease and the RNA target.[251] Those catalysts were shown to cleave RNA only within a bulge[i] in the target strand.[252]

[i] A bulge is defined as a region of unpaired nucleobases within a double strand region forming a loop

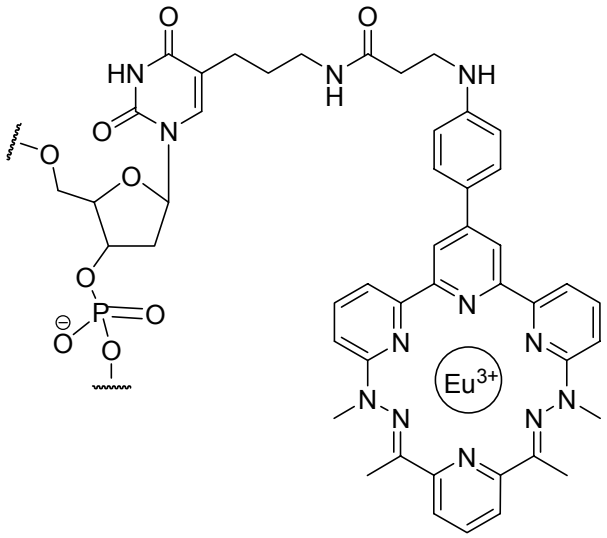

Fig. 5.17: *A Modified T-DNA Monomer with an RNA Cleaving Moiety*

According to the PNA sequences synthesized in the preceding chapters, central functionalization in this project was planned to be achieved by replacing the central cytosine with a cleaving moiety (Tab. 5.7).

Tab. 5.7: *Sequences for Central Replacement of a Cytosine by a Cleaving Unit* ***x***

central	
Ac-tacc**x**tgtt-Lys	^{Ac}**4-x-4**^{K}
Ac-ttacc**x**tgtta-Lys	^{Ac}**5-x-5**^{K}
Ac-attacc**x**tgttat-Lys	^{Ac}**6-x-6**^{K}

The most self-evident way of doing so is the development of an additional PNA monomer consisting of an Aeg-backbone derivative connected to a ligand instead of a nucleobase.

An example of a ligand-substituted PNA backbone was published by *Achim et al.*[253] and represents a further development of the metal-labelled PNA monomers synthesized in our group[174] (see Chapter 5.5). Substitution of bipyridine for a nucleobase leads to modified PNA single strands that are bridged in the presence of Ni^{2+} into a duplex containing a combination of hydrogen and coordinative bonds (Tab. 5.12).

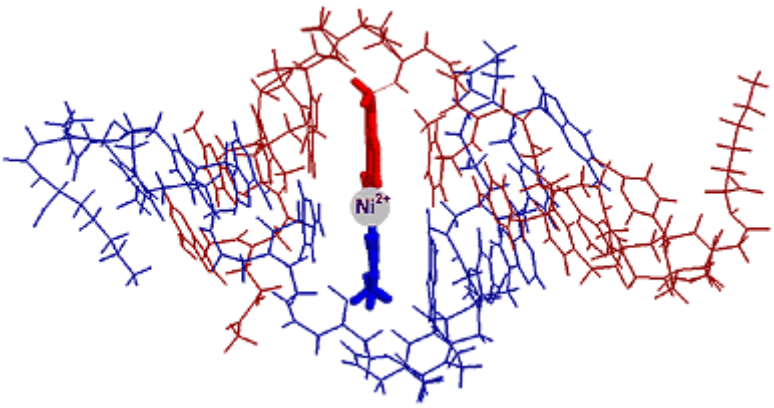

Fig. 5.18: *Cartoon Representation of a PNA Duplex Containing one Ni^{2+} Site*[253]

Balasubramanian et al. developed a cleavage monomer with a neocuproine ligand suitable to be incorporated into PNA SPS (Fig. 5.19).[81] PNA oligomers with this unit at the *N*-terminus and at an internal site were hybridized with complementary RNA sequences, and cleavage experiments in the presence of Zn(II) provided the first demonstration of a PNA-based ribonuclease mimic utilizing a metal-cleaving system. The melting temperatures (74°C and 70°C) turned out to be quasi similar, so it can be assumed that only one half of the internally modified oligomer actually binds to the RNA strand, whereas the other half sticks out which is not mentioned by the authors.
This observation makes the compound unusable in a catalytic sense.

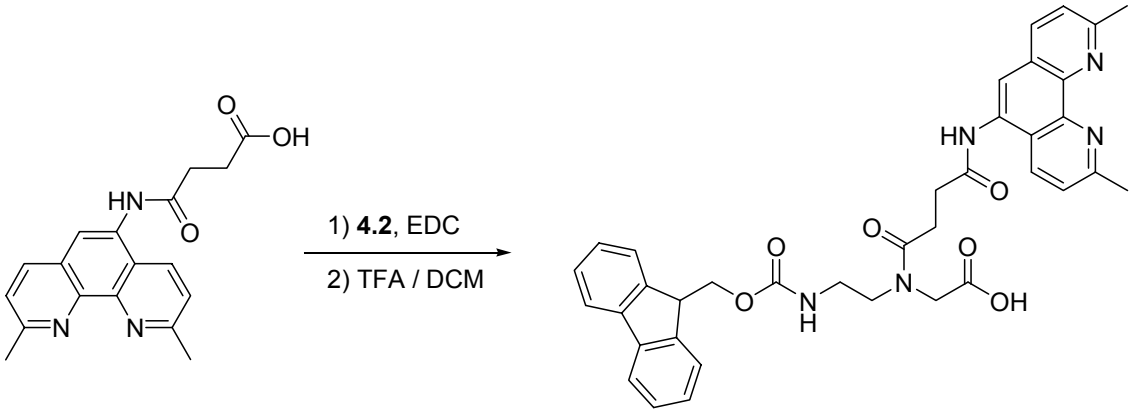

Fig. 5.19: *Coupling of Neocuproine to the PNA Backbone*

Maiorana et al. labelled thymine monomers by attaching a Fischer-type chromium carbene complex to the α-carbon of the glycine part of the backbone[254] and by condensating a benzaldehyde chromium complex via an Ugi reaction,[255] retaining the Watson-Crick base pairing properties of the nucleobase (Fig. 5.20).

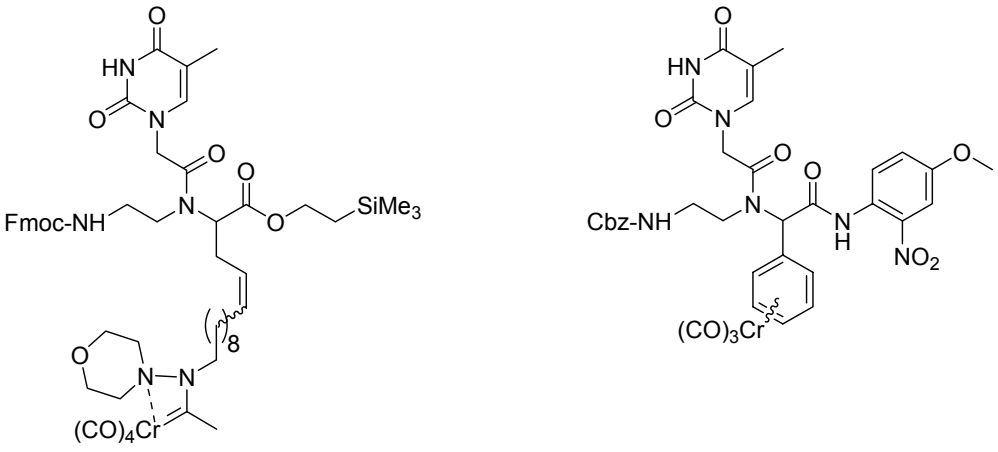

Fig. 5.20: *Backbone Labelling of PNA Thymine Monomers*

Another mentionable α-derivatization of the PNA backbone, not involving metal atoms, but modulating the pharmacokinetic properties of PNA was developed by *Hamzavi et al.*[256] by replacing the glycine part of a thymine PNA monomer by miscellaneous amino acids with derivatizable side chains and subsequent glycosylation.

A different possibility of synthesizing a metal-labelled PNA monomer is the connection of metal complexes or organometallic moieties to a PNA nucleobase instead of the backbone.[257, 258] For example, 5-iodo-derivatized uracil PNA monomers are accessible for Sonogashira coupling of alkyne residues (R=Fc-CONH) which was shown by *Hudson et al.* (Fig. 5.21).[259]

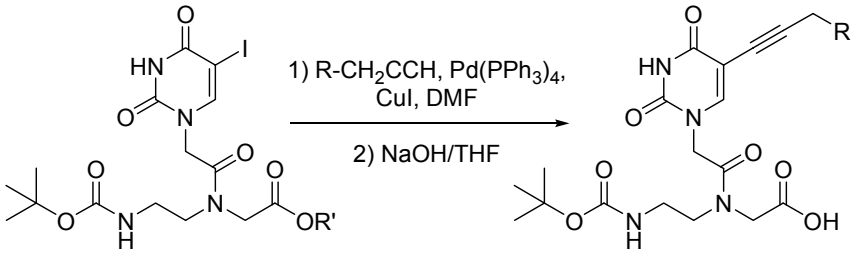

Fig. 5.21: *Sonogashira Coupling of 5-Iodo-Uracil PNA*

In contrast to the examples of *N*-derivatized PNA backbone mentioned above, in these two cases the base-pairing properties of the monomer are at least partially maintained. For a universal application (meaning arbitrary choice of sequences), four monomers would have to be provided, which does not favour this concept for an all-round use.

Unfortunately, all mentioned methods of introducing a ligand-PNA monomer require a solution phase synthesis of their own including workup and analysis which makes these methods time-consuming, circumstantial and constricted. An all-purpose concept should facilitate the implementation of various substituents into the chain and thus be more universal.

Early efforts to couple the ligand **3.5** to the PNA backbone failed, but were not pursued in favour of developing a new strategy based on the fact that the PNA backbone has exactly the length of two amino acids (repeating unit of six atoms) which suggests the replacement of one PNA monomer unit by an isostructural dipeptide, consisting of one functionalized phenylalanine and one glycine and being amenable to preparation by SPPS (Fig. 5.22).

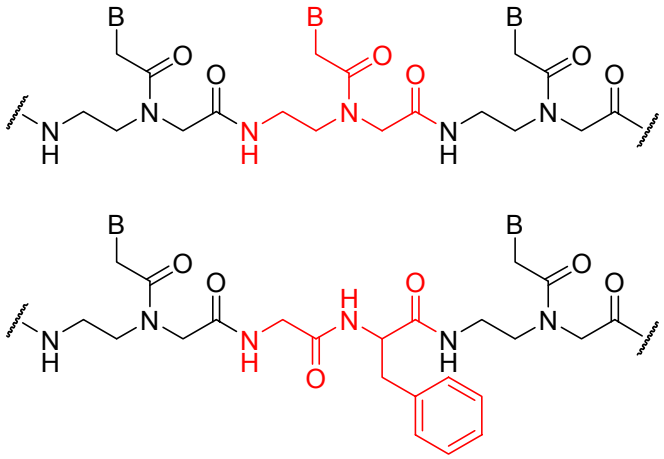

Fig. 5.22: *Standard PNA and PNA with a GlyPhe-Dipeptide Spacer*

In order to be able to attach carboxyl ligands to the abasic site, nitro-phenylalanine was chosen to be incorporated into the sequence. An on-resin reduction of the aromatic nitro group of Phe does not require additional orthogonal side-chain protection and therefore simplifies the synthesis planning (Fig. 5.23).

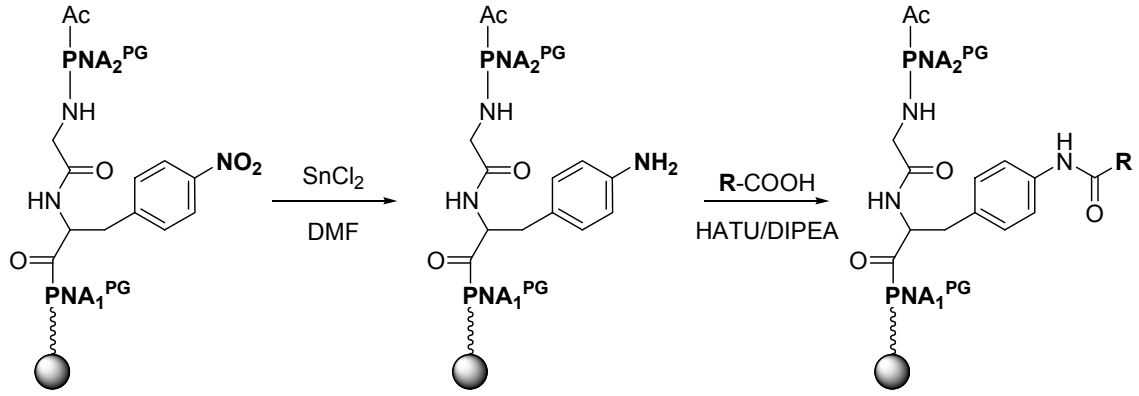

Fig. 5.23: *Strategy for the Central Attachment of Carboxylic Acid Derivatives*

The strategy of introducing functionalizable amino acids into the PNA sequence is very promising in terms of the mentioned versatility; any moiety bearing a carboxyl group should be able to be attached. This equals the *N*-terminal functionalization to the internal one, because most of the known terminal PNA bioconjugates are connected via peptide bonds, as well.

In addition to that, this method offers the possibility of synthesizing the entire oligomer on solid support which facilitates the whole process.

Finally, the chain length variability of the used amino acids (e.g. use of β-alanine or γ-amino butyric acid instead of glycine etc.) gives the opportunity to easily modify the disturbing impact of the internal building block (see melting experiments below) by simply incorporating another component into the SPPS. Thus, hybridization on both sides of the cleavage moiety should be achieved at the same time.

In this subchapter, the replacement of the PNA backbone with two amino acids, their functionalization and the attachment of ligands will be described.

5.6.1 Replacement of a PNA Monomer with a Dipeptide

The fact that the PNA backbone consists of a poly-aminoethylglycine chain and is synthesized by SPPS suggests the incorporation of other amino acids or peptides into the PNA synthesis. Several PNA-peptide chimera have been synthesized in order to enhance cellular uptake to eukaryotic cells,[260-262] bacteria[263] and tumors.[264]
In all those examples, the peptide residue is connected to the *N*-terminus of the PNA strand – either on resin or in solution. This can be achieved by finalizing the PNA sequence with an *N*-terminal cysteine[265] (a method originally developed for DNA[266]) which is thus accessible for peptide attachment.[267] For example, *van Boom et al.* reported the convergent synthesis of a PNA-peptide conjugate by chemical ligation of a thioester peptide fragment containing a nuclear localization signal (NLS) sequence with an *N*-terminal cysteine PNA derivative.[268]
Interest in the development of peptide analogues of DNA (besides and before PNA with its beneficial properties) lead to building blocks incorporating dipeptidic subunits like Ser(CH_2**B**)-Gly[269] and Ala(**B**)-Pro[270] (**B** = A, C; G, T).

Up to now, only little information about the influence of the replacement of PNA monomers with amino acids within a sequence is known except investigations concerning backbone modifications in order to modify PNA properties in general.[271]
Zuckermann et al. moved the amide carbonyl of the acetic acid linker of PNA away from the nucleobase to the backbone and replaced it with a methylene group, the resulting molecule lacking the stabilizing hydrogen bond.[272] Those modifications emerged to completely prevent oligomer interaction with DNA.
Vilaivan et al. developed backbone-modified PNA monomers which, in fact, consist of the dipeptide GlyPro(**B**) (**B** = A, C, G, T) in order to obtain a configurationally and conformationally constrained PNA.[273-275]
Trifilieff et al. presented a PNA derivative with a real polypeptide backbone instead of aminoethylglycine.[276] Melting experiments suggested self-aggregation, caused by the semi-rigid structure of this chiral molecule making it difficult to adopt the double helical structure in solution.

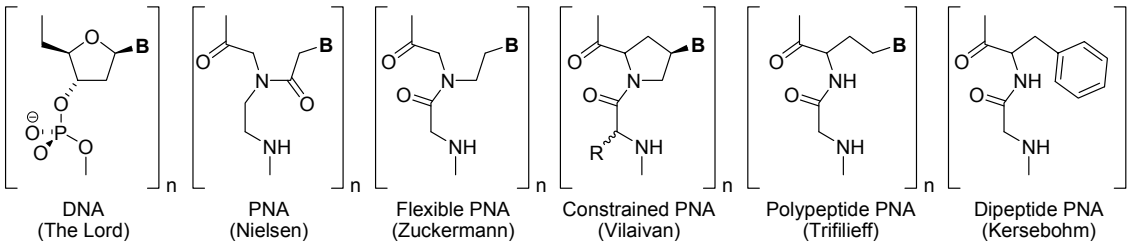

Fig. 5.24: *PNA Modifications*

Seitz et al. connected amino acids to PNA and used a complementary oligonucleotide-template to accelerate a peptide ligation (Fig. 5.25).[277]

The resulting PNA oligomers with an internal abasic site (dipeptide spacer) were identified by MALDI-TOF spectrometry,[278] but their hybridization properties were not investigated. In a recent paper,[279] *Seitz et al.* reported melting experiments with the unligated PNA-AA precursors, but assumed a dehybridization after the ligation having taken place (Fig. 5.25) and therefore did not study the duplex formation of the products. In their case, the dissociation of the resulting double strand was intended, whereas for a cleavage purpose, the duplex should reopen not until cleavage has occured.

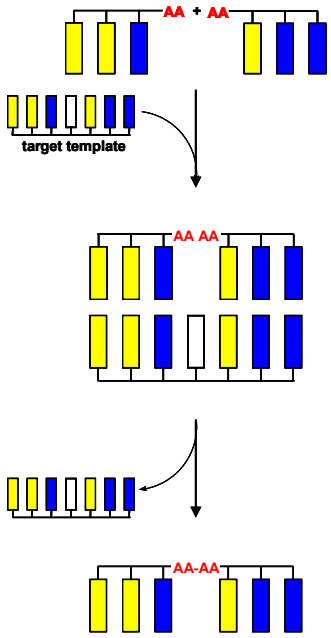

Fig. 5.25: *PNA Ligation Mediated by a DNA Template*

5.6.2 Synthesis of PNA Oligomers with a Central Dipeptide Unit

In order to investigate the properties and melting behaviour of PNA oligomers with two internal amino acids in general, the central cytosine of the I-Sce I sequence fragment was replaced by the unfunctionalized dipeptide GlyPhe. All oligomers were synthesized pursuing the SPPS standard protocol, incorporating the Fmoc-protected amino acids into the procedure (Fig. 5.26).

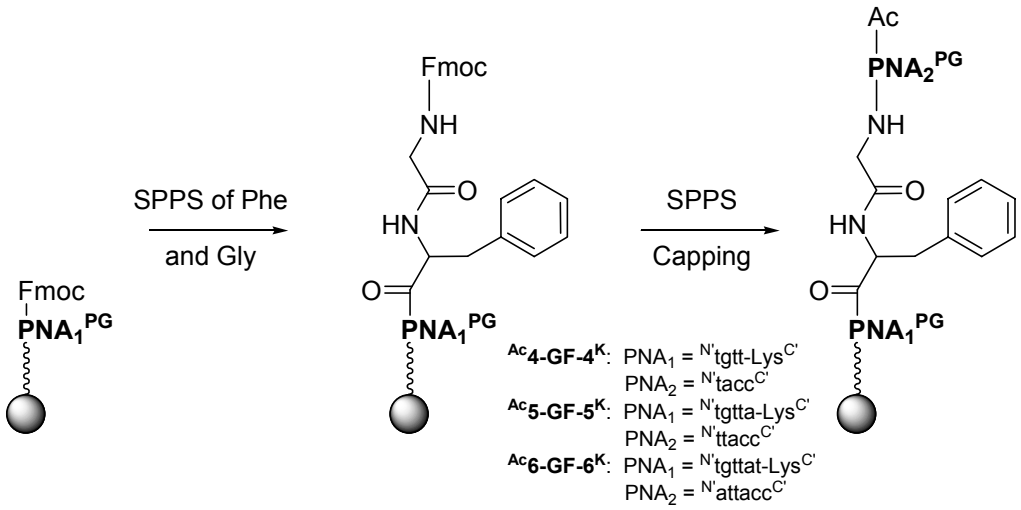

Fig. 5.26: *Incorporation of Amino Acids into the PNA Sequence*

Purification was performed by reverse-phase HPLC, and the oligomers were characterized by MALDI-TOF mass spectrometry.

Tab. 5.8: *PNA Sequences with a Central Dipeptide Unit*

central		M_{calc}	M_{found}
Ac-tacc-GlyPhe-tgtt-Lys	^{Ac}**4-GF-4**^{K}	2525.0	2526.7
Ac-ttacc-GlyPhe-tgtta-Lys	^{Ac}**5-GF-5**^{K}	3066.3	3067.6
Ac-attacc-GlyPhe-tgttat-Lys	^{Ac}**6-GF-6**^{K}	3608.5	3608.5

G-rich Oligomers

Guanine and cytosine rich oligonucleotides show an increased binding affinity to complementary strands because of the formation of three hydrogen bonds in the duplex in contrast to two hydrogen bonds in the case of adenine and thymine.

In order to test the increase of melting temperature by raising the G/C content of the oligomer, two G-rich sequences with a central dipeptide were synthesized (Fig. 5.27)

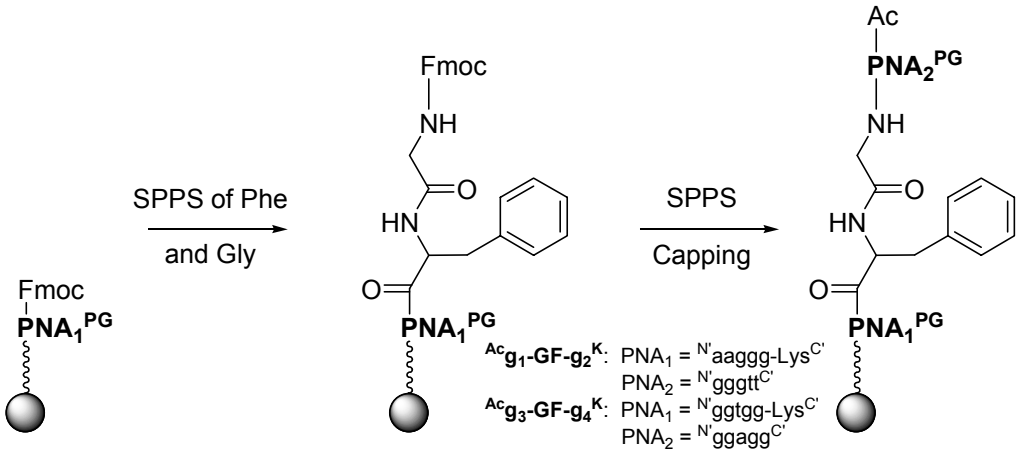

Fig. 5.27: *Synthesis of G-rich Sequences with Central Dipeptide Unit*

Purification was performed by reverse-phase HPLC, and the oligomers were characterized by MALDI-TOF mass spectrometry.

Tab. 5.9: *G-Rich PNA Sequences with a Central Dipeptide Unit*

central		$\mathbf{M_{calc}}$	$\mathbf{M_{found}}$
Ac-gggtt-GlyPhe-aaggg-Lys	$^{Ac}\mathbf{g_1}\text{-}\mathbf{GF}\text{-}\mathbf{g_2}^{K}$	3221.3	3221.3
Ac-ggagg-GlyPhe-ggtgg-Lys	$^{Ac}\mathbf{g_3}\text{-}\mathbf{GF}\text{-}\mathbf{g_4}^{K}$	3262.3	3263.0

5.6.3 Synthesis of Fmoc-Phe(NO_2)-OH

The incorporation of ligands into a PNA sequence containing phenylalanine requires its preceding functionalization which was, in this case, achieved by the nitration of the phenyl side chain, followed by Fmoc-protection and subsequent reduction (see next subchapter).

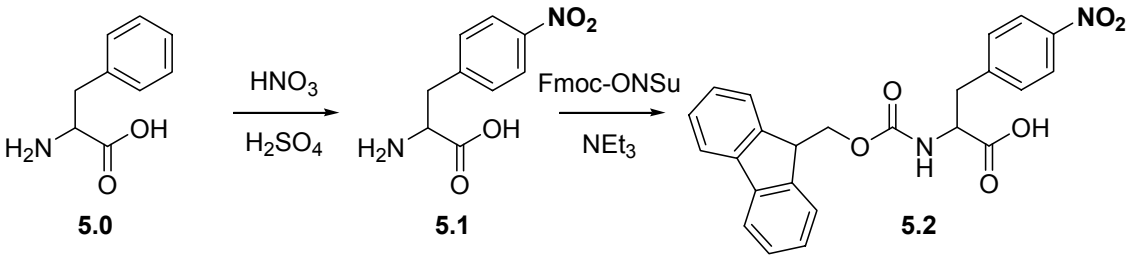

Fig. 5.28: *Synthesis Scheme for Fmoc-Phe(NO_2)-OH* ***5.2***

In the first step, phenylalanine was nitrated with HNO_3/H_2SO_4, and the product was precipitated with aqueous NaOH at pH7. Fmoc-protection was carried out in a mixture of H_2O and MeCN with triethylamine as a base. After removal of the volatiles, the resulting red oil was dissolved in water and at neutral pH, the crude product precipitated. Recrystallization from EtOAc yielded 53% of pure **5.2**.

The synthesis steps were easy to be observed by ^{1}H-NMR spectroscopy (see Fig. 5.32), and the compounds were characterized by ^{13}C-NMR, MS and IR, as well. HPLC analysis revealed them to be of satisfactory purity.

Nitro-phenylalanine is stable under SPPS conditions and is therefore suitable for its integration into a PNA sequence.
Avoiding orthogonal protection of the Phe side chain, the nitro group was planned to be reduced on resin, followed by attachment of the carboxyl ligand.

5.6.4 Synthesis of Fmoc-Phe(NH_2)-OH

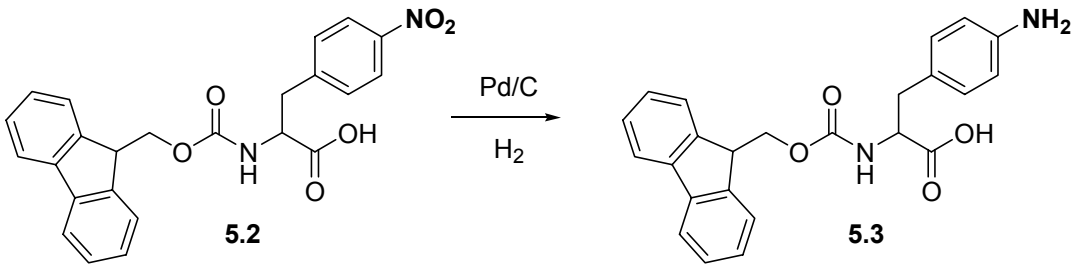

Fig. 5.29: *Reduction of Fmoc-Phe(NO_2)-OH* ***5.2***

In order to show that the aromatic nitro group of Fmoc-protected phenylalanine can be reduced without affecting the rest of the molecule, the compound was subjected to a catalytic reduction with Pd/C and H_2 in dioxane/MeOH (4:1).

The reaction progress was monitored by HPLC, impressively showing the decrease of Fmoc-Phe(NO_2)-OH **5.2** in favour of the amino compound **5.3** (Fig. 5.30).

During the first three hours of reaction, the percentages of the two major components changed significantly, just to change into a linear transformation (Fig. 5.31). Interestingly, the composition of the samples changed upon standing even when the catalyst was filtered of (maybe due to Pd residues), so that HPLC was performed immediately after sampling to assure reproducibility.

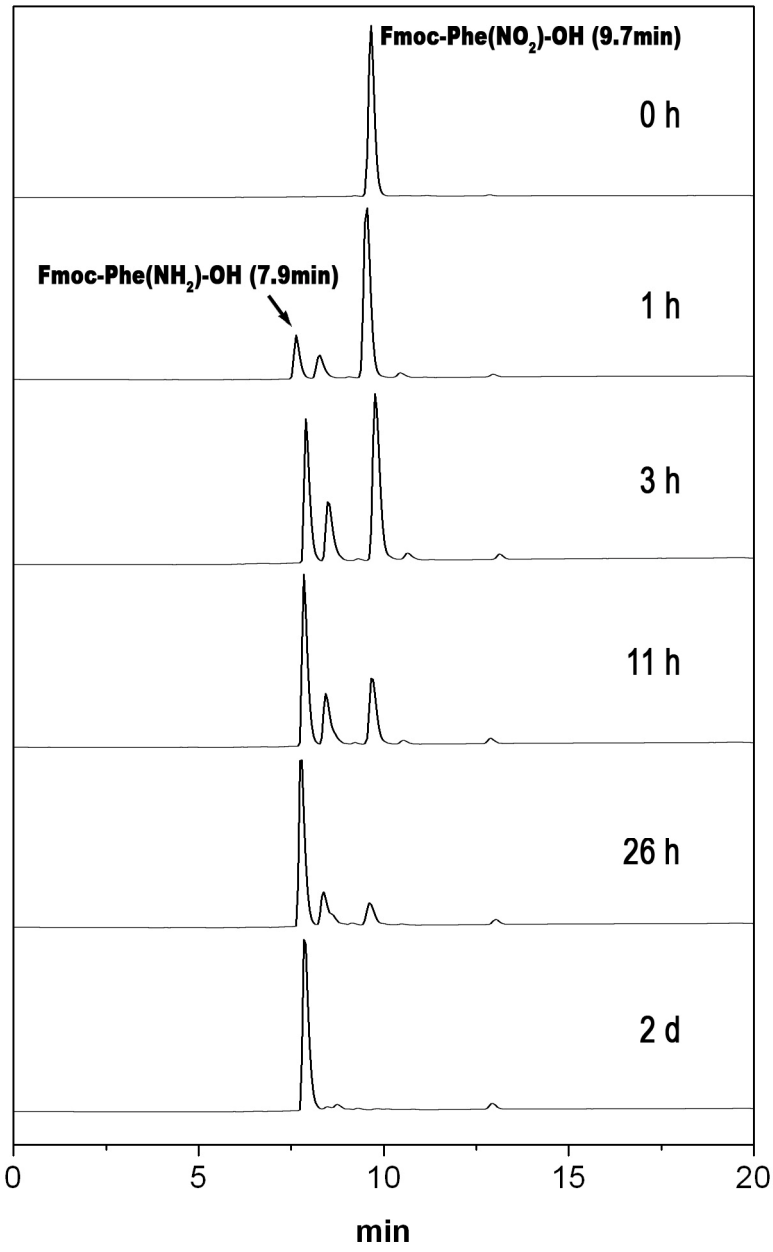

Fig. 5.30: *HPLC-Monitored Reduction of Fmoc-Phe(NO_2)-OH* ***5.2*** *with Supposed Nitroso-Intermediate at 8.5min*

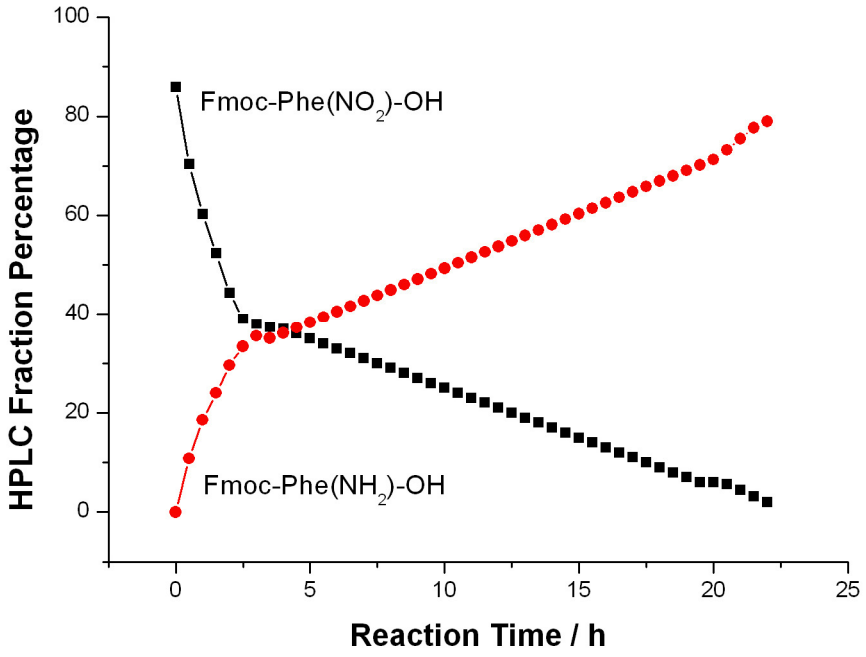

Fig. 5.31: *Percentage of HPLC Fractions During the Progress of the Reduction of* ***5.2***

The selective reduction of Fmoc-protected nitro-phenylalanine was thus shown to be straightforward even under harsh conditions by converting the compound with Pd/C catalyst and hydrogen.

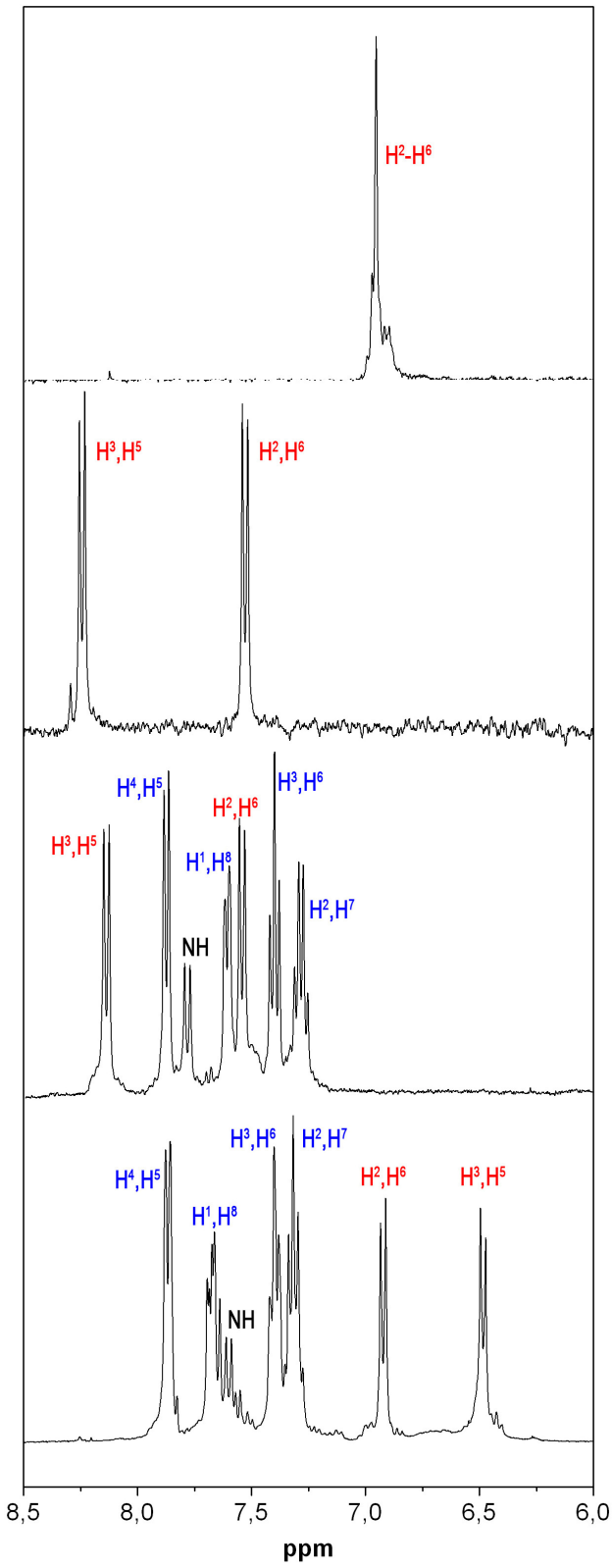

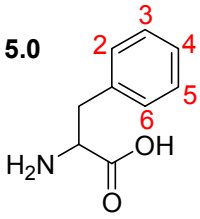

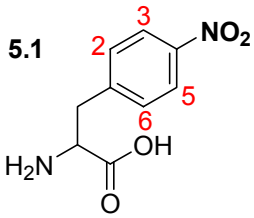

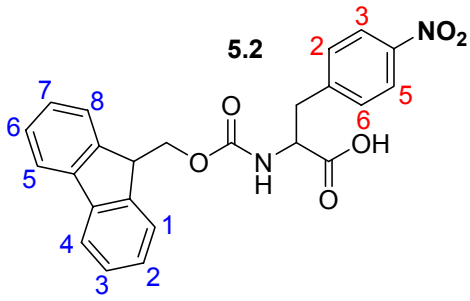

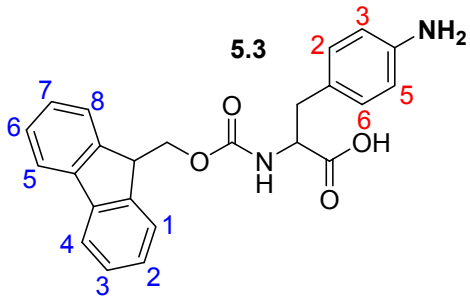

Fig. 5.32: *[1]H-NMR Spectra of Phe-Derivatives* ***5.0-5.3***

The successful reduction of Fmoc-Phe(NO_2)-OH **5.2** to the amine **5.3** showed the suitability of the compound to be incorporated into solid phase synthesis.

Attempts to couple the activated terpyridine ligand **3.5** to Fmoc-Phe(NH_2)-OH **5.3** *in solution* (Fig. 5.33) failed and supported the plan of performing the whole synthesis based on SPPS.

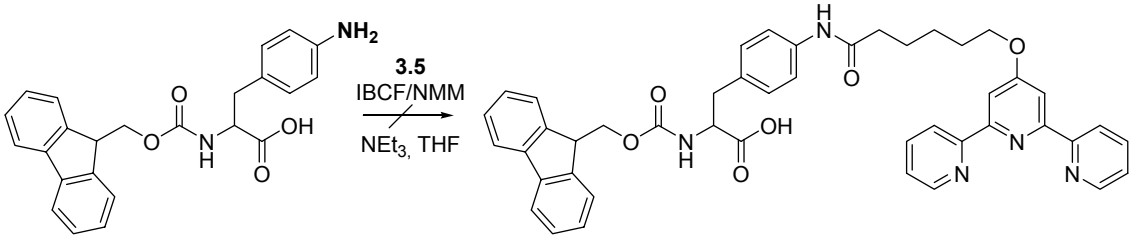

Fig. 5.33: *Attempting to Couple Ligand **3.5** to Fmoc-Phe(NH_2)-OH **5.3** in Solution*

Further experiments with modified conditions and coupling reagents are expected to afford the desired cleavage monomer, but were not pursued because of the undoubted advantages of the SPPS pathway.

5.6.5 Synthesis of PNA Oligomers with Central Ligand

The advantages of SPPS lead to the concept of performing the entire synthesis of internally functionalized PNA oligomers *on resin* (Fig. 5.23).

As a preliminary investigation, the oligomer Ac-tacc-GlyPhe(NO_2)-tgtt-Lys (^{Ac}**4-GF^{O}-4^{K}**) was synthesized. After assembly of the PNA-peptide chain, incorporating nitro-phenylalanine into the sequence, a test cleavage was performed with some resin beads, and the MALDI spectrum confirmed the formation of the intermediate (Fig. 5.34).

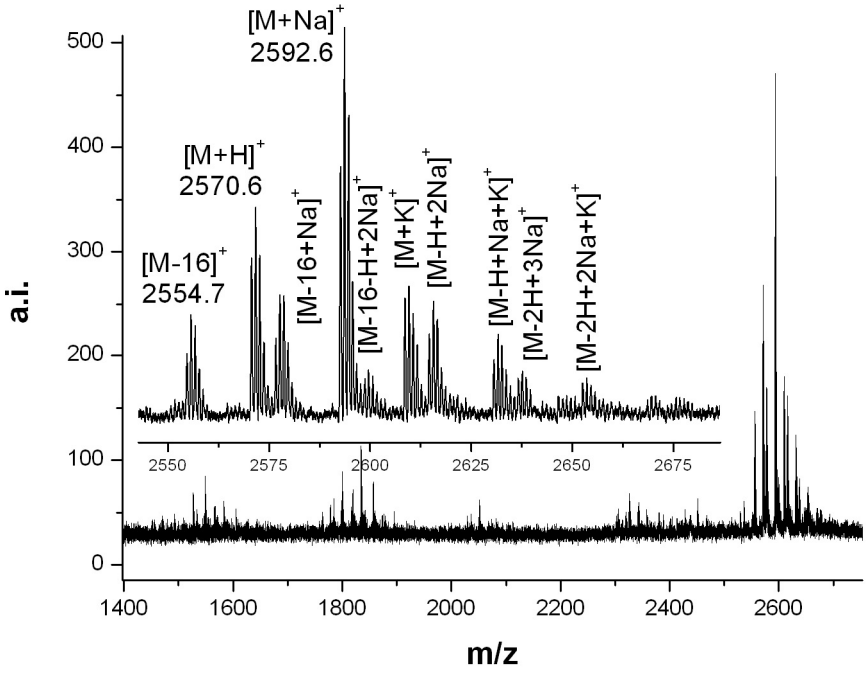

Fig. 5.34: *MALDI Spectrum of* ***^{Ac}4-GF^{O}-4^{K}***

Subsequent reduction was carried out by converting the resin-bound oligomer nitro group with 0.9M $SnCl_2$ in DMF overnight, followed by ligand coupling with HATU/DIPEA in DMF (Fig. 5.35).

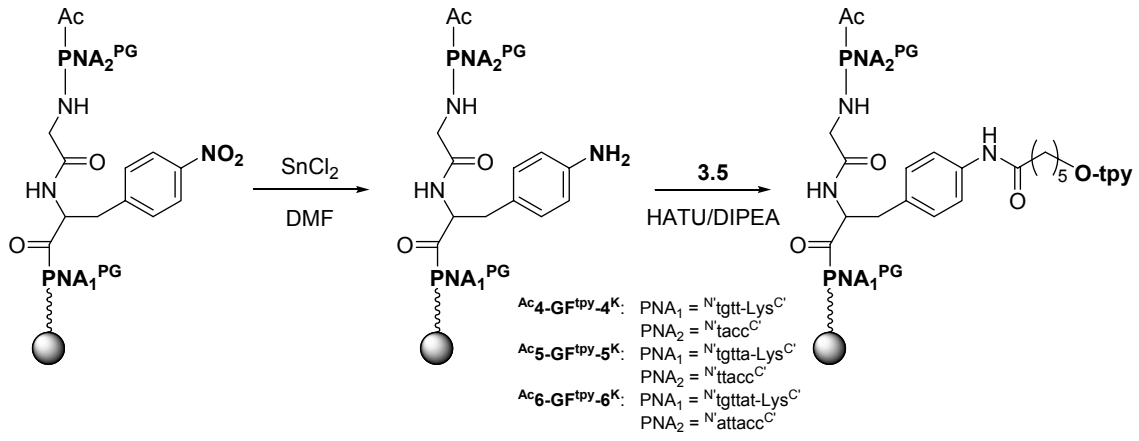

Fig. 5.35: *Strategy of Attaching the Ligand **3.5** to a Central Phenylalanine*

A MALDI spectrum of the supposed products (Fig. 5.36) revealed that neither the reduction nor the ligand coupling had been quantitative which may be explainable with the sterical shielding by the PNA chain.

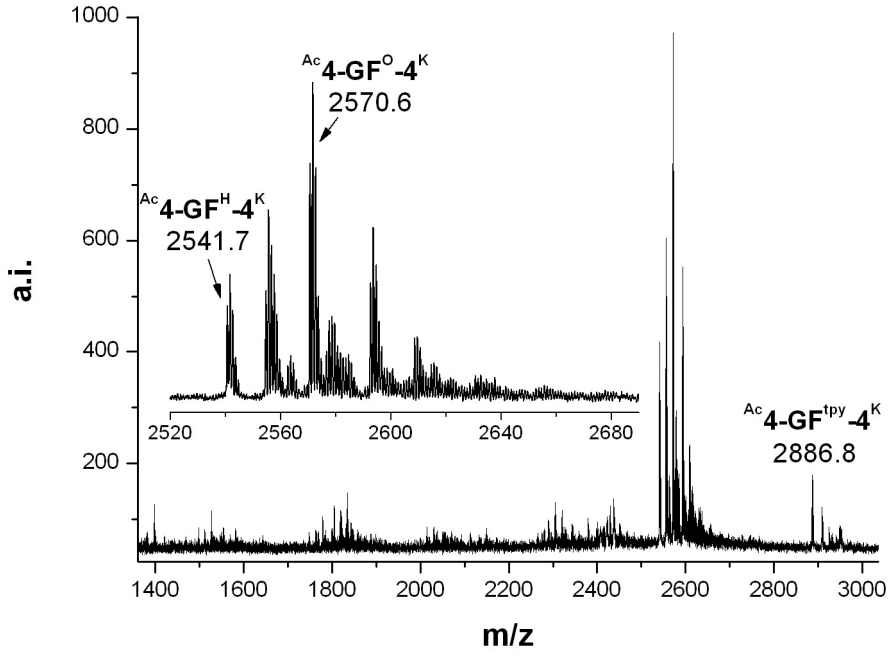

Fig. 5.36: *MALDI Spectrum after the Futile Synthesis of ^{Ac}4-GF^{tpy}-4^{K}*

Tab. 5.10: *Overview of Intermediates of* ^{Ac}***4-GF***^{tpy}***-4***^{K}

		M_{calc}	M_{found}
Ac-ttacc-GlyPhe(NO_2)-tgtta-Lys	^{Ac}**4-GF**^{O}**-4**^{K}	2569.0	2570.6
Ac-ttacc-GlyPhe(NH_2)-tgtta-Lys	^{Ac}**4-GF**^{H}**-4**^{K}	2539.1	2541.7
Ac-ttacc-GlyPhe(tpy*)-tgtta-Lys	^{Ac}**4-GF**^{tpy}**-4**^{K}	2885.2	(2886.8)

Instead of optimizing or modifying this pathway, a change of strategy seemed to me more promising. In order to prevent the PNA chain from hindering the subsequent steps, the oligomer assembly was interrupted after glycine, and continued after reducing the nitro group and coupling of the ligand (Fig. 5.37).

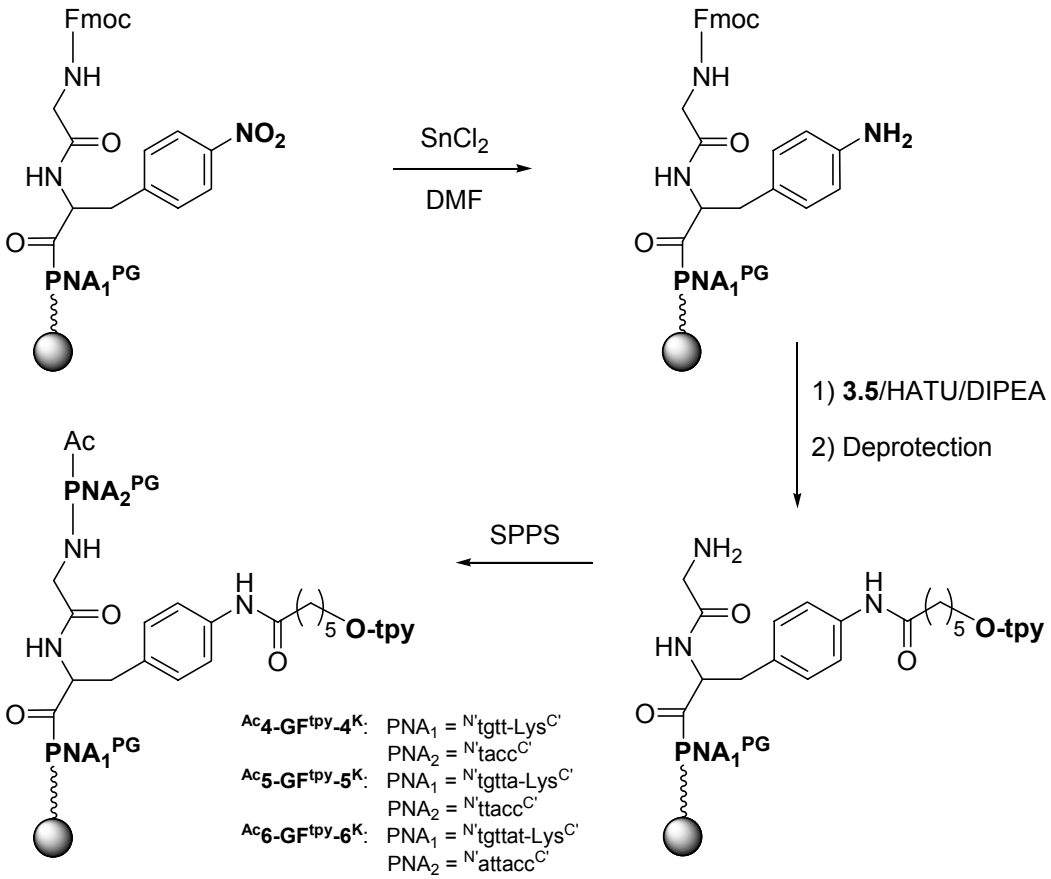

Fig. 5.37: *Improved Strategy of Internal Ligand Coupling*

The whole process was monitored by performing MALDI spectrometry after each single step, and the particular intermediates revealed an unobstructed progression. Exemplarily, the MALDI spectra of the intermediates shown in Fig. 5.37 are presented for ^{Ac}**6-GF**^{tpy}**-6**^{K} (Fig. 5.38, Fig. 5.39)

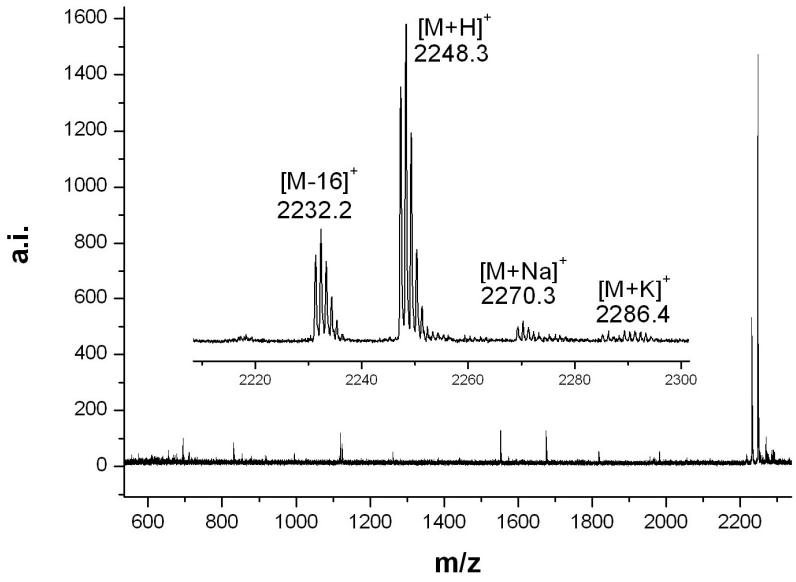

Fig. 5.38: *MALDI Spectrum of* ^{Fmoc}***GF***^{O}***-6***^{K}

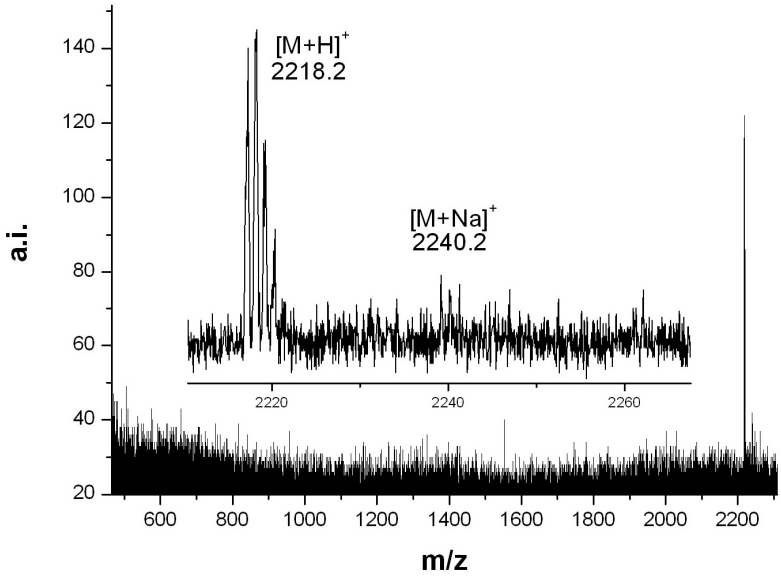

Fig. 5.39: *MALDI Spectrum of* ^{Fmoc}***GF***^{H}***-6***^{K}

A test spectrum of Fmoc-GlyPhe(tpy*)-tgttat-Lys (^{Fmoc}**GF**^{tpy}**-6**^{K}) showed unreacted Fmoc-GlyPhe(NH_2)-tgttat-Lys (^{Fmoc}**GF**^{H}**-6**^{K}). This may be due to the reduced reactivity of aromatic amino groups towards the formation of peptide bonds. As a consequence, the ligand coupling was prolonged and performed twice. In addition, the standard coupling conditions were optimized for this special purpose (see Experimental Part).

The MALDI spectrum of ^{H}**GF**^{tpy}**-6**^{K}after the successful coupling of **3.5** to the Phe(NH_2) side chain and terminal deprotection (Fig. 5.40) shows some capping products of intermediate steps, and an iron peak which is observed in all cases, but was easy to remove by performing HPLC on the final crude product (the effect of iron contamination of tpy* conjugates already has been mentioned in Chapter 3).
Impurities in intermediate spectra were ignored, as long as only some beads were cleaved for monitoring and thus the spectrum not being representative. Furthermore, HPLC-purification was performed on the final product.

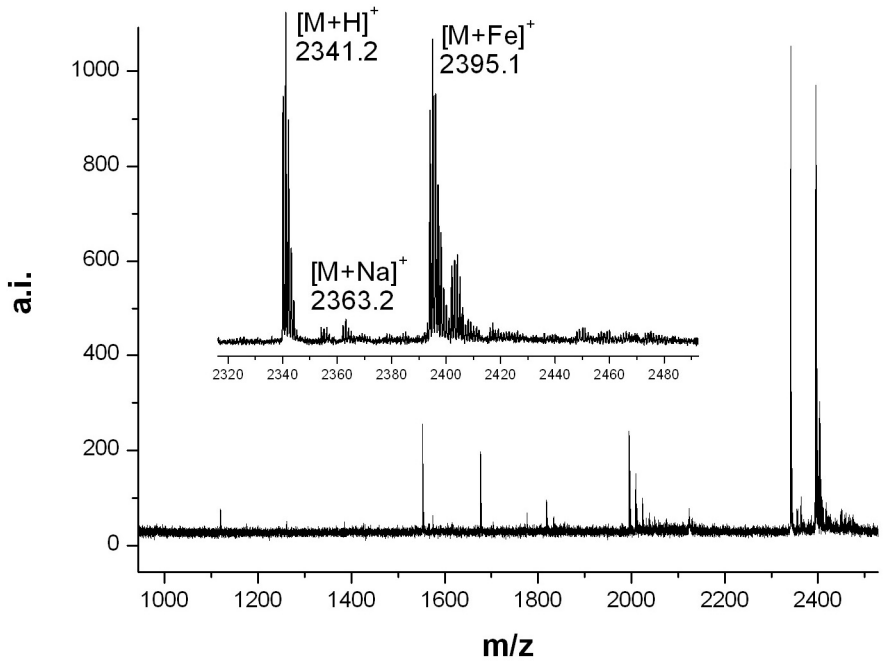

Fig. 5.40: *MALDI Spectrum of* ^{H}***GF***^{tpy}***-6***^{K}

The amino terminus was deprotected, and the chain extension was continued till the end (Fig. 5.37). After cleavage from the resin, the final crude product was purified by HPLC, and the MALDI spectrum showed the success of the reaction (Fig. 5.41).

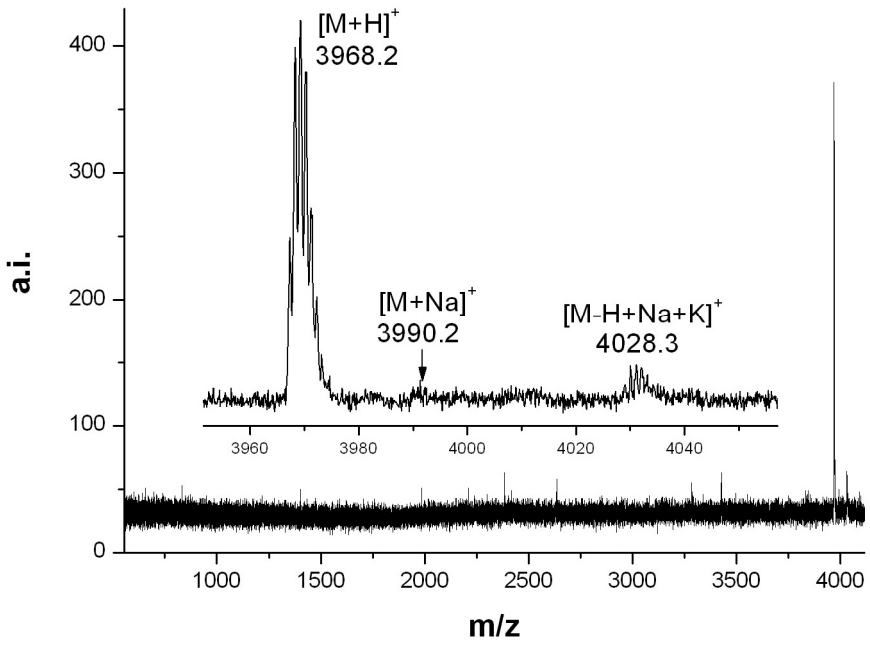

Fig. 5.41: *MALDI Spectrum of* ^{Ac}**6-GF**^{tpy}**-6**^{K} *without Iron Contamination (m/z=4022.3)*

Tab. 5.11: *Overview of Intermediates of* ^{Ac}**6-GF**^{tpy}**-6**^{K}

		M_{calc}	M_{found}
Fmoc-GlyPhe(NO_2)-tgttat-Lys	^{Fmoc}**GF**^{O}**-6**^{K}	2247.9	2248.3
Fmoc-GlyPhe(NH_2)-tgttat-Lys	^{Fmoc}**GF**^{H}**-6**^{K}	2217.9	2218.2
H-GlyPhe(tpy*)-tgttat-Lys	^{H}**GF**^{tpy}**-6**	2341.0	2341.2
Ac-attacc-GlyPhe(tpy*)-tgttat-Lys	^{Ac}**6-GF**^{tpy}**-6**^{K}	3967.6	3968.2

The same strategy was applied on two other PNA oligomers, completing the three varying chain lengths (Tab. 5.12). All compounds were purified by HPLC and characterized by MALDI spectrometry.

Tab. 5.12: *Overview of PNA Oligomers with Central tpy* Attachment*

central		$\mathbf{M_{calc}}$	$\mathbf{M_{found}}$
Ac-tacc-GlyPhe(tpy*)-tgtt-Lys	^{Ac}**4-GF^{tpy}-4^{K}**	2885.2	2886.2
Ac-ttacc-GlyPhe(tpy*)-tgtta-Lys	^{Ac}**5-GF^{tpy}-5^{K}**	3426.4	3428.6
Ac-attacc-GlyPhe(tpy*)-tgttat-Lys	^{Ac}**6-GF^{tpy}-6^{K}**	3967.6	3968.8

bpa

The same synthesis strategy (as shown in Fig. 5.37) could be applied on the bpa ligand **3.6**, and MALDI spectra of the HPLC purified products proved a successful reaction.

Tab. 5.13: *Overview of PNA Oligomers with Central bpa* Attachment*

central		$\mathbf{M_{calc}}$	$\mathbf{M_{found}}$
Ac-tacc-GlyPhe(bpa*)-tgtt-Lys	^{Ac}**4-GF^{bpa}-4^{K}**	2855.2	2855.1
Ac-ttacc-GlyPhe(bpa*)-tgtta-Lys	^{Ac}**5-GF^{bpa}-5^{K}**	3396.4	3397.8

5.7 Summary

In the preceding Chapter, several unmodified PNA oligomers were synthesized, corresponding both to terminally and centrally substituted sequences. An overview of the synthesized sequences in this Chapter is given in the Appendix. All oligomers were purified by HPLC, and MALDI-TOF spectrometry showed pure products in all cases.

The ligands **3.5** and **3.6** could be successfully coupled to the *N*-terminus of PNA. Attempts to attach the amino ligand phen*-H **3.8** to the *N*-terminus which was successfully converted into a *C*-terminus prior to coupling, exposed the difficulty of on-resin carboxyl activation by the use of HATU.

A versatile method for an internal attachment of carboxyl ligands to a PNA chain was developed, consisting of the incorporation of Fmoc-protected *p*-nitro-phenylalanine and a glycine spacer. The chain assembly was interrupted after that, the nitro group was successfully reduced on resin, and after coupling of the particular ligand, the oligomer synthesis was continued to the end.

As a comparison, the corresponding PNA oligomers bearing an unfunctionalized internal dipeptide spacer and guanine rich oligomers with a central GlyPhe unit were synthesized, as well.

6 Hybridization Experiments

6.1 Introduction

The so-called melting of oligonucleotide double strands describes the thermal denaturation of a duplex, caused by the breaking of Watson-Crick base pairings with increasing temperature (Fig. 6.1).

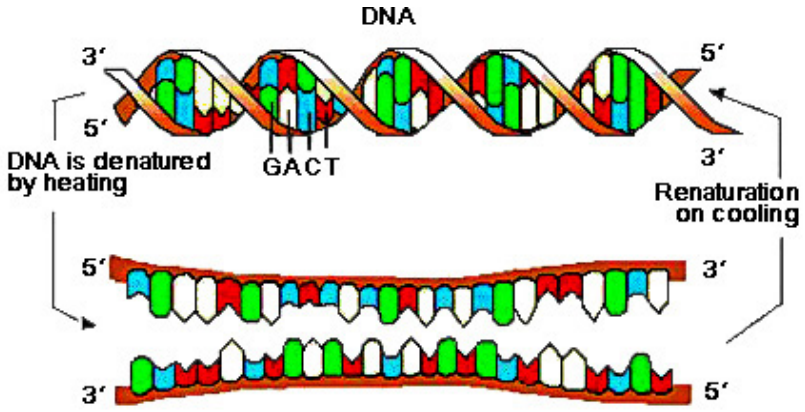

Fig. 6.1: *Denaturation and Renaturation of DNA*

This process can be observed by measuring at certain wavelengths (260nm) the absorbance of a solution of two more or less complementary single strands versus the temperature.[280] The change of absorbance with increasing temperature is caused by the hyperchromicity due to the loss of π-stacking present in oligonucleotide helices. The absorption coefficient of nucleobases is higher in single strand oligonucleotides than in the duplex which leads to an increase of absorbance with rising temperature.

Melting curves show a sigmoidal shape (Fig. 6.2) because of the melting being a cooperative effect: If some base pairs are already broken up, adjacent base pairs will break up easier.

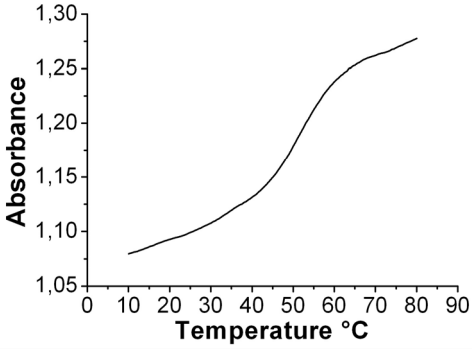

Fig. 6.2: *Melting Curve of PNA* ^{Ac}***6-c-6***^{K} • *DNA* $^{3'}$***6-G-11***$^{5'}$

The melting temperature T_M is defined as the temperature at which 50% of the species in solution is hybridized, meaning equal amounts of base-paired and unpaired single strands are present. It is determined by the maximum of the first derivative melting curve. The α value of a system describes the fraction of single strands in the duplex state; α will be 0.5 at T_M (Fig. 6.3).

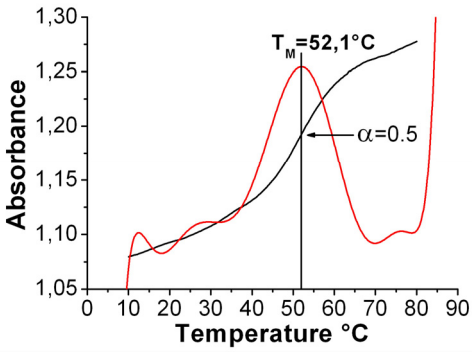

Fig. 6.3: *Melting Curve (black) of PNA* ^{Ac}***6-c-6***^{K} • *DNA* $^{3'}$***6-G-11***$^{5'}$ *and its First Derivative (red)*

T_M has been found to correlate well with the thermodynamic equilibrium constant, K, and is, thus, generally a good measure for duplex stability.[281, 282]

Fro DNA • DNA, T_M is strongly dependent on the concentration of oligonucleotides and the salt concentration, because the repulsion of negatively charged single strands is compensated by metal ions. As a result, T_M decreases with decreasing salt concentration. For that reason, a phosphate buffer with 0.1M NaCl is used for melting experiments. Under physiological conditions, Zn^{2+} & Mg^{2+} can take over the role of those

counter ions. In the case of PNA, melting is relatively independent of the salt concentration because of PNA being an uncharged molecule.[157, 283] PNA oligomers readily hybridize with complementary DNA strands, preferably in an antiparallel way.[156, 284]
The antiparallel PNA•DNA duplex forms a DNA like, right-handed double helix,[150, 285, 286] but with a tighter coiling than in the case of dsDNA (Fig. 6.4). B-DNA has 10 base pairs in one turn, whereas in PNA•DNA duplexes, the major groove is enlarged at the expense of the minor groove, which leads to a coil of 13 bp.

According to NMR experiments, PNA•DNA mixed-sequence duplexes adopt a structure possessing features of both A-form and B-form DNA.[283]

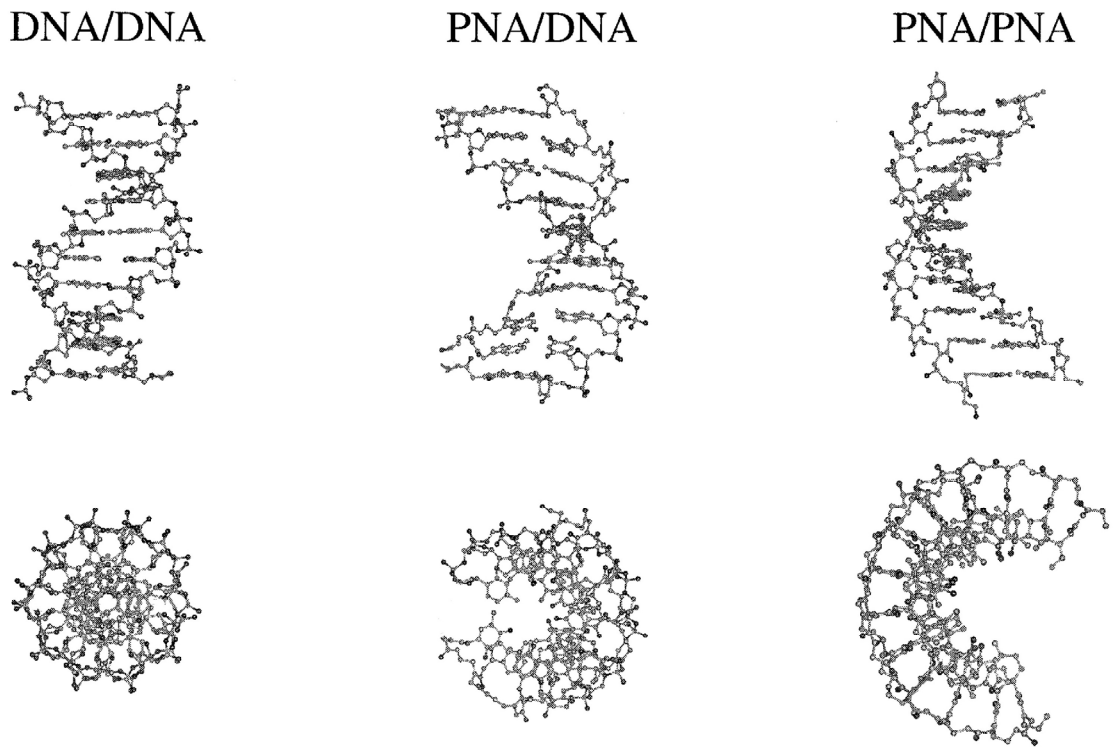

Fig. 6.4: *Models illustrating the three different types of duplexes. From left to right: DNA•DNA, PNA•DNA, and PNA•PNA, with side views in the upper row and top views in the lower*[284]

If a nucleobase within a sequence is replaced with another one not matching to the complementary strand (mutation), this is called a mismatch. The difference between the melting temperature of a fully complementary duplex and the melting temperature of a duplex with one or more mismatches is referred to as ΔT_M. PNA possesses a higher mismatch-sensitivity than DNA,[287] leading to a ΔT_M (DNA • PNA) of up to 15°C in decamers.

This results in a higher sequence selectivity[143, 158] and binding specificity[288] due to the fact that PNAs will preferably bind to their perfect complementary sequence, because the affinity to a single mismatch sequence will be significantly lower.

The higher melting temperature of PNA • DNA duplexes in contrast to DNA • DNA duplexes[157, 288] makes even short sequences suitable for targeting.

6.2 Melting Curve Analysis

Because of the melting temperature of an oligonucleotide being defined as the point of highest slope in the absorbance melting curve, the maximum of the first derivative indicates this temperature. Each experiment was carried out at least four times with fresh solutions, the inflection point for each curve was determined by this means, and the average was calculated after leaving out mavericks. In this Chapter and in the Appendix, only one example of each duplex is displayed; average data is given in Chapter 6.4.

Significance

The mere consideration of the melting temperature turned out to be not significant enough for comparing different sequences.

Melting curves of apparently inferior matching strands sometimes showed a higher melting temperature than obtained from the 100% matching experiment.

For example, a curve from an obviously not hybridizing system (concerning the shape of the melting curve) was transformed into a quite nice first derivative curve by simply cropping the melting data at both ends, and a melting point was obtained (Fig. 6.5).

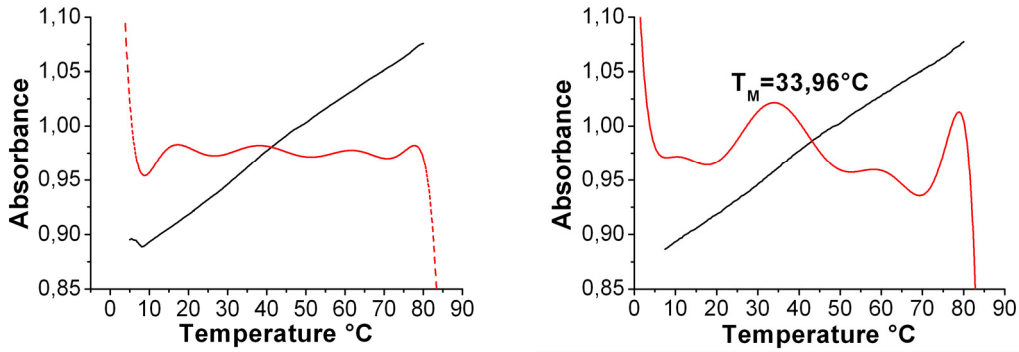

Fig. 6.5: *Melting Curve of PNA* ^{Ac}***6-GF-6***^{K} • *DNA* $^{3'}$***6-G-11***$^{5'}$ *– Different Data Ranges*

Also by rescaling the y-axis and cutting the first derivative curve, the result could be embellished (Fig. 6.6).

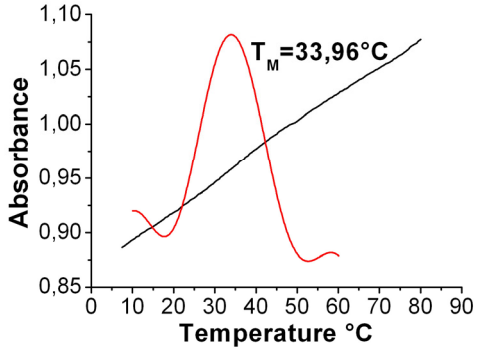

Fig. 6.6: *Melting Curve of PNA* ^{Ac}***6-GF-6***^{K} • *DNA* $^{3'}$***6-G-11***$^{5'}$ *– Cropped 1*st *Derivative*

The same experiment with the corresponding DNA match sequence (with the central guanine omitted; these results are forestalled and will be discussed later) showed a lower melting temperature, but a clear sigmoidal shape (Fig. 6.7).

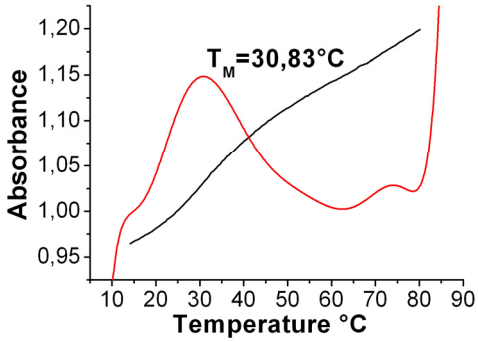

Fig. 6.7: *Melting Curve of PNA* ^{Ac}***6-GF-6***^{K} • *DNA* $^{3'}$***6-11***$^{5'}$

By only indicating the melting temperatures of these two examples, one could conclude that the first PNA • DNA duplex is more stable than the second one which is not coherent and also not true.

In order to overcome these problems, the shape of the melting curve was taken into consideration by the development of a factor representing the pertinence of the curve.

Aspects of a significant melting process besides the melting temperature are:

Melting Curve:

- Difference between Upper and Lower Baseline
  (Offset / Increase of Absorbance)

1st Derivative:

- Maximum (representing the slope of the melting curve at T_M)
- Minima (left & right)
- Peak Height (Max minus Average Min)
- Max/Min-Ratio
- Full Width at Half Maximum (FWHM)
- **Ratio between Peak Height and FWHM**

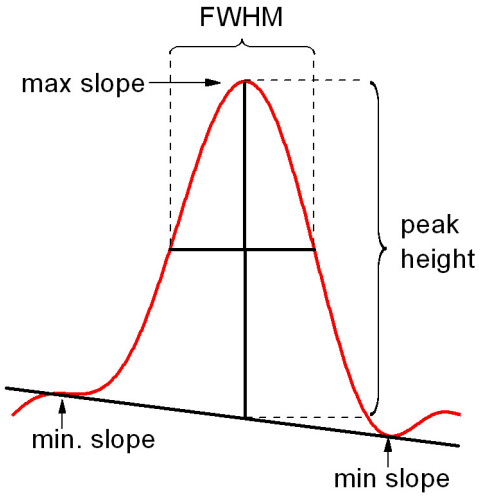

The latter coefficient is higher with increasing height and decreasing width of the first derivative melting curve. Those two values directly depend on the sigmoidality. The first derivative of a highly curved graph is very sharp and clear cut, and the ratio peak height / FWHM is high. This quotient therefore was deemed to be a valuable measure for the relevance of a melting curve and will be referred to as $\mathbf{f_M}$ in the following. Every value was multiplied with 10^4 and indicated as nondimensional.

Another important aspect is the so-called self-melting of PNA.

Self-melting

The concentration of PNA solutions has to be determined at 70°C. The reason for this is the self-stacking of nucleobases in PNA oligomer strands (which is not observed for DNA), so that only at higher temperature, the absorbance of PNA solutions will significantly represent its concentration. Stacking of nucleobases causes a decrease of absorbance (hypochromicity) and therefore falsifies the concentration.

A PNA•DNA melting experiment with two non-match single strands can result in a change of absorbance suggesting hybridization.

Literature does not provide any information about the significance of melting curves, only mentioning melting points or thermodynamical data. The fact that single stranded PNA has a melting temperature for itself was mentioned by Ray and Nordén,[151] only specifying the T_M of the single strand (44.7°C) without comparison or valuation. This T_M is even higher than that obtained from a duplex melting experiment (39.0°C), but the authors do not comment this fact, so that no information is given whether hybridization or only self-melting takes place.

The self-stacking of PNA oligomers has little impact, however, on the hyperchromicity of the melting curves of PNA•DNA duplexes, as they will typically melt at temperatures above 45°C.[149, 284] Normally, the effect of single-strand order at low temperatures should not represent a severe complication when analyzing absorbance melting curves. At low temperatures, the duplex is strongly favoured over the isolated single strand and as the temperature (and consequently the number of single strands) increases, the order of the single strands decreases.[289] In the case of shorter sequences and disturbed complementarity as in this Thesis, this fact has to be implied, because if no hybridization occurs, the self-melting effect (giving a sigmoidal curve even without hybridization) could be mistaken for a melting which does in fact not take place at all.

In order to evaluate this, each PNA monomer was “molten” without addition of the corresponding DNA strand. The ratio between f_M of the double-strand melting curve and f_M of the single strand melting experiment ($\mathbf{q_M}$) provides information about the significance of the melting curve in comparison to the self-melting effect ($q_M = f_M^{ds}/f_M^{sm}$).

Buffer Baseline

In order to prove that only PNA is responsible for sigmoidality, absorbance curves both of pure buffer (Fig. 6.8) and pure DNA (Fig. 6.9) were measured.

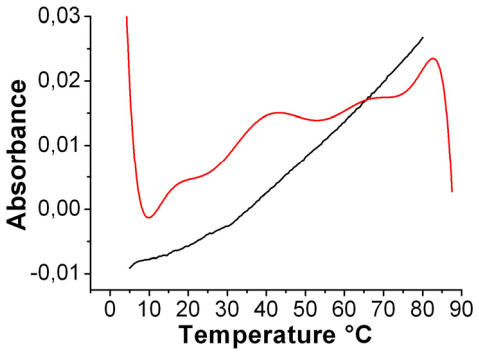

Fig. 6.8: *Absorbance Curve of Pure Buffer*

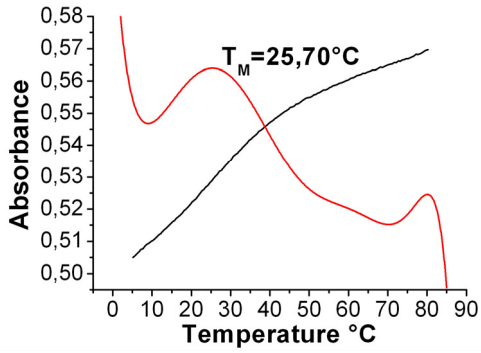

Fig. 6.9: *Absorbance Curve of Pure DNA* **$^{3'}$6-G-11$^{5'}$**

The buffer curve shows hyperchromicity which turns out to be negligible, because it only amounts to a total of 3%. Experiments with a blank cuvette filled with buffer only, being subtracted from the actual absorbance values, did not reveal any significant difference in the shape of the melting curve, and the T_M values were similar to the uncorrected ones.

Tab. 6.1: *Typical Hyperchromicity Values*

	$A_{80°C} - A_{5°C}$
buffer only	0.035 (3%)
DNA only	0.065 (13%)
PNA only	0.05-0.10 (20-30%)
PNA • DNA	0.25-0.30 (20-30%)
DNA • DNA	0.30-0.40 (25-35%)

The percentage increases of absorbance (hyperchromicity) values are indicated below the particular melting curves in the Appendix.

Concentration Accuracy

In order to examine the influence of concentration inaccuracies on the melting temperature, hybridization experiments were carried out with 20% excess of DNA and 20% excess of PNA, respectively. Surprisingly, the melting temperature was only changed by an average value of 1.3°C, so that this potential systematic error did not have to be worried about.

6.3 Measurements

Every melting experiment was done at least four times according to the procedure described in the Experimental Part. 3μM solutions of the HPLC purified oligomers were prepared in phosphate buffer with 0.1M NaCl, and the mixtures were heated from 5°C to 80°C with a rate of 0.5°C/min, measuring the absorbance at 260nm. The resulting melting curves were differentiated and polynomially fitted (9^{th} order / 1000 data points). The T_M values obtained from the melting curves were averaged (Eq. 1) after deleting mavericks, and standard deviations were determined according to Eq. 2:

$$\bar{x} = \frac{\sum x_i}{N} \quad (1) \qquad \sigma_x = \sqrt{\frac{1}{N}\sum_{i=1}^{N}(x_i - \bar{x})^2} \quad (2)$$

All PNA oligomers were readily soluble in phosphate buffer, except as indicated.

Self-melting experiments were carried out once on every single strand sequence and DNA • DNA hybridization was performed for every combination, as well.

PNA • DNA melting experiments were performed with the prepared oligomers and compared with the results obtained from self-melting curves and the corresponding DNA • DNA duplexes.

In the Appendix, one example of each curve is shown; the averaged T_M data and the f_M values of the particular example curve are collected and discussed in Chapter 6.4.

The following DNA oligonucleotides were used for hybridisation:

DNA targets	
3'-TAATGGGACAATAGGGAT-5'	$^{3'}$**6-G-11**$^{5'}$
3'-TAATGG ACAATAGGGAT-5'	$^{3'}$**6-11**$^{5'}$
3'-ACAATAGG-5'	$^{3'}$**8**$^{5'}$
3'-ACAATAGGGAT-5'	$^{3'}$**11**$^{5'}$
3'-TAATGG-5'	$^{3'}$**6**$^{5'}$

DNA as PNA representatives	
5'-TGTTATCC-3'	$^{5'}$**8**$^{3'}$
5'-TGTTATCCC-3'	$^{5'}$**9**$^{3'}$
5'-TGTTATCCCT-3'	$^{5'}$**10**$^{3'}$
5'-TACCCTGTT-3'	$^{5'}$**4-C-4**$^{3'}$
5'-TTACCCTGTTA-3'	$^{5'}$**5-C-5**$^{3'}$
5'-ATTACCCTGTTAT-3'	$^{5'}$**6-C-6**$^{3'}$
5'-TACC TGTT-3'	$^{5'}$**4-4**$^{3'}$
5'-TTACC TGTTA-3'	$^{5'}$**5-5**$^{3'}$
5'-ATTACC TGTTAT-3'	$^{5'}$**6-6**$^{3'}$

Be careful not to mix $^{3'}$**8**$^{5'}$ and $^{5'}$**8**$^{3'}$ – they are complementary and do NOT represent the same sequence.

Distinguishing between them will be easy in the context of the experiments.

6.3.1 Terminal Sequences

As a comparison, DNA • DNA hybridization experiments were carried out with the following sequences and DNA $^{3'}$**6-G-11**$^{5'}$:

terminal	DNA
5'-TGTTATCC-3'	$^{5'}$**8**$^{3'}$
5'-TGTTATCCC-3'	$^{5'}$**9**$^{3'}$
5'-TGTTATCCCT-3'	$^{5'}$**10**$^{3'}$

For all sequences with and without ligand, melting was investigated for PNA alone (self-melting) and PNA • DNA $^{3'}$**6-G-11**$^{5'}$:

terminal	PNA
Ac-tgttatcc-Lys	^{Ac}**8**^{K}
Ac-tgttatccc-Lys	^{Ac}**9**^{K}
Ac-tgttatccct-Lys	^{Ac}**10**^{K}
tpy*-tgttatcc-Lys	^{tpy}**8**^{K}
tpy*-tgttatccc-Lys	^{tpy}**9**^{K}
tpy*-tgttatccct-Lys	^{tpy}**10**^{K}
bpa*-tgttatcc-Lys	$^{bpa'}$**8**^{K}

In order to examine the influence of a DNA overhang on the hybridization behaviour of the substituted and unsubstituted PNA oligomers, additional melting experiments were undertaken for the following combinations as a comparison:

PNA ^{tpy}**8**^{K} • DNA $^{3'}$**8**$^{5'}$ PNA ^{Ac}**8**^{K} • DNA $^{3'}$**8**$^{5'}$

PNA $^{bpa'}$**8**^{K} • DNA $^{3'}$**8**$^{5'}$ DNA $^{5'}$**8**$^{3'}$ • DNA $^{3'}$**8**$^{5'}$

6.3.2 Central Sequences

6.3.2.1 Unmodified PNA Oligomers

Balasubramanian et al.[81] published results suggesting the hybridization of only one half of the PNA sequence when a central ligand is attached. In order to obtain more information about the influence of an internal disturbing factor on the melting behaviour, melting experiments were performed for all possible combinations of omitted / present central nucleobases within the sequences for central functionalization.

As a comparison, DNA • DNA hybridization experiments were carried out with the following sequences and DNA $^{3'}$**6-G-11**$^{5'}$ & $^{3'}$**6-11**$^{5'}$:

central	DNA
5'-TACCCTGTT-3'	$^{5'}$**4-C-4**$^{3'}$
5'-TTACCCTGTTA-3'	$^{5'}$**5-C-5**$^{3'}$
5'-ATTACCCTGTTAT-3'	$^{5'}$**6-C-6**$^{3'}$
5'-TACC TGTT-3'	$^{5'}$**4-4**$^{3'}$
5'-TTACC TGTTA-3'	$^{5'}$**5-5**$^{3'}$
5'-ATTACC TGTTAT-3'	$^{5'}$**6-6**$^{3'}$

With the following PNA sequences, melting was performed for PNA alone (self-melting), PNA • DNA $^{3'}$**6-G-11**$^{5'}$ and PNA • DNA $^{3'}$**6-11**$^{5'}$:

central	PNA
Ac-taccctgtt-Lys	^{Ac}**4-c-4**^{K}
Ac-ttaccctgtta-Lys	^{Ac}**5-c-5**^{K}
Ac-attaccctgttat-Lys	^{Ac}**6-c-6**^{K}
Ac-tacctgtt-Lys	^{Ac}**4-4**^{K}
Ac-ttacctgtta-Lys	^{Ac}**5-5**^{K}
Ac-attacctgttat-Lys	^{Ac}**6-6**^{K}

6.3.2.2 PNA Oligomers with Central Dipeptide

For all three PNA sequences with an internal GlyPhe unit, T_M curves were determined for PNA alone, PNA • DNA $^{3'}$**6-G-11**$^{5'}$ and PNA • DNA $^{3'}$**6-11**$^{5'}$:

central	**PNA**
Ac-tacc-GlyPhe-tgtt-Lys	^{Ac}**4-GF-4**^{K}
Ac-ttacc-GlyPhe-tgtta-Lys	^{Ac}**5-GF-5**^{K}
Ac-attacc-GlyPhe-tgttat-Lys	^{Ac}**6-GF-6**^{K}

G-rich Sequences

In the presence of TFA, the synthesized guanine rich sequences (^{Ac}**g$_1$-GF-g$_2$**^{K}, ^{Ac}**g$_3$-GF-g$_4$**^{K}) were clearly soluble, but they turned out to be nearly insoluble in phosphate buffer used for hybridization experiments. As a consequence, it was impossible to reach a concentration sufficing for UV-Vis spectroscopy. This fact corresponds to the experience *Nielsen et al.* gained with several PNA sequences;[290] purine rich sequences tend to aggregate despite of the protonation of the amino groups (lysine residues) at neutral pH. In order to rise the G/C content of the sequence, the synthesis of cytosine rich sequences thus should be much more promising.

6.3.2.3 DNA Cleavage Fragments

The basic concept behind the development of cleavage moieties attached to the center of a sequence is its potential catalytic activity based on the assumption that the binding affinity of a PNA•DNA duplex will decrease after the reaction, leading to a dehybridization.[291] In order to investigate this concept, melting experiments were undertaken with "cleaved" DNA oligomers meaning fragments of the target sequence from both sides of the cleavage spot.

The following DNA and PNA sequences were hybridized with both halves of the DNA target ($^{3'}$**6**$^{5'}$ and $^{3'}$**11**$^{5'}$):

central	**DNA**
5'-ATTACCCTGTTAT-3'	$^{5'}$**6-C-6**$^{3'}$
5'-ATTACC TGTTAT-3'	$^{5'}$**6-6**$^{3'}$

central	**PNA**
Ac-attaccctgttat-Lys	^{Ac}**6-c-6**^{K}
Ac-attacctgttat-Lys	^{Ac}**6-6**^{K}
Ac-attacc-GlyPhe-tgttat-Lys	^{Ac}**6-GF-6**^{K}

6.3.2.4 PNA Sequences with Central Ligand

The internally functionalized PNA oligomers (**^{Ac}4-GF^{tpy}-4^{K}**, **^{Ac}5-GF^{tpy}-5^{K}**, **^{Ac}6-GF^{tpy}-6^{K}**, **^{Ac}4-GF^{bpa}-4^{K}**, **^{Ac}5-GF^{bpa}-5^{K}**) turned out to be insoluble in buffer, although they did not resist being purified by HPLC in aqueous TFA/acetonitrile.

Several attempts were undertaken to examine the hybridization properties of these compounds (because the next step would have been to let them cleave DNA). A change of pH was out of the question; protonation of the DNA templates would have prevented significant results. A well-known way to get badly soluble oligonucleotides into solution is the addition of DMSO (the changing solvent effect could have been neglected). All compounds were clearly soluble in pure DMSO, but after adding one single drop of water (which is inevitable for hybridization because of the hydration equilibrium), the oligomers precipitated immediately.

This deficiency could be remedied by adding more lysine residues to the oligomer chain; an increased solubility could be achieved by this means.

Future research will be headed towards this direction.

6.4 Results

In this Chapter, only the data is discussed (apart from some examples); for plots of the particular melting curves, please refer to the Appendix.

6.4.1 Overview

Terminal

Tab. 6.2: *Overview of Melting Data for Terminal Sequences with DNA*

T_M[°C]±SD (f_M)	self-melting	• DNA $^{3'}$6-G-11$^{5'}$	• DNA $^{3'}$8$^{5'}$
PNA ^{Ac}8^{K}	31.3 (0.18)	27.6±0.1 (1.21)	18.2±0.3 (1.27)
PNA ^{tpy}8^{K}	44.4 (0.08)	38.4±0.3 (1.01)	24.8±0.4 (0.81)
PNA $^{bpa'}$8^{K}	n.o.	29.7±0.3 (1.54)	22.3±0.7 (1.38)
DNA $^{5'}$8$^{3'}$	n.m.	27.9±0.3 (2.06)	23.2±0.4 (1.86)
PNA ^{Ac}9^{K}	49.2 (0.20)	38.9±0.1 (1.80)	n.m.
PNA ^{tpy}9^{K}	49.9 (0.05)	46.8±0.2 (0.73)	n.m.
DNA $^{5'}$9$^{3'}$	n.m.	38.1±0.02 (2.76)	n.m.
PNA ^{Ac}10^{K}	29.0 (0.10)	43.8±0.4 (1.74)	n.m.
PNA ^{tpy}10^{K}	45.6 (0.15)	50.0±0.2 (1.76)	n.m.
DNA $^{5'}$10$^{3'}$	n.m.	41.8±0.1 (3.33)	n.m.

(n.m. = not measured; n.o. = not observed)

Central

Tab. 6.3: *Overview of Melting Data for Central Sequences with DNA Fragments*

T_M[°C]±SD (f_M)	• DNA $^{3'}6^{5'}$	• DNA $^{3'}11^{5'}$
PNA ^{Ac}6-c-6^{K}	44.0±0.1 (0.28)	44.3±2.6 (0.40)
DNA $^{5'}$6-C-6$^{3'}$	(22.7) (0.29)	(26.0) (0.36)
PNA ^{Ac}6-6^{K}	44.0±1.0 (0.20)	48.2±1.3 (0.32)
DNA $^{5'}$6-6$^{3'}$	(~4) (n.o.)	(33.3) (0.14)
PNA ^{Ac}6-GF-6^{K}	40.4±0.1 (0.26)	41.2±1.1 (0.68)

Tab. 6.4: *Overview of Melting Data for Central Sequences with DNA*

T_M[°C]±SD (f_M)	self-melting	• DNA $^{3'}$6-G-11$^{5'}$	• DNA $^{3'}$6-11$^{5'}$
PNA ^{Ac}4-c-4^{K}	40.2 (0.10)	41.8±0.5 (0.94)	18.6±1.0 (0.25)
DNA $^{5'}$4-C-4$^{3'}$	n.m.	34.2±0.2 (2.62)	13.1±0.1 (1.00)
PNA ^{Ac}4-4^{K}	n.o.	24.3±1.6 (0.54)	25.1±0.02 (0.81)
DNA $^{5'}$4-4$^{3'}$	n.m.	(~17) (1.91)	26.1±0.1 (1.86)
PNA ^{Ac}4-GF-4^{K}	22.0 (0.21)	(~31) (0.29)	11.0±0.1 (0.59)
PNA ^{Ac}5-c-5^{K}	39.1 (0.21)	47.4±0.3 (1.28)	29.9±2.8 (0.44)
DNA $^{5'}$5-C-5$^{3'}$	n.m.	41.1±0.2 (3.32)	23.4±0.3 (1.96)
PNA ^{Ac}5-5^{K}	56.0 (0.15)	29.4±1.6 (1.11)	35.3±0.1 (1.07)
DNA $^{5'}$5-5$^{3'}$	n.m.	23.5±0.5 (1.86)	34.5±0.1 (3.45)
PNA ^{Ac}5-GF-5^{K}	23.7 (0.35)	(~27) (0.47)	21.5±0.1 (1.41)
PNA ^{Ac}6-c-6^{K}	47.5 (0.25)	52.1±0.2 (2.55)	28.7±0.5 (0.42)
DNA $^{5'}$6-C-6$^{3'}$	n.m.	47.4±0.1 (5.94)	32.9±0.1 (3.97)
PNA ^{Ac}6-6^{K}	48.2 (0.53)	35.0±0.7 (0.99)	43.2±0.2 (1.59)
DNA $^{5'}$6-6$^{3'}$	n.m.	33.3±0.1 (3.96)	42.2±0.1 (4.88)
PNA ^{Ac}6-GF-6^{K}	44.2 (0.29)	(~33) (0.40)	30.7±0.2 (1.50)

(n.m. = not measured; n.o. = not observed)

6.4.2 Self-Melting

In Chapter 6.2, the aspect of significance was mentioned, and the coefficients f_M and q_M were introduced. On the basis of the obtained T_M data, the self-melting effect will be elaborated. Tab. 6.5 and Tab. 6.6 show the self-melting data of the PNA oligomers and the melting temperatures of the particular PNA • DNA duplexes, including the f_M values, written in brackets. The difference in T_M and the ratio between f_M^{ds} and f_M^{sm} (q_M) are indicated, providing information concerning the significance of a melting curve in comparison to the PNA single strand self-melting.

Tab. 6.5: *Terminal PNA Sequences – Self-Melting and Hybridization Data*

PNA	T_M^{sm} (f_M^{sm})	• DNA $^{3'}$6-G-11$^{5'}$ T_M^{ds} (f_M^{ds})	$\Delta T^{sm/ds}$ (q_M)	• DNA $^{3'}$8$^{5'}$ T_M^{ds} (f_M^{ds})	$\Delta T^{sm/ds}$ (q_M)
^{Ac}**8**^{K}	31.3 (0.18)	27.6 (1.21)	-3.7 (6.7)	18.2 (1.27)	-13.1 (7.1)
^{tpy}**8**^{K}	44.4 (0.08)	38.4 (1.01)	-6.0 (12.6)	24.8 (0.81)	-19.6 (10.1)
^{Ac}**9**^{K}	49.2 (0.20)	38.9 (1.80)	-10.3 (9.0)	n.m.	/
^{tpy}**9**^{K}	49.9 (0.05)	46.8 (0.73)	-3.1 (14.6)	n.m.	/
^{Ac}**10**^{K}	29.0 (0.10)	43.8 (1.74)	14.8 (17.4)	n.m.	/
^{tpy}**10**^{K}	45.6 (0.15)	50.0 (1.76)	4.4 (11.7)	n.m.	/

For terminal oligomers, f_M^{ds} significantly differs from f_M^{sm} (f_M^{ds} ranges from 0.73-1.80, f_M^{sm} from 0.05-0.20). As a consequence, q_M has values of 6.7-14.6 and increases with growing chain length. $\Delta T^{sm/ds}$ does not provide any information about stability; it differs as the case arises and is invalid as long as T_M^{sm} is not significant according to the corresponding f_M values. It can be concluded that melting in fact takes place, and q_M of more than 5-6 can be regarded as significant.

Tab. 6.6: *Central PNA Sequences – Self-Melting and Hybridization Data*

PNA	T_M^{sm} (f_M^{sm})	•DNA 3'6-G-11 5' T_M^{ds} (f_M^{ds})	$\Delta T^{sm/ds}$ (q_M)	•DNA 3'6-11 5' T_M^{ds} (f_M^{ds})	$\Delta T^{sm/ds}$ (q_M)
^{Ac}**4-c-4**^{K}	40.2 (0.10)	41.8 (0.94)	1.6 (9.4)	18.6 (0.25)	-21.6 (2.5)
^{Ac}**4-4**^{K}	n.o.	24.3 (0.54)	/	25.1 (0.81)	/
^{Ac}**4-GF-4**^{K}	22.0 (0.21)	(~31) (0.29)	(9.0) (1.4)	11.0 (0.59)	-11.0 (2.8)
^{Ac}**5-c-5**^{K}	39.1 (0.21)	47.4 (1.28)	8.3 (6.1)	29.9 (0.44)	-9.2 (2.1)
^{Ac}**5-5**^{K}	56.0 (0.15)	29.4 (1.11)	26.6 (7.4)	35.3 (1.07)	-20.7 (7.1)
^{Ac}**5-GF-5**^{K}	23.7 (0.35)	(~27) (0.47)	(3.3) (1.3)	21.5 (1.41)	-2.2 (4.0)
^{Ac}**6-c-6**^{K}	47.5 (0.25)	52.1 (2.55)	4.6 (10.2)	28.7 (0.42)	-18.8 (1.7)
^{Ac}**6-6**^{K}	48.2 (0.53)	35.0 (0.99)	-13.2 (1.9)	43.2 (1.59)	-5.0 (3.0)
^{Ac}**6-GF-6**^{K}	44.2 (0.29)	(~33) (0.40)	(11.2) (1.4)	30.7 (1.50)	-13.5 (5.2)

Similar to the terminal sequences, the self-melting temperatures of the central PNA single strands appear to be coincidental. The f_M^{sm} values are higher than the terminal ones (0.10-0.53), which can be explained by partial self-complementarity. An antiparallel hybridization of two similar PNA strands e.g. for ^{Ac}**6-c-6**^{K} shows eight matches that increase the stability of the duplex, albeit they form double matches that are not adjacent to each other (and therefore not cooperative). Eight separated complements in a strand are not sufficient for the self-aggregation of PNA, but obviously intensify the self-melting effect. f_M^{sm} increases with growing chain length, because more matches are present:

Lys- t a t t g t c c c a t t a -Ac
Ac- a t t a c c c t g t t a t -Lys

^{Ac}**6-C-6**^{K}

For the terminal sequences, only four matches can be expected:

Lys- t c c c t a t t g t -Ac
Ac- t g t t a t c c c t -Lys

^{Ac}**10**^{K}

As a consequence for the central sequences, f_M^{sm} increases, and q_M is smaller on average, reaching from 1.4-10.2. As a preliminary conclusion, it can be stated that f_M can at the most serve for comparison, and should be carefully used as an absolute value.

6.4.3 Terminal Sequences

Comparison of Chain Lengths

With increasing length, the melting temperature of oligonucleotide duplexes usually rises, because more base pairs cooperatively contribute to the overall stability.
Tab. 6.7 shows that for PNA and DNA, the increase in T_M between 8- and 9mers is approximately twice as high as between 9- and 10mers. The f_M values tendentially increase with the chain length.

Tab. 6.7: *Comparison of Terminal Chain Lengths*

• DNA $^{3'}$6-G-11$^{5'}$	T_M[°C] (f_M)	ΔT_M
PNA ^{Ac}8^{K}	27.6 (1.21)	11.3
PNA ^{Ac}9^{K}	38.9 (1.80)	4.9
PNA ^{Ac}10^{K}	43.8 (1.74)	
PNA ^{tpy}8^{K}	38.4 (1.01)	8.4
PNA ^{tpy}9^{K}	46.8 (0.73)	3.2
PNA ^{tpy}10^{K}	50.0 (1.76)	
DNA $^{5'}$8$^{3'}$	27.9 (2.06)	10.2
DNA $^{5'}$9$^{3'}$	38.1 (2.76)	3.7
DNA $^{5'}$10$^{3'}$	41.8 (3.33)	

Comparison of PNA and DNA

Tab. 6.8: *Comparison of Terminal PNA and DNA With (left) and Without Overhang (right)*

T_M[°C]	• DNA $^{3'}$6-G-11$^{5'}$			• DNA $^{3'}$8$^{5'}$		
	DNA	**PNA**	**ΔT_M**	**DNA**	**PNA**	**ΔT_M**
$^{5'}$**8**$^{3'}$ / ^{Ac}**8**^{K}	27.9	27.6	-0.3	23.2	18.2	-5.0
$^{5'}$**8**$^{3'}$ / ^{tpy}**8**^{K}	27.9	38.4	**10.5**	23.2	24.8	1.6
$^{5'}$**8**$^{3'}$ / ^{bpa}**8**^{K}	27.9	29.7	1.8	23.2	22.3	-0.9
$^{5'}$**9**$^{3'}$ / ^{Ac}**9**^{K}	38.1	38.9	0.8	n.m.	n.m.	n.m.
$^{5'}$**9**$^{3'}$ / ^{tpy}**9**^{K}	38.1	46.8	**8.7**	n.m.	n.m.	n.m.
$^{5'}$**10**$^{3'}$ / ^{Ac}**10**^{K}	41.8	43.8	2.0	n.m.	n.m.	n.m.
$^{5'}$**10**$^{3'}$ / ^{tpy}**10**^{K}	41.8	50.0	**8.2**	n.m.	n.m.	n.m.

Compared to DNA • DNA duplexes, PNA • DNA hybrids in general show a higher stability because of the lack of charge repulsion due to the neutral PNA backbone. In fact, this can be affirmed in line with the results displayed in Tab. 6.8. Some examples show a lower T_M for PNA • DNA. This is in the range of measuring inaccuracies, which are probable especially for short sequences with low T_M values. The acetylated PNA oligomers display only small ΔT_M, which might be explainable by a repulsive and destabilizing effect of the acetyl group. This effect decreases with growing chain length, because the attractive influence of the double strand gets the upper hand.

In the case of tpy-substitution, the melting temperatures show a more significant increase of T_M relative to the corresponding DNA • DNA values in comparison to acetylated oligomers ($\varnothing$=9.1°C). This leads to the conclusion that terpyridine must have a stabilizing effect on the particular duplex which is not observed in the case of bpa. The complementary DNA sequence without overhang (DNA $^{3'}$**8**$^{5'}$) does not reveal this result, so that a single strand effect can be reasoned – an overhang should not cause any difference if tpy-interaction with the PNA • DNA double strand (groove binding) took place. On the other hand, the stabilizing effect of lysine is not present any more. In contrast to repulsion, stabilizing interactions decrease with growing chain length, as in this case.

Comparison of Substitution

As shown on the basis of Tab. 6.8, a terminal tpy ligand seems to have a stabilizing effect on the PNA•DNA duplex in comparison with DNA•DNA melting experiments. This is confirmed by regarding ΔT_M of different substituents (Tab. 6.9). Furthermore, the influence of an overhang of target DNA was examined by performing melting experiments with DNA $^{3'}\mathbf{8}^{5'}$.

Tab. 6.9: *Comparison of Terminally Substituted Sequences*

T_M[°C] PNA•DNA	**x=Ac**	**x=tpy**	**ΔT_M**
$^{x}\mathbf{8}^{K}\bullet{}^{3'}\mathbf{6\text{-}G\text{-}11}^{5'}$	27.6	38.4	**10.8**
$^{x}\mathbf{9}^{K}\bullet{}^{3'}\mathbf{6\text{-}G\text{-}11}^{5'}$	38.9	46.8	**7.9**
$^{x}\mathbf{10}^{K}\bullet{}^{3'}\mathbf{6\text{-}G\text{-}11}^{5'}$	43.8	50.0	**6.2**
$^{x}\mathbf{8}^{K}\bullet{}^{3'}\mathbf{8}^{5'}$	18.2	24.8	6.6

T_M[°C] PNA•DNA	**x=Ac**	**x=bpa**	**ΔT_M**
$^{x}\mathbf{8}^{K}\bullet{}^{3'}\mathbf{6\text{-}G\text{-}11}^{5'}$	27.6	29.7	2.1
$^{x}\mathbf{8}^{K}\bullet{}^{3'}\mathbf{8}^{5'}$	18.2	22.3	4.1

T_M[°C] PNA•DNA	**x=bpa**	**x=tpy**	**ΔT_M**
$^{x}\mathbf{8}^{K}\bullet{}^{3'}\mathbf{6\text{-}G\text{-}11}^{5'}$	29.7	38.4	8.7
$^{x}\mathbf{8}^{K}\bullet{}^{3'}\mathbf{8}^{5'}$	22.3	24.8	2.5

The stabilizing effect of tpy in comparison to a terminal acetyl group is much higher than for bpa. Again, ΔT_M decreases with growing chain length, representing the evanescent influence in comparison to the attractive base-pairing interaction. In addition to that, the overhang interacting with the lysine residue becomes shorter. The difference between the T_Ms of bpa- and tpy-substituted sequences is *inter alia* explainable by the enhanced flexibility of the tpy-linker in contrast to the more rigid bpaBzl, so that the stabilizing effect of bpa is reduced to its electrostatic interaction with the DNA phosphate backbone due to protonation of the pyridine nitrogen atoms.

Comparison of DNA $^{3'}$**6-G-11**$^{5'}$ and DNA $^{3'}$**8**$^{5'}$ (Overhang Influence)

Tab. 6.10: *Terminal DNA Targets With and Without Overhang*

T_M[°C]	• DNA $^{3'}$6-G-11$^{5'}$	• DNA $^{3'}$8$^{5'}$	ΔT_M
PNA ^{Ac}8^{K}	27.6	18.2	-9.4
PNA ^{tpy}8^{K}	38.4	24.8	**-13.6**
PNA ^{bpa}8^{K}	29.7	22.3	-7.4
DNA $^{5'}$8$^{3'}$	27.9	23.2	-4.7

Similar to the observed effect whether a DNA overhang is present or not, the increase of stability of the bpa-PNA duplex in comparison to the Ac-PNA can be explained by electrostatic attractions similar to those between Lys residues and the complementary DNA strand. In the case of terpyridine, this circumstance is not sufficient enough to elucidate a ΔT_M of more than 10°C. Intercalation (which is, *per definitionem*, the insertion of molecules between the stacked nucleobases of double stranded DNA) by terpyridine is only known from its metal complexes (Pt(II), Ru(II)) which insert one of their ligands between two base pairs.[292-294] In addition, intercalation usually leads to destabilization of double strands, not to an increase of melting temperature. A valid explanation for the enhanced binding affinity of tpy-PNA could be the π-stacking of its pyridine rings between the nucleobases of the overhanging DNA single strand which is, certainly, a kind

of intercalation. This interaction takes place in the single strand region, because a missing overhang has a significant influence. The attractive interaction of the ligand with the complementary strand is promoted, because the partners are already close to each other due to the hybridization of the particular strands.

Intercalation usually is favoured for large π-systems. For example, ethidium bromide (Fig. 6.10), the prime intercalator example, possesses an expanded aromatic ring system which enables it to interact with and thus stack between nucleobases. In the case of terpyridine, this π-system is combined with an enhanced flexibility which enables the intercalator to adapt to a binding pocket. A model for the intercalation of an internally linked intercalator is shown in Fig. 6.11.

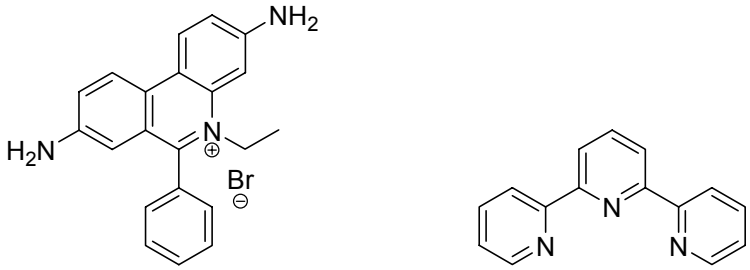

Fig. 6.10: *Structures of the Intercalators Ethidium Bromide and Terpyridine*

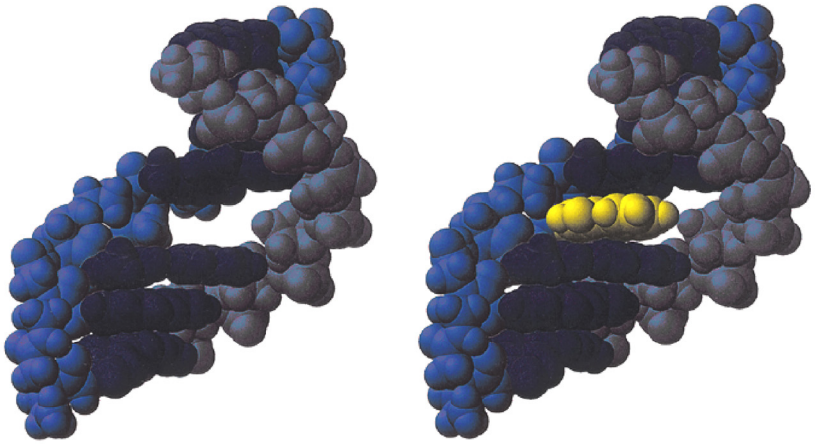

Fig. 6.11: *Intercalation of Anthraquinone into a PNA:DNA Double Strand*[155]

6.4.4 Central Sequences

In Tab. 6.11 and Tab. 6.12, only the fully complementary data is displayed; partial non-complementarity should not be taken into account in this context and will be discussed later.

Comparison of Chain Lengths

Tab. 6.11: *Comparison of Central Chain Lengths*

• DNA $^{3'}$**6-G-11**$^{5'}$	T_M[°C]	ΔT_M	• DNA $^{3'}$**6-11**$^{5'}$	T_M[°C]	ΔT_M
PNA ^{Ac}**4-c-4**^{K}	41.8	5.6	**PNA** ^{Ac}**4-4**^{K}	25.1	10.2
PNA ^{Ac}**5-c-5**^{K}	47.4		**PNA** ^{Ac}**5-5**^{K}	35.3	
PNA ^{Ac}**6-c-6**^{K}	52.1	4.5	**PNA** ^{Ac}**6-6**^{K}	43.2	7.9
DNA $^{5'}$**4-C-4**$^{3'}$	34.2	6.9	**DNA** $^{5'}$**4-4**$^{3'}$	26.1	8.4
DNA $^{5'}$**5-C-5**$^{3'}$	41.1		**DNA** $^{5'}$**5-5**$^{3'}$	34.5	
DNA $^{5'}$**6-C-6**$^{3'}$	47.4	6.3	**DNA** $^{5'}$**6-6**$^{3'}$	42.2	7.7

For the central sequences, the increase of T_M is similar in nearly all cases and as high as for the terminal sequences, although the number of base pairs is each time raised by two. For DNA $^{3'}$**6-11**$^{5'}$, the differences are higher.

Comparison of PNA and DNA

Tab. 6.12: *Comparison of Central PNA and DNA With and Without Guanine*

T_M[°C]	• DNA $^{3'}$6-G-11$^{5'}$		
	DNA	**PNA**	**ΔT_M**
$^{5'}$4-C-4$^{3'}$ / ^{Ac}4-c-4^{K}	**34.2**	**41.8**	**7.6**
$^{5'}$5-C-5$^{3'}$ / ^{Ac}5-c-5^{K}	**41.1**	**47.4**	**6.3**
$^{5'}$6-C-6$^{3'}$ / ^{Ac}6-c-6^{K}	**47.4**	**52.1**	**4.7**

T_M[°C]	• DNA $^{3'}$6-11$^{5'}$		
	DNA	**PNA**	**ΔT_M**
$^{5'}$4-4$^{3'}$ / ^{Ac}4-4^{K}	**26.1**	**25.1**	**-1.0**
$^{5'}$5-5$^{3'}$ / ^{Ac}5-5^{K}	**34.5**	**35.3**	**0.8**
$^{5'}$6-6$^{3'}$ / ^{Ac}6-6^{K}	**42.2**	**43.2**	**1.0**

The fully matching sequences show a difference of ~5-8°C for DNA $^{3'}$**6-G-11**$^{5'}$ and nearly no difference for DNA $^{3'}$**6-11**$^{5'}$ (±1°C). Nevertheless, a decrease of ΔT_M is observed in the first case and an increase in the second one.

Comparison of Cleavage Fragments

In order to prove that after a hypothetical oligonucleotide cleavage, the fragments will dehybridize again to release the PNA conjugate for further turnovers in a catalytic sense, both halves of the DNA target were investigated.

Tab. 6.13: *Comparison of Cleavage Fragments*

T_M[°C] (q_M)	• DNA $^{3'}\mathbf{6}^{5'}$	• DNA $^{3'}\mathbf{11}^{5'}$
PNA ^{Ac}6-c-6^{K}	44.0 (1.1)	44.3 (1.6)
PNA ^{Ac}6-6^{K}	44.0 (0.4)	48.2 (0.6)
PNA ^{Ac}6-GF-6^{K}	40.4 (0.9)	41.2 (2.3)

At first glance, one could conclude that even with the short sequences, melting takes place, because a melting profile is observed. Concerning the shape of the melting curves (see Appendix), represented by f_M, those conclusion is disproved, because the observed sigmoidality must be only due to self-melting (similar f_M values; q_M~1). In addition, the corresponding DNA • DNA experiments (not indicated in Tab. 6.13) showed no melting at all. Furthermore, the overhang only present in the case of DNA $^{3'}\mathbf{11}^{5'}$ does not make any difference in melting behaviour, compared to DNA $^{3'}\mathbf{6}^{5'}$ (without overhang). It can be concluded that after an assumed cleavage, the fragments would dehybridize again, and centrally derivatized PNA oligomers can be used as catalyst for DNA cleavage.

Internal Modifications – Bulge Formation

For some central sequences, internal modifications were carried out, comprising the omission of one central nucleobase and incorporation of a dipeptidic abasic site, so that destabilization of the duplexes is expected. As a matter of fact, all those changes are reflected in a decrease of q_M in comparison to a fully matching duplex.
On this occasion, the observations will be discussed considering the melting curves.

The first example depicts the influence of a PNA bulge on the hybridization (Fig. 6.12).

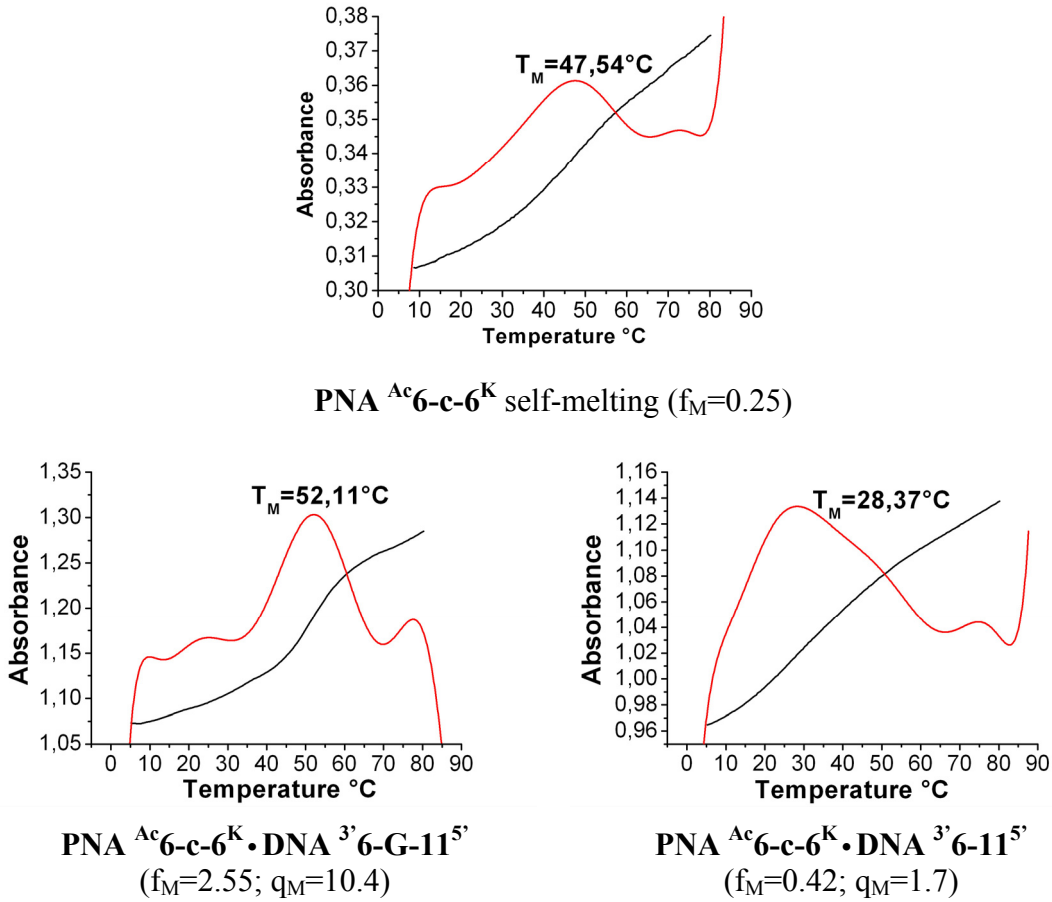

PNA ^{Ac}6-c-6^{K} self-melting (f_M=0.25)

PNA ^{Ac}6-c-6^{K} • DNA $^{3'}$6-G-11$^{5'}$
(f_M=2.55; q_M=10.4)

PNA ^{Ac}6-c-6^{K} • DNA $^{3'}$6-11$^{5'}$
(f_M=0.42; q_M=1.7)

Fig. 6.12: *Influence of a PNA Bulge on Hybridization*

The self-melting curve of PNA ^{Ac}**6-c-6**^{K} shows a sigmoidal shape and an f_M value of 0.25. As one can clearly see at first glance, this oligomer hybridizes with the complementary DNA like a textbook example. Don't be confused by the deceiving shape of the self-melting curve – it looks more sigmoidal than it is, because its hyperchromic offset is much lower than in the case of a duplex experiment. This is reflected by f_M of the matching experiment which is more than ten times higher in comparison to self-melting (q_M=10.4). In contrast to that, a DNA gap (in other words: PNA bulge) leads to a decrease of T_M and q_M at the same time.

The converse experiment was carried out with a DNA bulge, and the results turned out to be *vice versa*; the DNA bulge (PNA gap) is tolerated, but leads to a significant decrease of stability. Again, it must be concluded that considering f_M and q_M may only serve as a comparison as the case arises.

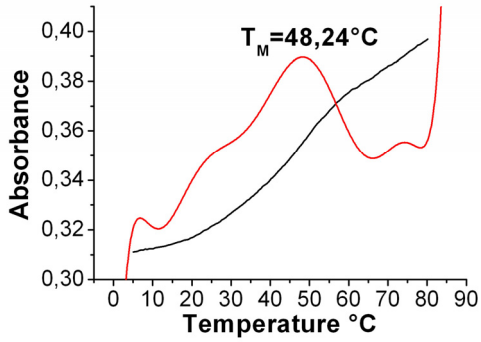

PNA ^{Ac}6-6^{K} self-melting (f_M=0.53)

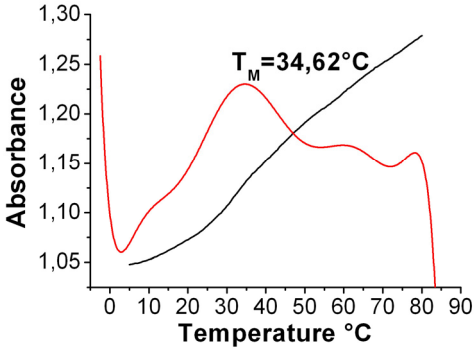

PNA ^{Ac}6-6^{K} • DNA $^{3'}$6-G-11$^{5'}$
(f_M=0.99; q_M=1.9)

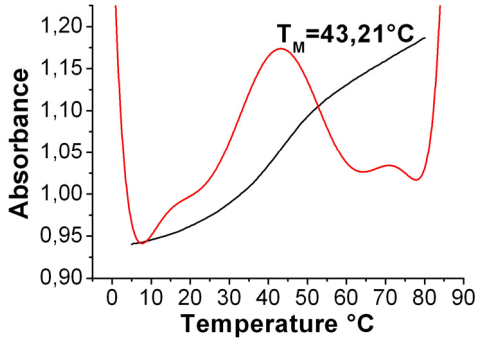

PNA ^{Ac}6-6^{K} • DNA $^{3'}$6-11$^{5'}$
(f_M=1.59; q_M=3.0)

Fig. 6.13: *Influence of a DNA Bulge on Hybridization*

In the case of an internal dipeptide spacer as an abasic site, the experiments with the complementary DNA sequences resulted in nearly linear absorbance curves (see Appendix). Depending on the data range used for the derivative, the curves appeared in a completely different shape, although maxima are obtained. This was an important hint for the dubiety of a mere melting temperature without taking the shape into account. This point has been already discussed elaborately in Chapter 6.2.

The shape of the melting curves (see Appendix) and the random values of the melting temperature lead to the conclusion that no hybridization has taken place at all. Reflecting on the influence of the amino acids preventing the single strands from hybridization lead to the idea of omitting the corresponding nucleobases in the DNA sequence in order to investigate if a bulge formation is taking place. One example of these experiments is displayed in Fig. 6.14 (the same curves already were shown in Chapter 6.2).

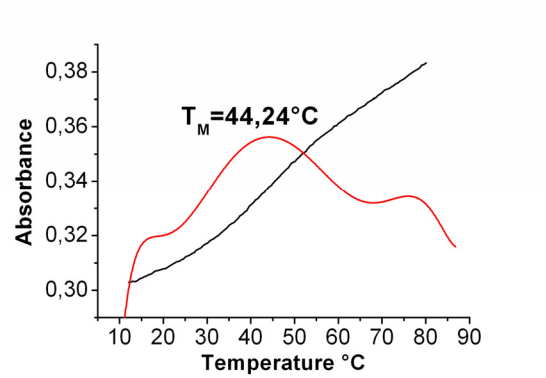

PNA ^{Ac}6-GF-6^{K} self-melting (f_M=0.29)

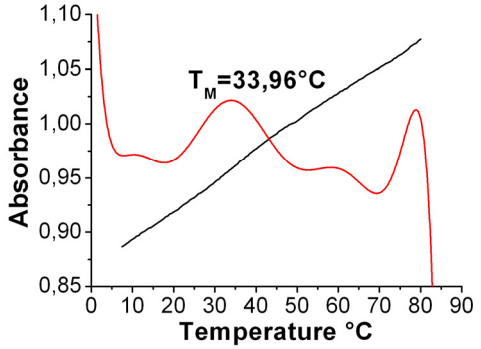

PNA ^{Ac}6-GF-6^{K}•DNA $^{3'}$6-G-11$^{5'}$
(f_M=0.40; q_M=1.4)

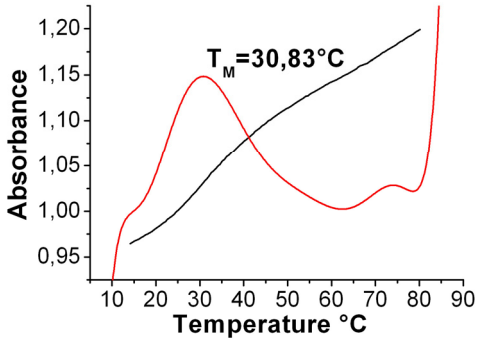

PNA ^{Ac}6-GF-6^{K}•DNA $^{3'}$6-11$^{5'}$
(f_M=1.50; q_M=5.1)

Fig. 6.14: *Influence of a Dipeptide Bulge on Hybridization*

Concerning the q_M values of the two melting experiments, the toleration of the dipeptide bulge is obvious. The higher melting temperature for PNA ^{Ac}**6-GF-6^{K}** • DNA $^{3'}$**6-G-11$^{5'}$** is voted down by the higher q_M for PNA ^{Ac}**6-GF-6^{K}** • DNA $^{3'}$**6-11$^{5'}$**.

The observations were similar for all other chain lengths. Both for PNA- and DNA bulges, a decrease of T_M was measured, although the bulge q_M values indicate an improper melting. The pretended decrease of stability for the dipeptide bulges is disproved by considering f_M and q_M.

Tab. 6.14: *Destabilization by a PNA Bulge*

T_M[°C] (q_M)	**• DNA $^{3'}$6-G-11$^{5'}$**	**• DNA $^{3'}$6-11$^{5'}$**		**• DNA $^{3'}$6-11$^{5'}$**		
PNA	**^{Ac}x-c-x^{K}**		**ΔT_M**	**^{Ac}x-x^{K}**	**^{Ac}x-c-x^{K}**	**ΔT_M**
x=4	41.8 (9.4)	18.6 (2.5)	-23.2	25.1 (/)	18.6 (2.5)	-6.5
x=5	47.4 (6.1)	29.9 (2.1)	-17.5	35.3 (7.1)	29.9 (2.1)	-5.4
x=6	52.1 (10.2)	28.7 (1.7)	-23.4	43.2 (3.0)	28.7 (1.7)	-14.5

Tab. 6.15: *Destabilization by a DNA Bulge*

T_M[°C] (q_M)	**• DNA $^{3'}$6-11$^{5'}$**	**• DNA $^{3'}$6-G-11$^{5'}$**		**• DNA $^{3'}$6-G-11$^{5'}$**		
PNA	**^{Ac}x-x^{K}**		**ΔT_M**	**^{Ac}x-c-x^{K}**	**^{Ac}x-x^{K}**	**ΔT_M**
x=4	25.1 (/)	24.3 (/)	-0.8	41.8 (9.4)	24.3 (/)	-17.5
x=5	35.3 (7.1)	29.4 (7.4)	-5.9	47.4 (6.1)	29.4 (7.4)	-18.0
x=6	43.2 (3.0)	35.0 (1.9)	-8.2	52.1 (10.2)	35.0 (1.9)	-17.1

Tab. 6.16: *Stabilization by a Dipeptide Bulge*

T_M[°C] (q_M)	**• DNA $^{3'}$6-G-11$^{5'}$**	**• DNA $^{3'}$6-11$^{5'}$**		**• DNA $^{3'}$6-11$^{5'}$**		
PNA	**^{Ac}x-GF-x^{K}**		**ΔT_M**	**^{Ac}x-x^{K}**	**^{Ac}x-GF-x^{K}**	**ΔT_M**
x=4	(~31) (1.4)	11.0 (2.8)	(-20)	25.1 (/)	11.0 (2.8)	-14.1
x=5	(~27) (1.3)	21.5 (4.0)	(-5.5)	35.3 (7.1)	21.5 (4.0)	-13.8
x=6	(~33) (1.4)	30.7 (5.2)	(-2.3)	43.2 (3.0)	30.7 (5.2)	-12.5

6.5 Summary

Due to the doubtful consideration of duplex melting temperatures without any ancillary information, the first task in this project was to develop an objective and comparable criterion for the significance of (de)hybridization experiments.
The ratio between height and full width at half maximum f_M was shown to correlate well with the sigmoidality of a first derivative melting curve and therefore can be consulted for comparison. The effect of PNA self-melting was included into these thoughts, and the coefficient q_M was established to distinguish between this effect and real duplex formation. Partial self-complementarity was found to contribute to the mere stacking aspect of self-melting.

Melting experiments were undertaken with the PNA oligomers described in Chapter 5 and miscellaneous DNA targets. As a comparison, DNA•DNA hybrids were investigated, as well. To summarize the vast number of data discussed in this Chapter, the following main aspects can be concluded:

- As known from literature, PNA•DNA duplexes show higher melting temperatures than the corresponding DNA•DNA duplexes.
- An increase of chain length increases the melting temperature as expected.
- Terminally PNA-bound terpyridine was found to intercalate in the single strand region of DNA and is therefore able to stabilize PNA•DNA duplexes.
- The sequences with internal functionalization are suitable for potential catalytic nuclease activity, because target fragments will dehybridize after cleavage.
- The destabilizing impact of an internal abasic site, consisting of a dipeptide spacer, can be compensated by the omitting of its DNA counterpart nucleobase. The formation of a bulge structure by the amino acids can be assumed.

7 Conclusion & Outlook

One of the most important actions in the context of replication *in vivo* and genetic engineering *in vitro* is the cutting of genes. The genetic information in every living organism is located in the DNA, whose oligonucleotide sequence encodes the structure of enzymes and peptides in general as a blueprint. In nature, the cleavage is performed by nucleases, catalytically hydrolyzing the phosphodiester backbone of the DNA. Often, metal atoms are involved in that process.

In a biotechnological laboratory, the cutting of oligonucleotides is carried out with restriction enzymes, isolated from bacteria. The limitation of those biotools to certain promoter sequences strongly demands the development of universal, artificial nucleases which are able to act at any desired sequence. Such a construct should consist of two main parts: a recognition domain and a cleavage domain.

The aim of this Thesis was the development of new ligand systems being able to bind copper ions, which is predestined as a catalytic metal center for oligonucleotide hydrolysis. In order to act in a sequence-specific way, PNA (peptide nucleic acid), a DNA mimic with a pseudopeptide backbone, was chosen to be connected to the ligand moiety. The ligands terpyridine, bis-picolylamine and phenanthroline (Fig. 7.1), which are known to cleave phosphodiester bonds in collaboration with copper, were functionalized in order to enable them to be incorporated into solid phase peptide synthesis (SPPS), which is the method of choice to generate a desired PNA sequence. The ligands were obtained in high purity and good yield, and characterized by NMR and MS techniques.

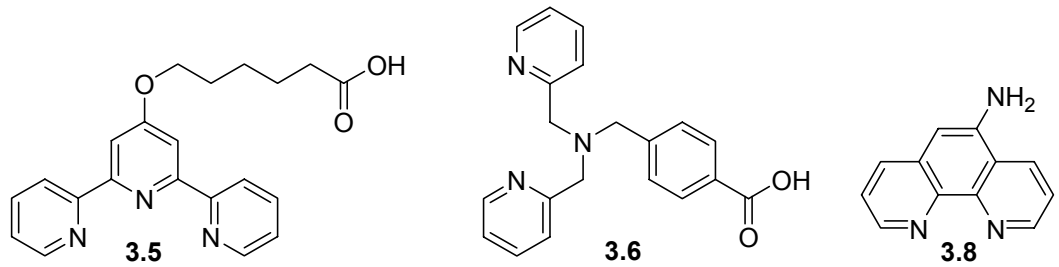

Fig. 7.1: *Overview of Functionalized Nitrogen Ligands*

The suitability of the ligands **3.5** and **3.6** for their coupling to amino groups was shown by the synthesis of conjugates with the amino acid phenylalanine. Furthermore, the ligands could be successfully connected to the peptide pseudoneurotensin, which may provide new metal markers for diagnosis and therapy (Fig. 7.2).

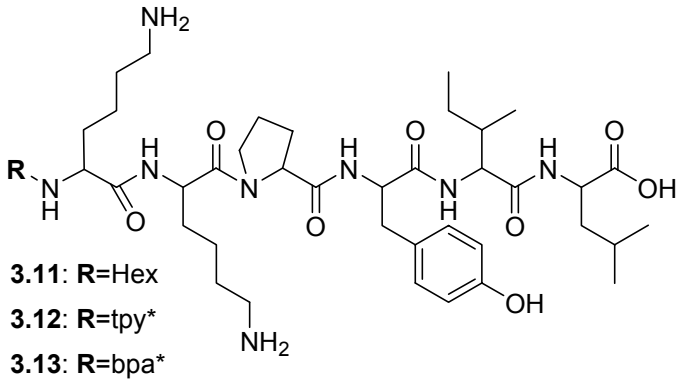

Fig. 7.2: *Pseudoneurotensin Conjugates*

Copper complexes of the free ligands and their conjugates were synthesized, and mass spectrometry revealed their ability to bind the metal center selectively in their nitrogen binding pockets. In order to obtain detailed information about the binding modes of these compounds, the particular conjugates were titrated with copper, measuring the change of absorbance in UV-Vis. These experiments disclosed different binding modes of the ligands; terpyridine was shown to form bivalent complexes with two ligands complexing one copper center (Fig. 7.3, left; Fig. 7.4). This was not observed for the peptide conjugate of this ligand (Fig. 7.3, right), so that incorporation into PNA oligomers seemed to be reasonable, as well. In the case of bis-picolylamine, the bivalent complex was formed irreversibly even with the peptide conjugate (Fig. 7.5; Fig. 7.6).

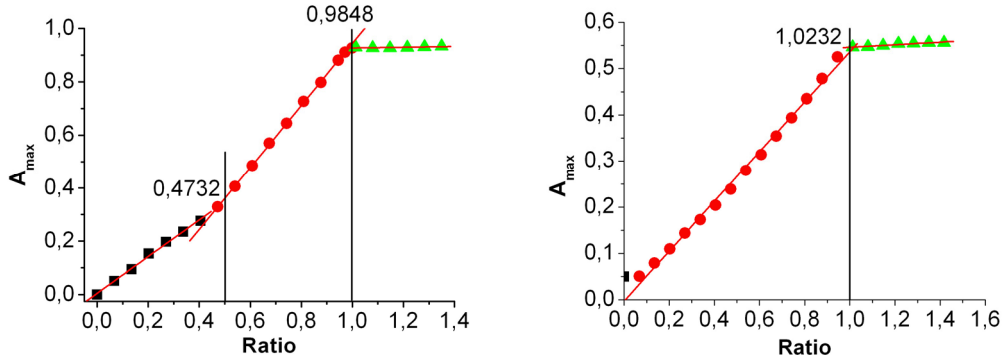

Fig. 7.3: *UV-Vis Copper Titration Curves for* ***3.5*** *(left) and* ***3.12*** *(right)*

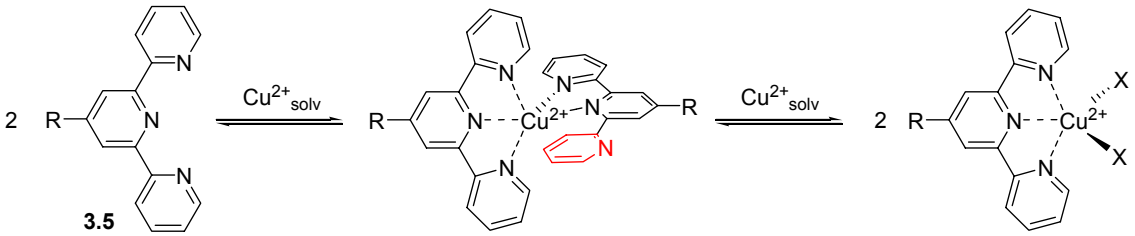

Fig. 7.4: *Binding Modes of Terpyridine*

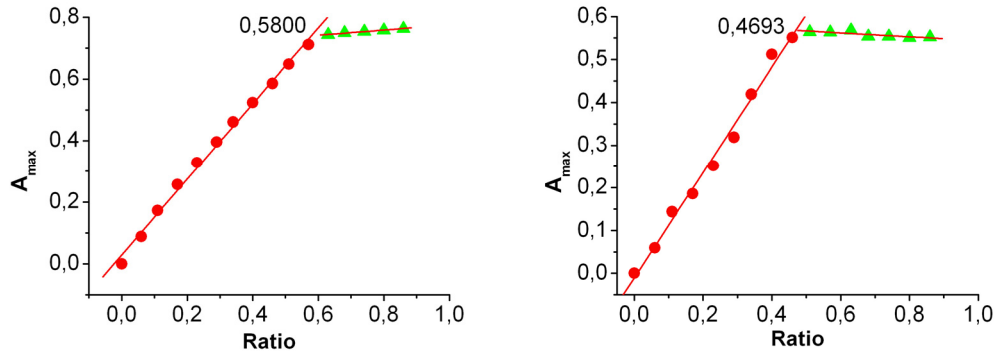

Fig. 7.5: *UV-Vis Copper Titration Curves for* ***3.6*** *(left) and* ***3.13*** *(right)*

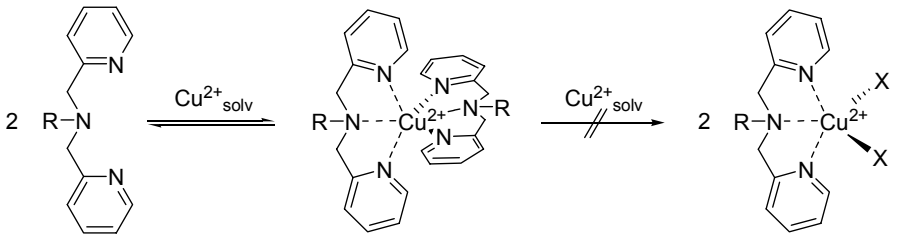

Fig. 7.6: *Binding Modes of Bis-Picolylamine*

Concerning the sequence specific recognition domain of a potential artificial nuclease, the synthesis of PNA monomers with base labile side chain protecting groups was optimized in the second part of this Thesis. The practicability of this system was shown on a random sequence.

The ligands mentioned above were connected to the amino terminus of PNA oligomers. Several sequences were synthesized by Fmoc SPPS, characterized by MALDI-TOF spectrometry and hybridized to complementary DNA strands, recording absorbance melting curves at 260nm. In the case of N-terminal terpyridine substitution, an intercalating effect of the uncomplexed ligand increased the stability of the PNA•DNA duplex, resulting in higher melting temperature in comparison to unsubstituted sequences and *N*-terminal bpa-conjugates.

Another important task in the context of this Thesis was the coupling of the ligands to the center of a PNA sequence in order to provide building blocks for catalytic artificial nucleases with multiple turnovers. This was achieved by the incorporation of a dipeptide (GlyPhe) into PNA SPS, whose phenylalanine was easy to functionalize by the use of its *p*-nitro derivative **5.2**. The chain assembly was interrupted after the glycine spacer, the aromatic nitro group was reduced on resin, and the activated carboxyl acid ligand was coupled to the resulting amino group, followed by finalization of the sequence and cleavage from the resin (Fig. 7.7).

The concept of a dehybridization of oligonucleotide cleavage fragments and thus a potential catalytic mode of action was proven by the fact that melting for DNA target fragments could not be observed.

Melting experiments with DNA and PNA monomers with an internal, unfunctionalized GlyPhe spacer revealed the formation of a bulge structure by the dipeptidic abasic site. Investigations in the future should examine the influence of varying chain lengths on the duplex formation. Molecular modelling could provide information about structure and stability.

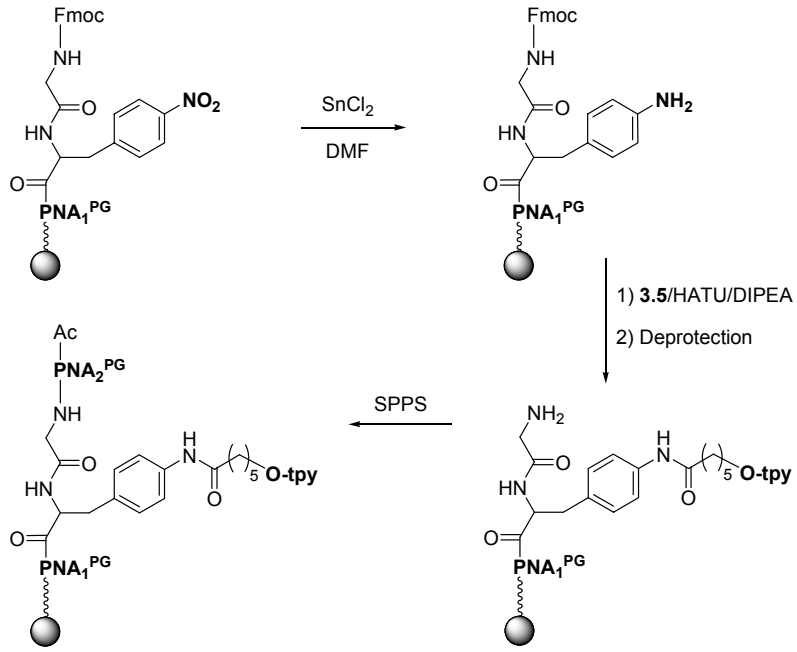

Fig. 7.7: *Synthesis Strategy for Internal Ligand Coupling to PNA*

Conjugates with internally attached ligands turned out to be insoluble in the buffer required for hybridization. This could be remedied by the incorporation of two or more lysine residues to the oligomers which should enhance solubility. Future research will be headed towards this direction. Nevertheless, in contrast to the time-consuming synthesis of a cleavage site in solution, this method is based on solid phase methods, exclusively, and can be applied on a large variety of ligands, organometallic moieties, fluorescent markers and every kind of biomolecule bearing a carboxylic group and is thus very promising for the future.

Another promising concept not mentioned in this Thesis is the use of Sonogashira coupling for the introduction of alkynyl functionalized ligands into PNA. Fmoc-protected *p*-iodophenylalanine was successfully incorporated into a PNA sequence, and a terpyridine alkyne was attempted to be coupled. This method provides another feasible method for the introduction of ligands.

The fact that PNA single strands alone show a sigmoidal absorbance melting curve due to base stacking (self-melting effect) was taken into consideration by the development of the coefficient f_M, helping to distinguish between self-melting and duplex formation. These examinations were shown to be indispensable for the assessment of hybridization data and should be incorporated into every melting curve analysis.
Theoretical calculations of the melting temperatures for the particular oligomers should provide additional information about the aspect of significance. Insights into thermodynamics could be obtained by further data processing of the melting curves.

The terpyridine ligand **3.5** will be coupled to DNA oligonucleotides in the future within a project in our institute.

Furthermore, the examination of the cleavage abilities of the compounds in this Thesis will provide information about their usability as real artificial nucleases.

8 Experimental Section / Materials & Methods

8.1 General Procedures

8.1.1 Synthesis & Workup

8.1.1.1 Chemicals

All chemicals and solvents were purchased from Acros (Geel, Belgium), Aldrich/Sigma/Fluka (Deisenhofen, Germany), Novabiochem (Laufelfingen, Switzerland), Roth (Karlsruhe, Germany) and IRIS Biotech (Marktredwitz, Germany) and used without further purification.

The preloaded polymer resins were purchased from Rapp Polymers (Tübingen, Germany), the acid labile PNA monomers from Applied Biosystems (Darmstadt, Germany), and the DNA oligonucleotides from IBA (Göttingen, Germany) in HPLC purity. All solutions were freshly prepared before use.

8.1.1.2 HPLC Purification

High Performance Liquid Chromatography (HPLC) purifications were performed on a Varian ProStar 210 System, equipped with column heater, PDA detector and auto sampler, using Varian DynaStar C-18 reverse phase columns for analytical (250·8mm) and preparative (250·21mm) runs. Water (Millipore®) and MeCN (Baker, HPLC-grade) were used as eluents, each containing 0.1% TFA. All analytical samples were measured at a flowrate of 1ml/min using the standard gradient indicated in Chapter 8.6. For purifications, the flowrate was 8ml/min. The samples were filtrated before injection using a 0.22µm syringe filter. Spectra were recorded at 254nm and 25°C.

8.1.1.3 Lyophilisation

All HPLC fractions were frozen in liquid nitrogen and lyophilized before subsequent processing using an Edwards Modulyo freeze dryer.

8.1.2 Physical Measurements

8.1.2.1 Elemental Analysis

Elemental Analysis were performed on a Foss Heraeus Vario EL Elementar Analysator in C,H,N mode.

8.1.2.2 Infrared Spectra

Infrared spectra were recorded on a Brucker Equinox 55 FT-IR spectrometer between NaCl windows in distilled $CHCl_3$, or as KBr discs, with a spectral resolution of 2.0cm^{-1}. Wavenumbers, *v*, are given in cm^{-1}.

8.1.2.3 NMR spectra

NMR spectra were determined either on a Bruker AM 360 spectrometer, ^1H operating at 360.14MHz and ^{13}C operating at 90.56MHz or on a Bruker AM 300 with frequencies of 300.16MHz (^1H) and 75.47MHz (^{13}C). Peak positions in both ^1H and ^{13}C are reported in ppm relative to TMS, the internal standard. Spectra of peptides are referenced to the residual DMSO signal (2.50ppm in ^1H, 39.52ppm in ^{13}C). All other compounds are referenced to the residual $CHCl_3$ signal (7.26ppm in ^1H, 77.16ppm in ^{13}C). Coupling constants, *J*, are given in Hz. Individual peaks are marked as: singlet (s), dublet (d), triplet (t) or multiplet (m). All chemical shifts are indicated in ppm.

8.1.2.4 Mass Spectrometry

The MALDI-TOF spectra were recorded on a Bruker Biflex III spectrometer at the Institute for Inorganic Chemistry (University of Heidelberg), using sinapinic acid as a matrix which was prepared by dissolving 6mg of sinapinic acid (from Bruker Daltonics, Leipzig, Germany) in 1ml of a mixture of MeCN and water (2:1) with 0.1% TFA added. The sample was dissolved in 0.1% TFA in water, and 1µl of probe solution was mixed with 2-3µl of matrix solution in a small Eppendorf tube. The ratio between these two components sometimes had to be adjusted in order to optimize the resulting spectrum. 2µl of this mixture were placed onto the plate and subjected to the measurement. Most of the spectra were measured in positive linear mode, thus suppressing fragmentation. Depending on the requirements, reflector mode was used, as well. The number of shots and the attenuation were adjusted as the case arised. For an overview of the use of MALDI-TOF spectrometry for the analysis of PNA oligomers, see Ref.[238]. EI (70eV) and FAB (glycerol or NBA matrix) spectra were measured on a MAT8200 instrument. Characteristic mass fragments with probable composition are given in brackets. For fragments containing metals only the isotopomer with highest intensity was described. All ESI (neg./pos.) spectra were recorded on a Finnigan TSQ700 at 4.5kV.

8.1.2.5 UV-Visible Spectrometry

All spectra were recorded on a Varian Cary 100 Conc UV-Vis spectrophotometer using 1cm quarz Suprasil cuvettes. Standard measurements were performed in dual beam mode with a cuvette filled with solvent serving as a blank sample. Before measuring, the instrument was zeroed without cuvettes, and after that, a baseline was recorded with both cuvettes filled with pure solvent. Data was saved in ASCII format and processed with ORIGIN.[j] Absorption maxima, λ_{max} and molar absorption coefficients, ε, are given in nm and $l \cdot mol^{-1} \cdot cm^{-1}$, respectively.

[j] V7.0303 © OriginLab Corporation 1991-2002

General procedure for UV-Vis titration:

In order to obtain absorbance curves in dependence of the Cu/L ratio, solutions were prepared allowing to titrate the reactants in a reasonable range of value.

Preliminary tests suggested the following course of action (20°C):

- Prepare a 10mM solution of the compound to be titrated
- Provide 400µl (4µmol) of this solution in the measuring cuvette
- Record a blank spectrum with pure analyte
- Add a 50mM solution of titer subsequently in 5µl-steps
- Let the mixture each time equilibrate for 3min
- Record a UV-Vis spectrum
- After 16 steps (80µl·50mM = 4µmol), equimolarity should be reached
- Record spectra up to $\tau > 1.5$
- Plot A_{max} versus titrant/analyte ratio
- Perform a linear fit on each line
- Determine the intersection point

All A_{max} values were determined after performing a polynomial fit (9^{th} order; 1000 data points) on the curve and corrected according to

$$A_{corr} = A \cdot \frac{400\mu l + n \cdot 5\mu l}{400\mu l}$$

in order to compensate the dilution effect by adding solvent during the titration.

The molar extinction coefficient ε at each state of the titration could be calculated with the formula $\varepsilon = \frac{A}{c \cdot \ell} = \frac{A \cdot (400\mu l + n \cdot 5\mu l)}{n \cdot 0.25\mu mol}$ [$l \cdot mol^{-1} \cdot cm^{-1} = 10^{-3}\ cm^2 \cdot \mu mol^{-1}$]

(with ℓ = 1cm and n = number of 50mM equivalents added, each one having a volume of 5µl and containing 0.25µmol of titrant).

8.1.2.6 Absorbance Melting Curves – General procedure

All melting curves were recorded at 260nm on a Varian Cary 100 Conc UV-Vis spectrophotometer equipped with peltier thermostatted multicell holders in order to assure a high probe throughput and a reproducible temperature control (high stability over time and a variation of ±0.05°C). Nitrogen purging was indispensable in order to prevent the cuvettes from steaming up at low temperatures.
Each melting curve was recorded at least four times in order to eliminate mavericks and to obtain weighted averages of melting points.

All samples were dissolved in phosphate buffer prepared as follows:

0.1M KH_2PO_4, 1.3609g per 100ml

0.1M $Na_2HPO_4 \cdot 2H_2O$, 1.7799g per 100ml

0.1M NaCl, 584.4mg per 100ml

Before use, the buffer was filtered through a 0.22µm syringe filter in order to remove bacteriological and other contaminations.

1) Determination of Extinction Coefficients at 260nm

The ε-values were calculated from the increments according to:

$$\varepsilon_{oligo} = \sum_{x} n_x \cdot \varepsilon_x \qquad (\varepsilon_{oligo} = n_A \cdot \varepsilon_A + n_G \cdot \varepsilon_G + n_C \cdot \varepsilon_C + n_T \cdot \varepsilon_T \text{ etc.})$$

Incremental extinction coefficients for the PNA and DNA monomers were obtained from literature:[149, 280]

$cm^2 \cdot \mu mol^{-1}$	ε_A	ε_G	ε_C	ε_T
DNA	15.3	12.2	7.6	8.7
PNA	13.7	11.7	6.6	8.6

In order to include the aromatic chromophores of the ligands and of phenylalanine into the calculations, the absorbance of known concentrations of the free building blocks was measured, and ε was calculated according to Lambert-Beer's law ($A = \varepsilon \cdot c \cdot \ell$).

$cm^2 \cdot \mu mol^{-1}$	ε_{Phe}	ε_{tpy}	ε_{bpa}
PNA	0.2	17.9	9.4

2) Determination of Concentration

PNA stock solutions were prepared by dissolving the lyophilisate of the pure HPLC fraction in buffer. DNA stock solutions were used as received from IBA.

The DNA and PNA stock concentrations were determined according to the following protocol which allows measuring a whole UV-Vis spectrum from 190-900nm and a number of absorbance values at 260nm at a time without preparing new sample solutions:

- Zero the instrument in the "Scan" mode without samples, adjust temperature
- Put 950µl of buffer in each of the two cuvettes and place them in slots 1 & 7
- Let buffer reach temperature for at least 5min. (DNA: 25°C – PNA: 70°C)
- Record a baseline in "Scan" mode
- Zero the instrument in "Simple Reads" mode (260nm)
- Add 50µl of DNA or PNA stock solution into the cuvette in slot 1
- Let mixture reach temperature at least for 5 min. (!)
- Perform 20 scans in „Simple Reads" mode and determine the average (Excel)
- Perform a scan in "Scan" mode with baseline being activated

Be sure that $A_{260(verd)}$ will be between 0.3 & 1.5 (best signal-to-noise ratio)

Calculate the stock concentration according to $c = 20 \cdot \frac{A_{260(verd)}}{\varepsilon}$ [mM].

3) Probe Composition

All melting experiments were carried out with 3µM solutions.

Based on the known stock concentrations, the required volumes were calculated following $V = \frac{3}{c}$ [µl], and the respective amounts of each stock solution were mixed in the cuvette already containing the amount of buffer required for topping up to 1ml (and used before for multizeroing – see below).

4) General Procedure for Melting Curves:

Using the multicell holder of the Cary 100 Conc allows to measure 12 curves (3 different experiments, 4 times each). Proceed as follows:

- Multizero the instrument with all four cuvettes filled with buffer (20°C)
- Add the calculated amounts of DNA & PNA stock solutions
- Seal the cuvettes with a Teflon plug in order to avoid the use of silicon oil
- Heat the cuvettes in a water bath to 70°C for 3min (this will completely dehybridize the strands and saturate the space above the solution with solvent)
- Supersonicate and cool down to ambient temperature
- Record A_{260}, starting at 20°C along the following profile:

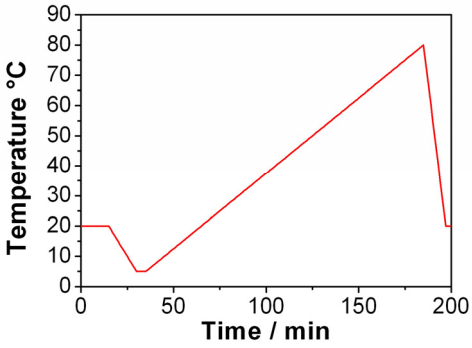

Data	Rate	End	Hold
0.5	1	5	15
0.5	0.5	80	5
2	5	20	0

- Ensure nitrogen purging below room temperature – steamy cuvettes will make the result useless

Data was collected as indicated, the files were saved in ASCII format and processed with ORIGIN.[k] In all cases, the cooling, holding and re-annealing data was discarded.

For interpretational details, see Chapter 6.2.

[k] V7.0303 © OriginLab Corporation 1991-2002

8.2 Synthesis of Ligands and Peptide Conjugates Thereof

Synthesis of 6-[4'-oxa-(2,2':6',2''-terpyridinyl)]hexanoic acid **3.5**

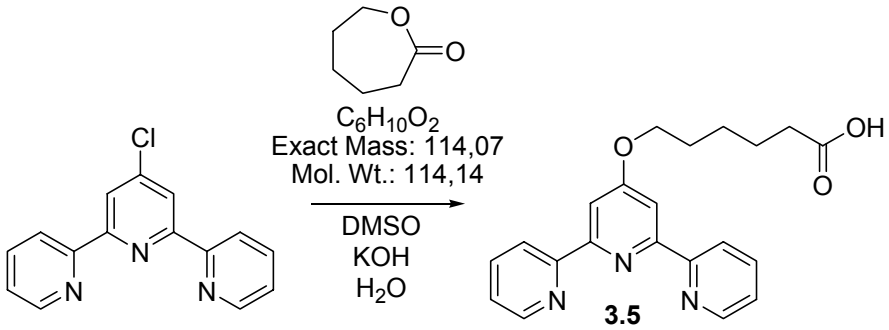

ε-Caprolactone (0.48g 99%, 4.2mmol) and powdered KOH (1.50g, 27mmol) were suspended in DMSO (25ml). After heating the slurry to 60°C, 4'-chloro-2,2':6',2''-terpyridine (1.13g 99%, 4.2mmol) and H_2O (75µl, 4.2mmol) were added. The mixture clouded and the KOH-particles turned red (caused by iron contamination). Refluxing at 60°C resulted in a red and clear solution, which clouded again after some days. After 7-10d of refluxing, the suspension was allowed to cool to RT and poured into 300ml of H_2O giving a light yellow and clear solution. The product was precipitated by adjusting the pH to 7 with 10% HCl. After 30min of stirring, the white solid was collected by filtration, washed with water (2x80ml) and dried *in vacuo*.
Yield: 1.186g (3.26mmol, 78%)

The synthesis of the tpy-derivatives with shorter chain lengths was carried out similar to this procedure.

Fig. 8.1: *Overview of tpy-Carboxylic Acids with various Chain Lengths*

	Lactone	$\mathbf{M_{lactone}}$	$\mathbf{M_{product}}$	**Yield**
3.2	Glycolic acid	76.04	307.30	50%
3.3	γ-Butyrolactone	86.09	335.35	57%
3.4	δ-Valerolactone	100.12	349.39	69%
3.5	ε-Caprolactone	114.14	363.41	78%

4'-Chloro-2,2':6',2''-terpyridine

^{1}H-NMR (360MHz, DMSO-d_6): δ = 8.74 (2H, d, H^{6}_{tpy}, $H^{6''}_{tpy}$), 8.62 (2H, d, H^{3}_{tpy}, $H^{3''}_{tpy}$), 8.42 (2H, s, $H^{3'}_{tpy}$, $H^{5'}_{tpy}$), 8.03 (2H, m, H^{4}_{tpy}, $H^{4''}_{tpy}$), 7.55 (2H, m, H^{5}_{tpy}, $H^{5''}_{tpy}$). ^{13}C-NMR (90.56MHz, DMSO-d_6): δ = 156.64 (s, $C^{2'}_{tpy}$, $C^{6'}_{tpy}$), 153.62 (s, C^{2}_{tpy}, $C^{2''}_{tpy}$), 149.47 (d, C^{6}_{tpy}, $C^{6''}_{tpy}$), 145.28 (d, $C^{4'}_{tpy}$), 137.64 (d, C^{4}_{tpy}, $C^{4''}_{tpy}$), 125.08 (d, C^{3}_{tpy}, $C^{3''}_{tpy}$), 121.13 (d, C^{5}_{tpy}, $C^{5''}_{tpy}$), 120.17 (d, $C^{3'}_{tpy}$, $C^{5'}_{tpy}$).

4'-Hydroxy-2,2':6',2''-terpyridine **3.1**

^{1}H-NMR (360MHz, DMSO-d_6): δ = 8.72 (2H, d, H^{6}_{tpy}, $H^{6''}_{tpy}$), 8.59 (2H, d, H^{3}_{tpy}, $H^{3''}_{tpy}$), 8.02 (2H, m, H^{4}_{tpy}, $H^{4''}_{tpy}$), 7.88 (2H, s, $H^{3'}_{tpy}$, $H^{5'}_{tpy}$), 7.51 (2H, m, H^{5}_{tpy}, $H^{5''}_{tpy}$). ^{13}C-NMR (90.56MHz, DMSO-d_6): δ = 166.59 (d, $C^{4'}_{tpy}$), 155.61 (s, $C^{2'}_{tpy}$, $C^{6'}_{tpy}$), 154.36 (s, C^{2}_{tpy}, $C^{2''}_{tpy}$), 148.97 (d, C^{6}_{tpy}, $C^{6''}_{tpy}$), 137.68 (d, C^{4}_{tpy}, $C^{4''}_{tpy}$), 124.52 (d, C^{3}_{tpy}, $C^{3''}_{tpy}$), 120.98 (d, C^{5}_{tpy}, $C^{5''}_{tpy}$), 108.51 (d, $C^{3'}_{tpy}$, $C^{5'}_{tpy}$). MS (EI, 70eV, 275°C): *m/z* (%) = 249 (100) [M^{+}], 221 (88), 193 (4), 167 (8.4).

2-[4'-Oxa-(2,2':6',2''-terpyridinyl)]acetic acid **3.2**

^{1}H-NMR (360MHz, DMSO-d_6): δ = 8.72 (2H, d, H^{6}_{tpy}, $H^{6'}{}_{tpy}$), 8.59 (2H, d, H^{3}_{tpy}, $H^{3''}_{tpy}$), 8.02 (2H, m, H^{4}_{tpy}, $H^{4''}_{tpy}$), 7.95 (2H, s, $H^{3'}_{tpy}$, $H^{5'}_{tpy}$), 7.50 (2H, m, H^{5}_{tpy}, $H^{5''}_{tpy}$), 2.08 (2H, s, H^{2}_{alk}). ^{13}C-NMR (90.56MHz, DMSO-d_6): δ = 174.32 (s, C^{1}_{alk}), 166.59 (d, $C^{4'}_{tpy}$), 156.62 (s, $C^{2'}_{tpy}$, $C^{6'}_{tpy}$), 154.88 (s, C^{2}_{tpy}, $C^{2''}_{tpy}$), 149.27 (d, C^{6}_{tpy}, $C^{6''}_{tpy}$), 137.32 (d, C^{4}_{tpy}, $C^{4''}_{tpy}$), 124.44 (d, C^{3}_{tpy}, $C^{3''}_{tpy}$), 120.82 (d, C^{5}_{tpy}, $C^{5''}_{tpy}$), 106.74 (d, $C^{3'}_{tpy}$, $C^{5'}_{tpy}$), 67.66 (t, C^{2}_{alk}).

4-[4'-Oxa-(2,2':6',2''-terpyridinyl)]butanoic acid **3.3**

^{1}H-NMR (360MHz, DMSO-d_6): δ = 8.73 (2H, d, H^{6}_{tpy}, $H^{6''}_{tpy}$), 8.58 (2H, d, H^{3}_{tpy}, $H^{3''}_{tpy}$), 7.99 (2H, m, H^{4}_{tpy}, $H^{4''}_{tpy}$), 7.94 (2H, s, $H^{3'}_{tpy}$, $H^{5'}_{tpy}$), 7.49 (2H, m, H^{5}_{tpy}, $H^{5''}_{tpy}$), 4.27 (2H, t, J=6.3, H^{4}_{alk}), 2.27 (2H, t, J=7.2, H^{2}_{alk}), 1.66 (2H, pseudo-quint, J=6.8, H^{3}_{alk}). ^{13}C-NMR (90.56MHz, DMSO-d_6): δ = 174.05 (s, C^{1}_{alk}), 166.63 (d, $C^{4'}_{tpy}$), 156.60 (s, $C^{2'}_{tpy}$, $C^{6'}_{tpy}$), 154.80 (s, C^{2}_{tpy}, $C^{2''}_{tpy}$), 149.13 (d, C^{6}_{tpy}, $C^{6''}_{tpy}$), 137.34 (d, C^{4}_{tpy}, $C^{4''}_{tpy}$), 124.34 (d, C^{3}_{tpy}, $C^{3''}_{tpy}$), 120.78 (d, C^{5}_{tpy}, $C^{5''}_{tpy}$), 106.76 (d, $C^{3'}_{tpy}$, $C^{5'}_{tpy}$), 67.21 (t, C^{4}_{alk}), 30.08 (t, C^{2}_{alk}), 24.04 (t, C^{3}_{alk}). MS (EI, 70eV, 275°C): *m/z* (%) = 335 [M^{+}] (3.9), 291 (68), 276 (55), 261 (84), 249 (98), 233 (50), 221 (100), 193 (22)

5-[4'-Oxa-(2,2':6',2''-terpyridinyl)]pentanoic acid **3.4**

^{1}H-NMR (360MHz, DMSO-d_6): δ = 8.71 (2H, d, H^{6}_{tpy}, $H^{6''}_{tpy}$), 8.60 (2H, d, H^{3}_{tpy}, $H^{3''}_{tpy}$), 8.02 (2H, m, H^{4}_{tpy}, $H^{4''}_{tpy}$), 7.96 (2H, s, $H^{3'}_{tpy}$, $H^{5'}_{tpy}$), 7.49 (2H, m, H^{5}_{tpy}, $H^{5''}_{tpy}$), 4.25 (2H, t, J=6.3, H^{5}_{alk}), 2.32 (2H, t, J=6.4, H^{2}_{alk}), 1.81 (2H, pseudo-quint, J=7.1, H^{3}_{alk}), 1.70 (2H, pseudo-quint, J=6.8, H^{4}_{alk}). ^{13}C-NMR (90.56MHz, DMSO-d_6): δ = 174.28 (s, C^{1}_{alk}), 166.62 (d, $C^{4'}_{tpy}$), 156.58 (s, $C^{2'}_{tpy}$, $C^{6'}_{tpy}$), 154.78 (s, C^{2}_{tpy}, $C^{2''}_{tpy}$), 149.14 (d, C^{6}_{tpy}, $C^{6''}_{tpy}$), 137.27 (d, C^{4}_{tpy}, $C^{4''}_{tpy}$), 124.40 (d, C^{3}_{tpy}, $C^{3''}_{tpy}$), 120.78 (d, C^{5}_{tpy}, $C^{5''}_{tpy}$), 106.66 (d, $C^{3'}_{tpy}$, $C^{5'}_{tpy}$), 33.22 (t, C^{2}_{alk}), 27.80 (t, C^{4}_{alk}), 21.01 (t, C^{3}_{alk}). MS (EI, 70eV, 275°C): *m/z* (%) = 348 [M^{+}] (0.9), 332 (0.7), 305 (30), 276 (19), 262 (41), 249 (78), 233 (14), 221 (100), 193 (4), 155 (1.7), 117 (7.2), 78 (14).

6-[4'-Oxa-(2,2':6',2''-terpyridinyl)]hexanoic acid **3.5**

^{1}H-NMR (360MHz, DMSO-d_6): δ = 8.71 (2H, d, H^{6}_{tpy}, $H^{6''}_{tpy}$), 8.60 (2H, d, H^{3}_{tpy}, $H^{3''}_{tpy}$), 7.99 (2H, m, H^{4}_{tpy}, $H^{4''}_{tpy}$), 7.95 (2H, s, $H^{3'}_{tpy}$, $H^{5'}_{tpy}$), 7.49 (2H, m, H^{5}_{tpy}, $H^{5''}_{tpy}$), 4.22 (2H, t, J=6.3, H^{6}_{alk}), 2.26 (2H, t, J=7.2, H^{2}_{alk}), 1.80 (2H, pseudo-quint, J=6.8, H^{5}_{alk}), 1.60 (2H, pseudo-quint, J=7.1, H^{3}_{alk}), 1.48 (2H, pseudo-quint, J=6.9, H^{4}_{alk}). ^{13}C-NMR (90.56MHz, DMSO-d_6): δ = 174.46 (s, C^{1}_{alk}), 166.73 (d, $C^{4'}_{tpy}$), 156.66 (s, $C^{2'}_{tpy}$, $C^{6'}_{tpy}$), 154.87 (s, C^{2}_{tpy}, $C^{2''}_{tpy}$), 149.24 (d, C^{6}_{tpy}, $C^{6''}_{tpy}$), 137.36 (d, C^{4}_{tpy}, $C^{4''}_{tpy}$), 124.49 (d, C^{3}_{tpy}, $C^{3''}_{tpy}$), 120.88 (d, C^{5}_{tpy}, $C^{5''}_{tpy}$), 106.72 (d, $C^{3'}_{tpy}$, $C^{5'}_{tpy}$), 67.85 (t, C^{6}_{alk}), 33.62 (t, C^{2}_{alk}), 28.14 (t, C^{5}_{alk}), 25.01 (t, C^{4}_{alk}), 24.22 (t, C^{3}_{alk}). MS (EI, 70eV, 275°C): *m/z* (%) = 362 [M^{+}] (7.9), 319 (79), 304 (27.4), 290 (37), 276 (79), 262 (100), 249 (89), 233 (71.4), 221 (97.3), 193 (11.5). MS (ESI-pos, MeOH): *m/z* = 364.3 $[M+H]^{+}$. MS (ESI-neg, MeOH): *m/z* = 361.98 $[M-H]^{-}$, 247.91 $[M-C_5H_{10}COOH]^{-}$

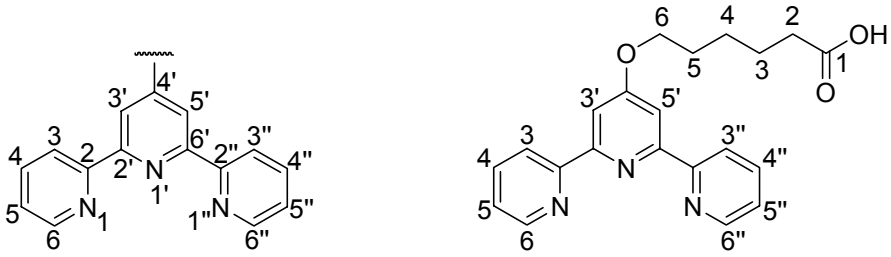

^{1}H-NMR (360MHz, DMSO-d_6)

δ (ppm)	tpy-Cl	3.1	3.2	3.3	3.4	3.5
H^{2}_{alk}	–	–	2.08	2.27	2.32	2.26
H^{3}_{alk}	–	–	–	1.66	1.81	1.60
H^{4}_{alk}	–	–	–	4.27	1.70	1.48
H^{5}_{alk}	–	–	–	–	4.25	1.80
H^{6}_{alk}	–	–	–	–	–	4.22
H^{5}_{tpy}, $H^{5''}_{tpy}$	7.55	7.51	7.50	7.49	7.49	7.49
$H^{3'}_{tpy}$, $H^{5'}_{tpy}$	**8.42**	**7.88**	**7.95**	**7.94**	**7.96**	**7.95**
H^{4}_{tpy}, $H^{4''}_{tpy}$	8.03	8.02	8.02	7.99	8.02	7.99
H^{3}_{tpy}, $H^{3''}_{tpy}$	8.62	8.59	8.59	8.58	8.60	8.60
H^{6}_{tpy}, $H^{6''}_{tpy}$	8.74	8.72	8.72	8.73	8.71	8.71

^{13}C-NMR (90.56MHz, DMSO-d_6)

δ (ppm)	tpy-Cl	3.1	3.2	3.3	3.4	3.5
C^{2}_{alk}	–	–	67.66	30.08	33.22	33.62
C^{3}_{alk}	–	–	–	24.04	21.01	24.22
C^{4}_{alk}	–	–	–	67.21	27.80	25.01
C^{5}_{alk}	–	–	–	–	67.61	28.14
C^{6}_{alk}	–	–	–	–	–	67.85
$C^{3'}_{tpy}$, $C^{5'}_{tpy}$	**120.17**	**108.51**	**106.74**	**106.76**	**106.66**	**106.72**
C^{5}_{tpy}, $C^{5''}_{tpy}$	121.13	120.98	120.82	120.78	120.78	120.88
C^{3}_{tpy}, $C^{3''}_{tpy}$	125.08	124.52	124.44	124.34	124.40	124.49
C^{4}_{tpy}, $C^{4''}_{tpy}$	137.64	137.68	137.32	137.34	137.27	137.36
C^{6}_{tpy}, $C^{6''}_{tpy}$	149.47	148.97	149.27	149.13	149.14	149.24
C^{2}_{tpy}, $C^{2''}_{tpy}$	153.62	154.36	154.88	154.80	154.78	154.87
$C^{2'}_{tpy}$, $C^{6'}_{tpy}$	156.64	155.61	156.62	156.60	156.58	156.66
$C^{4'}_{tpy}$	**145.28**	**166.59**	**166.59**	**166.63**	**166.62**	**166.73**
C^{1}_{alk}	–	–	174.32	174.05	174.28	174.46

Synthesis of *N*-(*p*-carboxybenzyl)bis(2-picolyl)amine **3.6**

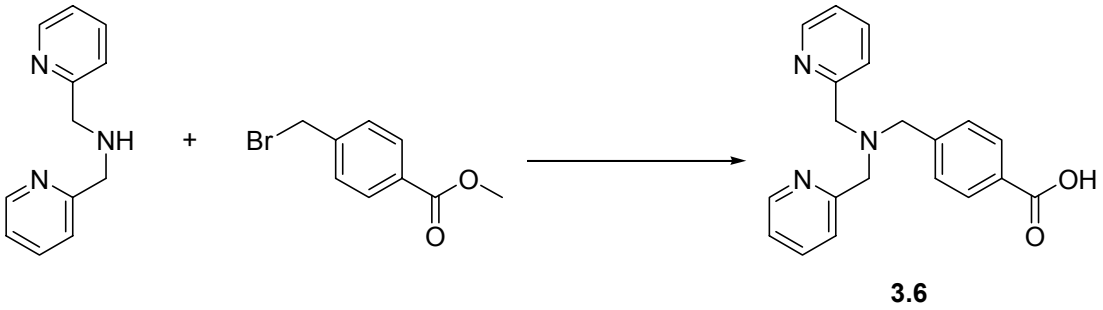

3.6

$C_{12}H_{13}N_3$	$C_9H_9BrO_2$	$C_{20}H_{19}N_3O_2$
Exact Mass: 199,11	Exact Mass: 227,98	Exact Mass: 333,15
Mol. Wt.: 199,25	Mol. Wt.: 229,07	Mol. Wt.: 333,38

Methyl ester

NEt_3 (0.69ml, 5.00mmol) was added to a solution of bis(2-picolyl)amine (1.0g, 5.0mmol) and methyl *p*-(bromomethyl)benzoate (1.15g, 5.00mmol) in THF (35ml), and the mixture was refluxed for 1.5h. The mixture was allowed to reach RT and subsequently filtered to remove a white precipitate. After removal of the solvent under reduced pressure, the oily residue was redissolved in Et_2O (40ml) and filtered to remove a red solid. Evaporation of the solvent yielded 1.4g (81%) of a light orange oil, which was used as such in the next step. M = 347.4 ($C_{21}H_{21}N_3O_2$).

^{1}H-NMR (250.1MHz, $CDCl_3$): δ = 8.49 (app. d, 2H, H_{pyr}), 7.95 (d, $^3J_{H,H}$=8.3Hz, 2H, H_{Ar}), 7.62 (pseudo t, 2H, H_{pyr}), 7.52 (pseudo d, 2H, H_{pyr}), 7.46 (d, ^3J=8.3Hz, 2H, H_{Ar}), 7.12 (pseudo t, 2H, H_{pyr}), 3.87 (s, 3H, OCH_3), 3.78 (s, 4H, $CH_{2,picolyl}$), 3.71 (s, 2H, CH_2). ^{13}C-NMR ($CDCl_3$, 100.6MHz): δ = 166.9 (C-O), 159.3 (Cq_{pyr}), 148.9 (C_{Pyr}), 144.5 ($C_{Ar,q}$), 136.3 (C_{Pyr}), 129.5 (C_{Ar}), 128.9 ($C_{Ar,q}$), 128.6 (C_{Ar}), 122.7 (C_{Pyr}), 122.0 (C_{Pyr}), 60.0 ($CH_{2,\ picolyl}$), 58.1 (CH_2), 51.9 (OCH_3). MS (EI, 70eV, 170°C): *m*/*z* (%) = 347 (2) [M^+], 316 (2) [M-OCH3]$^+$, 255 (100) [M-C_6H_6N]$^+$.

Saponification

1.4g (4.0mmol) of the product obtained from step 1 was dissolved in MeOH (20ml), a solution of NaOH (0.8g, 20mmol) in 5ml of H_2O was added, and the mixture was stirred for 2h at ambient temperature. The pH was adjusted to 7 by dropwise addition of 2M HCl, followed by removal of the solvent under reduced pressure. The sticky white residue was triturated with $CHCl_3$ (200ml), followed by filtration to remove NaCl. The $CHCl_3$ solution was dried with $MgSO_4$. Removal of the solvent under reduced pressure afforded a yellow sticky oil, to which CH_3CN (30ml) was added, followed by vigorous stirring. After approximately 15-30 min, a white precipitate formed. The solution was stored at 0°C for 2h, to effect further precipitation and the white solid was then isolated by filtration and dried in vacuo. Yield: 0.7g (53%).

^{1}H-NMR (250.1MHz, $CDCl_3$): δ = 11.35 (br, 1H, CO_2H), 8.59 (app. d, 2H, H_{Pyr}), 8.01 (d, $^3J_{H,H}$=8.0Hz, 2H, H_{Ar}), 7.66 (pseudo t, 2H, H_{Pyr}), 7.59 (app. d, 2H, H_{Pyr}), 7.44 (d, $^3J_{H,H}$=7.7Hz, 2H, H_{Ar}), 7.80 (pseudo t, 2H, H_{Pyr}), 3.85 (s, 4H, CH_2), 3.73 (s, 2H, $CH_{2,Bz}$). ^{13}C-NMR (62.9MHz, $CDCl_3$): δ = 169.3 (C-O), 159.8, 148.4, 143.1, 137.2, 130.0, 128.8, 123.4, 122.4, 122.0 (all C_{Ar}), 59.3 (CH_2), 58.2 ($CH_{2,Bz}$). MS (EI, 70eV, 175°C): *m*/*z* (%) = 333 (1) $[M]^+$, 241 (100) $[M\text{-}C_6H_6N]^+$.

Synthesis of 5-nitro-1,10-phenanthroline **3.7**

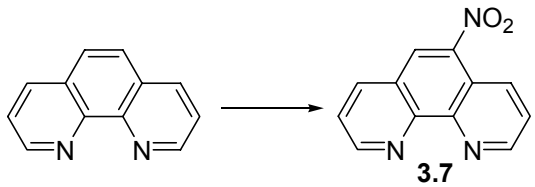

$C_{12}H_8N_2$
Exact Mass: 180,07
Mol. Wt.: 180,21

$C_{12}H_7N_3O_2$
Exact Mass: 225,05
Mol. Wt.: 225,2

In a 500ml three-necked flask equipped with thermometer, 100ml dropping funnel and reflux condenser, 1,10-Phenanthroline (25.45g 99%, 139mmol) was slowly dissolved in conc. H_2SO_4 (180ml) at 0°C resulting in a brown, clear solution which was allowed to reach RT. 90ml of conc. HNO_3 was added quickly, but carefully over a dropping funnel in a way letting the solution reach, but not exceed 95°C. The resulting mixture was stirred for another 30min, changing its colour to light yellow. It was heated to 115°C by a heating mantle for 1h to complete the reaction and get rid of nitric gases. After cooling down to RT, the solution was carefully poured over 2kg of crushed ice under continuous stirring. The resulting yellow suspension was brought to pH 7 with 320g of NaOH dissolved in 1.8L of water, changing its colour from yellow to orange. The precipitate was sucked off, washed with water and dried *in vacuo* for 24h. Yield: 23.3g (103mmol, 74%); Melting point: 202-204°C.

1,10-Phenanthroline

^{1}H-NMR (360MHz, DMSO-d_6): δ = 9.09 (2H, dd, J=1.71, 4.26, H^2, H^9), 8.44 (2H, dd, J=1.71, 8.07, H^4, H^7), 7.92 (2H, s, H^5, H^6), 7.73 (2H, pseudo-q, J=4.29, H^3, H^8). ^{13}C-NMR (90.56MHz, DMSO-d_6): δ = 123.23 (C^3, C^8), 136.15 (C^4, C^7), 128.37 (C^{4a}, C^{6a}), 126.58 (C^5, C^6), 145.39 (C^{10a}, C^{10b}), 149.84 (C^2, C^9). MS (EI, 70eV, 275°C): 180 [M^+] (100), 154 (17.9), 127 (9.1).

5-Nitro-1,10-phenanthroline **3.7**

^{1}H-NMR (360MHz, DMSO-d_6): δ = 9.28 (1H, dd, J=1.39, 4.15, H^9), 9.24 (1H, dd, J=1.07, 4.01, H^2), 9.04 (1H, s, H^6), 8.89 (1H, dd, J=1.10, 8.54, H^7), 8.78 (1H, dd, J=1.30, 8.08, H^4), 7.95 (2H, m, H^3, H^8). ^{13}C-NMR (90.56MHz, DMSO-d_6): δ = 153.38 (C^9), 151.19 (C^2), 146.79 (C^{10a}), 145.43 (C^5), 143.85 (C^{10b}), 138.12 (C^7), 132.12 (C^4),

126.00 (C^6), 125.56 (C^{6a}), 124.58 (C^3), 124.50 (C^8), 120.37 (C^{4a}). MS (EI, 70eV, 275°C): *m/z* (%) = 225 [M^+] (74.6), 196 (1.1), 179 (100), 167 (25.1), 152 (37.4), 125 (28.3), 99 (12.8), 75 (20.8), 63 (2.8), 51 (17.1), 28 (15.8).

Synthesis of 5-amino-1,10-phenanthroline **3.8**

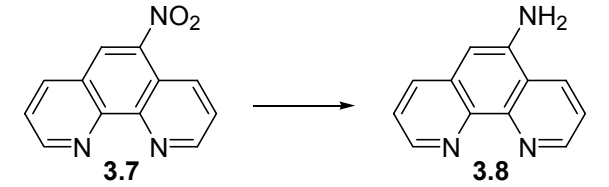

3.7
$C_{12}H_7N_3O_2$
Exact Mass: 225,05
Mol. Wt.: 225,2

3.8
$C_{12}H_9N_3$
Exact Mass: 195,08
Mol. Wt.: 195,22

In a 500ml three-necked round-bottomed flask equipped with a gas inlet tube and a bubble counter, 5-nitro-1,10-phenanthroline (9.52g, 42.27mmol) was dissolved in 210ml EtOH giving a yellow solution. 25% NH_3 (30ml) was added, and under stirring, H_2S was passed into the solution which became cloudy and warm and changed its colour to a brownish green. After saturation of the solution being complete, stirring was continued for 3d, saturating the solution with H_2S from time to time. 100ml EtOH and 20ml NH_3 were added, and the procedure was continued for another 4d. The clear and brown mixture was heated to 60°C on an oil bath, and the excess of gases and the solvents were removed with a water jet pump, followed by coevaporation with EtOH (2x200ml). The orange-coloured residue was suspended in 2% HCl (360ml), and the red solution was separated from the yellow solid. The filtrate was brought to pH8 with 25% NH_3, the yellow product was sucked off, dried *in vacuo* and recrystallized from isopropanol. Yield: 3.19g (16.2mmol, 39%)

^{1}H-NMR (360MHz, DMSO-d_6): δ = 9.04 (1H, d, H^2), 8.68 (1H, d, H^9), 8.62 (1H, d, H^4), 8.02 (1H, d, H^7), 7.72 (1H, dd, H^3), 7.50 (1H, dd, H^8), 6.86 (1H, s, H^6), 6.13 (2H, s, NH_2). ^{13}C-NMR (90.56MHz, DMSO-d_6): δ = 149.33 (C^2), 146.17 (C^5), 144.81 (C^9), 142.65 (C^{10a}), 140.50 (C^{10b}), 132.69 (C^4), 130.79 (C^7), 130.55 (C^{6a}), 123.19 (C^3), 122.06 (C^8), 121.80 (C^{4a}), 101.75 (C^6). MS (EI, 70eV, 275°C): *m/z* (%) = 195 [M^+] (100), 168 (14.9), 140 (6.8), 114 (2.3).

^{1}H-NMR (360MHz, DMSO-d_6)

δ (ppm)	phen	3.7	3.8
H^2	9.09	9.24	9.04
H^3	7.73	7.95	7.72
H^4	8.44	8.78	8.62
H^5	7.92	–	–
H^6	**7.92**	**9.04**	**6.86**
H^7	8.44	8.89	8.02
H^8	7.73	7.95	7.50
H^9	9.09	9.28	8.68
NH_2	–	–	6.13

^{13}C-NMR (90.56MHz, DMSO-d_6)

δ (ppm)	phen	3.7	3.8
C^2	149.84	151.19	149.33
C^3	123.23	124.58	123.19
C^4	136.15	132.12	132.69
C^{4a}	128.37	120.37	121.80
C^5	126.58	145.43	146.17
C^6	126.58	126.00	101.75
C^{6a}	128.37	125.56	130.55
C^7	136.15	138.12	130.79
C^8	123.23	124.50	122.06
C^9	149.84	153.38	144.81
C^{10a}	145.39	146.79	142.65
C^{10b}	145.39	143.85	140.50

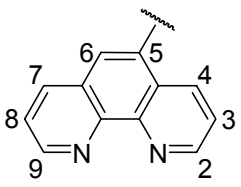

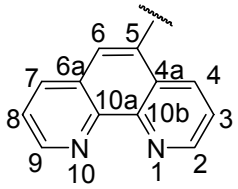

Synthesis of tpy*-Phe-OMe **3.9**

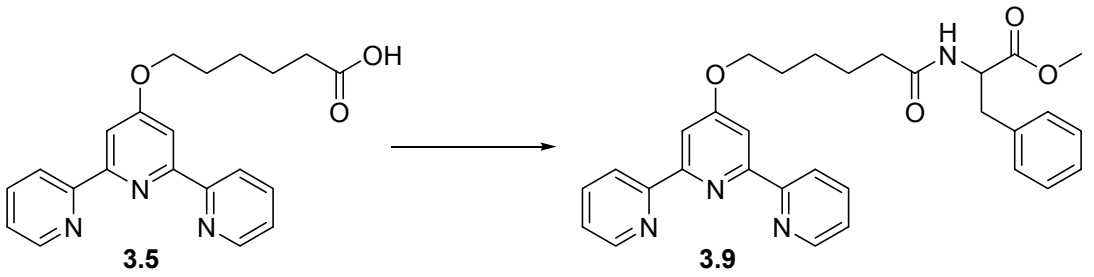

3.5

$C_{21}H_{21}N_3O_3$
Exact Mass: 363,16
Mol. Wt.: 363,41

3.9

$C_{31}H_{32}N_4O_4$
Exact Mass: 524,24
Mol. Wt.: 524,61

Phenylalanine methyl ester hydrochloride (108mg, 0.5mmol) was dissolved in DMF (15ml), and ligand **3.5** (186mg, 0.5mmol) was added, resulting in a clear, light yellow solution. EDC·HCl (100mg, 0.55mmol) was added, and the solution was stirred at RT overnight. The solvent was removed *in vacuo* to leave a pink oil which was coevaporated with MeOH (3x). H_2O (10ml) was added, followed by stirring overnight at RT. The slurry was filtrated, whereupon a pink filtrate and a white precipitate were separated. Yield: 205mg (78%)

^{1}H-NMR (360MHz, DMSO-d_6): δ = 8.72 (2H, d, $H^6{}_{tpy}$, $H^{6''}{}_{tpy}$), 8.62 (2H, d, $H^3{}_{tpy}$, $H^{3''}{}_{tpy}$), 8.30 (1H, d, NH), 7.96-8.02 (4H, m, $H^4{}_{tpy}$, $H^{4''}{}_{tpy}$, $H^{3'}{}_{tpy}$, $H^{5'}{}_{tpy}$), 7.50 (2H, m, $H^5{}_{tpy}$, $H^{5''}{}_{tpy}$), 7.20-7.28 (7H, m, $H_{Phe\text{-}o}$, $H_{Phe\text{-}m}$, $H_{Phe\text{-}p}$), 4.46-4.52 (1H, m, $H_{Phe\text{-}\alpha}$), 4.24 (2H, m, $H^6{}_{alk}$), 3.60 (3H, s, H_{OMe}), 3.19-3.03 (2H, m, $H_{Phe\text{-}\beta}$). 2.28 (t, 2H, $H^2{}_{alk}$), 1.81 (2H, pseudo-quint, J=6.8, $H^5{}_{alk}$), 1.74 (2H, pseudo-quint, J=7.1, $H^3{}_{alk}$), 1.50 (2H, pseudo-quint, J=6.9, $H^4{}_{alk}$). ^{13}C-NMR (90.56MHz, DMSO-d_6): δ = 174.35 (s, $C^1{}_{alk}$), 172.10 (CO_{Phe}), 166.65 (d, $C^{4'}{}_{tpy}$), 156.58 (s, $C^{2'}{}_{tpy}$, $C^{6'}{}_{tpy}$), 154.78 (s, $C^2{}_{tpy}$, $C^{2''}{}_{tpy}$), 149.15 (d, $C^6{}_{tpy}$, $C^{6''}{}_{tpy}$), 137.28 (d, $C^4{}_{tpy}$, $C^{4''}{}_{tpy}$), 128.94 ($C_{Phe\text{-}o}$), 128.08 ($C_{Phe\text{-}m}$), 126.35 ($C_{Phe\text{-}p}$), 124.41 (d, $C^3{}_{tpy}$, $C^{3''}{}_{tpy}$), 120.79 (d, $C^5{}_{tpy}$, $C^{5''}{}_{tpy}$), 106.63 (d, $C^{3'}{}_{tpy}$, $C^{5'}{}_{tpy}$), 67.77 (t, $C^6{}_{alk}$), 53.25 ($C_{Phe\text{-}\alpha}$), 51.70 (C_{OMe}), 36.57 ($C_{Phe\text{-}\beta}$). 33.52 (t, $C^2{}_{alk}$), 28.05 (t, $C^5{}_{alk}$), 24.91 (t, $C^4{}_{alk}$), 24.27 (t, $C^3{}_{alk}$). MS (EI, 70eV, 265°C): *m/z* (%) = 525 (32) $[M]^+$, 494 (2) $[M\text{-}OMe]^+$, 466 (38) $[M\text{-}COOMe]^+$, 434 (25) $[M\text{-}Bzl]^+$, 391 (5), 347 (3), 319 (16) $[tpyOC_5H_{10}]^+$305 (9) $[tpyOC_4H_8]^+$291 (6) $[tpyOC_3H_6]^+$277 (16) $[tpyOC_2H_4]^+$263 (53) $[tpyOCH_2]^+$, $[M\text{-}tpyOCH_2]^+$251 (100) $[tpyO]^+$ 248 (5) $[M\text{-}tpyOC_2H_4]^+$235 (7) $[M\text{-}tpyOC_3H_6]^+$ 221 (24) $[M\text{-}tpyOC_4H_8]^+$.

Synthesis of bpa*-Phe-OMe **3.10**

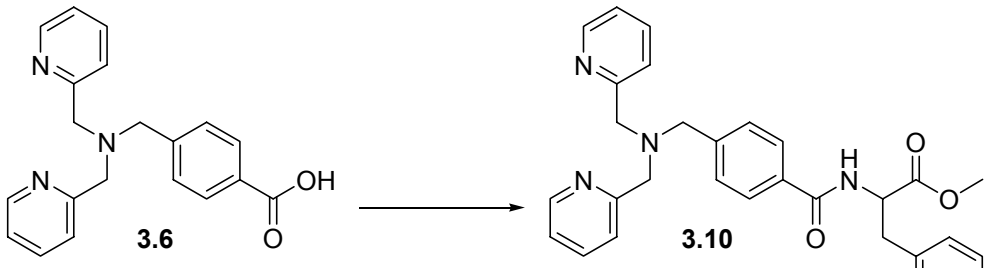

Acid **3.6** (333mg, 1.00mmol) was suspended in acetonitrile (10ml), and phenylalanine methyl ester hydrochloride (216mg, 1.00mmol), TBTU (323mg, 1.00mmol) and DIPEA (1.20ml, 7.20mmol) were added. The yellow reaction mixture was stirred for 1h at room temperature and thereafter the solvent was evaporated *in vacuo*. To the residue dichloromethane (75ml) was added and washed with saturated $NaHCO_3$ solution (75ml) and water (2×75ml). After drying the organic phase over Na_2SO_4 and filtration, the solvent was removed *in vacuo* and the crude product purified by column chromatography on silica (35g, ∅=2.5 cm, ethyl acetate:acetonitrile = 9:1), R_f(**3.10**)=0.12. Yield: 400mg (80.9mmol, 80.9%) of colorless oil.

^{1}H-NMR (360MHz, DMSO-d_6): δ = 8.82 (1H, d, NH, *J*=7.7), 8.50-8.47 (2H, m, H^6_{Py}), 7.87-7.69 (4H, m, H^3_{Bzl}, H^4_{Py}), 7.57 (2H, d, *J*=7.6, H^3_{Py}), 7.49 (2H, d, *J*=7.9, H^2_{Bzl}), 7.31-7.22 (7H, m, $H_{Phe\text{-}o}$, $H_{Phe\text{-}m}$, $H_{Phe\text{-}p}$, H^5_{Py}), 4.68-4.60 (1H, m, $H_{Phe\text{-}\alpha}$), 3.70 (4H, s, $H_{Py\text{-}\alpha}$), 3.67 (2H, s, H_1), 3.62 (3H, s, H_{OMe}), 3.19-3.03 (2H, m, $H_{Phe\text{-}\beta}$). ^{13}C-NMR (90.56MHz, DMSO-d_6): δ = 172.2 ($C{=}O_{Phe}$), 166.4 ($C{=}O_{Bzl}$), 158.9 (C^2_{Py}), 148.9 (C^6_{Py}), 142.6 (C^1_{Bzl}), 137.7 ($C_{Phe\text{-}i}$), 136.7 (C^4_{Py}), 132.5 (C^4_{Bzl}) 129.1 (C^2_{Bzl}), 128.4 (C^3_{Bzl}), 128.3 ($C_{Phe\text{-}o}$), 127.4 ($C_{Phe\text{-}m}$), 126.5 ($C_{Phe\text{-}p}$), 122.6 (C^3_{Py}), 122.2 (C^5_{Py}), 59.1 ($C_{Py\text{-}\alpha}$), 57.1 (C^1), 54.3 ($C_{Phe\text{-}\alpha}$), 52.0 (C_{OMe}), 36.2 ($C_{Phe\text{-}\beta}$). HRMS (EI, 70eV): 494.2317. MS (EI, 70eV, 265°C): *m/z* (%) = 494 (6) $[M]^+$, 463 $[M\text{-}OMe]^+$, 402 (100) $[M\text{-}Bzl]^+$, 198 (31) $[bpa]^+$, 134 (5) $[PyCH_2N(CH_2)_2]^+$, 121 (1) $[PyCH_2NHCH_2]^+$, 107 (1) $[PyCH_2NH]^+$, 93 (64) $[PyCH_2]^+$, 78 (2) $[Py]^+$.

Synthesis of Pseudoneurotensin-Conjugates

The assembly of the pnt conjugates **3.11**-**3.13** was performed according to the standard SPPS procedure described in Chapter 8.6 including the modified ligand coupling protocol explained in that context. A preloaded Fmoc-Leu-Wang resin (0.68mmol/g) was used instead of the resin mentioned there.

A ^{1}H-NMR spectrum was obtained of the hexanoic acid capped pnt derivative **3.11**. The assignment of the proton signals was done with the help of HH-COSY.

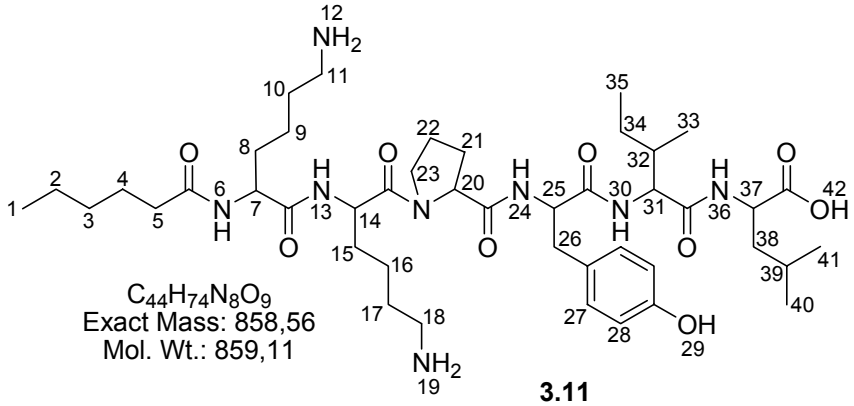

3.11

^{1}H-NMR (360MHz, DMSO-d_6): δ = 8.18 (1H, d, $NH^{24}{}_{Tyr}$), 8.00 (1H, d, $NH^{6}{}_{Lys}$), 7.92 (1H, d, $NH^{30}{}_{Ile}$), 7.83 (1H, d, $NH^{13}{}_{Lys}$), 7.76 (4H, br, $NH_2{}^{12}{}_{Lys}$, $NH_2{}^{19}{}_{Lys}$), 7.72 ($NH^{36}{}_{Leu}$), 6.97 (2H, d, $CH^{27}{}_{Tyr}$), 6.60 (2H, d, $H^{28}{}_{Tyr}$), 4.38-4.42 (2H, br, $CH^{7}{}_{Lys}$, $CH^{14}{}_{Lys}$), 4.31 (1H, d, $CH^{31}{}_{Ile}$), 4.18-4.23 (4H, br, $CH^{25}{}_{Tyr}$, $CH^{37}{}_{Leu}$), 2.52 (2H, m, $CH_2{}^{23}{}_{Pro}$), 2.87 (1H, t, $CH^{20}{}_{Pro}$), 2.65-2.78 (6H, br, $CH_2{}^{11}{}_{Lys}$, $CH_2{}^{18}{}_{Lys}$, $CH_2{}^{26}{}_{Tyr}$), 2.09 (2H, t, $CH_2{}^{5}{}_{Hex}$), 1.94 (1H, m, $CH^{39}{}_{Leu}$), 1.78 (4H, br, $CH_2{}^{21}{}_{Pro}$, $CH_2{}^{22}{}_{Pro}$), 1.42-1.18 (15H, br. m, ($CH_2{}^{38}{}_{Leu}$, $CH_2{}^{34}{}_{Ile}$, $CH_2{}^{8}{}_{Lys}$, $CH_2{}^{9}{}_{Lys}$ $CH_2{}^{10}{}_{Lys}$, $CH_2{}^{15}{}_{Lys}$, $CH_2{}^{16}{}_{Lys}$, $CH_2{}^{17}{}_{Lys}$), 1.15-1.40 (6H, br. m, $CH_2{}^{2}{}_{Hex}$, $CH_2{}^{3}{}_{Hex}$, $CH_2{}^{4}{}_{Hex}$,), 1.05 (1H, m, $CH^{32}{}_{Ile}$), 0.76-0.90 (15H, m, $CH_3{}^{1}{}_{Hex}$, $CH_3{}^{33}{}_{Ile}$, $CH_3{}^{35}{}_{Ile}$, $CH_3{}^{40}{}_{Leu}$, $CH_3{}^{41}{}_{Leu}$). MS (ESI-pos): *m/z* = 859.8, 430.5.

8.3 Synthesis of Copper Complexes

For the in situ preparation of Cu complexes, equimolar amounts of ligand / bioconjugate and copper solution were mixed to obtain a 10mM dilution which was subjected to MS. This procedure was performed for all tpy-substituted compounds and for bpa*-pnt (see Chapter 3.5.1 for MS data). The short-chain bpa*-conjugate complexes were isolated according to the following.

Synthesis of (bpa*-OMe)$Cu(NO_3)_2$

Solutions of bpa*-OMe (86.8mg, 0.25mmol) and $Cu(NO_3)_2 \cdot 3H_2O$ (60.4mg, 0.25mmol) in methanol (10ml each) were mixed at 50°C and cooled down slowly. After 2 days, the product was collected by filtration. Yield 73.0mg (0.14mmol, 55%) of blue crystals.
M_r ($C_{21}H_{21}N_5O_8Cu$) = 534.99. MS (ESI-pos): m/z 472 $[M\text{-}NO_3]^+$, 455 $[M\text{-}Py]^+$, 441 $[M\text{-}PyCH_2]^+$, 427 $[M\text{-}PyCH_2\text{-}Me]^+$, 410 $[M\text{-}2NO_3]^+$, 346 $[M\text{–}Cu(NO_3)_2]^+$, 317 $[M\text{-}2NO_3\text{-}PyCH_2]^+$, 260 $[Cu\text{-}bpa]^+$. MS (FAB-pos, glycerol): m/z 472 $[M\text{-}NO_3]^+$, 410 $[M\text{-}2NO_3]^+$, 346 $[M\text{-}Cu(NO_3)_2]^+$, 317 $[M\text{-}2NO_3\text{-}PyCH_2]^+$, 260 $[Cu\text{-}bpa]^+$. HRMS (FAB-pos, glycerol, PEG300): m/z exp 472.0819 and calc. 472.0808 for $[C_{21}H_{21}N_4O_5{}^{63}Cu]^+$, exp. 410.0915 and calc. 410.0930 for $[C_{21}H_{21}N_3O_2{}^{63}Cu]^+$.

Synthesis of (bpa*-OH)$CuNO_3$ **3.6_{Cu}**

Solutions of ligand **3.6** (83.4mg, 0.25 mmol) and $Cu(NO_3)_2 \cdot 3H_2O$ (60.4mg, 0.25mmol) in methanol (10ml each) were mixed at 50°C and cooled down slowly. After standing overnight, product **3.6_{Cu}** was collected by filtration. Yield 89mg (0.17mmol, 68%) of blue crystals.
M_r ($C_{20}H_{18}N_4O_5Cu$) = 457.93. MS (ESI-pos): m/z 396 $[M\text{-}NO_3]^+$. MS (FAB-pos, glycerol): m/z 458 $[M]^+$, 396 $[M\text{-}NO_3]^+$, 352 $[M\text{-}NO_3\text{-}CO_2]^+$, 303 $[M\text{-}NO_3\text{-}PyCH_2]^+$ 260 $[Cu\text{–}bpa]^+$. HRMS (FAB-pos, glycerol, PEG300): m/z exp. 458.0585 and calc. 458.0651 for $[C_{20}H_{19}N_4O_5{}^{63}Cu]^+$, exp. 396.0780 and calc. 396.0773 for $[C_{20}H_{19}N_3O_2{}^{63}Cu]^+$.

Synthesis of (bpa*-Phe-OMe)$Cu(NO_3)_2$ **3.10_{Cu}**

Solutions of **3.10** (49.5mg, 0.10mmol) and $Cu(NO_3)_2 \cdot 3H_2O$ (24.2mg, 0.10mmol) in ethanol (5ml each) were mixed at 50°C and cooled down slowly. After 4 days, product **3.10_{Cu}** was collected by filtration. Yield: 23mg (34µmol, 34%) of blue powder.
M_r ($C_{30}H_{30}N_6O_9Cu$) = 682.17. MS (ESI-pos): 619 $[M\text{-}NO_3]^+$, 602 $[M\text{-}Py]^+$, 588 $[M\text{-}NO_3\text{-}OMe]^+$, 557 $[M\text{-}2NO_3]^+$, 496 $[M - Cu(NO_3)_2]^+$. MS (FAB-pos, glycerol): m/z 619 $[M\text{-}NO_3]^+$, 557 $[M\text{-}2NO_3]^+$, 497 $[M\text{-}Cu(NO_3)_2]^+$, 351 $[Cu\text{-}bpaBzl]^+$, 260 $[Cu\text{-}bpa]^+$. HRMS (FAB-pos, NBA, PEG600): m/z exp. 619.1451 and calc. 619.1492 for $[C_{30}H_{30}N_5O_6{}^{63}Cu]^+$, exp. 557.1575 and calc. 557.1614 for $[C_{30}H_{30}N_4O_3{}^{63}Cu]^+$.

8.4 Synthesis of Modified Amino Acids

Synthesis of *p*-nitro-phenylalanine **5.1**

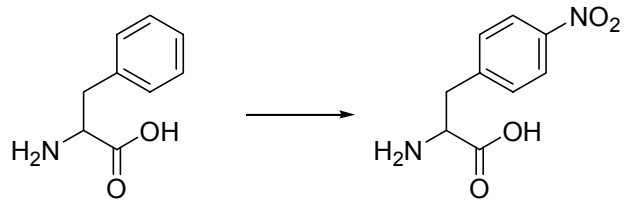

5.1

$C_9H_{11}NO_2$
Exact Mass: 165,08
Mol. Wt.: 165,19

$C_9H_{10}N_2O_4$
Exact Mass: 210,06
Mol. Wt.: 210,19

At 0°C, conc. H_2SO_4 (120ml) was slowly added under stirring to 120ml of conc. HNO_3. H-Phe-OH (100g, 605mmol) was added in portions over a period of 20min., giving a yellow, sticky solution. Stirring was continued overnight, the resulting slurry was poured over crushed ice and brought to pH7 with NaOH. The white precipitate was separated by filtration and dried *in vacuo*. Yield: 92.6g (441mmol, 72.8%)

Phenylalanine

^{1}H-NMR (360MHz, DMSO-d6): δ = 7.26 (5H, m, H^2_{Bz}, H^3_{Bz}, H^4_{Bz}, H^5_{Bz}, H^6_{Bz}), 3.74 (1H, t, Hα), 3.18 (2H, m, Hβ). ^{13}C-NMR (90.56MHz, DMSO-d6): δ = 169.31 (CO), 137.85 (C^1_{Bz}), 129.29 (C^4_{Bz}), 128.25 (C^2_{Bz}, C^6_{Bz}), 126.32 (C^3_{Bz}, C^5_{Bz}), 55.60 (Cα), 37.13 (Cβ).

p-Nitro-phenylalanine **5.1**

^{1}H-NMR (360MHz, DMSO-d6): δ = 8.16 (2H, d, H^3_{Bz}, H^5_{Bz}), 7.45 (2H, d, H^2_{Bz}, H^6_{Bz}), 3.98 (1H, t, Hα), 3.27 (2H, m, Hβ). ^{13}C-NMR (90.56MHz, DMSO-d6): δ = 173.86 (CO), 144.41 (C^1_{Bz}, C^4_{Bz}), 131.42 (C^2_{Bz}, C^6_{Bz}), 125.01 (C^3_{Bz}, C^5_{Bz}), 56.52 (Cα), 37.24 (Cβ). MS (EI, 70eV, 210°C): *m/z* (%) = 210 [M^+] (0.5), 165 (38.1), 137 (63.7), 119 (27.0), 107 (23.6), 90 (31.1), 74 (100.0), 46 (26.6), 28 (70.7).

Synthesis of Fmoc-*p*-nitro-phenylalanine **5.2**

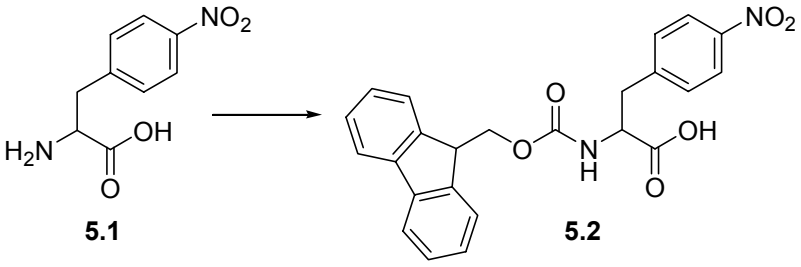

5.1

$C_9H_{10}N_2O_4$
Exact Mass: 210,06
Mol. Wt.: 210,19

5.2

$C_{24}H_{20}N_2O_6$
Exact Mass: 432,13
Mol. Wt.: 432,43

5.45g (25mmol) of *p*-nitro-phenylalanine was dissolved in a mixture of each 50ml of H_2O and CH_3CN and treated with 1 equivalent of NEt_3 (2.5g, 25mmol). After 10min. of stirring, 8.0g (23.75mmol 95%) of Fmoc-ONSu in 50ml of CH_3CN was added dropwise over a period of 20min, while pH was adjusted to 8.5-9.0. After 2h of continuous stirring and successive filtration, the solvents were removed *in vacuo* and a red oil remained. The residue was again dissolved in water and afterwards neutralized using 1N HCl until the crude product precipitated. Recrystallization from EtOAc yielded 5.9g (53%) of pure product as a white solid.

^{1}H-NMR (360 MHz, DMSO-d6): δ = 8.11 (2H, d, H^3_{Bz}, H^5_{Bz}), 7.84 (2H, d, H^4_{Fmoc}, H^5_{Fmoc}), 7.78 (1H, d, NH), 7.60 (2H, d, H^1_{Fmoc}, H^8_{Fmoc}), 7.53 (2H, d, H^2_{Bz}, H^6_{Bz}), 7.38 (2H, m, H^3_{Fmoc}, H^6_{Fmoc}), 7.27 (2H, m, H^2_{Fmoc}, H^7_{Fmoc}), 4.30 (2H, d, H^{10}_{Fmoc}), 4.23 (1H, t, H^9_{Fmoc}), 4.15 (1H, t, Hα), 3.25 (2H, m, Hβ). ^{13}C-NMR (90.56 MHz, DMSO-d6): δ = 172.91 (CO), 155.97 (C^{11}_{Fmoc}), 146.46 (C^1_{Bz}), 146.23 (C^4_{Bz}) 143.71 (C^{8a}_{Fmoc}, C^{9a}_{Fmoc}), 140.72 (C^{4a}_{Fmoc}, C^{4b}_{Fmoc}), 130.46 (C^2_{Bz}, C^6_{Bz}), 127.62 (C^1_{Fmoc}, C^8_{Fmoc}), 127.06 (C^4_{Fmoc}, C^5_{Fmoc}), 125.11 (C^2_{Fmoc}, C^7_{Fmoc}), 123.23 (C^3_{Bz}, C^5_{Bz}), 120.18 (C^3_{Fmoc}, C^6_{Fmoc}), 65.67 (C^{10}_{Fmoc}), 54.84 (Cα), 46.69 (C^9_{Fmoc}), 36.17 (Cβ). MS (FAB-pos): *m/z* = 433 $[M+H]^+$, 255 [M-Fluorenyl]$^+$, 165 [Fluorenyl]$^+$.

Synthesis of Fmoc-*p*-amino-phenylalanine **5.3**

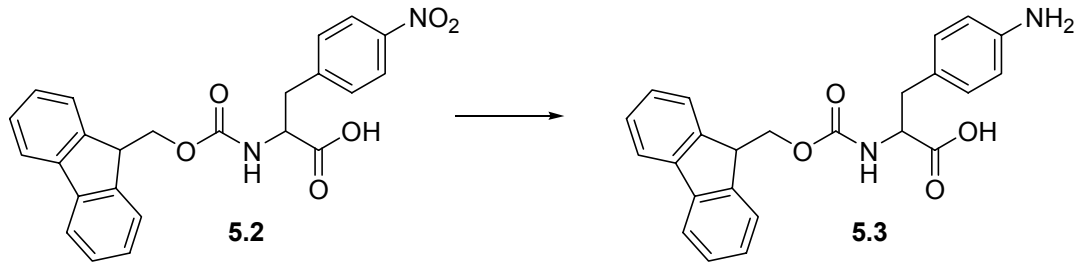

5.2

$C_{24}H_{20}N_2O_6$
Exact Mass: 432,13
Mol. Wt.: 432,43

5.3

$C_{24}H_{22}N_2O_4$
Exact Mass: 402,16
Mol. Wt.: 402,44

In a three-necked, round-bottomed flask, equipped with a gas inlet tube and a bubble counter, Fmoc-Phe(NO_2)-OH **5.2** (3g, 6.9mmol) was dissolved in a mixture of 200ml dioxane and 30ml EtOH. After some heating, a clear solution of light yellow colour formed. 200mg of Pd/C catalyst was added, followed by the inlet of dihydrogen. The progress of the reaction was monitored by HPLC, taking 0.2ml samples from the reaction mixture every 30min. These samples were diluted with MeCN (1:50), the catalyst was removed with a syringe filter, and the solution was centrifuged. Each sample was subjected to HPLC, using a standard gradient with MeCN/H_2O. After 24h, the HPLC peaks showed the completeness of the reduction, and the mixture was filtrated. After removal of the solvents on a rotary evaporator and drying of the residue *in vacuo*, a light brown solid was obtained. Yield: 2.18g (5.4mmol, 78%)

^{1}H-NMR (360 MHz, DMSO-d6): δ = 7.88 (2H, d, H^4_{Fmoc}, H^5_{Fmoc}), 7.68 (2H, d, H^1_{Fmoc}, H^8_{Fmoc}), 7.58 (1H, d, NH), 7.43 (2H, m, H^3_{Fmoc}, H^6_{Fmoc}), 7.32 (2H, m, H^2_{Fmoc}, H^7_{Fmoc}), 6.90 (2H, d, H^2_{Bz}, H^6_{Bz}), 6.47 (2H, d, H^3_{Bz}, H^5_{Bz}), 4.24 (2H, d, H^{10}_{Fmoc}), 4.19 (1H, t, H^9_{Fmoc}), 4.15 (1H, t, Hα), 4.03 (2H, m, NH_2), 2.88 (2H, m, Hβ). ^{13}C-NMR (90.56 MHz, DMSO-d6): δ = 173.57 (CO), 155.87 (C^{11}_{Fmoc}), 146.99 (C^1_{Bz}), 143.77 (C^{8a}_{Fmoc}, C^{9a}_{Fmoc}), 140.65 (C^{4a}_{Fmoc}, C^{4b}_{Fmoc}), 129.52 (C^2_{Bz}, C^6_{Bz}), 127.61 (C^1_{Fmoc}, C^8_{Fmoc}), 127.04 (C^4_{Fmoc}, C^5_{Fmoc}), 125.29 (C^2_{Fmoc}, C^7_{Fmoc}), 124.75 (C^4_{Bz}), 124.16 (C^3_{Bz}, C^5_{Bz}), 120.07 (C^3_{Fmoc}, C^6_{Fmoc}), 65.26 (C^{10}_{Fmoc}), 56.10 (Cα), 46.64 (C^9_{Fmoc}), 35.86 (Cβ). MS (EI, 70eV, 210°C): *m/z* = 402 (1.3) $[M+H]^+$, 324 (0.5), 252 (0.4), 224 (3.0), 206 (1.5), 194 (5.6), 178 (49), 165 (21), 152 (5.5), 106 (100). MS (FAB-pos, NBA): *m/z* = 403 $[M+H]^+$, 391, 307, 289, 252, 240, 179, 154, 136.

^{1}H-NMR (360MHz, DMSO-d_6)

δ (ppm)	H-Phe-OH	5.1	5.2	5.3
NH_2	–	–	–	4.03
H^4_{Bz}	7.26	–	–	–
H^3_{Bz}, H^5_{Bz}	**7.26**	**8.16**	**8.11**	**6.47**
H^2_{Bz}, H^6_{Bz}	**7.26**	**7.45**	**7.53**	**6.90**
NH	–	–	7.78	7.58
H^4_{Fmoc}, H^5_{Fmoc}	–	–	7.84	7.88
H^1_{Fmoc}, H^8_{Fmoc}	–	–	7.60	7.68
H^3_{Fmoc}, H^6_{Fmoc}	–	–	7.38	7.43
H^2_{Fmoc}, H^7_{Fmoc}	–	–	7.27	7.32
Hα	3.74	3.98	4.15	4.15
Hβ	3.18	3.27	3.25	2.88
H^{10}_{Fmoc}	–	–	4.30	4.24
H^9_{Fmoc}	–	–	4.23	4.19

^{13}C-NMR (90.56MHz, DMSO-d_6)

δ (ppm)	H-Phe-OH	5.1	5.2	5.3
CO	169.31	173.86	172.91	173.57
C^1_{Bz}	**137.85**	**144.41**	**146.46**	**146.99**
C^3_{Bz}, C^5_{Bz}	126.32	125.01	123.23	124.16
C^2_{Bz}, C^6_{Bz}	128.25	131.42	130.46	129.52
C^4_{Bz}	**129.29**	**144.41**	**146.23**	**124.75**
Cα	**55.60**	**56.52**	**54.84**	**65.26**
Cβ	37.13	37.24	36.17	35.86
C^1_{Fmoc}, C^8_{Fmoc}	–	–	127.62	127.61
C^2_{Fmoc}, C^7_{Fmoc}	–	–	125.11	125.29
C^3_{Fmoc}, C^6_{Fmoc}	–	–	120.18	120.07
C^4_{Fmoc}, C^5_{Fmoc}	–	–	127.06	127.04
C^{4a}_{Fmoc}, C^{4b}_{Fmoc}	–	–	140.72	140.65
C^{8a}_{Fmoc}, C^{9a}_{Fmoc}	–	–	143.71	143.77
C^9_{Fmoc}	–	–	46.69	46.64
C^{10}_{Fmoc}	–	–	65.67	65.26
C^{11}_{Fmoc}	–	–	155.97	155.87

8.5 Synthesis of PNA-Monomers

The numbering of atoms for PNA monomers is conceived according to IUPAC:

Cytosine

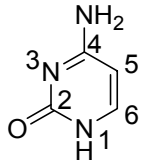

Thymine

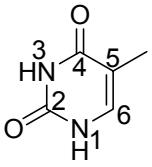

Adenine

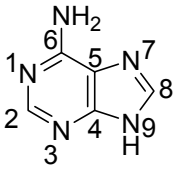

Guanine

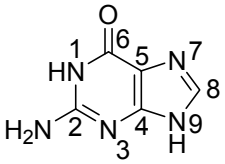

PG

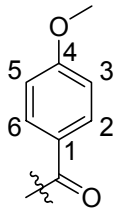

Backbone

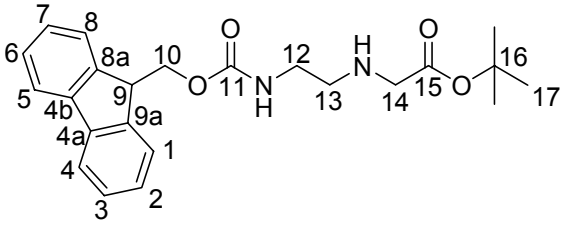

Synthesis of ethylendiamine acetic acid *t*Bu-ester **4.1**

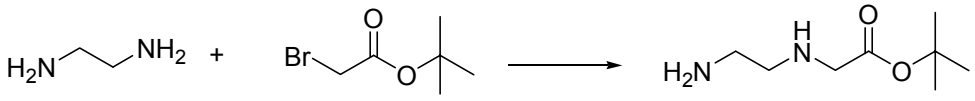

4.1

$C_2H_8N_2$	$C_6H_{11}BrO_2$	$C_8H_{18}N_2O_2$
Exact Mass: 60,07	Exact Mass: 193,99	Exact Mass: 174,14
Mol. Wt.: 60,1	Mol. Wt.: 195,05	Mol. Wt.: 174,24

55.3g (62ml, 920mmol, 8.5eq.) of ethylenediamine (d=0.89g/ml) (which does not necessarily have to be distilled before use, even if yellow) was dissolved in 400ml CH_2Cl_2 in a 1L round-bottomed flask. At 0°C, a solution of 16ml (21.1g, 108mmol) *tert*-Butylbromoacetate in 80ml CH_2Cl_2 was added dropwise under stirring over 3-4h forming a white precipitate. Sometimes, two phases may occur, which can be ignored. The solution was allowed to slowly reach room temperature and stirred overnight. After that, it was washed three times with 100ml of water in order to remove the excess of ethylenediamine and the HBr formed during the reaction. These 300ml of water were washed with 100ml CH_2Cl_2, and the combined (clear and colourless) organic phases were dried over $MgSO_4$. The yellow aqueous phase was discarded. After removing the $MgSO_4$, the solution was used directly for the next step assuming a yield of 80% (86mmol).

Synthesis of backbone·HCl

(9H-fluoren-9-yl)methyl-2-((*tert*-butoxycarbonyl)methylamino)ethylcarbamate **4.2**

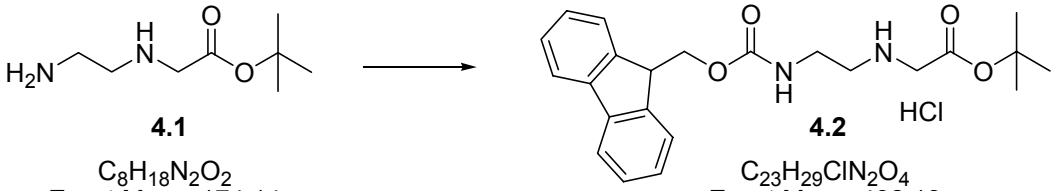

4.1

$C_8H_{18}N_2O_2$
Exact Mass: 174,14
Mol. Wt.: 174,24

4.2

$C_{23}H_{29}ClN_2O_4$
Exact Mass: 432,18
Mol. Wt.: 432,94

After adding 15ml (86mmol) DIPEA to the solution of **4.1** obtained from the previous step, a solution of 29g (86mmol) Fmoc-ONSu in 150ml of CH_2Cl_2 was added at RT over a period of 3h, followed by stirring overnight. The solution was washed 5 times with 100ml 1N HCl and once with 100ml brine. The aqueous phases were combined, washed with 100ml of CH_2Cl_2 and the combined organic phases were dried over $MgSO_4$. After filtering the solid, the solution was concentrated to ¼ by evaporation. The product crystallized out of the clear solution overnight at -10°C forming white crystals which were separated and washed with 30ml of hexane. The product was dried *in vacuo* yielding 20.45g (48mmol, 55%) the hydrochloride as white, amorphous powder.

^{1}H-NMR (360MHz, DMSO-d_6): δ = 9.54 (2H, br, NH_{BB}), 7.88 (2H, d, $H^4{}_{Fmoc}$, $H^5{}_{Fmoc}$), 7.70 (2H, d, $H^1{}_{Fmoc}$, $H^8{}_{Fmoc}$), 7.40 (2H, m, $H^3{}_{Fmoc}$, $H^6{}_{Fmoc}$), 7.30 (2H, m, $H^2{}_{Fmoc}$, $H^7{}_{Fmoc}$), 4.28 (2H, d, $H^{10}{}_{Fmoc}$), 4.20 (1H, t, $H^9{}_{Fmoc}$), 3.85 (2H, s, $H^{14}{}_{BB}$), 3.37 (2H, t, $H^{12}{}_{BB}$), 3.02 (2H, t, $H^{13}{}_{BB}$), 1.44 (9H, s, $H^{17}{}_{BB}$). ^{13}C-NMR (90.56MHz, DMSO-d_6): δ = 165.57 ($C^{15}{}_{BB}$), 156.28 ($C^{11}{}_{Fmoc}$), 143.80 ($C^{8a}{}_{Fmoc}$, $C^{9a}{}_{Fmoc}$), 140.74 ($C^{4a}{}_{Fmoc}$, $C^{4b}{}_{Fmoc}$), 127.64 ($C^1{}_{Fmoc}$, $C^8{}_{Fmoc}$), 127.08 ($C^4{}_{Fmoc}$, $C^5{}_{Fmoc}$), 125.20 ($C^2{}_{Fmoc}$, $C^7{}_{Fmoc}$), 120.12 ($C^3{}_{Fmoc}$, $C^6{}_{Fmoc}$), 82.97 ($C^{16}{}_{BB}$), 65.68 ($C^{10}{}_{Fmoc}$), 47.24 ($C^{14}{}_{BB}$), 46.66 ($C^9{}_{Fmoc}$), 46.42 ($C^{13}{}_{BB}$), 36.62 ($C^{12}{}_{BB}$), 27.61 ($C^{17}{}_{BB}$). MS (EI, 70eV, 165°C): *m/z* (%) = 396 (1.7) [M^+-HCl], 351 (0.2), 340 (9.0), 322 (10.1), 295 (61.4), 196 (2.5), 178 (100.0), 165 (24.8), 152 (6.2), 117 (19.1), 99 (13.0), 88 (89.4), 73 (24.6), 57 (47.3), 44 (19.3), 30 (12.5).

^{1}H-NMR (360MHz, DMSO-d_6)

δ (ppm)	4.2
NH_{BB}	9.54
H^{4}_{Fmoc}, H^{5}_{Fmoc}	7.88
H^{1}_{Fmoc}, H^{8}_{Fmoc}	7.70
H^{3}_{Fmoc}, H^{6}_{Fmoc}	7.40
H^{2}_{Fmoc}, H^{7}_{Fmoc}	7.30
H^{10}_{Fmoc}	4.28
H^{9}_{Fmoc}	4.20
H^{14}_{BB}	3.85
H^{12}_{BB}	3.37
H^{13}_{BB}	3.02
H^{17}_{BB}	1.44

^{13}C-NMR (90.56MHz, DMSO-d_6)

δ (ppm)	4.2
C^{1}_{Fmoc}, C^{8}_{Fmoc}	127.64
C^{2}_{Fmoc}, C^{7}_{Fmoc}	125.20
C^{3}_{Fmoc}, C^{6}_{Fmoc}	120.12
C^{4}_{Fmoc}, C^{5}_{Fmoc}	127.08
C^{4a}_{Fmoc}, C^{4b}_{Fmoc}	140.74
C^{8a}_{Fmoc}, C^{9a}_{Fmoc}	143.80
C^{9}_{Fmoc}	46.66
C^{10}_{Fmoc}	65.68
C^{11}_{Fmoc}	156.28
C^{12}_{BB}	36.62
C^{13}_{BB}	46.42
C^{14}_{BB}	47.24
C^{15}_{BB}	156.57
C^{16}_{BB}	82.97
C^{17}_{BB}	27.61

Synthesis of thymine-acetic acid **4.3**

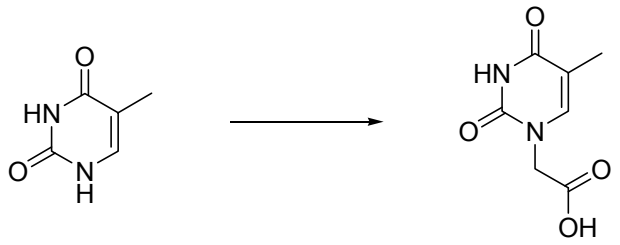

4.3

$C_5H_6N_2O_2$
Exact Mass: 126,04
Mol. Wt.: 126,11

$C_7H_8N_2O_4$
Exact Mass: 184,05
Mol. Wt.: 184,15

In a 1L round-bottomed flask, a solution of KOH (17.15g, 0.3mol) in H_2O (50ml) was heated to 40-50°C. After dissolving 10.1g (80.2mmol) of thymine, a solution of 16.5g (118.7mmol, 1.5eq.) bromo-acetic acid in 25ml H_2O was added dropwise during 1h, maintaining the temperature at 40-50°C. After stirring overnight at RT, the pH was adjusted to 5.5 with conc. HCl. The flask was stored at -10°C for 2h, and the excess of thymine was filtered off. The pH was brought to 2 with conc. HCl, and the white product precipitated. After storage for 2h at -10°C, it was filtered and dried *in vacuo* yielding a white powder. Yield: 11.8g (64mmol, 80%)

^{1}H-NMR (360MHz, D_2O): δ = 11.29 (1H, s, NH_{Th}), 7.38 (1H, s, $H^6{}_{Th}$), 4.48 (2H, s, $H\alpha_{Ac}$); 1.83 (3H, s, Me_{Th}). ^{1}H-NMR (360MHz, DMSO-d_6): 11.29 (1H, s, NH_{Th}), 7.48 (1H, s, $H^6{}_{Th}$); 4.33 (2H, s, $H\alpha_{Ac}$); 1.75 (3H, s, Me_{Th}). ^{13}C-NMR (90.56MHz, DMSO-d_6): δ = 170.94 (CO_{Ac}), 165.92 ($C^4{}_{Th}$), 152.25 ($C^2{}_{Th}$), 143.06 ($C^6{}_{Th}$), 109.82 ($C^5{}_{Th}$), 49.58 ($C\alpha_{Ac}$), 12.94 (Me_{Th}). MS (EI, 70eV, 165°C): *m/z* (%) = 184 (32.9), 140 (54.9), 126 (1.3), 113 (4.0), 96 (100.0), 82 (4.3), 68 (16.9), 55 (13.2), 41 (39.5), 28 (6.6).

Synthesis of thymine-backbone **4.4**

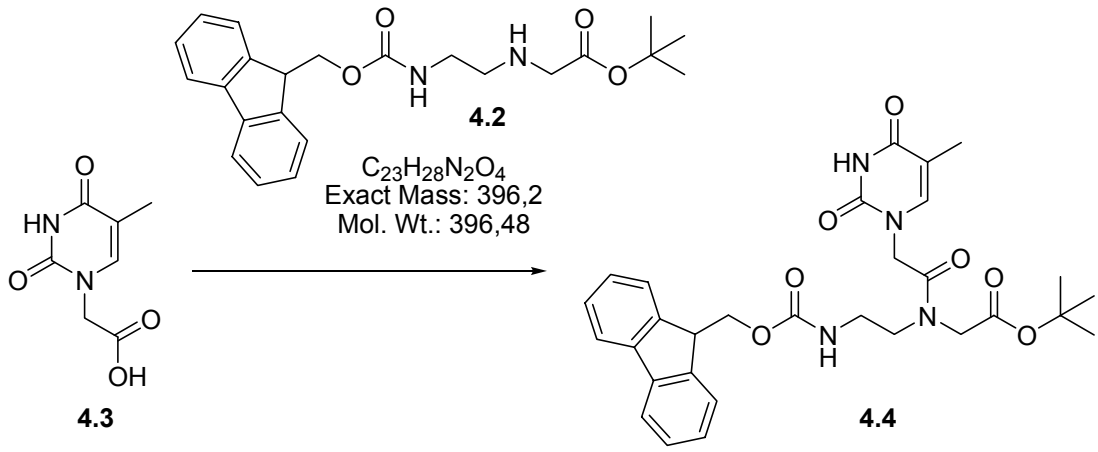

Backbone·HCl **4.2** (3.25g, 7.5mmol) was suspended in dichloromethane (30ml) in an extraction funnel and $NaHCO_3$ (sat. aq, 30ml) was added. After extraction, the dichloromethane layer was dried over $MgSO_4$ for 10min. and the solvent was removed on a rotary evaporator. The resulting solid was dissolved in a dry 250ml Schlenk flask in DMF (50ml, dried over molecular sieves), and thymine-acetic acid **4.3** (4.03g, 22mmol) was added. After complete dissolution, 3.41g (22mmol) EDC was added in two portions within 30min, followed by stirring overnight at RT. The solvent was evaporated in vacuo, and the residue was coevaporated with 2x40ml methanol. 100ml of degassed water was added under stirring. The precipitate was filtered off, washed again with 100ml of degassed water and dried in vacuo. Yield: 4.03g (7.2mmol, 72%)

Flash Chromatography:

Crude Fmoc-T-PNA-OtBu **4.4** (1.7g) and dichloromethane were stirred overnight. Then silica (0.040-0.063mm, 1g) was added and dichloromethane removed under reduced pressure. The solvent mixture was prepared (CH_2Cl_2:MeOH=97.5:2.5) and a flash column filled with fresh silica (0.040-0.063mm, 40g). Flash chromatography was carried out and the fractions (20ml) analyzed by TLC. Fractions 8-13 were combined and evaporated under reduced pressure yielding 542mg of pure product as a white powder. Fractions containing impurities were chromatographed again.

^{1}H-NMR δ (360MHz, DMSO-d_6): δ = 11.26 (2H, br, NH_{Th}), 7.90 (2H, d, H^{4}_{Fmoc}, H^{5}_{Fmoc}), 7.69 (2H, d, H^{1}_{Fmoc}, H^{8}_{Fmoc}), 7.42 (2H, m, H^{3}_{Fmoc}, H^{6}_{Fmoc}), 7.32 (2H, m, H^{2}_{Fmoc}, H^{7}_{Fmoc}), 7.26 (1H, s, H^{6}_{Th}), 4.65 (1.2H, s, $H\alpha^{maj}_{Ac}$), 4.47 (0.8H, s, $H\alpha^{min}_{Ac}$), 4.35 (2H, d, H^{10}_{Fmoc}), 4.22 (1H, t, H^{9}_{Fmoc}), 3.93 (2H, s, H^{14}_{BB}), 3.40 (1.2H, t, H^{12maj}_{BB}), 3.31 (0.8H, t, H^{12min}_{BB}), 3.25 (1.2H, t, H^{13maj}_{BB}), 3.09 (0.8H, t, H^{13min}_{BB}), 1.74 (3H, s, Me_{Th}), 1.46 (3.6H, s, H^{17min}_{BB}), 1.41 (5.4H, s, H^{17maj}_{BB}). ^{13}C-NMR (90.56MHz, DMSO-d_6): δ = 170.82 (CO_{Ac}), 167.58 (C^{15}_{BB}), 165.11 (C^{11}_{Fmoc}), 164.64 (C^{4}_{Th}), 151.23 (C^{2}_{Th}), 143.61 (C^{8a}_{Fmoc}, C^{9a}_{Fmoc}), 142.42 (C^{6}_{Th}), 140.72 (C^{4a}_{Fmoc}, C^{4b}_{Fmoc}), 128.03 (C^{1}_{Fmoc}, C^{8}_{Fmoc}), 126.87 (C^{4}_{Fmoc}, C^{5}_{Fmoc}), 125.26 (C^{2}_{Fmoc}, C^{7}_{Fmoc}), 120.51 (C^{3}_{Fmoc}, C^{6}_{Fmoc}), 108.53 (C^{5}_{Th}), 83.14 (C^{16}_{BB}), 65.48 (C^{10}_{Fmoc}), 49.14 ($C\alpha_{Ac}$), 47.65 (C^{14}_{BB}), 46.91 (C^{13}_{BB}), 46.27 (C^{9}_{Fmoc}), 39.02 (C^{12}_{BB}), 27.55 (C^{17}_{BB}), 11.92 (Me_{Th}).

Synthesis of thymine monomer **4.5**

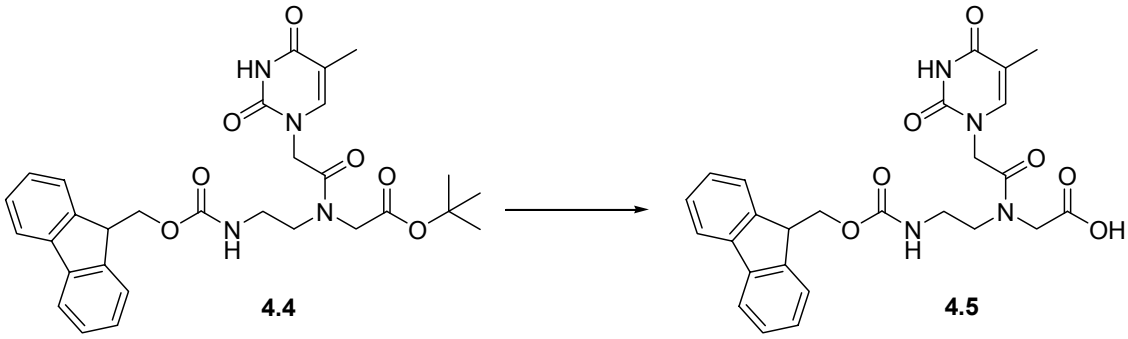

4.4

$C_{30}H_{34}N_4O_7$
Exact Mass: 562,24
Mol. Wt.: 562,61

4.5

$C_{26}H_{26}N_4O_7$
Exact Mass: 506,18
Mol. Wt.: 506,51

Thymine-backbone **4.4** (584mg, 1mmol) was suspended in a 100ml round-bottomed flask in 20ml DCM together with 0.1ml TIS and 0.1ml water and cooled to 0°C. TFA (4ml) was added dropwise over a period of 5min, and after 15min of stirring, the mixture was allowed to reach RT. and left under stirring overnight (16h). The solvent was removed by rotary evaporation and dried *in vacuo*. After coevaporation with acetonitrile (4x20ml), the resulting white solid was dried for 8h *in vacuo* giving the product in quantitative yield.

Alternatively, the *t*Bu-ester cleavage can be carried out with HCl, which avoids TFA contamination of the product. Thymine-backbone **4.4** (7g, 12.4mmol) was suspended in a mixture of 50ml acetic acid and 25ml 4N HCl and stirred for 48h. The solution got clear first, and after a while, the product precipitated. The solvent was removed by rotary evaporation, the residue was dissolved in THF and precipitated from hexane:toluene 3:1, followed by drying *in vacuo*. Yield: 5.8g (11.5mmol, 92%)

^{1}H-NMR δ (360MHz, DMSO-d_6): δ = 11.24 (2H, br, NH_{Th}), 7.87 (2H, d, $H^4{}_{Fmoc}$, $H^5{}_{Fmoc}$), 7.67 (2H, d, $H^1{}_{Fmoc}$, $H^8{}_{Fmoc}$), 7.40 (2H, m, $H^3{}_{Fmoc}$, $H^6{}_{Fmoc}$), 7.32 (2H, m, $H^2{}_{Fmoc}$, $H^7{}_{Fmoc}$), 7.25 (1H, s, $H^6{}_{Th}$), 4.64 (1.2H, s, $H\alpha^{maj}{}_{Ac}$), 4.46 (0.8H, s, $H\alpha^{min}{}_{Ac}$), 4.31 (2H, d, $H^{10}{}_{Fmoc}$), 4.21 (1H, t, $H^9{}_{Fmoc}$), 3.97 (2H, s, $H^{14}{}_{BB}$), 3.38 (1.2H, t, $H^{12maj}{}_{BB}$), 3.30 (0.8H, t, $H^{12min}{}_{BB}$), 3.22 (1.2H, t, $H^{13maj}{}_{BB}$), 3.05 (0.8H, t, $H^{13min}{}_{BB}$), 1.72 (3H, s, Me_{Th}). ^{13}C-NMR (90.56MHz, DMSO-d_6): δ = 170.73 (CO_{Ac}), 167.58 ($C^{15}{}_{BB}$), 165.31 ($C^{11}{}_{Fmoc}$),

164.38 (C^{4}_{Th}), 150.95 (C^{2}_{Th}), 143.81 (C^{8a}_{Fmoc}, C^{9a}_{Fmoc}), 142.04 (C^{6}_{Th}), 140.69 (C^{4a}_{Fmoc}, C^{4b}_{Fmoc}), 127.59 (C^{1}_{Fmoc}, C^{8}_{Fmoc}), 127.04 (C^{4}_{Fmoc}, C^{5}_{Fmoc}), 125.01 (C^{2}_{Fmoc}, C^{7}_{Fmoc}), 120.08 (C^{3}_{Fmoc}, C^{6}_{Fmoc}), 108.08 (C^{5}_{Th}), 65.42 (C^{10}_{Fmoc}), 49.32 ($C\alpha_{Ac}$), 47.64 (C^{14}_{BB}), 46.86 (C^{13}_{BB}), 46.68 (C^{9}_{Fmoc}), 38.81 (C^{12}_{BB}), 11.86 (Me_{Th}). MS (ESI-neg): *m/z* = 1011.5 $[2M-H]^-$, 506.3 $[M-H]^-$. MALDI-TOF (pos, CCA): *m/z* = 507.2 $[M+H]^+$, 529.2 $[M+Na]^+$, 545.2 $[M+K]^+$, 551.2 $[M-H+2Na]^+$, 567.2 $[M-H+Na+K]^+$.

^{1}H-NMR (360MHz, DMSO-d$_6$)

δ (ppm)	**4.3**	**4.4**	**4.5**
NH_{Th}	11.29	11.26	11.24
H^{4}_{Fmoc}, H^{5}_{Fmoc}	–	7.90	7.87
H^{1}_{Fmoc}, H^{8}_{Fmoc}	–	7.69	7.67
H^{3}_{Fmoc}, H^{6}_{Fmoc}	–	7.42	7.40
H^{2}_{Fmoc}, H^{7}_{Fmoc}	–	7.32	7.32
H^{6}_{Th}	7.48	7.26	7.25
$H\alpha_{Ac}^{maj}$	4.33	4.65	4.64
$H\alpha_{Ac}^{min}$	4.33	4.47	4.46
H^{10}_{Fmoc}	–	4.35	4.31
H^{9}_{Fmoc}	–	4.22	4.21
H^{14}_{BB}	–	3.93	3.97
H^{12maj}_{BB}	–	3.40	3.38
H^{12min}_{BB}	–	3.31	3.30
H^{13maj}_{BB}	–	3.25	3.22
H^{13min}_{BB}	–	3.09	3.05
Me_{Th}	1.75	1.74	1.72
H^{17maj}_{BB}	–	1.46	–
H^{17min}_{BB}	–	1.41	–

^{13}C-NMR (90.56MHz, DMSO-d_6)

δ (ppm)	4.3	4.4	4.5
CO_{Ac}	170.94	170.82	170.73
C^{2}_{Th}	152.25	151.23	150.95
C^{4}_{Th}	165.92	164.64	164.38
C^{5}_{Th}	109.82	108.53	108.08
C^{6}_{Th}	143.06	142.42	142.04
$C\alpha_{Ac}$	49.58	49.14	49.32
Me_{Th}	12.94	11.92	11.86
C^{1}_{Fmoc}, C^{8}_{Fmoc}	–	128.03	127.59
C^{2}_{Fmoc}, C^{7}_{Fmoc}	–	125.26	125.01
C^{3}_{Fmoc}, C^{6}_{Fmoc}	–	120.51	120.08
C^{4}_{Fmoc}, C^{5}_{Fmoc}	–	126.87	127.04
C^{4a}_{Fmoc}, C^{4b}_{Fmoc}	–	140.72	140.69
C^{8a}_{Fmoc}, C^{9a}_{Fmoc}	–	143.61	143.81
C^{9}_{Fmoc}	–	46.27	46.68
C^{10}_{Fmoc}	–	65.48	65.42
C^{11}_{Fmoc}	–	165.11	165.31
C^{12}_{BB}	–	39.02	38.81
C^{13}_{BB}	–	46.91	46.86
C^{14}_{BB}	–	47.65	47.64
C^{15}_{BB}	–	167.58	167.58
C^{16}_{BB}	–	83.14	–
C^{17}_{BB}	–	27.55	–

Synthesis of N4-(4-methoxybenzoyl)cytosine **4.6**

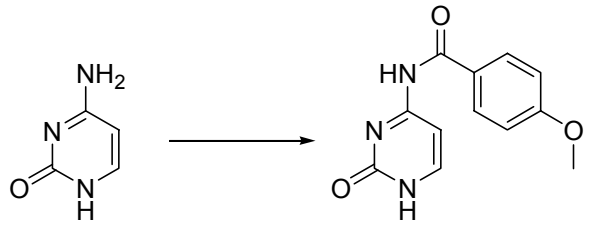

4.6

$C_4H_5N_3O$
Exact Mass: 111,04
Mol. Wt.: 111,1

$C_{12}H_{11}N_3O_3$
Exact Mass: 245,08
Mol. Wt.: 245,23

Cytosine (29.2g, 99%, 180mmol) was suspended in 650ml dry or freshly distilled pyridine in a 1L three-necked flask under stirring. Anisoylchloride (30.7g, 23ml, 180mmol) was added over a dropping funnel over a period of 30min. The solution gets clear at first, but after some time a white, sticky precipitate forms, eventually affording the addition of some more solvent. After stirring overnight at RT, the mixture was refluxed for 1h to 80-100°C, giving a clear solution which precipitates again. After that, stirring was continued overnight at RT, followed by evaporation of the pyridine at HV (40°C) and coevaporation with MeOH (2x250ml). The white powder was dried *in vacuo* and turned out to be nearly insoluble in any common solvent. For that reason, no NMR spectrum was prepared, and the product was used for the next step without further purification.
Yield: 39,60g (161.5mmol, 90%)

^{1}H-NMR (360MHz, DMSO-d_6): δ = 9.48 (2H, br. s, NH^1_{Cy}, NH^4_{Cy}), 8.01 (2H, d, H^2_{Bz}, H^6_{Bz}), 7.74 (1H, d, H^6_{Cy}), 6.93 (2H, d, H^3_{Bz}, H^5_{Bz}), 7.41 (2H, d, H^5_{Cy}), 3.83 (9H, s, Me_{Bz}). ^{13}C-NMR (90.56MHz, DMSO-d_6): δ = 166.72 (CO_{Bz}), 162.92 (C^4_{Cy}), 155.89 (C^2_{Cy}), 163.62 (C^4_{Bz}), 151.08 (C^6_{Cy}), 124.98 (C^1_{Bz}), 130.58 (C^2_{Bz}, C^6_{Bz}), 113.81 (C^3_{Bz}, C^5_{Bz}), 96.03 (C^5_{Cy}), 55.49 (Me_{Bz}). MS (EI, 80eV, 165°C): *m/z* (%) = 245 (27) $[M]^+$, 223 (12), 197 (17), 154 (2.9), 135 (100).

Synthesis of N4-(4-methoxybenzoyl)-1-(methoxycarbonylmethyl)cytosine **4.7**

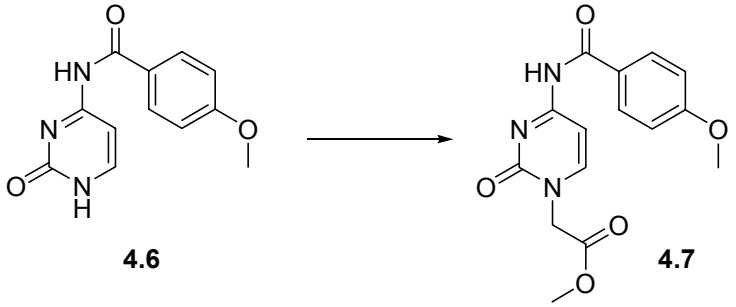

4.6 **4.7**

$C_{12}H_{11}N_3O_3$
Exact Mass: 245,08
Mol. Wt.: 245,23

$C_{15}H_{15}N_3O_5$
Exact Mass: 317,1
Mol. Wt.: 317,3

The crude product N4-(4-methoxybenzoyl)cytosine **4.6** (39.60g, 161.5mmol) was suspended in dry DMF (500ml), and K_2CO_3 (22.3g, 161.5mmol) and methylbromoacetate (15.5ml, 161.5mmol) was added. After stirring at RT overnight, a yellow suspension was obtained. The KBr was filtered off, washed with DMF and discarded; the filtrated was reduced to dryness. After the addition of 160ml of water and 7.2ml 4N HCl, stirring was continued for 20min. The precipitate was collected by filtration and dried *in vacuo*. Yield: 41.0g (129.2mmol, 80%)

^{1}H-NMR (360MHz, DMSO-d_6): δ = 11.10 (2H, br. s, NH^4_{Cy}), 8.03 (2H, d, H^2_{Bz}, H^6_{Bz}), 8.11 (1H, d, H^6_{Cy}), 7.07 (2H, d, H^3_{Bz}, H^5_{Bz}), 7.34 (2H, d, H^5_{Cy}), 3.84 (3H, s, Me_{Bz}), 3.70 (3H, s, Me_{Ac}), 4.68 (2H, s, $H\alpha_{Ac}$). ^{13}C-NMR (90.56MHz, DMSO-d_6): δ = 168.44 (CO_{Ac}), 166.65 (CO_{Bz}), 162.89 (C^4_{Cy}), 155.16 (C^2_{Cy}), 163.80 (C^4_{Bz}), 150.30 (C^6_{Cy}), 125.19 (C^1_{Bz}), 130.65 (C^2_{Bz}, C^6_{Bz}), 113.75 (C^3_{Bz}, C^5_{Bz}), 96.14 (C^5_{Cy}), 50.57 ($C\alpha_{Ac}$), 55.42 (Me_{Bz}), 52.27 (Me_{Ac}). MS (EI, 80eV, 160°C): *m/z* (%) = 317 (26.9) $[M]^+$, 288 (9.1), 244 (3.5), 210 (2.9), 135 (100).

Synthesis of N4-(4-methoxybenzoyl)-1-(carboxymethyl)cytosine **4.8**

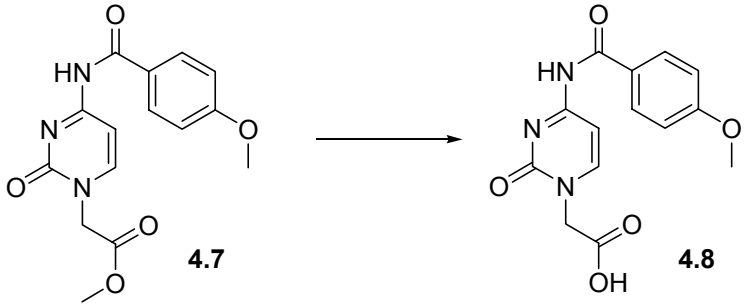

$C_{15}H_{15}N_3O_5$
Exact Mass: 317,1
Mol. Wt.: 317,3

$C_{14}H_{13}N_3O_5$
Exact Mass: 303,09
Mol. Wt.: 303,27

N4-(4-Methoxybenzoyl)-1-(methoxycarbonylmethyl)cytosine **4.7** (41.0g, 129.2mmol) was added under stirring to a solution of NaOH (9.36g, 234mmol, 1.5eq.) in water (350ml) in a beaker. After stirring for 1h, the product was precipitated by adding 4M HCl (54ml, 260mmol). The product was isolated by filtration, coevaporated with MeOH and dried *in vacuo*. Yield: 28.2g (93.0mmol, 72%)

^{1}H-NMR (360MHz, DMSO-d_6): δ = 11.07 (2H, br. s, NH^4_{Cy}), 8.02 (2H, d, H^2_{Bz}, H^6_{Bz}), 8.08 (1H, d, H^6_{Cy}), 7.04 (2H, d, H^3_{Bz}, H^5_{Bz}), 7.30 (2H, d, H^5_{Cy}), 3.84 (3H, s, Me_{Bz}), 4.56 (2H, s, $H\alpha_{Ac}$). ^{13}C-NMR (90.56MHz, DMSO-d_6): δ = 169.30 (CO_{Ac}), 166.67 (CO_{Bz}), 162.87 (C^4_{Cy}), 155.19 (C^2_{Cy}), 163.59 (C^4_{Bz}), 150.44 (C^6_{Cy}), 125.24 (C^1_{Bz}), 130.62 (C^2_{Bz}, C^6_{Bz}), 113.76 (C^3_{Bz}, C^5_{Bz}), 95.90 (C^5_{Cy}), 50.61 ($C\alpha_{Ac}$), 55.54 (Me_{Bz}). MS (EI, 80eV, 216°C): *m/z* (%) = 303 (5.1) $[M]^+$, 259 (15.0), 230 (3.5), 152 (9.8), 135 (100).

Synthesis of N4-(4-*t*-butylbenzoyl)cytosine **4.9**

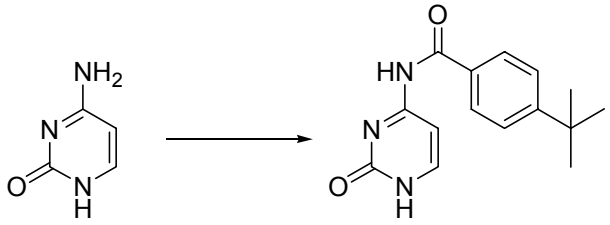

4.9

$C_4H_5N_3O$
Exact Mass: 111,04
Mol. Wt.: 111,1

$C_{15}H_{17}N_3O_2$
Exact Mass: 271,13
Mol. Wt.: 271,31

In a 1L three-necked flask, cytosine (22.2g, 99%, 200mmol) was suspended under stirring in 750ml dry or freshly distilled DMF together with triethylamine (30.8ml, 0.22mol). 4-tert-butylbenzoylchloride (37.2ml, 200mmol) was added over a dropping funnel over a period of 30min. After 4h of stirring, additional 4-tert-Butylbenzoylchloride (7.4ml, 40mmol) was added, and the mixture was stirred overnight at RT. The DMF was removed *in vacuo* using glassware, exclusively because of the weakening of the hoses by the solvent. The residue was coevaporated twice with MeOH. DCM was added, and the product was separated by filtration, followed by washing with DCM and after that with water until the filtrate being colourless. The white product was dried *in vacuo*. Yield: 40-60%

^{1}H-NMR (360MHz, DMSO-d_6): δ = 11.25 (2H, br. s, NH^1_{Cy}, NH^4_{Cy}), 7.98 (2H, d, H^2_{Bz}, H^6_{Bz}), 7.88 (1H, d, H^6_{Cy}), 7.51 (2H, d, H^3_{Bz}, H^5_{Bz}), 7.22 (2H, d, H^5_{Cy}), 1.32 (9H, s, *t*Bu_{Bz}). ^{13}C-NMR (90.56 MHz, DMSO-d_6): δ = 166.68 (CO_{Bz}), 164.82 (C^4_{Cy}), 155.82 (C^2_{Cy}), 129.68 (C^1_{Bz}), 128.4 (C^2_{Bz}, C^6_{Bz}), 125.92 (C^3_{Bz}, C^5_{Bz}), 93.50 (C^5_{Cy}), 34.75 (Cq_{Bz}), 31.24 (*t*Bu_{Bz}). MS (FAB-pos, glycerol): *m/z* = 272.1 $[M+H]^+$, 185.1, 161.1 $[M-Cy]^+$, 112.1 $[M-Bz]^+$, 93.1.

Synthesis of N4-(4-*t*-butylbenzoyl)-1-(methoxycarbonylmethyl)cytosine **4.10**

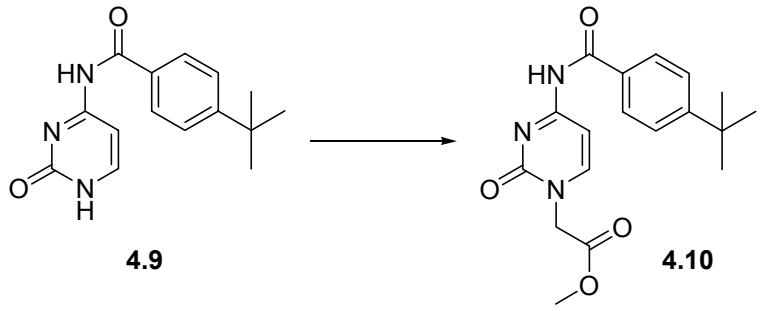

4.9 **4.10**

$C_{15}H_{17}N_3O_2$
Exact Mass: 271,13
Mol. Wt.: 271,31

$C_{18}H_{21}N_3O_4$
Exact Mass: 343,15
Mol. Wt.: 343,38

N4-(4-*t*-Butylbenzoyl)cytosine **4.9** (20g, 73.73mmol) was suspended in dry DMF (330ml). NaH (1.76g, 77.33mmol, 1.05eq.) was added in two portions. The suspension was stirred for 2-3h at 50°C. Methylbromoacetate (6.9ml, 74.66mmol) was added over a dropping funnel over a period of 1h and stirred overnight at 50°C, leading to a light pink slurry. The solvent was removed *in vacuo* and the residue was suspended in DCM which was washed with water (5x). The colourless organic phase and was dried over Na_2SO_4 and reduced to 1/4. After crystallisation at 5°C, the precipitate was collected by filtration and recrystallized from isopropanole yielding a white product.
Yield: 30-40%

^{1}H-NMR (360MHz, DMSO-d_6): δ = 11.11 (1H, s, NH^4_{Cy}), 8.10 (1H, d, H^6_{Cy}), 7.94 (2H, d, H^2_{Bz}, H^6_{Bz}), 7.51 (2H, d, H^3_{Bz}, H^5_{Bz}), 7.34 (2H, d, H^5_{Cy}), 4.66 (2H, s, $H\alpha_{Ac}$), 3.68 (3H, s, Me_{Ac}), 1.31 (9H, s, $t Bu_{Bz}$). ^{13}C-NMR (90.56 MHz, DMSO-d_6): δ = 157.06 (C^2_{Cy}), 151.16 (C^6_{Cy}), 128.89 (C^2_{Bz}, C^6_{Bz}), 126.12 (C^3_{Bz}, C^5_{Bz}), 97.32 (C^5_{Cy}), 51.47 (Me_{Bz}), 49.21 ($C\alpha_{Ac}$), 31.14 ($t Bu_{Bz}$). MS (FAB-pos, Glycerol): *m/z* = 344.1 $[M]^+$, 161.1 $[Bz]^+$.

Synthesis of N4-(4-*t*-butylbenzoyl)-1-(carboxymethyl)cytosine **4.11**

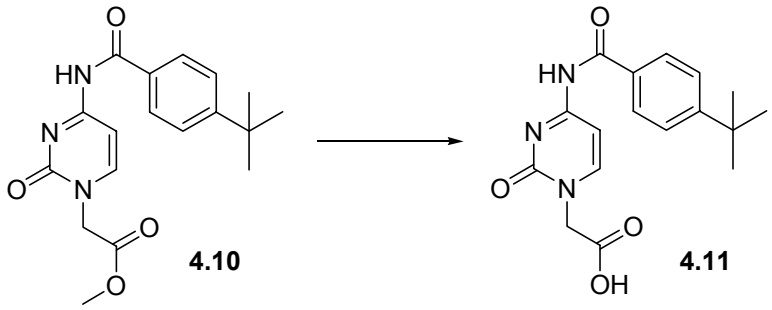

$C_{18}H_{21}N_3O_4$
Exact Mass: 343,15
Mol. Wt.: 343,38

$C_{17}H_{19}N_3O_4$
Exact Mass: 329,14
Mol. Wt.: 329,35

N4-(4-*t*-Butylbenzoyl)-1-(methoxycarbonylmethyl)cytosine **4.10** (8.0g, 24mmol) obtained from step 2 was suspended in a mixture of dioxane (50ml) and water (10ml) and brought to pH11 with 2N NaOH, resulting in a colour change to yellow and the dissolution of the compound. The mixture was stirred overnight at RT. Then, the pH was adjusted to 3 with 1N HCl, forming a white precipitate. A pH below 3 will dissolve the product again. After some time, the product was separated by filtration and dissolved in $NaHCO_3$ (sat., aq) (sometimes, some 2N NaOH has to be added to complete the dissolution). After that, the product was precipitated again by addition of 1N HCl until pH 3 was reached. The white product was separated by filtration, washed with water and dried *in vacuo*. Yield: 5.53g (16.8mmol, 70%)

^{1}H-NMR (360MHz, DMSO-d_6): δ = 11.05 (1H, s, NH^4_{Cy}), 8.10 (1H, d, H^6_{Cy}), 7.94 (2H, d, H^2_{Bz}, H^6_{Bz}), 7.50 (2H, d, H^3_{Bz}, H^5_{Bz}), 7.30 (2H, d, H^5_{Cy}), 4.55 (2H, s, $H\alpha_{Ac}$), 1.29 (9H, s, $t\text{Bu}_{Bz}$). ^{13}C-NMR (90.56MHz, DMSO-d_6): δ = 169.34 (CO_{Ac}), 167.16 (CO_{Bz}), 163.55 (C^4_{Cy}), 155.85 (C^2_{Cy}), 155.24 (C^4_{Bz}), 150.64 (C^6_{Cy}), 130.36 (C^1_{Bz}), 128.39 (C^2_{Bz}, C^6_{Bz}), 125.33 (C^3_{Bz}, C^5_{Bz}), 95.94 (C^5_{Cy}), 50.66 ($C\alpha_{Ac}$), 34.80 (Cq_{Bz}), 30.85 ($t\text{Bu}_{Bz}$).

Synthesis of cytosine-backbone **4.12**

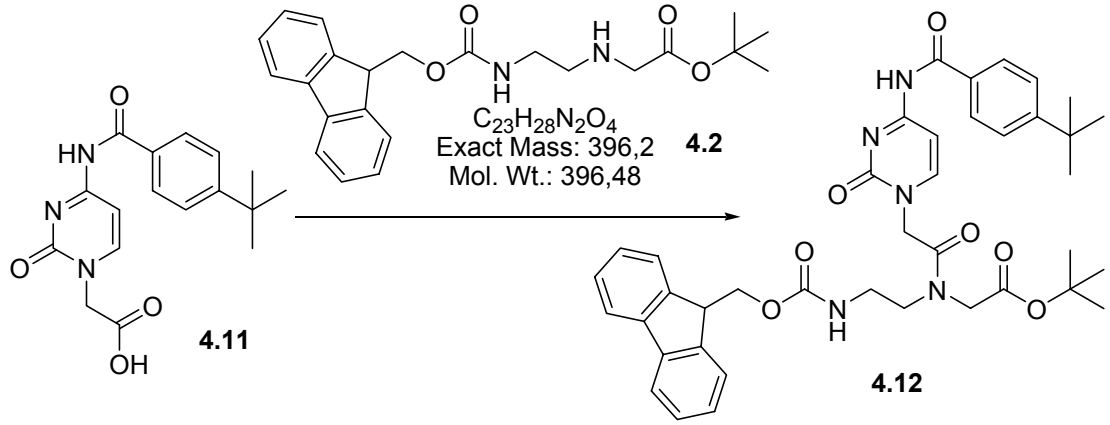

Cytosine-acetic acid **4.11** (4.0g, 12.15mmol), TBTU (7.8g, 24.3mmol) and HOBt (3.7g, 24.3mmol) were suspended in DMF (120ml). Meanwhile, backbone·HCl **4.2** (10.5g, 24.3mmol) was suspended in dichloromethane (160ml) in an extraction funnel and $NaHCO_3$ (sat. aq, 80ml) was added. After extraction, the dichloromethane layer was dried over $MgSO_4$ for 10min. Then DIPEA (4.3g, 24.3mmol) was added to the DMF solution, and the colour changed to yellow. After 2min of activation, the organic phase was filtered into the DMF solution, and the extraction funnel was washed with dichloromethane (20ml). This mixture was stirred at RT for 20h. After evaporation of the solvent in vacuo (10^{-2}mbar, 50°C), the orange-yellow residue was resolved in dichloromethane (180ml), washed with HCl (1M, 3x100ml), $NaHCO_3$ (sat. aq, 3x100ml) and brine (100ml). The clear and dark yellow organic extract was dried over $MgSO_4$, filtered and evaporated to yield the crude product (10.47g) as a yellow oil.

TLC (EtOAc) of the crude product showed two significant spots, R_f 0.30 (unreacted backbone) and R_f 0.15 (product). Both absorb at 254nm, but only the product absorbs at 366nm. The crude product was purified by flash chromatography (SiO_2, 60g, Ø2.5cm, tube volume 20ml, 3.0g of crude) with EtOAc, until the spot with R_f 0.30 has been washed out. Then the eluent was changed to EtOAc:MeOH = 9:1 and two coloured

bands started moving. The faster is slightly yellow (product), while the later one is green. Fractions with R_f 0.15 in EtOAc were evaporated and dried.

Alternatively to Flash chromatography, the crude product can be washed with MeOH leading to similar purity.

^{1}H-NMR (360MHz, DMSO-d_6): δ = 8.67 (1H, s, NH^4_{Cy}), 7.81 (2H, d, H^2_{Bz}, H^6_{Bz}), 7.75 (1H, d, H^6_{Cy}), 7.89 (2H, d, H^4_{Fmoc}, H^5_{Fmoc}), 7.61 (2H, d, H^1_{Fmoc}, H^8_{Fmoc}), 7.51(1H, t, NH_{BB}), 7.49 (2H, d, H^3_{Bz}, H^5_{Bz}), 7.40 (1H, d, H^5_{Cy}), 7.38 (2H, m, H^3_{Fmoc}, H^6_{Fmoc}), 7.30 (2H, m, H^2_{Fmoc}, H^7_{Fmoc}), 4.62 (1.2H, s, $H\alpha^{maj}_{Ac}$), 4.58 (0.8H, s, $H\alpha^{min}_{Ac}$), 4.44 (2H, d, H^{10}_{Fmoc}), 4.22 (1H, t, H^9_{Fmoc}), 3.96 (2H, s, H^{14}_{BB}), 3.60 (1.2 H, t, H^{12maj}_{BB}), 3.45 (2H, br. m, H^{12min}_{BB}, H^{13maj}_{BB}), 3.39 (0.8H, t, H^{13min}_{BB}), 1.30 (9H, s, $t\mathrm{Bu}_{Bz}$), 1.42 (3.6H, s, H^{17min}_{BB}), 1.38 (5.4H, s, H^{17maj}_{BB}). ^{13}C-NMR (90.56MHz, DMSO-d_6): δ = 167.05 (C^{15}_{BB}), 163.33 (C^4_{Cy}), 155.71 (C^4_{Bz}), 143.80 (C^{8a}_{Fmoc}, C^{9a}_{Fmoc}), 140.66 (C^{4a}_{Fmoc}, C^{4b}_{Fmoc}), 130.30 (C^1_{Bz}), 128.30 (C^2_{Bz}, C^6_{Bz}), 127.00 (C^4_{Fmoc}, C^5_{Fmoc}), 125.22 (C^3_{Bz}, C^5_{Bz}), 125.05 (C^2_{Fmoc}, C^7_{Fmoc}), 120.05 (C^{10}_{Fmoc}), 95.67 (C^{10}_{Fmoc}), 65.43 (C^{10}_{Fmoc}), 49.50 ($C\alpha_{Ac}$), 46.65 (C^9_{Fmoc}), 34.70 (Cq_{Bz}), 30.40 ($t\mathrm{Bu}_{Bz}$), 27.60 ($t\mathrm{Bu}_{BB}$). MS (FAB-pos, NBA): *m/z* = 708.0 $[M+H]^+$, 397.0 $[BB]^+$, 341.0, 179.0, 161.0 $[Bz]^+$.

Synthesis of cytosine monomer **4.13**

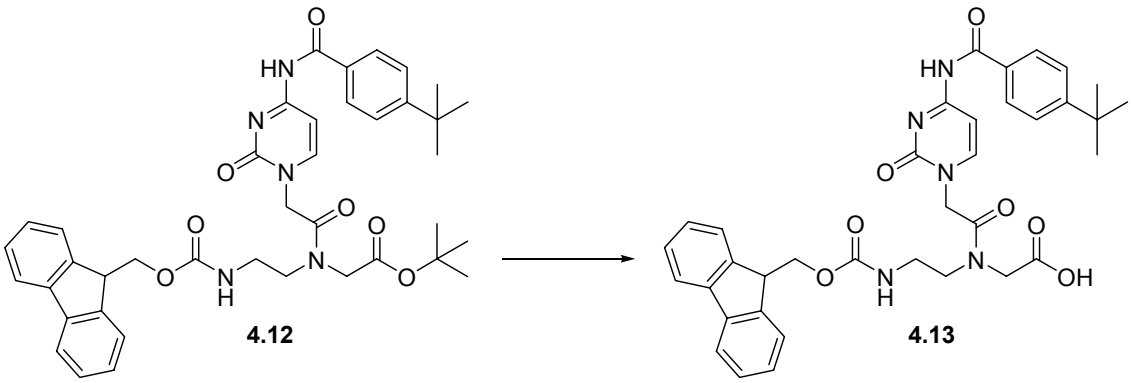

4.12

$C_{40}H_{45}N_5O_7$
Exact Mass: 707,33
Mol. Wt.: 707,81

4.13

$C_{36}H_{37}N_5O_7$
Exact Mass: 651,27
Mol. Wt.: 651,71

A suspension of cytosine-backbone **4.12** (708mg, 1mmol), TIS (0.1ml) and water (0.1ml) in dichloromethane (20ml) was cooled to 0°C in a round-bottomed flask (50ml). TFA (4.75ml) was added over a period of 5min, and after 15min, the ice-bath was removed. After stirring overnight at RT, the volatiles were removed under reduced pressure, coevaporated with acetonitrile until the colour of the residue changed from yellow to white (>10x20ml) followed by drying for 16h (20°C, $5 \cdot 10^{-3}$mbar) forming a white solid in quantitative yield.

^{1}H-NMR (360MHz, DMSO-d_6): δ = 11.08 (1H, s, NH^4_{Cy}), 7.98 (2H, d, H^2_{Bz}, H^6_{Bz}), 7.94 (1H, d, H^6_{Cy}), 7.89 (2H, d, H^4_{Fmoc}, H^5_{Fmoc}), 7.68 (2H, d, H^1_{Fmoc}, H^8_{Fmoc}), 7.53 (2H, d, H^3_{Bz}, H^5_{Bz}), 7.51(1H, t, NH_{BB}), 7.43 (1H, d, H^5_{Cy}), 7.41 (2H, m, H^3_{Fmoc}, H^6_{Fmoc}), 7.33 (2H, m, H^2_{Fmoc}, H^7_{Fmoc}), 4.88 (1.2H, s, $H\alpha^{maj}_{Ac}$), 4.70 (0.8H, s, $H\alpha^{min}_{Ac}$), 4.35 (2H, d, H^{10}_{Fmoc}), 4.26 (1H, t, H^9_{Fmoc}), 4.02 (2H, s, H^{14}_{BB}), 3.48 (1.2 H, t, H^{12maj}_{BB}), 3.37 (0.8H, br. m, H^{12min}_{BB}), 3.31 (1.2H, br. m, H^{13maj}_{BB}), 3.14 (0.8H, t, H^{13min}_{BB}), 1.30 (9H, s, tBu$_{Bz}$). ^{13}C-NMR (90.56MHz, DMSO-d_6): δ = 170.63 (CO_{Ac}), 167.73 (C^{15}_{BB}), 167.37 (CO_{Bz}), 163.57 (C^4_{Cy}), 156.61 (C^{11}_{Fmoc}), 156.03 (C^2_{Cy}), 155.26 (C^4_{Bz}), 151.32 (C^6_{Cy}), 144.13 (C^{8a}_{Fmoc}, C^{9a}_{Fmoc}), 140.97 (C^{4a}_{Fmoc}, C^{4b}_{Fmoc}), 130.63 (C^1_{Bz}), 128.61 (C^2_{Bz}, C^6_{Bz}), 127.84 (C^1_{Fmoc}, C^8_{Fmoc}), 127.30 (C^4_{Fmoc}, C^5_{Fmoc}), 125.50 (C^3_{Bz}, C^5_{Bz}), 125.36 (C^2_{Fmoc}, C^7_{Fmoc}), 120.33 (C^3_{Fmoc}, C^6_{Fmoc}), 95.97 (C^5_{Cy}), 65.77 (C^{10}_{Fmoc}), 49.83 ($C\alpha_{Ac}$), 48.00 (C^{14}_{BB}), 47.20 (C^{13}_{BB}), 46.97 (C^9_{Fmoc}), 38.21 (C^{12}_{BB}), 35.02 (Cq_{Bz}), 31.06 (tBu$_{Bz}$). MS (FAB-pos, NBA): *m/z* =652.0 $[M]^+$, 312.0, 272.0 [**9**+H]$^+$, 178.0 $[Fmoc]^+$, 161.0 $[Bz]^+$.

^{1}H-NMR (360MHz, DMSO-d_6)

δ (ppm)	**4.6**	**4.7**	**4.8**	**4.9**	**4.10**	**4.11**	**4.12**	**4.13**
Me_{Bz}	3.83	3.84	3.84	–	–	–	–	–
tBu_{Bz}	–	–	–	1.32	1.31	1.29	1.30	1.30
$H^3{}_{Bz}$, $H^5{}_{Bz}$	6.93	7.07	7.04	7.51	7.51	7.50	7.49	7.53
$H^2{}_{Bz}$, $H^6{}_{Bz}$	8.01	8.03	8.02	7.98	7.94	7.94	7.81	7.98
$NH^1{}_{Cy}$	9.48	–	–	11.25	–	–	–	–
$NH^4{}_{Cy}$	9.48	11.10	11.07	11.25	11.10	11.05	8.67	11.08
$H^5{}_{Cy}$	7.41	7.34	7.30	7.22	7.34	7.30	7.40	7.43
$H^6{}_{Cy}$	7.74	8.11	8.08	7.88	8.10	8.10	7.75	7.94
Me_{Ac}	–	3.70	–	–	3.68	–	–	–
NH_{BB}	–	–	–	–	–	–	7.51	7.51
$H^4{}_{Fmoc}$, $H^5{}_{Fmoc}$	–	–	–	–	–	–	7.89	7.89
$H^1{}_{Fmoc}$, $H^8{}_{Fmoc}$	–	–	–	–	–	–	7.61	7.68
$H^3{}_{Fmoc}$, $H^6{}_{Fmoc}$	–	–	–	–	–	–	7.38	7.41
$H^2{}_{Fmoc}$, $H^7{}_{Fmoc}$	–	–	–	–	–	–	7.30	7.33
$H\alpha^{maj}{}_{Ac}$	–	4.68	4.56	–	4.66	4.55	4.62	4.88
$H\alpha^{min}{}_{Ac}$	–	4.68	4.56	–	4.66	4.55	4.58	4.70
$H^{10}{}_{Fmoc}$	–	–	–	–	–	–	4.44	4.35
$H^9{}_{Fmoc}$	–	–	–	–	–	–	4.22	4.26
$H^{14}{}_{BB}$	–	–	–	–	–	–	3.96	4.02
$H^{12maj}{}_{BB}$	–	–	–	–	–	–	3.60	3.48
$H^{12min}{}_{BB}$	–	–	–	–	–	–	3.45	3.37
$H^{13maj}{}_{BB}$	–	–	–	–	–	–	3.45	3.31
$H^{13min}{}_{BB}$	–	–	–	–	–	–	3.39	3.14
$H^{17min}{}_{BB}$	–	–	–	–	–	–	1.42	–
$H^{17maj}{}_{BB}$	–	–	–	–	–	–	1.38	–

^{13}C-NMR (90.56MHz, DMSO-d_6)

δ (ppm)	4.6	4.7	4.8	4.9	4.10	4.11	4.12	4.13
Me_{Bz}	55.49	55.42	55.54	–		–	–	–
Cq_{Bz}	–	–	–	34.75	34.75	34.80	34.73	35.02
$t\mathrm{Bu}_{Bz}$	–	–	–	31.24	31.14	30.85	30.78	31.06
$C^1{}_{Bz}$	124.98	125.19	125.24	129.68	n.o.	130.36	130.30	130.63
$C^3{}_{Bz}$, $C^5{}_{Bz}$	113.81	113.75	113.76	125.92	126.12	125.33	125.22	125.50
$C^2{}_{Bz}$, $C^6{}_{Bz}$	130.58	130.65	130.62	128.40	128.89	128.39	128.30	128.61
$C^4{}_{Bz}$	163.62	163.80	163.59	164.82	n.o.	155.24	n.o.	155.26
CO_{Bz}	166.72	166.65	166.67	166.68	n.o.	167.16	167.05	167.37
$C^2{}_{Cy}$	155.89	155.16	155.19	155.82	157.06	155.85	155.71	156.03
$C^4{}_{Cy}$	162.92	162.89	162.87	n.o.	n.o.	163.55	163.33	163.57
$C^5{}_{Cy}$	96.03	96.14	95.90	93.50	97.32	95.94	95.67	95.97
$C^6{}_{Cy}$	151.08	150.30	150.44	n.o.	151.16	150.64	n.o.	151.32
$C\alpha_{Ac}$	–	50.57	50.61	–	49.21	50.66	49.50	49.83
CO_{Ac}	–	168.44	169.30	–	n.o.	169.34	n.o.	170.63
Me_{Ac}	–	52.27	–	–	51.47	–	–	–
$C^1{}_{Fmoc}$, $C^8{}_{Fmoc}$	–	–	–	–	–	–	127.55	127.84
$C^2{}_{Fmoc}$, $C^7{}_{Fmoc}$	–	–	–	–	–	–	125.05	125.36
$C^3{}_{Fmoc}$, $C^6{}_{Fmoc}$	–	–	–	–	–	–	120.05	120.33
$C^4{}_{Fmoc}$, $C^5{}_{Fmoc}$	–	–	–	–	–	–	127.00	127.30
$C^{4a}{}_{Fmoc}$, $C^{4b}{}_{Fmoc}$	–	–	–	–	–	–	140.66	140.97
$C^{8a}{}_{Fmoc}$, $C^{9a}{}_{Fmoc}$	–	–	–	–	–	–	143.80	144.13
$C^9{}_{Fmoc}$	–	–	–	–	–	–	46.65	46.97
$C^{10}{}_{Fmoc}$	–	–	–	–	–	–	65.43	65.77
$C^{11}{}_{Fmoc}$	–	–	–	–	–	–	n.o.	156.61
$C^{12}{}_{BB}$	–	–	–	–	–	–	n.o.	38.21
$C^{13}{}_{BB}$	–	–	–	–	–	–	n.o.	47.20
$C^{14}{}_{BB}$	–	–	–	–	–	–	n.o.	48.00
$C^{15}{}_{BB}$	–	–	–	–	–	–	n.o.	167.73
$C^{16}{}_{BB}$	–	–	–	–	–	–	80.91	–
$C^{17}{}_{BB}$	–	–	–	–	–	–	27.60	–

Synthesis of N6-(4-methoxybenzoyl)adenine **4.14**

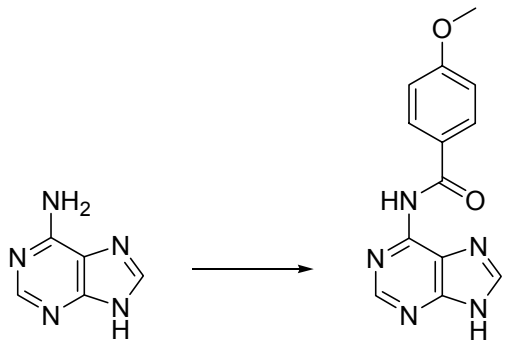

4.14

$C_5H_5N_5$
Exact Mass: 135,05
Mol. Wt.: 135,13

$C_{13}H_{11}N_5O_2$
Exact Mass: 269,09
Mol. Wt.: 269,26

Adenine (20.3g, 150mmol) was suspended in pyridine (400ml, dried over mol. sieves) and 4-methoxybenzoylchloride (20.3ml, 150mmol) was added over a dropping funnel. The yellow slurry was heated to 100°C for 3h, changed to a clear, brown-red solution and was stirred at RT overnight. Methanol (30ml) was added over a dropping funnel, the solvent was removed *in vacuo* and coevaporated with toluene (2x150ml). The residue was refluxed with *i*-propanol (300ml) for 3h and left in the fridge overnight. The solid was filtered, dried on air overnight and at HV for 3h yielding 37g (92%) of the white product being clean enough to be used for the next step without further purification.

^{1}H-NMR (360MHz, DMSO-d_6): δ = 11.41 (1H, br. s, NH^6_{Ad}), 8.76 (1H, s, H^8_{Ad}), 8.68 (1H, s, H^2_{Ad}), 8.56 (1H, d, NH^9_{Ad}), 8.15 (2H, d, J=8.5, H^2_{Bz}, H^6_{Bz}), 7.11 (2H, d, J=8.5, H^3_{Bz}, H^5_{Bz}), 3.88 (3H, s, Me_{Bz}). ^{13}C-NMR (90.56MHz, DMSO-d_6): δ = 165.89 (CO_{Bz}), 162.86 (C^4_{Bz}), 160.85 (C^4_{Ad}), 151.16 (C^2_{Ad}), 145.68 (C^8_{Ad}), 145.38 (C^6_{Ad}), 130.79 (C^2_{Bz}, C^6_{Bz}), 124.79 (C^1_{Bz}), 115.28 (C^5_{Ad}), 113.80 (C^3_{Bz}, C^5_{Bz}), 55.56 (Me_{Bz}). MS (EI, 70eV, 165°C): *m/z* (%) = 269 [M^+] (37), 241 (27), 136 (21), 135 (100), 107 (15), 92 (34), 77 (45), 64 (14).

Synthesis N6-(4-methoxybenzoyl)-9-(methoxycarbonylmethyl)adenine **4.15a** and N6-(4-methoxybenzoyl)-7-(methoxycarbonylmethyl)adenine **4.15b**

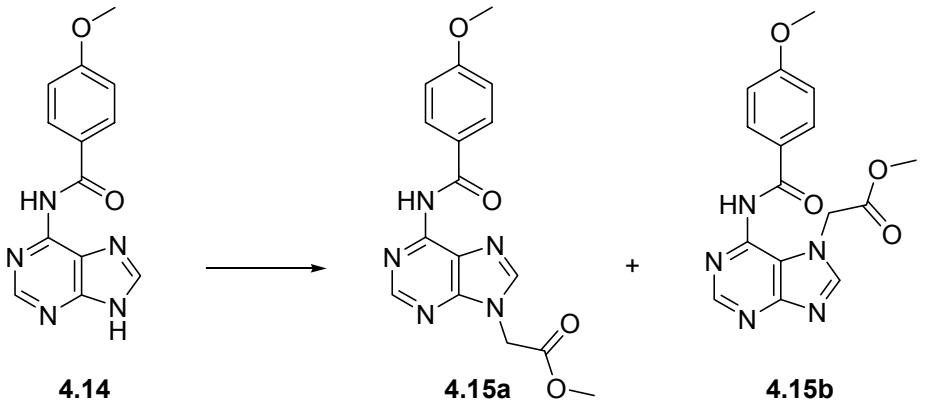

4.14

$C_{13}H_{11}N_5O_2$
Exact Mass: 269,09
Mol. Wt.: 269,26

4.15a

$C_{16}H_{15}N_5O_4$
Exact Mass: 341,11
Mol. Wt.: 341,32

4.15b

$C_{16}H_{15}N_5O_4$
Exact Mass: 341,11
Mol. Wt.: 341,32

N6-(4-Methoxybenzoyl)adenine **4.14** (2.69g, 10mmol), anhydrous K_2CO_3 (1.38g, 10mmol) and anhydrous Cs_2CO_3 (236mg, 1mmol) were suspended in dry DMF (40ml). After stirring for 5min at RT, methyl-bromo acetate (1.05ml, 11mmol) was added over a dropping funnel. The almost clear solution (containing some undissolved carbonate) becomes a slurry after 15min. After stirring the mixture for 24h, the solvent was removed *in vacuo*, and the residue was stirred overnight with ethyl acetate (175ml) and water (70ml). The white precipitate was isolated by filtration **4.15b** and the filtrate was separated in a separatory funnel. The ethyl acetate was washed with brine (1x100ml) and water (2x100ml), dried over Na_2SO_4, filtered and the solvent was removed by rotary evaporation. m=1.42g (4.16mmol, 41.6%)

300mg of the residue was purified by column chromatography (37g SiO_2, CH_2Cl_2:*i*-PrOH=92.5:7.5) yielding 73mg (0.21mmol, 2.1%) of pure **4.15a**.

4.15a:

^{1}H-NMR (360MHz, DMSO-d_6): δ = 11.05 (1H, br. s, NH^6_{Ad}), 8.70 (1H, s, H^8_{Ad}), 8.42 (1H, s, H^2_{Ad}), 8.03 (2H, d, J=8.5, H^2_{Bz}, H^6_{Bz}), 7.07 (2H, d, J=8.5, H^3_{Bz}, H^5_{Bz}), 5.22 (2H, s, $H\alpha_{Ac}$), 3.84 (3H, s, Me_{Bz}), 3.72 (3H, s, Me_{Ac}). ^{13}C-NMR (90.56MHz, DMSO-d_6): δ = 168.35 (CO_{Ac}), 165.11 (CO_{Bz}), 162.69 (C^4_{Bz}), 152.51 (C^4_{Ad}), 151.76 (C^2_{Ad}), 150.52

(C^6_{Ad}), 144.91 (C^8_{Ad}), 130.67 (C^2_{Bz}, C^6_{Bz}), 125.57 (C^5_{Ad}), 124.85 (C^1_{Bz}), 113.17 (C^3_{Bz}, C^5_{Bz}), 55.59 (Me_{Bz}), 52.67 (Me^2_{Ac}), 44.20 ($C\alpha_{Ac}$). MS (EI, 70eV, 170°C): *m/z* (%) = 341 [M^+] (21), 340 (15), 313 (45), 312 (35), 136 (21), 135 (100), 107 (14), 92 (30), 77 (38), 64 (10).

4.15b:

^{1}H-NMR (360MHz, DMSO-d_6): δ = 8.67 (1H, br. s, H^8_{Ad}), 8.57 (1H, s, H^2_{Ad}), 8.06 (2H, d, J=8.5, H^2_{Bz}, H^6_{Bz}), 7.07 (2H, d, J=8.5, H^3_{Bz}, H^5_{Bz}), 5.33 (2H, br. s, $H\alpha_{Ac}$), 3.86 (3H, s, Me_{Bz}), 3.61 (s, 3H, Me^2_{Ac}). ^{13}C-NMR (90.56MHz, DMSO-d_6): δ = 130.33 (C^2_{Bz}, C^6_{Bz}), 168.08 (CO_{Ac}), 162.50 (C^4_{Bz}), 113.46 (C^3_{Bz}, C^5_{Bz}), 55.28 (Me_{Bz}), 52.08 (Me_{Ac}), 47.69 ($C\alpha_{Ac}$). MS (EI, 70eV, 165°C): *m/z* (%) = 341 [M^+] (24), 234 (7), 136 (21), 135 (100), 107 (8), 92 (10), 77 (19), 44 (23).

Synthesis of N6-(4-methoxybenzoyl)-9-(*t*-butoxycarbonylmethyl)adenine **4.16a** and N6-(4-methoxybenzoyl)-7-(*t*-butoxycarbonylmethyl)adenine **4.16b**

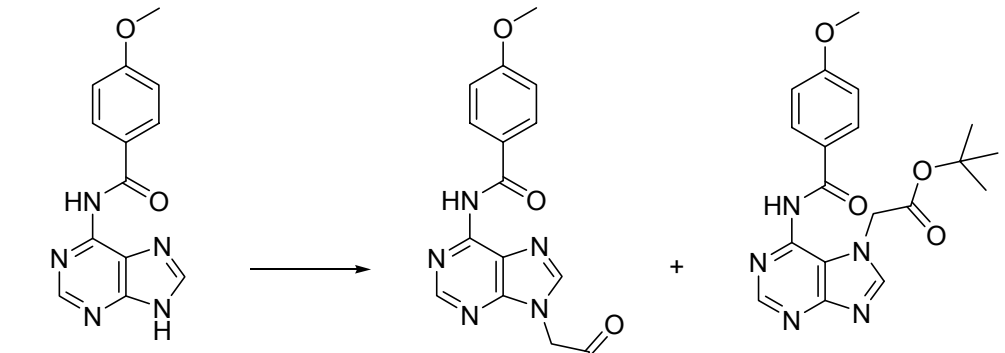

4.14
$C_{13}H_{11}N_5O_2$
Exact Mass: 269,09
Mol. Wt.: 269,26

4.16a
$C_{19}H_{21}N_5O_4$
Exact Mass: 383,16
Mol. Wt.: 383,4

4.16b
$C_{19}H_{21}N_5O_4$
Exact Mass: 383,16
Mol. Wt.: 383,4

N6-(4-methoxybenzoyl)adenine **4.14** (23.66g, 88mmol), anhydrous K_2CO_3 (12.16g, 88mmol) and anhydrous Cs_2CO_3 (2.87g, 8.8mmol) were suspended in dry DMF (400ml). After stirring for 5min at RT, *t*-butylbromoacetate (14.11ml, 97mmol) was added over a dropping funnel. The almost clear solution (containing some undissolved carbonate) becomes a slurry after 15min. After stirring the mixture for 24h, the solvent

was removed *in vacuo*, and the residue was stirred overnight with ethyl acetate (400ml) and water (200ml). The white precipitate was isolated by filtration. m=18.54g (54.4%), ^{1}H-NMR: **4.16a**: **4.16b** = 2:1. The crude product was recrystallized from ethyl acetate (2.25L) yielding 9.58g (28.2%) of **4.16a** of >98% purity.

4.16a:

^{1}H-NMR (360MHz, DMSO-d_6): δ = 11.04 (1H, br. s, NH^{6}_{Ad}), 8.72 (1H, s, H^{8}_{Ad}), 8.43 (1H, s, H^{2}_{Ad}), 8.05 (2H, d, J=8.5, H^{2}_{Bz}, H^{6}_{Bz}), 7.08 (2H, d, J=8.5, H^{3}_{Bz}, H^{5}_{Bz}), 5.10 (2H, s, $H\alpha_{Ac}$), 3.86 (3H, s, Me_{Bz}), 1.44 (9H, s, tBu^{2}_{Ac}). ^{13}C-NMR (90.56MHz, DMSO-d_6): δ = 166.67 (CO_{Ac}), 165.98 (CO_{Bz}), 162.53 (C^{4}_{Bz}), 152.44 (C^{4}_{Ad}), 151.53 (C^{2}_{Ad}), 150.38 (C^{6}_{Ad}), 144.85 (C^{8}_{Ad}), 130.53 (C^{2}_{Bz}, C^{6}_{Bz}), 125.60 (C^{5}_{Ad}), 124.81 (C^{1}_{Bz}), 113.67 (C^{3}_{Bz}, C^{5}_{Bz}), 82.27 (Cq_{Ac}), 55.45 (Me_{Bz}), 44.79 ($C\alpha_{Ac}$), 27.61 (tBu_{Ac}). MS (EI, 70eV, 155°C): *m/z* (%) = 383 [M^{+}] (11), 355 (12), 299 (16), 298 (11), 136 (10), 135 (100), 107 (8), 92 (11), 77 (19), 57 (14), 44 (14), 41 (11).

4.16b:

^{1}H-NMR (360MHz, DMSO-d_6): δ = 8.66 (1H, s, H^{8}_{Ad}), 8.56 (1H, s, H^{2}_{Ad}), 8.12 (2H, d, J=8.5, H^{2}_{Bz}, H^{6}_{Bz}), 7.07 (2H, d, J=8.5, H^{3}_{Bz}, H^{5}_{Bz}), 5.22 (2H, s, $H\alpha_{Ac}$), 3.86 (3H, s, Me_{Bz}), 1.26 (9H, s, tBu^{2}_{Ac}). ^{13}C-NMR (90.56MHz, DMSO-d_6): δ = 166.87 (CO_{Ac}), 162.65 (C^{4}_{Bz}), 130.74 (C^{2}_{Bz}, C^{6}_{Bz}), 113.58 (C^{3}_{Bz}, C^{5}_{Bz}), 82.13 (Cq_{Ac}), 55.49 (Me_{Bz}), 48.52 ($C\alpha_{Ac}$), 27.43 (tBu_{Ac}). MS (EI, 70eV, 170°C): *m/z* (%) = 383 [M^{+}] (9), 327 (5), 269 (5), 136 (9), 135 (100), 107 (5), 92 (10), 77 (14), 57 (14), 56 (5), 41 (15).

Synthesis of N6-(4-methoxybenzoyl)-9-(carboxymethyl)adenine **4.17**

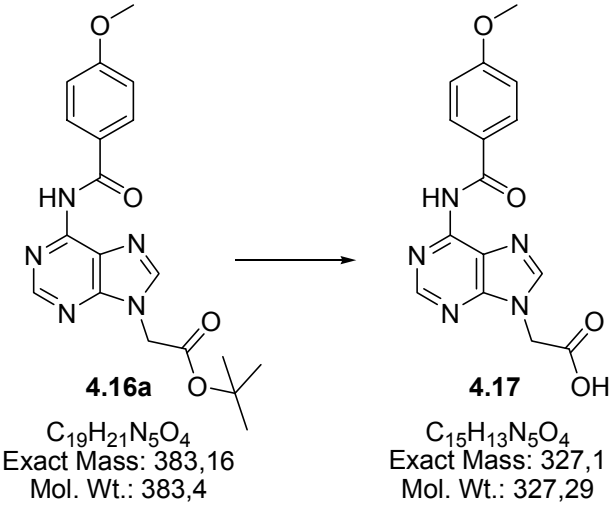

N6-(4-Methoxybenzoyl)-9-(*t*-butoxycarbonylmethyl)adenine **4.16a** (8.74g, 22.8mmol) was suspended in dichloromethane (200ml) and triisopropylsilane (0.47ml, 2.3mmol) was added. TFA (100ml) was slowly added at 0°C over a period of 1h. The clear solution was stirred overnight, followed by evaporation of all volatile compounds and coevaporation with CH_2Cl_2 (3x50ml). The crude product, a yellow foam, is pure enough for the next step. Yield: 6.82g (92%)

^{1}H-NMR (360MHz, DMSO-d_6): δ = 8.73 (1H, s, $H^8{}_{Ad}$), 8.52 (1H, s, $H^2{}_{Ad}$), 8.06 (2H, d, J=9.0, $H^2{}_{Bz}$, $H^6{}_{Bz}$), 7.09 (2H, d, J=9.0, $H^3{}_{Bz}$, $H^5{}_{Bz}$), 5.13 (2H, s, $H\alpha_{Ac}$), 3.87 (3H, s, Me_{Bz}). ^{13}C-NMR (90.56MHz, DMSO-d_6): δ = 169.01 (CO_{Ac}), 165.18 (CO_{Bz}), 162.66 ($C^4{}_{Bz}$), 152.40 ($C^4{}_{Ad}$), 151.58 ($C^2{}_{Ad}$), 150.15 ($C^6{}_{Ad}$), 145.00 ($C^8{}_{Ad}$), 130.64 ($C^2{}_{Bz}$, $C^6{}_{Bz}$), 125.44 ($C^5{}_{Ad}$), 124.13 ($C^1{}_{Bz}$), 113.75 ($C^3{}_{Bz}$, $C^5{}_{Bz}$), 55.52 (Me_{Bz}), 44.38 ($C\alpha_{Ac}$). MS (FAB-pos, NBA): *m/z* = 366, 328 [M+H$^+$], 192, 155, 154, 149, 137, 136, 135, 107, 90, 89, 78, 77, 69, 63, 57, 55, 51, 50, 43, 41. MS (EI, 70eV, 161°C): 355 (3), 327 [M$^+$] (8), 135 (82), 92 (11), 77 (16), 69 (61), 51 (30), 50 (13), 45 (100), 44 (92), 43 (15).

Synthesis of adenine-backbone **4.18**

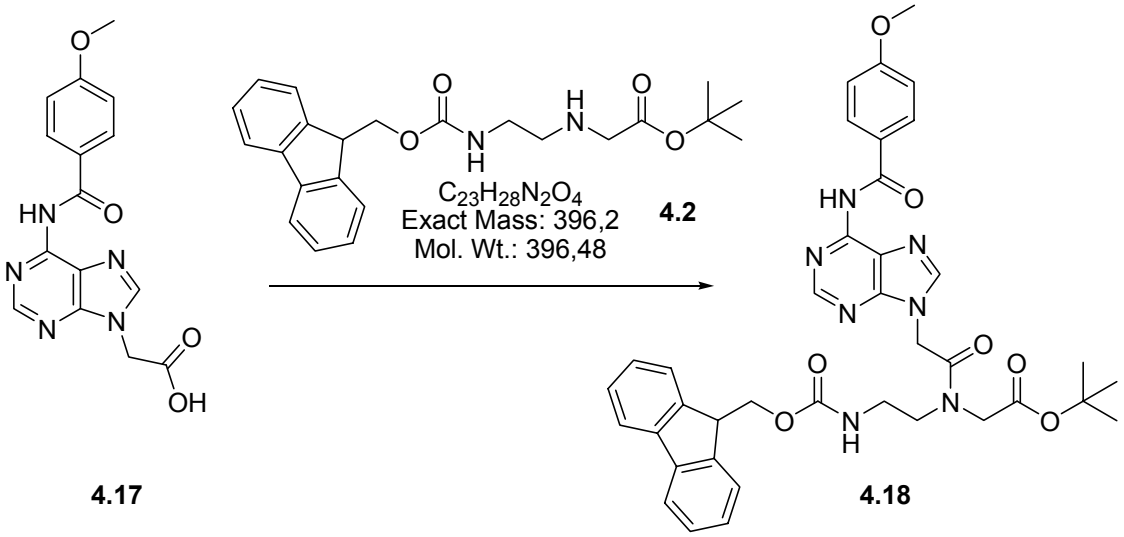

Adenine-acetic acid **4.17** (1.64g, 5mmol), TBTU (2.41g, 7.5mmol) and HOBt (1.15g, 7.5mmol) were resolved in DMF (60ml) with orange colour. Meanwhile, backbone·HCl **4.2** (3.25g, 7.5mmol) was suspended in dichloromethane (30ml) in an extraction funnel and $NaHCO_3$ (sat. aq, 30ml) was added. After extraction, the dichloromethane layer was dried over $MgSO_4$ for 10min. Then DIPEA (1.7ml, 10mmol) was added to the DMF solution, and the colour changed to yellow. After 2min. of activation, the organic phase was filtered into the DMF solution and the extraction funnel was washed with dichloromethane (10ml). This mixture was stirred at RT for 4h. After evaporation of the solvent in vacuo (10^{-2}mbar, 50°C), the residue was resolved in dichloromethane (100ml), washed with HCl (1M, 3x100ml), $NaHCO_3$ (sat. aq, 3x100ml) and brine (100ml). The organic extract was dried, filtered and evaporated to yield 3.07g (87%) of crude product as brownish foam.

TLC (EtOAc) of the crude product showed two significant spots, R_f 0.30 (unreacted Backbone) and R_f 0.15 (product). Both absorb at 254nm, but only the product absorbs at 366nm.

The crude product was purified by flash chromatography (SiO_2, 60g, Ø2.5cm, tube volume 20ml, 3.0g of crude) with EtOAc, until the spot with R_f 0.30 was washed out. Then the eluent was changed to EtOAc:MeOH = 9:1 and two coloured bands started moving. The faster is slightly yellow (product), while the latter one is green. Fractions with R_f 0.15 in EtOAc were evaporated and dried. Yield: 2.2g (62%) as a white foam.

^{1}H-NMR (360MHz, DMSO-d_6): δ = 10.96 (1H, s, NH^6_{Ad}), 8.67 (1H, s, H^8_{Ad}), 8.62 (1H, s, H^2_{Ad}), 8.04 (2H, d, J=9.0, H^2_{Bz}, H^6_{Bz}), 7.87 (2H, d, H^4_{Fmoc}, H^5_{Fmoc}), 7.67 (2H, d, H^1_{Fmoc}, H^8_{Fmoc}), 7.49 (1H, t, NH_{BB}), 7.40 (2H, m, H^3_{Fmoc}, H^6_{Fmoc}), 7.31 (2H, m, H^2_{Fmoc}, H^7_{Fmoc}), 7.07 (2H, d, J=9.0, H^3_{Bz}, H^5_{Bz}), 5.36 (1.2H, s, $H\alpha^{maj}_{Ac}$), 5.17 (0.8H, s, $H\alpha^{min}_{Ac}$), 4.43-4.15 (3H , br. m, H^9_{Fmoc}, H^{10}_{Fmoc}), 3.97 (2H , s, H^{14}_{BB}), 3.86 (3H, s, Me_{Bz}), 3.56 (1.2 H, t, H^{12maj}_{BB}); 3.35 (2H, br. m, $H^{12min}_{BB,}$ H^{13maj}_{BB}); 3.13 (0.8H, t, H^{13min}_{BB}), 1.51 (3.6H, s, H^{17min}_{BB}), 1.44 (5.4H, s, H^{17maj}_{BB}).

Synthesis of adenine monomer **4.19**

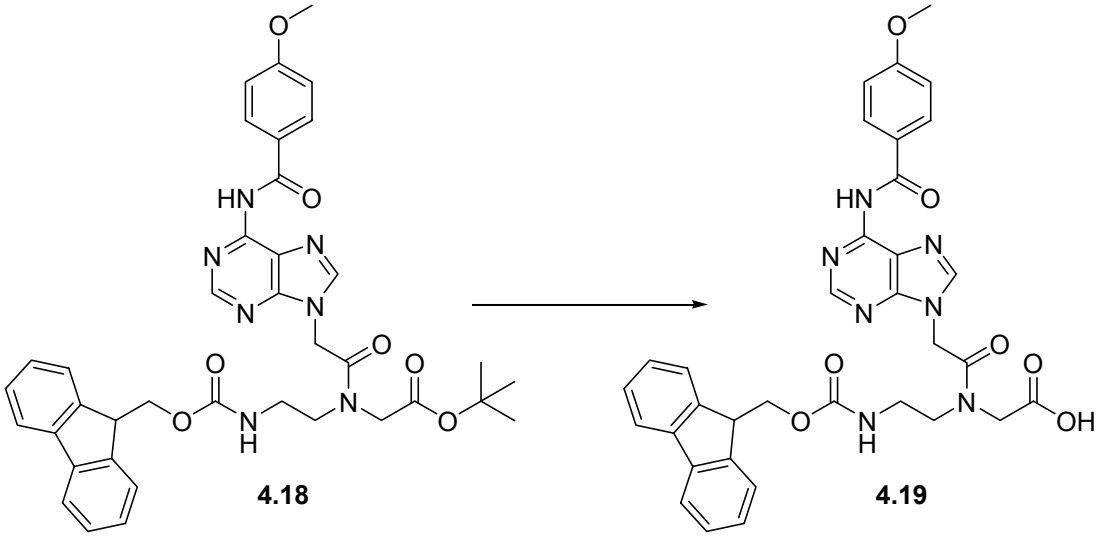

4.18

$C_{38}H_{39}N_7O_7$
Exact Mass: 705,29
Mol. Wt.: 705,76

4.19

$C_{34}H_{31}N_7O_7$
Exact Mass: 649,23
Mol. Wt.: 649,65

A suspension of adenine-backbone **4.18** (706mg, 1mmol), TIS (0.125ml) and water (0.125ml) in CH_2Cl_2 (10ml) was cooled to 0°C in a round-bottomed flask (50ml). TFA (4.75ml) was added over a period of 5min, and after 15min, the ice-bath was removed. After stirring overnight at RT, the volatiles were removed under reduced pressure, coevaporated with acetonitrile (4x20ml) followed by drying for 16h (20°C, $5 \cdot 10^{-3}$mbar) forming a white solid in quantitative yield.

^{1}H-NMR (360MHz, DMSO-d_6): δ = 11.14 (1H, s, NH^6_{Ad}), 8.71 (1H, s, H^8_{Ad}), 8.66 (1H, s, H^2_{Ad}), 8.06 (2H, d, J=9.0, H^2_{Bz}, H^6_{Bz}), 7.87 (2H, d, H^4_{Fmoc}, H^5_{Fmoc}), 7.67 (2H, d, H^1_{Fmoc}, H^8_{Fmoc}), 7.51(1H, t, NH_{BB}), 7.39 (2H, m, H^3_{Fmoc}, H^6_{Fmoc}), 7.30 (2H, m, H^2_{Fmoc}, H^7_{Fmoc}), 7.08 (2H, d, J=9.0, H^3_{Bz}, H^5_{Bz}), 5.40 (1.2H, s, $H\alpha^{maj}_{Ac}$), 5.23 (0.8H, s, $H\alpha^{min}_{Ac}$), 4.37 (2H, d, H^{10}_{Fmoc}), 4.28 (1H, t, H^9_{Fmoc}), 4.02 (2H, s, H^{14}_{BB}), 3.85 (3H, s, Me_{Bz}), 3.57 (1.2 H, t, H^{12maj}_{BB}), 3.36 (2H, br. m, H^{12min}_{BB}, H^{13maj}_{BB}), 3.14 (0.8H, t, H^{13min}_{BB}).

^{1}H-NMR (360MHz, DMSO-d$_6$)

δ (ppm)	4.14	4.15a	4.15b	4.16a	4.16b	4.17	4.18	4.19
Me_{Bz}	3.88	3.84	3.86	3.86	3.86	3.87	3.86	3.85
H^3_{Bz}, H^5_{Bz}	7.11	7.07	7.07	7.08	7.07	7.09	7.07	7.08
H^2_{Bz}, H^6_{Bz}	8.15	8.03	8.06	8.05	8.12	8.06	8.04	8.06
NH^6_{Ad}	11.41	11.05	n.o.	11.04	n.o.	n.o.	10.96	11.14
H^2_{Ad}	8.68	8.42	8.57	8.43	8.56	8.52	8.62	8.66
H^8_{Ad}	8.76	8.70	8.67	8.72	8.66	8.73	8.67	8.71
NH^9_{Ad}	8.56	–	–	–	–	–	–	–
Me^2_{Ac}	–	3.72	3.61	–	–	–	–	–
tBu^2_{Ac}	–	–	–	1.44	1.26	–	–	–
NH_{BB}	–	–	–	–	–	–	7.49	7.51
H^4_{Fmoc}, H^5_{Fmoc}	–	–	–	–	–	–	7.87	7.87
H^1_{Fmoc}, H^8_{Fmoc}	–	–	–	–	–	–	7.67	7.67
H^3_{Fmoc}, H^6_{Fmoc}	–	–	–	–	–	–	7.40	7.39
H^2_{Fmoc}, H^7_{Fmoc}	–	–	–	–	–	–	7.31	7.30
$H\alpha^{maj}_{Ac}$	–	5.22	5.33	5.10	5.22	5.13	5.36	5.40
$H\alpha^{min}_{Ac}$	–	5.22	5.33	5.10	5.22	5.13	5.17	5.23
H^{10}_{Fmoc}	–	–	–	–	–	–	4.43	4.37
H^9_{Fmoc}	–	–	–	–	–	–	4.15	4.28
H^{14}_{BB}	–	–	–	–	–	–	3.97	4.02
H^{12maj}_{BB}	–	–	–	–	–	–	3.56	3.57
H^{12min}_{BB}	–	–	–	–	–	–	3.35	3.36
H^{13maj}_{BB}	–	–	–	–	–	–	3.35	3.36
H^{13min}_{BB}	–	–	–	–	–	–	3.13	3.14
H^{17min}_{BB}	–	–	–	–	–	–	1.51	–
H^{17maj}_{BB}	–	–	–	–	–	–	1.44	–

^{13}C-NMR (90.56MHz, DMSO-d_6)

δ (ppm)	4.14	4.15a	4.15b	4.16a	4.16b	4.17
Me_{Bz}	55.56	55.59	55.28	55.45	55.49	55.52
C^1_{Bz}	124.79	124.85	n.o.	124.81	n.o.	124.13
C^3_{Bz}, C^5_{Bz}	113.80	113.17	113.46	113.67	113.58	113.75
C^2_{Bz}, C^6_{Bz}	130.79	130.67	130.33	130.53	130.74	130.64
C^4_{Bz}	162.86	162.69	162.50	162.53	162.65	162.66
CO_{Bz}	165.89	165.11	n.o.	165.98	n.o.	165.18
C^2_{Ad}	151.16	151.76	n.o.	151.53	n.o.	151.58
C^4_{Ad}	160.85	152.51	n.o.	152.44	n.o.	152.40
C^5_{Ad}	115.28	125.57	n.o.	125.60	n.o.	125.44
C^6_{Ad}	145.38	150.52	n.o.	150.38	n.o.	150.15
C^8_{Ad}	145.68	144.91	n.o.	144.85	n.o.	145.00
$C\alpha_{Ac}$	–	44.20	47.69	44.79	48.52	44.38
CO_{Ac}	–	168.35	168.08	166.67	166.87	169.01
Me_{Ac}	–	52.67	52.08	–	–	–
Cq_{Ac}	–	–	–	82.27	82.13	–
tBu_{Ac}	–	–	–	27.61	27.43	–

Synthesis of N2,9-diacetylguanine **4.20**

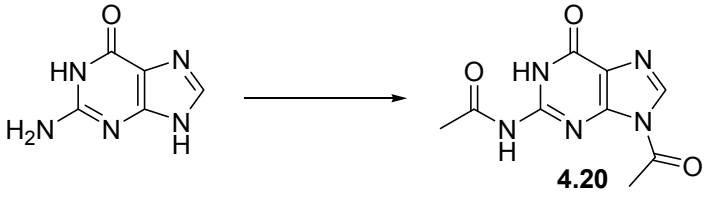

$C_5H_5N_5O$
Exact Mass: 151,05
Mol. Wt.: 151,13

$C_9H_9N_5O_3$
Exact Mass: 235,07
Mol. Wt.: 235,2

Guanine (15.11g, 100mmol) was suspended in 125 ml of dried DMAc. 25ml Ac_2O were added, and the mixture was stirred at 160°C for 6-7h. The resulting brown solution was allowed to reach RT, the crystalline product was filtered and washed with cold EtOH.
Yield: 16.1g (68.5mmol, 68.5%)

^{1}H-NMR (360MHz, DMSO-d_6): δ = 12.02 (1H, br. s, NH^1_{Gu}), 8.44 (1H, s, H^8_{Gu}), 2.81 (3H, s, Me^9_{Ac}), 2.21 (3H, s, Me^2_{Ac}). ^{13}C-NMR (90.56MHz, DMSO-d_6): δ = 173.74 (CO^2_{Ac}), 168.00 (CO^9_{Ac}), 154.61 (C^6_{Gu}), 148.37 (C^4_{Gu}), 147.82 (C^2_{Gu}), 137.44 (C^8_{Gu}), 121.45 (C^5_{Gu}), 24.64 (Me^2_{Ac}), 23.82 (Me^9_{Ac}). MS (EI, 70eV, 200°C): *m/z* (%) = 444 (6.7) (?), 235 (9.9) $[M]^+$, 193 (63.6), 151 (86.5), 109 (30.1). MS (FAB-pos, Glycerol): *m/z* = 236 $[M+H]^+$, 194, 185, 171.

Synthesis of N2-acetyl-O6-diphenylcarbamoylguanine **4.21**

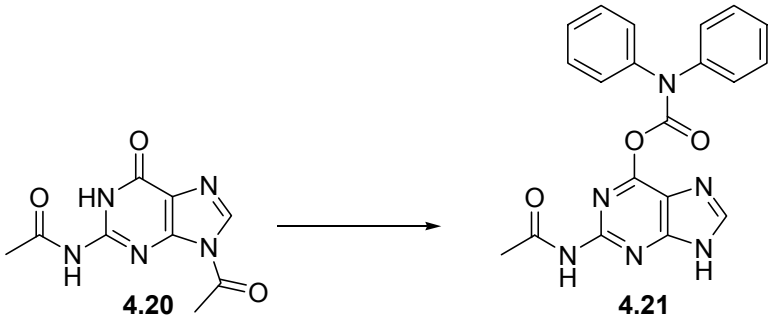

Diphenylcarbamoylchloride (6.37g, 27.5mmol) was added in portions to a suspension of 2-*N*,9-diacetylguanine **4.20** (5.88g, 25mmol) in 8.7ml (50mmol) DIPEA and 120ml dry or freshly distilled pyridine. After stirring the mixture for 1h at RT, it was quenched with 10ml H_2O and stirred for 10min. The solvent was removed *in vacuo* and coevaporated with toluene (3x50ml). The residue was refluxed at 100°C with 300ml of EtOH/H_2O (1:1) for 1.5h. The mixture was cooled down again, filtered and the product was washed with EtOH to yield a violet solid. Yield: 8.8g (22.7mmol, 90.6%)

^{1}H-NMR (360MHz, DMSO-d_6): δ = 13.53 (1H, s, NH^9_{Gu}) 10.63 (1H, s, NH^2_{Gu}), 8.45 (1H, s, H^8_{Gu}), 7.50 (2H, d, H^4_{Bz}), 7.44 (4H, m, H^2_{Bz}, H^6_{Bz}), 7.31 (4H, m, H^3_{Bz}, H^5_{Bz}), 2.17 (3H, s, Me^2_{Ac}). ^{13}C-NMR (90.56MHz, DMSO-d_6): δ = 168.58 (CO^2_{Ac}), 153.54 (CO_{Bz}), 151.97 (C^6_{Gu}), 150.28 (C^4_{Gu}), 141.67 (C^1_{Bz}), 119.10 (C^2_{Bz}, C^6_{Bz}), 148.22 (C^2_{Gu}), 137.51 (C^8_{Gu}), 129.40 (C^3_{Bz}, C^5_{Bz}), 121.26 (C^5_{Gu}), 118.32 (C^4_{Bz}), 24.43 (Me^2_{Ac}). MS (EI, 70eV, 200°C): *m/z* (%) = 388 (0.7) $[M]^+$, 346 (0.1) $[M\text{-}CH_3CO]^+$, 302 (0.4), 269 (1.5) $[M\text{-}CH_3CO\text{-}C_6H_5]^+$, 253 (0.3), 211 (9.6), 196 (7.5), 193 (7.7), 177 (4.3), 169 (100.0). MS (FAB-pos, Glycerol): *m/z* = 389 $[M+H]^+$, 277, 196, 185, 171, 130.

Synthesis of N2-acetyl-O6-diphenylcarbamoyl-9-methoxycarbonylmethylguanine **4.22**

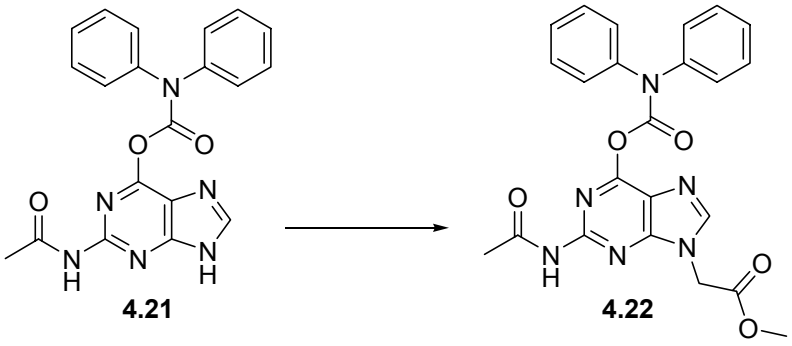

4.21

$C_{20}H_{16}N_6O_3$
Exact Mass: 388,13
Mol. Wt.: 388,38

4.22

$C_{23}H_{20}N_6O_5$
Exact Mass: 460,15
Mol. Wt.: 460,44

N2-acetyl-O6-diphenylcarbamoylguanine **4.21** (6g, 15.5mmol) was suspended in DMF (75ml) together with DIPEA (5.3ml) and heated until a clear solution formed. Methyl-2-bromoacetate (2.6g, 17mmol) was added, and the solution was stirred overnight at RT. The solvent was evaporated *in vacuo* and the residue was resolved in MeOH (75ml). Under vigorous stirring, this solution was poured into water (250ml), and after 30min of stirring, the precipitation of the product is complete. The product was separated by filtration, washed with water and resolved in MeOH. The solvent was removed *in vacuo*, washed repeatedly with EtOAc and finally with Et_2O to yield 4.4g (9.6mmol, 61.7%) of a light violet powder.

^{1}H-NMR (360MHz, DMSO-d_6): δ = 10.72 (1H, s, NH^2_{Gu}), 8.44 (1H, s, H^8_{Gu}), 7.51 (2H, d, H^4_{Bz}), 7.45 (4H, m, H^2_{Bz}, H^6_{Bz}), 7.32 (4H, m, H^3_{Bz}, H^5_{Bz}), 5.16 (2H, s, $H\alpha_{Ac}$), 3.72 (3H, s, Me^9_{Ac}), 2.19 (3H, s, Me^2_{Ac}). ^{13}C-NMR (90.56MHz, DMSO-d_6): δ = 168.83 (CO^2_{Ac}), 167.95 (CO^9_{Ac}), 154.94 (C^6_{Gu}), 155.07 (CO_{Bz}), 152.31 (C^4_{Gu}), 148.41 (C^2_{Gu}), 141.57 (C^1_{Bz}), 138.22 (C^8_{Gu}), 129.38 (C^3_{Bz}, C^5_{Bz}), 121.78 (C^5_{Gu}), 119.37 (C^2_{Bz}, C^6_{Bz}), 52.59 ($C\alpha_{Ac}$), 44.28 (Me^9_{Ac}), 24.50 (Me^2_{Ac}). MS (ESI-pos): *m/z* = 943 $[2M+Na]^+$, 483 [M+Na]+, 461 $[M+H]^+$ MS (FAB-pos, glycerol): *m/z* = 461 $[M+H]^+$, 266, 250, 224, 207, 196, 168.

Synthesis of N2-acetyl-O6-diphenylcarbamoyl-9-carboxymethylguanine **4.23**

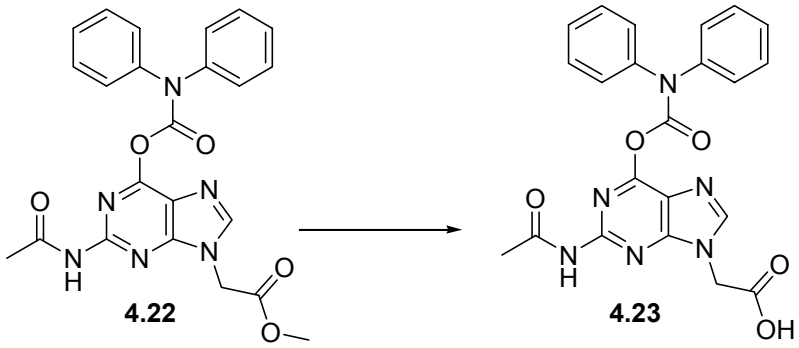

4.22

$C_{23}H_{20}N_6O_5$
Exact Mass: 460,15
Mol. Wt.: 460,44

4.23

$C_{22}H_{18}N_6O_5$
Exact Mass: 446,13
Mol. Wt.: 446,42

N2-Acetyl-O6-diphenylcarbamoyl-9-methoxycarbonylmethylguanine **4.22** (10g, 21.7mmol) was suspended in a mixture of MeOH (25ml), 1,4-dioxane (100ml) and water (50ml). NaOH (1M, 22ml) was added and the mixture was stirred for 1h at RT. The clear, brown solution was adjusted to pH 6 with 1M HCl, followed by removing the organic solvents on the rotary evaporator. Water (500ml) was added, and the pH was brought to 3 with 1M HCl. A jelly-like precipitate formed which was separated by filtration with difficulty and washed with ice-cold water. Yield: 7.7g (17.2mmol, 79.5%)

^{1}H-NMR (360MHz, DMSO-d_6): δ = 10.73 (1H, s, NH^2_{Gu}), 8.46 (1H, s, H^8_{Gu}), 7.50 (2H, d, H^4_{Bz}), 7.44 (4H, m, H^2_{Bz}, H^6_{Bz}), 7.31 (4H, m, H^3_{Bz}, H^5_{Bz}), 5.02 (2H, s, $H\alpha_{Ac}$), 2.20 (3H, s, Me^2_{Ac}). ^{13}C-NMR (90.56MHz, DMSO-d_6): δ = 169.13 (CO^2_{Ac}), 168.38 (CO^9_{Ac}), 154.74 (CO_{Bz}), 154.62 (C^6_{Gu}), 151.83 (C^4_{Gu}), 146.04 (C^2_{Gu}), 141.32 (C^1_{Bz}), 137.89 (C^8_{Gu}), 129.07 (C^3_{Bz}, C^5_{Bz}), 120.99 (C^5_{Gu}), 119.59 (C^2_{Bz}, C^6_{Bz}), 119.10 (C^4_{Bz}), 54.58 ($C\alpha_{Ac}$), 24.17 (Me^2_{Ac}). MS (FAB-pos, Glycerol): *m/z* = 539 $[M+glycerol]^+$, 509, 469 $[M+Na]^+$, 447 $[M+H]^+$, 405, 274 $[M+Na-(C_6H_5)_2NCO]^+$, 268, 252, 210, 196, 168.

Synthesis of guanine-backbone **4.24**

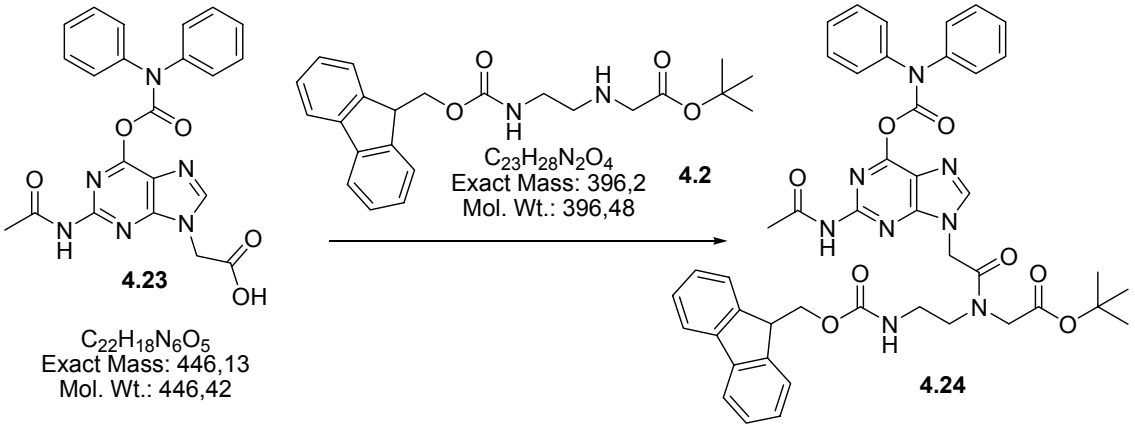

Guanine-acetic acid **4.23** (3.57g, 8mmol), TBTU (5.14g, 16mmol) and HOBt (2.45g, 16mmol) were suspended in DMF (80ml). Meanwhile, backbone·HCl **4.2** (3.46g, 8mmol) was suspended in dichloromethane (80ml) in an extraction funnel and $NaHCO_3$ (sat. aq, 40ml) was added. After extraction, the dichloromethane layer was dried over $MgSO_4$ for 10min. Then DIPEA (2.8ml, 2.08g, 16mmol) was added to the DMF solution, and the colour changed to yellow. After 2min of activation, the organic phase was filtered into the DMF solution, and the extraction funnel was washed with dichloromethane (20ml). This mixture was stirred at RT for 2h. After evaporation of the solvent in vacuo (10^{-2}mbar, 50°C), the brown residue was filtered and washed with EtOAc (3x50ml) until the colour disappears, followed by recrystallisation from EtOH (3L).

^{1}H-NMR (360MHz, DMSO-d_6): δ = 10.62 (1H, s, NH^2_{Gu}), 8.31 (1H, s, H^8_{Gu}), 7.86 (2H, d, H^4_{Fmoc}, H^5_{Fmoc}), 7.65 (2H, d, H^1_{Fmoc}, H^8_{Fmoc}), 7.43 (1H, t, NH_{BB}), 7.38 (2H, m, H^3_{Fmoc}, H^6_{Fmoc}), 7.31 (2H, m, H^2_{Fmoc}, H^7_{Fmoc}), 7.28 (4H, d, H^3_{Bz}, H^5_{Bz}), 7.45 (4H, d, H^2_{Bz}, H^6_{Bz}), 7.52 (1H, s, H^4_{Bz}), 5.25 (1.2H, s, $H\alpha^{maj}_{Ac}$), 5.08 (0.8H, s, $H\alpha^{min}_{Ac}$), 4.34 (2H, d, H^{10}_{Fmoc}), 4.20 (1H, t, H^9_{Fmoc}), 3.95 (2H, s, H^{14}_{BB}), 3.50 (1.2 H, t, H^{12maj}_{BB}), 3.10 (0.8H, t, H^{13min}_{BB}), 2.18 (3H, s, Me^2_{Ac}). ^{13}C-NMR (90.56MHz): δ = 169.02 (CO^2_{Ac}), 168.49 (CO^9_{Ac}), 166.82 (C^{15}_{BB}), 156.30 (C^{11}_{Fmoc}), 155.11 (C^6_{Gu}),154.91 (CO_{Bz}), 150.08 (C^4_{Gu}), 146.14 (C^2_{Gu}), 143.77 (C^{8a}_{Fmoc}, C^{9a}_{Fmoc}), 141.55 (C^1_{Bz}), 140.66 (C^{4a}_{Fmoc}, C^{4b}_{Fmoc}), 138.14 (C^8_{Gu}), 129.34 (C^3_{Bz}, C^5_{Bz}), 127.52 (C^1_{Fmoc}, C^8_{Fmoc}), 126.93 (C^4_{Fmoc}, C^5_{Fmoc}), 124.93

(C^2_{Fmoc}, C^7_{Fmoc}), 121.31 (C^5_{Gu}), 120.03 (C^3_{Fmoc}, C^6_{Fmoc}), 119.96 (C^2_{Bz}, C^6_{Bz}), 119.29 (C^4_{Bz}), 80.96 (C^{16}_{BB}), 65.34 (C^{10}_{Fmoc}), 54.98 ($C\alpha_{Ac}$), 48.44 (C^{14}_{BB}), 47.12 (C^{13}_{BB}), 46.63 (C^9_{Fmoc}), 38.02 (C^{12}_{BB}), 27.58 (C^{17}_{BB}), 24.49 (Me^2_{Ac}). MS (ESI-pos): *m/z* = 847 $[M+Na]^+$, 825 $[M+H]^+$. MS (FAB-pos, NBA): *m/z* = 825 $[M+H]^+$.

Synthesis of guanine monomer **4.25a & 4.25b**

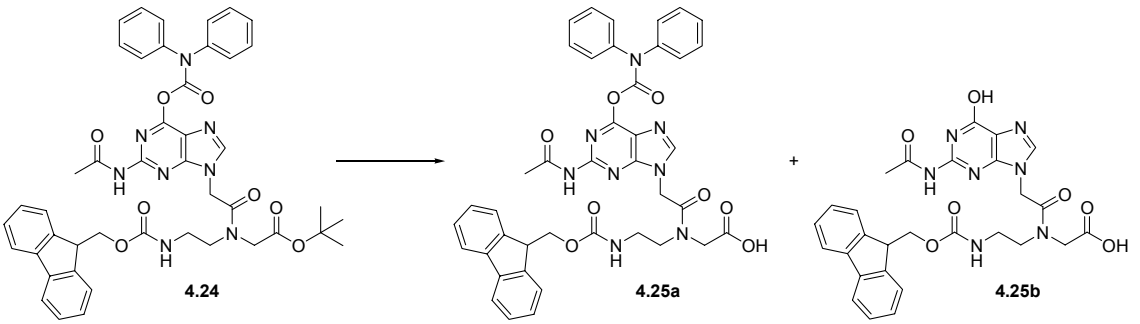

Guanine-backbone **4.24** (2g, 2.4mmol) was suspended in CH_2Cl_2 (30ml), followed by addition of 1,3-dimethoxybenzene (0.4ml, 2.9mmol) and TFA (22.6ml, 292mmol). The mixture clarified and was stirred for 8h at RT. The volatiles were removed *in vacuo*, the residue was coevaporated with acetonitrile (5x30ml), washed with ethyl acetate and recrystallized from EtOH.

^{1}H-NMR (360MHz, DMSO-d_6): δ = 7.97 (1H, s, H^8_{Gu}), 7.87 (2H, d, H^4_{Fmoc}, H^5_{Fmoc}), 7.66 (2H, d, H^1_{Fmoc}, H^8_{Fmoc}), 7.47 (1H, t, NH_{BB}), 7.40 (2H, m, H^3_{Fmoc}, H^6_{Fmoc}), 7.35 (2H, m, H^2_{Fmoc}, H^7_{Fmoc}), 7.22 (4H, d, H^3_{Bz}, H^5_{Bz}), 7.07 (4H, d, H^2_{Bz}, H^6_{Bz}), 6.81 (1H, s, H^4_{Bz}), 6.49 (NH^2_{Gu}), 5.14 (1.2H, s, $H\alpha^{maj}_{Ac}$), 4.98 (0.8H, s, $H\alpha^{min}_{Ac}$), 4.38 (2H, d, H^{10}_{Fmoc}), 4.28 (1H, t, H^9_{Fmoc}), 4.02 (2H, s, H^{14}_{BB}), 3.50 (1.2 H, t, H^{12maj}_{BB}), 3.34 (2H, br. m, H^{12min}_{BB}, H^{13maj}_{BB}), 3.13 (0.8H, t, H^{13min}_{BB}), 2.15 (3H, s, Me^2_{Ac}). MS (FAB-pos, Glycerol): *m/z* = 636 [M(**25a**)-Fmoc], 574 $[M(\mathbf{25b})+H]^+$. MALDI-TOF (CCA, DMSO): *m/z* = 573.9

^{1}H-NMR (360MHz, DMSO-d_6)

δ (ppm)	4.20	4.21	4.22	4.23	4.24	4.25a
H^{4}_{Bz}	–	7.50	7.51	7.50	7.52	6.81
H^{3}_{Bz}, H^{5}_{Bz}	–	7.31	7.32	7.31	7.28	7.07
H^{2}_{Bz}, H^{6}_{Bz}	–	7.44	7.45	7.44	7.45	7.22
NH^{1}_{Gu}	12.02	–	–	–	–	–
NH^{2}_{Gu}	n.a.	10.63	10.72	10.73	10.62	6.49
H^{8}_{Gu}	8.44	8.45	8.44	8.46	8.31	7.97
NH^{9}_{Gu}	–	13.53	–	–	–	–
Me^{2}_{Ac}	2.21	2.17	2.19	2.20	2.18	2.15
Me^{9}_{Ac}	2.81	–	–	–	–	–
Me^{9}_{Ac}	–	–	3.72	–	–	–
NH_{BB}	–	–	–	–	7.43	7.47
H^{4}_{Fmoc}, H^{5}_{Fmoc}	–	–	–	–	7.86	7.87
H^{1}_{Fmoc}, H^{8}_{Fmoc}	–	–	–	–	7.65	7.66
H^{3}_{Fmoc}, H^{6}_{Fmoc}	–	–	–	–	7.38	7.40
H^{2}_{Fmoc}, H^{7}_{Fmoc}	–	–	–	–	7.31	7.35
$H\alpha^{maj}_{Ac}$	–	–	5.16	5.02	5.25	5.14
$H\alpha^{min}_{Ac}$	–	–	5.16	5.02	5.08	4.98
H^{10}_{Fmoc}	–	–	–	–	4.34	4.38
H^{9}_{Fmoc}	–	–	–	–	4.20	4.28
H^{14}_{BB}	–	–	–	–	3.95	4.02
H^{12maj}_{BB}	–	–	–	–	3.50	3.50
H^{12min}_{BB}	–	–	–	–	n.a.	3.34
H^{13maj}_{BB}	–	–	–	–	n.a.	3.34
H^{13min}_{BB}	–	–	–	–	3.10	3.13
H^{17min}_{BB}	–	–	–	–	1.48	–
H^{17maj}_{BB}	–	–	–	–	1.36	–

^{13}C-NMR (90.56MHz, DMSO-d_6)

δ (ppm)	4.20	4.21	4.22	4.23	4.24
C^{1}_{Bz}	–	141.67	141.57	141.32	141.55
C^{3}_{Bz}, C^{5}_{Bz}	–	129.40	129.38	129.07	129.34
C^{2}_{Bz}, C^{6}_{Bz}	–	119.10	119.37	119.59	119.96
C^{4}_{Bz}	–	118.32	118.43	119.10	119.29
CO_{Bz}	–	153.54	155.07	154.74	154.91
C^{2}_{Gu}	147.82	148.22	148.41	146.04	146.14
C^{4}_{Gu}	148.37	150.28	152.31	151.83	150.08
C^{5}_{Gu}	121.45	121.26	121.78	120.99	121.31
C^{6}_{Gu}	154.61	151.97	154.94	154.62	155.11
C^{8}_{Gu}	137.44	137.51	138.22	137.89	138.14
$C\alpha_{Ac}$	–	–	52.59	54.58	54.98
CO^{2}_{Ac}	173.74	168.58	168.83	169.13	169.02
Me^{2}_{Ac}	24.64	24.43	24.50	24.17	24.49
CO^{9}_{Ac}	168.00	–	167.95	168.38	168.49
Me^{9}_{Ac}	23.82	–	–	–	–
Me^{9}_{Ac}	–	–	44.28	–	–
C^{1}_{Fmoc}, C^{8}_{Fmoc}	–	–	–	–	127.52
C^{2}_{Fmoc}, C^{7}_{Fmoc}	–	–	–	–	124.93
C^{3}_{Fmoc}, C^{6}_{Fmoc}	–	–	–	–	120.03
C^{4}_{Fmoc}, C^{5}_{Fmoc}	–	–	–	–	126.93
C^{4a}_{Fmoc}, C^{4b}_{Fmoc}	–	–	–	–	140.66
C^{8a}_{Fmoc}, C^{9a}_{Fmoc}	–	–	–	–	143.77
C^{9}_{Fmoc}	–	–	–	–	46.63
C^{10}_{Fmoc}	–	–	–	–	65.34
C^{11}_{Fmoc}	–	–	–	–	156.30
C^{12}_{BB}	–	–	–	–	38.02
C^{13}_{BB}	–	–	–	–	47.12
C^{14}_{BB}	–	–	–	–	48.44
C^{15}_{BB}	–	–	–	–	166.82
C^{16}_{BB}	–	–	–	–	80.96
C^{17}_{BB}	–	–	–	–	27.58

8.6 Synthesis of PNA Oligomers – General Procedure

Primary attempts in SPPS in our group were carried out on a peptide synthesizer (Fig. 8.2), but due to solubility problems of the cytosine monomer, persistent tube leaking and the device requiring permanent surveillance, a "low tech procedure" was established comprising a one-way plastic syringe as a reaction vessel (Fig. 8.3) affording considerable advantages such as enhanced accessibility and easy customizing.

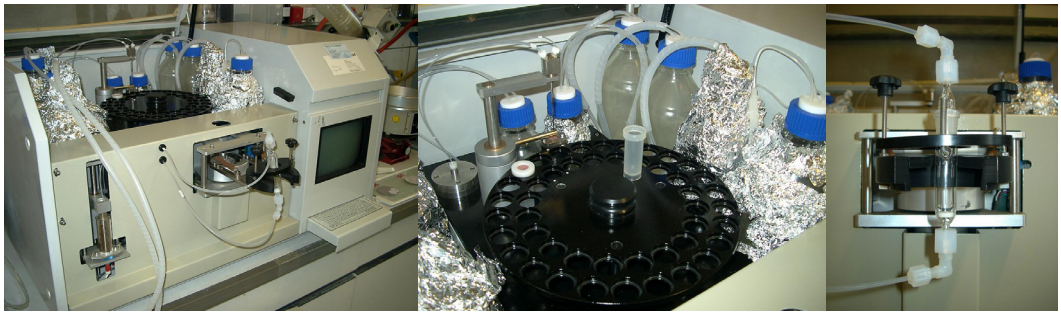

Fig. 8.2: *Automated Solid Phase Peptide Synthesizer*

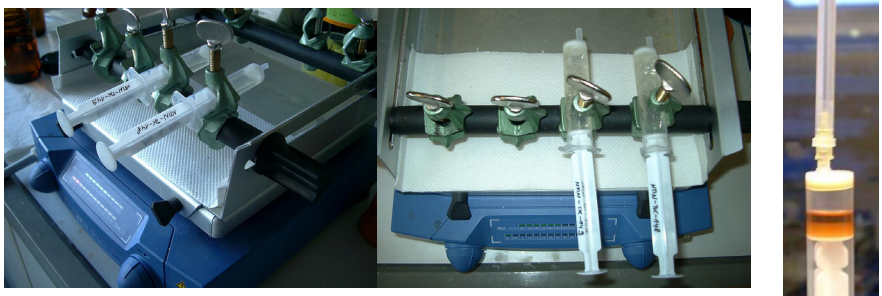

Fig. 8.3: *Mechanical Shaker with PNA Reaction Syringes and Syringe for PNA SPS with Coupling Solution (brown) and Resin beads (yellow)*

All reactions and washings were performed on a mechanical shaker with 640rpm (Fig. 8.3), soaking approximately 5-8ml of the particular solution into the syringe. Washing was always done for at least 15sec. Before starting, all solutions were freshly prepared:

- Deprotection solution: 20% piperidine in DMF
- Activation mixture: 0.3M lutidine & 0.2M DIPEA in DMF
- Capping solution: 5% acetic anhydride & 6% DIPEA in DMF

Amino acids and linkers were incorporated into the sequence exactly like PNA monomers, except as indicated. For the synthesis of PNA oligomers with base labile side chain protection (Chapter 4), the whole procedure was similar, except for the use of a different resin and the final cleavage which was carried out with 5% hydrazine in DMF.

132.35mg of TentaGel R RAM-Lys(Boc)Fmoc resin (0.17mmol/g) (22.5µmol of loading) were placed in a 10ml syringe equipped with a frit ("batch reactor") and washed five times with DMF, followed by swelling in DMF for 1h.

1) Deprotection

   The preloaded resin was deprotected with 20% piperidine in DMF for 2x3min, washed with DMF (3x), DCM (3x) and again DMF (3x).

2) Coupling

   HATU (4.5 equivalents in order to avoid HATU capping) was dissolved in 0.6ml of activation mixture (cytosine: 1.8ml !), added to an excess of 5 equivalents (112.5µmol) of PNA monomer and shaken for 3min. until a clear solution was obtained. Cytosine sometimes afforded longer activation and vigorous shaking and triturating because of decreased solubility. All containers were rinsed with 0.2ml of activation mixture.

   The coupling was performed for 1h, and the resin was washed with DMF (5x).

3) Kaiser test

   In order to assure the coupling being quantitative, a Kaiser test was performed after each coupling step.

4) Capping

   Free amine groups were capped once with 5% acetic anhydride & 6% DIPEA in DMF (3min), followed by washing with DMF (5x).

   Whenever the synthesis had to be interrupted overnight, the reactor with the resin was sealed with parafilm and stored in the fridge *after this step*.

(repeat steps 1 - 4 for further monomers)

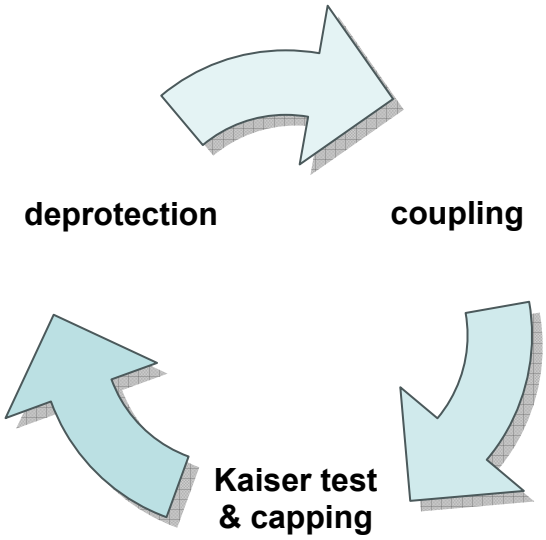

Fig. 8.4: *Synthesis Cacle for PNA Oligomers*

After the last coupling step, the final amine group was either acetylated or equipped with the particular ligand (see next chapter). The synthesis of oligomers with a central modification will also be described below.

5) Deprotection

The final oligomer was deprotected with 20% piperidine in DMF for 2x3min, washed with DMF (3x), DCM (3x) and again DMF (3x).

6) Acetylation

The free amine groups were acetylated twice with 5% acetic anhydride & 6% DIPEA in DMF (2x3min), followed by washing with DMF (5x).

7) Shrinking

The resin was washed with MeOH (5x) and shrunk with MeOH for 30min. After that, it was transferred into a weighed 50ml flask and dried *in vacuo*.

8) Cleavage

The dried resin was cleaved in the flask for 3h with 95% TFA / 2.5% TIS / 2.5% H_2O (Σ=10ml), filtered into another 50ml flask through the batch reactor used for synthesis and rinsed with 2-3ml of TFA. The combined filtrates were evaporated to dryness in HV, using an additional nitrogen trap in order to prevent TFA from damaging the pump.

9) Workup

The residue was precipitated with 5ml of ice-cold diethyl ether, centrifuged in a bluecap and washed 3-4x with ice cold ether which was discarded afterwards. Drying was performed on air flow.

10) Purification

All oligomers were purified using semi-preparative RP-HPLC.[237] The crude product was dissolved in 4ml 0.1% TFA, 2ml of which were injected into the loop after syringe filtration. Purification was carried out using a standard gradient suitable both for analytical and preparative runs with 0.1%TFA in acetonitrile and 0.1% TFA in H_2O (flow: 8ml/min).

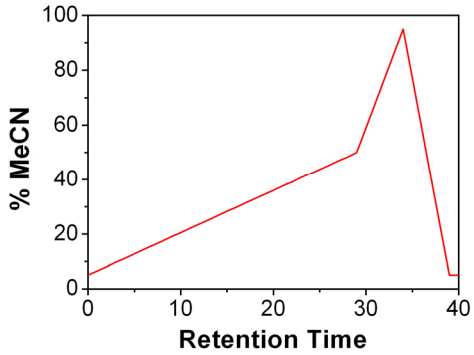

t	%MeCN
0	5
30	50
35	95
40	5

11) Analytics

All samples were dissolved in 0.1% TFA for MALDI-TOF. MALDI spectra were measured before and after HPLC purification of the crude product.

Monitoring

In order to supervise the progress of syntheses, some resin beads were taken out of the vessel after the questionable step (omitting deprotection / acetylation, shrinking and drying), transferred into a flask and cleaved with for 2h with 95% TFA / 2.5% TIS / 2.5% H_2O (Σ=2ml). The solution was filtered through a 0.22µm syringe filter, and the TFA was removed *in vacuo*. Workup was similar to that of the final crude product, and the sample was subjected to MALDI-TOF.

8.7 Synthesis of PNA Oligomers – Specific Sequences and Modifications

The synthesis of *N*-acetylated PNA oligomers has been described before.

The concept of incorporating ligands to the end and to the center of the sequence was designed to be compatible with the standard protocol in terms of peptide coupling.
All amino acids (Fmoc-Phe-OH, Fmoc-Phe(NO_2)-OH **5.2** and Fmoc-Gly-OH as a spacer), and the aminohexanoic acid linker (Fmoc-Ahx-OH) were introduced into the PNA chain according to the standard method mentioned in the previous chapter and thus treated like PNA monomers. Differing procedures will be described in the following:

Attachment of Carboxyl Ligands

In order to obtain a central anchoring group for carboxyl-functionalized ligands, Phe(NO_2) was inserted into the sequence, followed by on-resin reduction and ligand coupling. The phenylalanine nitro group was reduced twice overnight with a 0.9M solution of $SnCl_2 \cdot 2H_2O$ (406mg / 1.8mmol) in DMF (2ml).

For the attachment of ligands to free amino groups both at the end and in the center of the sequence, the following protocol turned out to be optimum:

Tab. 8.1: *Ligand coupling (for 22.5µmol of resin)*

	M [g/mol]	
95µmol HATU	380.20	36.12mg
440µl DMF	/	440µl
1mmol (10eq.) DIPEA	129.24	129.24mg = 174µl
100µmol Ligand	363.42	36.34mg

1) Deprotection

The resin was deprotected with 20% piperidine in DMF for 2x3min, washed with DMF (3x), DCM (3x) and again DMF (3x).

2) Coupling

HATU was dissolved in DMF (440µl) together with DIPEA (174µl), added to 4.4 equivalents (100µmol) of ligand and shaken for 15min. at 640rpm. The coupling was performed twice overnight, and the resin was washed with DMF (5x).

3) Kaiser test

In order to assure the coupling being quantitative, a Kaiser test was performed.

4) Capping

Free amine groups were capped once with 5% acetic anhydride & 6% DIPEA in DMF (3min), followed by washing with DMF (5x).

Attachment of Amino Ligands

In order to couple amino groups to the PNA chain, the *N*-terminus thereof first of all had to be converted into a *C*-terminus. This was achieved by the introduction of a dicarboxylic acid linker (Fig. 8.5).

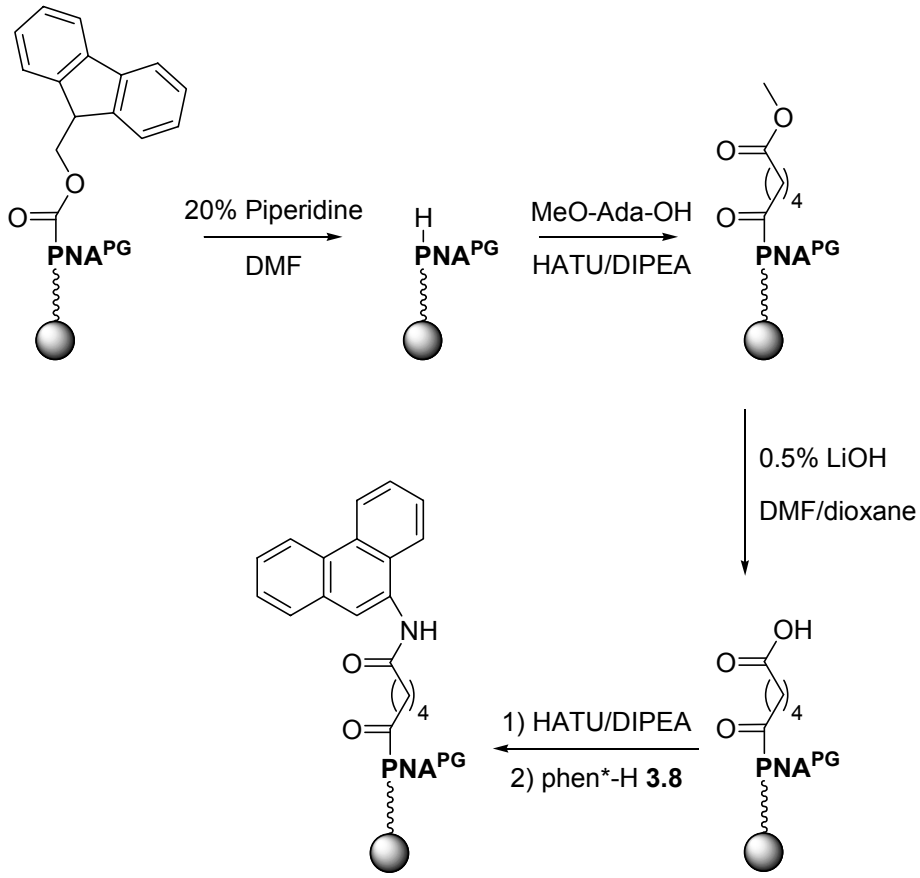

Fig. 8.5: *Pathway for the attachment of amino ligands to N-terminal PNA*

Tab. 8.2: *Linker coupling (for 22.5µmol of resin)*

	M [g/mol]	
95µmol HATU	380.20	36.12mg
440µl DMF	/	440µl
1mmol (10eq.) DIPEA	129.24	129.24mg = 174µl
100µmol Linker	160.17	16.02mg

1) Deprotection

The resin was deprotected with 20% piperidine in DMF for 2x3min, washed with DMF (3x), DCM (3x) and again DMF (3x).

2) Coupling

HATU was dissolved in DMF (440µl) together with DIPEA (174µl), added to 4.4 equivalents (100µmol) of linker and shaken for 15min. at 640rpm.

The coupling was performed twice overnight, and the resin was washed with DMF (5x).

3) Kaiser test

In order to assure the coupling being quantitative, a Kaiser test was performed.

4) Capping

Free amine groups were capped once with 5% acetic anhydride & 6% DIPEA in DMF (3min), followed by washing with DMF (5x).

After the coupling, the methyl ester was cleaved overnight with 0.5% LiOH in DMF/dioxane, followed by washing with dioxane and DMF.

HATU (7.2mg, 19µmol) and DIPEA (25µl, 200µmol) were dissolved in DMF (200µl), and the resin-bound carboxylic groups were activated overnight.

Phen*-H **3.8** (19.52mg, 100µmol) was dissolved in DMF (600µl) and added to the activated resin. Coupling was performed overnight. The solution changed its colour from orange to green-brown.

Tab. 8.3: *Amine Coupling*

	M [g/mol]	
19µmol HATU	380.20	7.2mg
800µl DMF	/	200µl+600µl
200µmol (11eq.) DIPEA	129.24	25.85mg = 35µl
100µmol Ligand	195.23	19.52mg

A MALDI spectrum was performed after each step with some cleaved resin beads in order to verify the particular reaction.

References

1. Frieden, E., New perspectives on the essential trace elements. *J. Chem. Ed.* **1985,** *62*, (11), 917-923.
2. Williams, R. J. P., The fundamental nature of life as a chemical system: the part played by inorganic elements. *J. Inorg. Biochem.* **2002,** *88*, 241-250.
3. Guo, Z.; Sadler, P. J., Metals in Medicine. *Angew. Chem. Int. Ed.* **1999,** *38*, (11), 1512-1531.
4. Metzler-Nolte, N., Labeling of Biomolecules for Medicinal Applications - Bioorganometallic Chemistry at Its Best. *Angew. Chem. Int. Ed.* **2001,** *40*, (6), 1040-1043.
5. vanStaveren, D. R.; Mundwiler, S.; Hoffmanns, U.; Pak, J. K.; Spingler, B.; Metzler-Nolte, N.; Alberto, R., Conjugation of a novel histidine derivative to biomolecules and labelling with $[^{99m}Tc(OH_2)_3(CO)_3]^+$. *Org. Biomol. Chem.* **2004,** *2*, 2593-2603.
6. Jaouen, G.; Top, S.; Vessières, A.; Alberto, R., New Paradigms for Synthetic Pathways Inspired by Bioorganometallic Chemistry. *J. Organomet. Chem.* **2000,** *600*, (1-2), 23-36.
7. Eisenhut, M.; Hull, W. H.; Mohammed, A.; Mier, W.; Lay, D.; Just, W.; Gorgas, K.; Lehmann, W. D.; Haberkorn, U., Radioiodinated *N*-(2-Diethylaminoethyl)benzamide Derivatives with High Melanoma Uptake; Structure-Affinity Relationship Studies, Metabolic Fate and Intracellular Localisation. *J. Med. Chem.* **2000,** *43*, 3913-3922.
8. Rosenberg, B.; VanCamp, L., Platinum Compounds: a New Class of Potent Antitumor Agents. *Nature* **1969,** *222*, 385-386.
9. Heeg, M. J.; Jurisson, S. S., The Role of Inorganic Chemistry in the Development of Radiometal Agents for Cancer Therapy. *Acc. Chem. Res.* **1999,** *32*, 1053-1060.
10. Beck, W.; Severin, K., Biometallorganische Chemie. *Chemie in unserer Zeit* **2002,** *36*, (6), 356-365.
11. MacKinnon, R., Potassium Channels and the Atomic Basis of Selective Ion Conduction (Nobel Lecture). *Angew. Chem. Int. Ed.* **2004,** *43*, 4265-4277.
12. Volbeda, A.; Charon, M.-H.; Piras, C.; Hatchikian, E. C.; Frey, M.; Fontecilla-Camps, J. C., Crystal structure of the nickel-iron hydrogenase from Desulfovibrio gigas. *Nature* **1995,** *373*, (6515), 580-587.
13. Schilling, O.; Wenzel, N.; Naylor, M.; Vogel, A.; Crowder, M.; Makaroff, C.; Meyer-Klaucke, W., Flexible Metal Binding of the Metallo-β-lactamase Domain: Glyoxalase II Incorporates Iron, Manganese, and Zinc in Vivo. *Biochemistry* **2003,** *42*, (40), 11777-11786.
14. Finney, L. A.; O'Halloran, T. V., Transition Metal Speciation in the Cell: Insights from the Chemistry of Metal Ion Receptors. *Science* **2003,** *300*, (5621), 931-936.
15. Battersby, A. R., Biosynthesis of Vitamin B_{12}. *Acc. Chem. Res.* **1993,** *26*, (1), 15-21.
16. Perutz, M. F., Relation between structure and sequence of haemoglobin. *Nature* **1962,** *194*, 914-917.
17. Monmenteau, M.; Reed, C. A., Synthetic Heme Dioxygen Complexes. *Chem. Rev.* **1994,** *94*, (3), 659-698.
18. Kobayashi, M.; Shimizu, S., Cobalt proteins. *Eur. J. Biochem.* **1999,** *261*, (1), 1-9.

19. Williams, R. J. P., Metallo-enzyme catalysis. *Chem. Comm.* **2003**, (10), 1109-1113.

20. Fischer, E., Einfluss der Configuration auf die Wirkung der Enzyme. *Ber. Dt. Chem. Ges.* **1894,** *27*, (3), 2985-2993.

21. Klug, A.; Rhodes, D., "Zinc Fingers": A Novel Protein Motif for Nucleic Acid Recognition. *Trends Biochem. Sci* **1987,** *12*, 464-469.

22. Berg, J. M., Proposed Structure for the Zinc-Binding Domains from Transcription Factor IIIA and Related Proteins. *Proc. Natl. Acad. Sci. U.S.A.* **1988,** *85*, (1), 99-102.

23. Wingender, F.; Seifart, K. H., Transcription in Eukaryotes - The Role of Transcription Complexes and Their Components. *Angew. Chem. Int. Ed.* **1987,** *26*, (3), 218-227.

24. Houbaviy, H. B.; Usheva, A.; Shenk, T.; Burley, S. K., Cocrystal Structure of YY1 bound to the Adeno-Associated Virus P5 Initiator. *Proc. Natl. Acad. Sci. U.S.A.* **1996,** *93*, 13577-13582.

25. Lee, M. S.; Gippert, G. P.; Soman, K. V.; Case, D. A.; Wright, P. E., Three-dimensional solution structure of a single zinc finger DNA-binding domain. *Science* **1989,** *245*, 635-637.

26. Omichinski, J. G.; Clore, G. M.; Appella, E.; Sakaguchi, K.; Gronenborn, A. M., High-resolution three-dimensional structure of a single zinc finger from a human enhancer binding protein in solution. *Biochemistry* **1990,** *29*, (40), 9324 - 9334.

27. Bashkin, J. K.; Jenkins, L. A., The role of metals in the hydrolytic cleavage of DNA and RNA. *Comments Inorg. Chem.* **1994,** *16*, (1-2), 77-93.

28. Kim, J. H.; Cin, J., Dimethyl Phosphate Hydrolysis at Neutral pH. *J. Am. Chem. Soc.* **1992,** *114*, (25), 9792-9795.

29. Borah, B.; Chen, C. W.; Egan, W.; Miller, M.; Wlodawer, A.; S., C. J., Nuclear magnetic resonance and neutron diffraction studies of the complex of ribonuclease A with uridine vanadate, a transition-state analog. *Biochemistry* **1985,** *24*, (8), 2058 - 2067.

30. Kessler, C.; Manta, V., Specificity of restriction endonucleases and DNA modification methyltransferases - a review. *Gene* **1990,** *91*, (1-2), 1-234.

31. Arber, W.; Linn, S., DNA Modification and Restriction. *Ann. Rev. Biochem.* **1969,** *38*, 467-500.

32. Arber, W., The Role of DNA Methylation in the Control by the Host of Modification of the Bacteriophage. *Path. Microbiol.* **1965,** *28*, (2), 71-72.

33. Barnard, E. A., Ribonucleases. *Annu. Rev. Biochem.* **1969,** *38*, 677-732.

34. Herschlag, D.; Cech, T. R., DNA cleavage catalysed by the ribozyme from Tetrahymena. *Nature* **1990,** *344*, (6265), 405-409.

35. Pyle, A. M.; Cech, T. R., Ribozyme recognition of RNA by tertiary interactions with specific ribose 2'-OH groups. *Nature* **1991,** *350*, (6319), 628-631.

36. Tann, C.-M.; Qi, D.; Distefano, M. D., Enzyme design by chemical modification of protein scaffolds. *Curr. Opin. Chem. Biol.* **2001,** *5*, (6), 696-704.

37. Stubbe, J.; Kozarich, J. W., Mechanisms of Bleomycin-Induced DNA Degradation. *Chem. Rev.* **1987,** *87*, (5), 1107-1136.

38. Cowan, J. A., Metal-mediated hydrolysis of biological phosphate esters - A critcal analysis of the essential metal ion stoichiometry for magnesium-dependent nuclease activation. *J. Biol. Inorg. Chem.* **1997,** *2*, (2), 168-176.

39. Basile, L. A.; Barton, J. K., Metallonnucleases: Real and Artificial. *Met. Ions Biol. Syst.* **1989,** *25*, 38.

40. Chin, J., Developing artificial hydrolytic metalloenzymes by a unified mechanistic approach. *Acc. Chem. Res.* **1991,** *24*, (5), 145-152.

41. Uppenberg, J.; Lindqvist, F.; Svensson, C.; Ek-Rylander, B.; Andersson, G., Crystal structure of a mammalian purple acid phosphatase. *J. Mol. Biol.* **1999,** *290*, (1), 201-211.

42. Guddat, L. W.; McAlpine, A. S.; Hume, D.; Hamilton, S.; deJersey, J.; Martin, J. L., Crystal structure of mammalian purple acid phosphatase. *Structure* **1999,** *7*, (7), 757-767.

43. Strater, N.; Klabunde, T.; Tucker, P.; Witzel, H.; Krebs, B., Crystal structure of a purple acid phosphatase containing a dinuclear Fe(III)-Zn(II) active site. *Science* **1995,** *268*, (5216), 1489-1492.

44. Lindqvist, Y.; Johansson, E.; Kaija, H.; Vihko, P.; Schneider, G., Three-dimensional structure of a mammalian purple acid phosphatase at 2.2 Å resolution with a μ-(hydr)oxo bridged di-iron center. *J. Mol. Biol.* **1999,** *291*, (1), 135-147.

45. Durmus, A.; Eicken, C.; Sift, B. H.; Kratel, A.; Kappl, R.; Hüttermann, J.; Krebs, B., The active site of purple acid phosphatase from sweet potatoes (Ipomoea batatas) Metal content and spectroscopic characterization. *Eur. J. Biochem.* **1999,** *260*, (3), 709-716.

46. Klenow, H.; Henningsen, I., Selective Elimination of the Exonuclease Activity of the Deoxyribonucleic Acid Polymerase from Escherichia coli B by Limited Proteolysis. *Proc. Natl. Acad. Sci. U.S.A.* **1970,** *65*, (1), 168-175.

47. Beese, L. S.; Steitz, T. A., Structural basis for the 3'-5' exonuclease activity of Escherichia coli DNA polymerase I: a two metal ion mechanism. *EMBO J.* **1991,** *10*, 25-33.

48. Brautigam, C. A.; Steitz, T. A., Structural principles for the inhibition of the 3′-5′ exonuclease activity of Escherichia coli DNA polymerase I by phosphorothioates. *J. Mol. Biol.* **1998,** *277*, (2), 363-377.

49. Trawick, B.; Daniher, A. T.; Bashkin, J. K., Inorganic Mimics of Ribonucleases and Ribozymes: From Random Cleavage to Sequence-Specific Chemistry to Catalytic Antisense Drugs. *Chem. Rev.* **1998,** *98*, 939-960.

50. Ott, R.; Krämer, R., DNA hydrolysis by inorganic catalysts. *Appl. Microbiol. Biotechnol.* **1999,** *52*, (6), 761-767.

51. Häner, R.; Hall, J., The sequence-specific cleavage of RNA by artificial chemical ribonucleases. *Antisense Nucleic Acid Drug Dev.* **1997,** *7*, (4), 423-430.

52. Matsuda, S.; Ishikuba, A.; Kuzuya, A.; Yashiro, M.; Komiyama, M., Konjugate eines zweikernigen Zink(II)-Komplexes mit DNA-Oligomeren als sequenzselektive künstliche Ribonucleasen. *Angew. Chem.* **1998,** *110*, (23), 3477-3479.

53. Pogozelski, W. K.; Tullius, T. D., Oxidative Strand Scission of Nucleic Acids: Routes Initiated by Hydrogen Abstraction from the Sugar Moiety. *Chem. Rev.* **1998,** *98*, (3), 1089-1107.

54. Burrows, C. J.; Muller, J. G., Oxidative Nucleobase Modifications Leading to Strand Scission. *Chem. Rev.* **1998,** *98*, (3), 1109-1152.

55. Chin, J., Artificial dinuclear phosphoesterases. *Curr. Opin. Chem. Biol.* **1997,** *1*, 514-521.

56. Cowan, J. A., Chemical nucleases. *Curr. Opin. Chem. Biol.* **2001,** *5*, (6), 634-642.

57. Pratviel, G.; Bernadou, J.; Meunier, B., Oxidative DNA damage mediated by a manganese-oxo porphyrin. *Adv. Inorg. Chem.* **1998,** *45*, 251-311.

58. Crooke, S. T., Molecular mechanisms of action of antisense drugs. *Biochim. Biophys. Acta* **1999,** *1489*, (1), 31-44.

59. Kostrewa, D.; Winkler, F. K., Mg^{2+} Binding to the Active Site of EcoRV Endonuclease: A Crystallographic Study of Complexes with Substrate and Product DNA at 2A Resolutions. *Biochemistry* **1995,** *34*, (2), 683-696.

60. Stein, C. A.; Cheng, Y. C., Antisense oligonucleotides as therapeutic agents - Is the bullet really magical? *Science* **1993,** *261*, 1004-1012.

61. Gewirtz, A. M.; Stein, C. A.; Glazer, P. M., Facilitating oligonucleotide delivery: Helping antisense deliver on its promise. *Proc. Natl. Acad. Sci. U.S.A.* **1996,** *93*, 3161-3163.

62. Morelli, D.; Pozzi, B.; Maier, J. A.; Menard, S.; Colnaghi, M. I.; Balsari, A., A monoclonal antibody extends the half-life of an anti-HIV oligodeoxynucleotide and targets it to CD4+ cells. *Nucleic Acids Res.* **1995,** *23*, 4603-4607.

63. Corey, D. R.; Pei, D.; Schultz, P. G., Generation of a Catalytic Sequence-Specific Hybrid DNase. *Biochemistry* **1989,** *28*, (21), 8277-8286.

64. Ma, W. P. M.; Hamilton, S. E.; Stowell, J. G.; Byrn, S. R.; Davisson, V. J., Sequence specific cleavage of messenger RNA by a modified ribonuclease H. *Bioorg. Med. Chem. Lett.* **1994,** *2*, 169-179.

65. Kanaya, S.; Nakai, C.; Konishi, A.; Inoue, H.; Ohtsuka, E.; Ikehara, M., A hybrid ribonuclease H. A novel RNA cleaving enzyme with sequence- specific recognition. *J. Biol. Chem.* **1992,** *267*, (12), 8492-8498.

66. Metteucci, M.; Lin, K.-Y.; Huang, T.; Wagner, R.; Sternbach, D. D.; Mehrotra, M.; Besterman, J. M., *J. Am. Chem. Soc.* **1997,** *119*, 6939.

67. Sigman, D. S.; Mazumder, A.; Perrin, D. M., Chemical Nucleases. *Chem. Rev.* **1993,** *93*, 2295-2316.

68. Chen, C.-H. B.; Sigman, D. S., Sequence-specific scission of RNA by 1,10-phenanthroline-copper linked to deoxyoligonucleotides. *J. Am. Chem. Soc.* **1988,** *110*, 6570-6572.

69. Sun, J.-S.; Francois, J.-C.; Lavery, R.; Saison-Behmoaras, E.; Montenay-Garestier, T.; Thuong, N. T.; Hélène, C., Sequence-Targeted Cleavage of Nucleic Acids by Oligo-a-thymidylate-Phenanthroline Conjugates: Parallel and Antiparallel Double Helices Are Formed with DNA and RNA, Respectively. *Biochemistry* **1988,** *27*, (16), 6039-6045.

70. Le Doan, T.; Perrouault, L.; Thuong, N. T., Targeted Cleavage of Polynucleotides by Complementary Oligonucleotides Covalently Linked to Iron-Porphyrins. *Biochemistry* **1986,** *25*, (22), 6736-6739.

71. Strobel, S. A.; Dervan, P. B., Single-site enzymatic cleavage of yeast genomic DNA mediated by triple helix formation. *Nature* **1991,** *350*, (6314), 172-174.

72. Strobel, S. A.; Dervan, P. B., Site Specific Cleavage of a Yeast Chromosome by Oligonucleotide Directed Triple Helix Formation. *Science* **1990,** *249*, 73-75.

73. Kurz, K., Hydrolytische Spaltung von Nucleinsäuren - vom Enzymmechanismus zum Enzymmodell. *Chemie in unserer Zeit* **1998,** *32*, (2), 94-103.

74. Zhou, D.-M.; Taira, K., The Hydrolysis of RNA: From Theoretical Calculations to the Hammerhead Ribozyme-Mediated Cleavage of RNA. *Chem. Rev.* **1998,** *98*, (3), 991-1026.

75. Pratviel, G.; Bernadou, J.; Meunier, B., Carbon - Hydrogen Bonds of DNA Sugar Units as Targets for Chemical Nucleases and Drugs. *Angew. Chem.* **1995,** *34*, (7), 746-769.

76. Hannon, C. L.; Anslyn, E. V., The Guanidinium Group: Its Biological Role and Synthetic Analogs. *Bioorg. Chem. Front* **1993,** *3*, 193-256.

77. Morrow, J. R., Artificial ribonucleases. *Adv. Inorg. Biochem.* **1994,** *9*, 41-74.

78. Morrow, J. R., Hydrolytic cleavage of RNA catalyzed by metal ion complexes. *Met. Ions Biol. Syst.* **1996,** *33*, 561-592.

79. Ott, R.; Krämer, R., Schnelle Phosphodiester-Hydrolyse durch Zirconium(IV). *Angew. Chem.* **1998,** *110*, (13/14), 2064-2067.

80. Zito, K.; Huttenhofer, A.; Peace, N. R., Lead-catalyzed cleavage of ribonuclease P RNA as a probe for integrity of tertiary structure. *Nucleic Acids Res.* **1993,** *21*, (25), 5916-5920.

81. Whitney, A.; Gavory, G.; Balasubramanian, S., Site-specific cleavage of human telomerase RNA using PNA-neocuproine·Zn(II) derivatives. *Chem. Comm.* **2003**, (1), 36-37.

82. Ihara, T.; Shimura, H.; Ohmori, K.; Tsuji, H.; Takeuchi, J.; Takagi, M., *Chem. Lett.* **1996,** *8*, 687-688.

83. Chin, J.; Banaszczyk, M.; Jubian, V.; Zou, X., Cobalt(III) complex-promoted hydrolysis of phosphate diesters: comparison in reactivity of rigid cis-diaquo(tetraaza)cobalt(III) complexes. *J. Am. Chem. Soc.* **1989,** *111*, (1), 186-190.

84. Dixon, N. E.; Geue, R. J.; Lambert, J. N.; Moghaddas, S.; Pearce, D. A.; Sargeson, A. M., DNA Hydrolysis by stable metal complexes. *Chem. Comm.* **1996**, (11), 1287-1288.

85. Chin, K. O. A.; Morrow, J. R., RNA Cleavage and Phosphate Diester Transesterification by Encapsulated Lanthanide Ions: Traversing the Lanthanide Series with Lanthanum(III), Europium(III), and Lutetium(III) Complexes of 1,4,7,10-Tetrakis(2-hydroxyalkyl)-1,4,7,10-tetraazacyclododecane. *Inorg. Chem.* **1994,** *33*, (22), 5036-5041.

86. Takasaki, B. K.; Chin, J., La(III)-Hydrogen Peroxide Cooperativity in Phosphate Diester Cleavage: A Mechanistic Study. *J. Am. Chem. Soc.* **1995,** *117*, (33), 8582-8585.

87. Henle, E. S.; Han, Z.; Tang, N.; Rai, P.; Luo, Y.; Linn, S., Sequence-specific DNA Cleavage by Fe^{2+}-mediated Fenton Reactions Has Possible Biological Implications. *J. Biol. Chem.* **1999,** *274*, 962-971.

88. Routier, S.; Vezin, H.; Lamour, E.; Bernier, E.; Catteau, J.-P.; Bailly, C., DNA cleavage by hydroxysalicylidene-ethylendiamine-iron complexes. *Nucl. Acids Res.* **1999,** *27*, (21), 4160-4166.

89. Sumaoka, J.; Azuma, Y.; Komiyama, M., Enzymatic manipulation of the fragments obtained by cerium (IV)-induced DNA scission: Characterization of hydrolytic termini. *Chem. Eur. J.* **1998,** *4*, (2), 205-209.

90. Branum, M. E.; Tipton, A. K.; Zhu, S.; Que, L., Double-Strand Hydrolysis of Plasmid DNA by Dicerium Complexes. *J. Am. Chem. Soc.* **2001,** *123*, 1898-1904.

91. Branum, M. E.; Que, L., Double-strand DNA hydrolysis by dilanthanide complexes. *J. Biol. Inorg. Chem.* **1999,** *4*, (5), 593-600.

92. Franklin, S. J., Lanthanide Mediated DNA Hydrolysis. *Curr. Opin. Chem. Biol.* **2001,** *5*, 201-208.

93. Copeland, K. D.; Fitzsimons, M. P.; Houser, R. P.; Barton, J. K., DNA Hydrolysis and Oxidative Cleavage by Metal-Binding Peptides Tetheres to Rhodium Intercalators. *Biochemistry* **2002,** *41*, 343-356.

94. Hegg, E. L. H.; Deal, K. A.; Laura, L.; Burstyn, J. N., Hydrolysis of Double-Stranded and Single-Stranded RNA in Hairpin Structures by the Copper(II) Makrocycle Cu([9]aneN_3)Cl_2. *Inorg. Chem.* **1997,** *36*, (8), 1715-1718.

95. Komiyama, M., Sequence-selective and hydrolytic scission of DNA and RNA by lanthanide complex-oligoDNA hybrids. *J. Biochem.* **1995,** *118*, 665-670.

96. Czlapinski, J. L.; Sheppard, T. L., Site-Specific Oxidative Cleavage of DNA by Metallosalen-DNA Conjugates. *Chem. Comm.* **2004**, (21), 2468-2469.

97. Sigman, D. S., Chemical Nucleases. *Biochemistry* **1990,** *29*, (39), 9097-9104.

98. Sigman, D. S.; Chen, C.-H. B., Chemical Nucleases: New Reagents in Molecular Biology. *Annu. Rev. Biochem.* **1990,** *59*, 207-236.

99. Sigman, D. S., Nuclease Activity of 1,10-Phenanthroline-Copper Ion. *Acc. Chem. Res.* **1986,** *19*, (6), 180-186.

100. Sigman, D. S., Oxygen-dependent Cleavage of DNA by the 1,10-Phenanthroline Cuprous Complex. *J. Biol. Chem.* **1979,** *254*, (24), 12269-12272.

101. Hertzberg, R. P.; Dervan, P. B., Cleavage of double helical DNA by methidium-propyl-EDTA-iron(II). *J. Am. Chem. Soc.* **1982,** *104*, (1), 313 - 315.

102. Tullius, T. D.; Dombroski, B. A., Hydroxyl Radical ``Footprinting": High-Resolution Information about DNA-Protein Contacts and Application to Repressor and Cro Protein. *Proc. Natl. Acad. Sci. U.S.A.* **1986,** *83*, (15), 5469-5473.

103. Doan, T. L.; Perrouault, L.; Helène, C.; Chassignol, M.; Nguyen, T. T., Targeted cleavage of polynucleotides by complementary oligonucleotides covalently linked to iron-porphyrins. *Biochemistry* **1986,** *25*, (22), 6736 - 6739.

104. Ward, B.; Skorobogaty, A.; Dabrowiak, J. C., DNA cleavage specificity of a group of cationic metalloporphyrins. *Biochemistry* **1986,** *25*, (22), 6875 - 6883.

105. Nielsen, P. E.; Jeppesen, C.; Buchardt, O., Uranyl salts as photochemical agents for cleavage of DNA and probing of protein-DNA contacts. *FEBS Lett.* **1988,** *235*, (1-2), 122-124.

106. Kirin, S. I.; Happel, C. M.; Hrubanova, S.; Weyhermüller, T.; Klein, C.; Metzler-Nolte, N., Synthesis, structure and comparison of the DNA cleavage ability of metal complexes M(II)L with the *N*-(2-ethoxyethanol)-bis(2-picolyl)amine ligand L (M = Co, Ni, Cu and Zn). *J. Chem. Soc., Dalton Trans.* **2004,** *8*, 1201-1207.

107. Neutrogena Corporation, **2001-2005**, http://www.neutrogena.com/ProductsDetails_107.asp.

108. U.S. Food and Drug Administration, **2004**, http://www.cfsan.fda.gov/~dms/supplmnt.html.

109. Deutsche Gesellschaft für Ernährung, **2003,** http://www.dge.de/Pages/navigation/fach_infos/referenzwerte/cumncrmo.html.

110. Jackman, M. P.; Hajnal, A.; Lerch, K., Albino Mutants of Streptomyces Glaucescens Tyrosinase. *Biochem. J.* **1991,** *274*, 707-713.

111. Spritz, R. A.; Ho, L.; Furumura, M.; Hearing, V. J., Mutational Analysis of Copper Binding by Human Tyrosinase. *J. Invest. Dermatol.* **1997,** *109*, 207-212.

112. Prohaska, J. R.; Gybina, A. A., Intracellular Copper Transport in Mammals. *J. Nutr.* **2004,** *134*, 1003-1006.

113. Lutsenko, S.; Petris, M. J., Function and Regulation of the Mammalian Copper-transporting AT-Pases: Insights from Biochemical and Cell Biological Approaches. *J. Membrane Biol.* **2002,** *191*, 1-12.

114. Kuo, Y.-M.; Zhou, B.; Cosco, D.; Gitschier, J., The copper Transporter CTR1 provides an essential Function in Mammalian Embryonic Development. *Proc. Natl. Acad. Sci. U.S.A.* **2001,** *98*, (12), 6836-6841.

115. Lee, J.; Prohaska, J. R.; Thiele, D. J., Essential Role for Mammalian Copper Transporter CTR1 in Copper Homeostasis and Embryonic Development. *Proc. Natl. Acad. Sci. U.S.A.* **2001,** *98*, (12), 6842-6847.

116. Klabunde, T.; Eicken, C.; Sacchettini, J. C.; Krebs, B., Crystal structure of a plant catechol oxidase containing a dicopper center. *Nat. Struct. Biol.* **1998,** *5*, 1084-1090.

117. Lerch, K., Amino acid sequence of tyrosinase from Neurospora crassa. *Proc. Natl. Acad. Sci. U.S.A.* **1978,** *75*, (8), 3635-3639.

118. Himmelwright, R. S.; Eickman, N. C.; LuBien, C. D.; Lerch, K.; Solomon, E. I., Chemical and Spectroscopic Studies of the Binuclear Copper Active Site of *Neurospora* Tyrosinase: Comparison to Hemocyanins. *J. Am. Chem. Soc.* **1980,** *102*, 7339-7344.

119. Lerch, K., Protein and Active-Site Structure of Tyrosinase. *Prog. Clin. Biol. Res.* **1988,** *256*, 85-98.

120. Tsai, T.-Y.; Lee, Y.-H., Roles of Copper LIgands in the Activation and Secretion of *Streptomyces* Tyrosinase. *J. Biol. Chem.* **1998,** *273*, (30), 19243-19250.

121. Solomon, E. I.; Chen, P.; Metz, M.; Lee, S. K.; Palmer, A. E., Oxygen Binding, Activation, and Reduction to ater by Copper Proteins. *Angew. Chem. Int. Ed.* **2001,** *40*, (24), 4570-4590.

122. Karlin, K. D.; Kaderli, S.; Zuberbühler, A. D., Kinetics and Thermodynamics of Copper(I)/Dioxygen Interaction. *Acc. Chem. Res.* **1997,** *30*, 139-147.

123. Zaitseva, I.; Zaitsev, V.; Card, G.; Moshkov, K.; Bax, B.; Ralph, A.; Lindley, P., The X-ray structure of human serum ceruloplasmin at 3.1 Å: nature of the copper centres. *J. Biol. Inorg. Chem.* **1996,** *1*, 15-23.

124. Kim, E.; Chufán, E. E.; Kamaraj, K.; Karlin, K. D., Synthetic Models for Heme-Copper Oxidases. *Chem. Rev.* **2004,** *104*, (2), 1077-1133.

125. Solomon, E. I.; Baldwin, M. J.; Lowery, M. D., Electronic Structures of Active Sites in Copper Proteins: Contributions to Reactivity. *Chem. Rev.* **1992,** *92*, 521-542.

126. Yang, Z.-S.; Wang, Y.-L.; Zhao, G.-C., The Interaction of Copper-Bipyridyl Complexes with DNA and Cleavage to DNA. *Anal. Sci.* **2004,** *20*, 1127-1130.

127. Lee, D.-H. W., N.; Murthy, N. N.; Tyeklar, Z.; Karlin, K. D.; Kaderli, S.; Jung, B.; Zuberbuehler, A. D., Reversible O_2 Binding to a Dinuclear Copper(I) Complex with Linked Tris(2-pyridylmethyl)amine Units: Kinetic-Thermodynamic Comparisons with Mononuclear Analogs. *J. Am. Chem. Soc.* **1995,** *117*, 12498 - 12513.

128. Humphreys, K. J.; Karlin, K. D.; Rokita, S. E., Recognition and Strand Scission at Junctions between Single- and Double-Stranded DNA by a Trinuclear Copper Complex. *J. Am. Chem. Soc.* **2001,** *123*, 5588-5589.

129. Chakravarty, A. R.; Reddy, P. A. N.; Santra, B. K.; Thomas, A. M., Copper Complexes as Chemical Nucleases. *Proc. Indian Acad. Sci. (Chem. Sci.)* **2002,** *114*, (4), 391-401.

130. Pitié, M.; Donnadieu, B.; Meunier, B., Preparation of the New Bis(phenanthroline) Ligand "Clip-Phen" and Evaluation of the Nuclease Activity of the Corresponding Copper Complex. *Inorg. Chem.* **1998,** *37*, 3486-3489.

131. Pitié, M.; Burrows, C. J.; Meunier, B., Mechanisms of DNA cleavage by copper complexes of 3-Clip-Phen and of its conjugate with a distamycin analogue. *Nucl. Acids Res.* **2000,** *28*, (24), 4856-4864.

132. Reddy, P. R.; Rao, K. S.; Mohan, S. K., Copper(II) Complexes Containing N,N-Donoer Ligands and Dipeptides Act as Hydrolytic DNA-Cleavage Agents. *Chemistry & Biodiversity* **2004,** *1*, 839-853.

133. Ren, R.; Yang, P.; Zheng, W.; Hua, Z., A Simple Copper(II)-Histidine System for Efficient Hydrolytic Cleavage of DNA. *Inorg. Chem.* **2000,** *39*, 5454-5463.

134. Häner, R., http://www.dcb.unibe.ch/groups/haener. **2004**.

135. Watson, J. D.; Crick, F. H. C., Molecular structure of Nucleic Acids. *Nature* **1953,** *171*, 737-738.

136. Gewirtz, A. M.; Sokol, D. L.; Ratajczak, M. Z., Nucleic Acid Therapeutics: State of the Art and Future Prospects. *Blood* **1998,** *92*, (3), 712-736.

137. Uhlmann, E.; Peyman, A., Antisense oligonucleotides: a new therapeutic principle. *Chem. Rev.* **1990,** *90*, (4), 543-584.

138. Hartmann, G.; Bidlingmaier, M.; Tschöp, K.; Eigler, A.; Hacker, U.; Endres, S., Antisense-Oligonukleotide. *Deutsches Ärzteblatt* **1998,** *95*, (24), A1524-A1530.

139. Thuong, N. T.; Hélène, C., Sequence-Specific Recognition and Modification of Double-Helical DNA by Oligonucleotides. *Angew. Chem. Int. Ed.* **1993,** *32*, (5), 666-690.

140. Marr, J. J., Ribozymes as therapeutic agents. *Drug Discovery Today* **1996,** *1*, 94-102.

141. Ellington, A. D.; Szostak, J. W., In vitro selection of RNA molecules that bind specific ligands. *Nature* **1990,** *346*, (6287), 818.

142. De Mesmaeker, A.; Häner, R.; Martin, P.; Moser, H. E., Antisense Nucleotides. *Acc. Chem. Res.* **1995,** *28*, 366-374.

143. Nielsen, P. E.; Egholm, M.; Berg, R. H.; Burchardt, O., Recognition of DNA by strand displacement with a thymine-substituted polyamide. *Science* **1991,** *254*, 1497-1500.

144. Hyrup, B. T. I.; Nielsen, P. E., Peptide nucleic acids (PNA): Synthesis, properties and potential applications. *Bioorg. Med. Chem.* **1996,** *4*, (1), 5-23.

145. Nielsen, P. E.; Egholm, M.; Buchardt, O., Peptide nucleic acid (PNA). A DNA mimic with a peptide backbone. *Bioconj. Chem.* **1994,** *5*, (1), 3-7.

146. Nielsen, P. E.; Haaima, G., Peptide Nucleic Acid (PNA). A DNA mimic with a pseudopeptide backbone. *Chem. Soc. Rev.* **1997,** *26*, (2), 73-78.

147. Demidov, V.; Potaman, V. N.; Frank-Kamenetskii, M. D.; Egholm, M.; Buchardt, O.; Sonnichsen, S. H.; Nielsen, P. E., Peptide nucleic acid delivery to human mitochondria. *Biochem. Pharmacol.* **1994,** *48*, 1310-1313.

148. Uhlmann, E.; Peyman, A.; Breipohl, G.; Will, D. W., PNAs: synthetische Polyamidnucleinsäuren mit außergewöhnlichen Bindungseigenschaften. *Angew. Chem.* **1998,** *110*, 2954-2983.

149. Nielsen, P. E.; Egholm, M., *Peptide Nucleic Acids - Protocols and Applications*. Horizon Scientific Press: 1999.

150. Eriksson, M.; Nielsen, P. E., Solution structure of a peptide nucleic acid-DNA duplex. *Nat. Struct. Biol.* **1996,** *3*, (5), 410-413.

151. Ray, A.; Nordén, B., Peptide Nucleic Acid (PNA): Its Medical and Biotechnical Applications and Promise for the Future. *FASEB J.* **2000,** *14*, 1041-1060.

152. Betts, L.; Josey, J. A.; Veal, J. M.; Jordan, S. R., A Nucleic Acid Triple Helix Formed by a Peptide Nucleic Acid-DNA Complex. *Science* **1995,** *270*, (5243), 1838-1841.

153. Demidov, V.; Frank-Kamenetskii, M. D.; Egholm, M.; Buchardt, O.; Nielsen, P. E., Sequence selective double strand DNA cleavage by peptide nucleic acid (PNA) targeting using nuclease S1. *Nucleic Acids Res.* **1993,** *21*, (9), 2103-2107.

154. Sabat, M.; Lippert, B., Metal ions in multiple-stranded DNA. *Met. Ions Biol. Syst.* **1996,** *33*, 143-176.

155. Armitage, B.; Koch, T.; Frydenlund, H.; Orum, H.; Schuster, G. B., Peptide nucleic acid (PNA)/DNA hybrid duplexes: intercalation by an internally linked anthraquinone. *Nucleic Acids Res.* **1998,** *26*, (3), 715-720.

156. Egholm, M.; Buchardt, O.; Christensen, L.; Behrens, C.; Freier, S. M.; Driver, D. A.; Berg, R. H.; Kim, S. K.; Nordén, B.; Nielsen, P. E., PNA hybridizes to complementary Oligonucleotides obeying the Watson-Crick hydrogen bonding rules. *Nature* **1993,** *365*, 556-558.

157. Tomac, S.; Sarkar, M.; Ratilainen, T.; Wittung, P.; Nielsen, P. E.; Nordén, B.; Gräslund, A., Ionic Effects on the stability and Conformation of Peptide Nucleic Acid (PNA) Complexes. *J. Am. Chem. Soc.* **1996,** *118*, 5544-5552.

158. Egholm, M.; Buchardt, O.; Nielsen, P. E.; Berg, R. H., Peptide nucleic acids (PNA). Oligonucleotide analogs with an achiral peptide backbone. *J. Am. Chem. Soc.* **1992,** *114*, 1895-1897.

159. Chinnery, P. F.; Taylor, R. W.; Diekert, K.; Lill, R.; Turnbull, D. M.; Lightowlers, R. N., Peptide Nucleic Acid Delivery to Human Mitochondria. *Gene Therapy* **1999,** *6*, 1919-1928.

160. Zhang, X.; Simmons, C. G.; Corey, D. R., Liver Cell Specific Targeting of Peptide Nucleic Acid Oligomers. *Bioorg. Med. Chem. Lett.* **2001,** *11*, 1269-1272.

161. Tyler, B. M.; McCormick, D. J.; Hoshall, C. V.; Douglas, C. L.; Jansen, K.; Lacy, B. W.; Cusack, B.; Richelson, E., Specific Gene Blockade shows that Peptide Nucleic Acids readily enter Neuronal Cells in vivo. *FEBS Lett.* **1998,** *421*, 280-284.

162. Tyler, B. M.; Jansen, K.; McCormick, D. J.; Douglas, C. L.; Boules, M.; Stewart, J. A.; Zhao, L.; Lacy, B.; Cusack, B.; Fauq, A.; Richelson, E., Peptide Nucleic Acids targeted to the Neurotensin Receptor and administered i.p. cross the Bloood-Brain Barrier and specifically reduce Gene Expression. *Proc. Natl. Acad. Sci. U.S.A.* **1999,** *96*, 7053-7058.

163. Møllegaard, N. E.; Buchardt, O.; Egholm, M.; Nielsen, P. E., Peptide Nucleic Acid·DNA Strand Displacement Loops as Artificial Transcription Promoters. *Proc. Natl. Acad. Sci. U.S.A.* **1994,** *91*, 3892-3895.

164. Mier, W.; Eritja, R.; Mohammed, A.; Haberkorn, U., Peptid-PNA-Konjugate: Gezielter Transport von Antisense-Therapeutika in Tumoren. *Angew. Chem.* **2003,** *115*, 2012-2015.

165. Haney, J. C.; Peffer, N. J.; Bisi, J. E.; Thomson, S. A.; Cadilla, R.; Josey, J. A.; Ricca, D. J.; Hassman, C. F.; Bonham, M. A.; Au, K. G.; Carter, S. G.; Bruckenstein, D. A.; Boyd, A. L.; Noble, S. A.; Babiss, L. E., *Science* **1992,** *258*, 1481-1485.

166. Soomets, U.; Hällbrink, M.; Langel, Ü., Antisense Properties of Peptide Nucleic Acids. *Frontiers in Bioscience* **1999,** *4*, 782-786.

167. Knudsen, H.; Nielsen, P. E., Antisense properties of duplex- and triplex-forming PNAs. *Nucleic Acids Res.* **1996,** *24*, 494-500.

168. Nielsen, P. E.; Egholm, M.; Berg, R. H.; Buchardt, O., Sequence specific inhibition of DNA restriction enzyme cleavage by PNA. *Nucleic Acids Res.* **1993,** *21*, (2), 197-200.

169. Carlsson, C.; Jonsson, M.; Nordén, B.; Dulay, M. T.; Zare, R. N.; Noolandi, J.; Nielsen, P. E.; Tsui, L.-Z.; Zielinski, J., Screening for Genetic Mutations. *Nature* **1996,** *380*, (6571), 207.

170. Orum, H.; Nielsen, P. E.; Egholm, M.; Berg, R. H.; Buchardt, O.; Stanley, C., Single base pair mutation analysis by PNA directed PCR clamping. *Nucleic Acids Res.* **1993,** *21*, (23), 5332-5336.

171. Nelson, K. E.; Levy, M.; Miller, S. L., Peptide nucleic acids rather than RNA may have been the first genetic molecule. *Proc. Natl. Acad. Sci. U.S.A.* **2000,** *97*, (8), 3868-3871.

172. Miller, S. L., A Production of Amino Acids Under Possible Primitive Earth Conditions. *Science* **1953,** *117*, 528-529.

173. Oró, J., Synthesis of Adenine from Ammonium Cyanide. *Biochem. Biophys. Res. Commun.* **1960,** *2*, 407-412.

174. Hess, A.; Metzler-Nolte, N., Transition Metal Labels on Peptide Nucleic Acid (PNA) monomers. *Chem. Comm.* **1999**, (8), 885-886.

175. Verheijen, J. C.; Van der Marel, G. A.; Van Boom, J. H.; Metzler-Nolte, N., Transition Metal Derivatives of Peptide Nucleic Acid (PNA) Oligomers - Synthesis, Characterization, and DNA binding. *Bioconj. Chem.* **2000,** *11*, (6), 741-743.

176. Hamzavi, R.; Happ, T.; Weitershaus, K.; Metzler-Nolte, N., The use of 3,3-bis(2-imidazolyl) propionic acid (bip-OH) as a new chelating ligand for $Re(CO)_3$ and Ru complexes: Formation of or-

ganometallic PNA oligomers with (bip)$Re(CO)_3$ and their interaction with complementary DNA. *J. Organomet. Chem.* **2004,** *689*, (25), 4745-4750.

177. Verheijen, J. C.; Deiman, B. A. L. M.; Yeheskiely, E.; Van der Marel, G. A.; Van Boom, J. H., Efficient Hydrolysis of RNA by a PNA - Diethylenetriamine Adduct. *Angew. Chem. Int. Ed.* **2000,** *39*, (2), 369-372.
178. Bigey, P.; Sönnichsen, S. H.; Meunier, B.; Nielsen, P. E., DNA Binding and Cleavage by a Cationic Manganese Porphyrin-Peptide Nucleic Acid Conjugate. *Bioconj. Chem.* **1997,** *8*, (3), 267-270.
179. Zelder, F. H.; Mokhir, A.; Krämer, R., Sequence Selective Hydrolysis of Linear DNA Using Conjugates of Zr(IV) Complexes and Peptide Nucleic Acids. *Inorg. Chem.* **2003,** *42*, 8618-8620.
180. Merrifield, R. B., Solid Phase Peptide Synthesis. I. The Synthesis of a Tetrapeptide. *J. Am. Chem. Soc.* **1963,** *85*, 2149-2154.
181. Moses, Genesis. *The Holy Bible, Int. Ed.* **30,** *1*, (20).
182. Foxon, S. P.; Walter, O.; Schindler, S., Synthesis and Characterization of Copper(II) Complexes of the New Ligands *N*-[(2-Pyridyl)methyl]-2,2'-dipyridylamine and *N*-[Bis(2-pyridyl)methyl]-2-pyridylamine. *Eur. J. Inorg. Chem.* **2002**, (1), 111-121.
183. Sammes, P. G.; Yahioglu, G., 1,10-Phenanthroline: a versatile ligand. *Chem. Soc. Rev.* **1994,** *23*, (5), 327 - 334.
184. D'Aurora, V.; Stern, A. M.; Sigman, D. S., Inhibition of E. coli DNA polymerase I by 1,10-phenanthroline. *Biochem. Biophys. Res. Commun.* **1977,** *78*, (1), 170-176.
185. D'Aurora, V.; Stern, A. M.; Sigman, D. S., 1,10-Phenanthroline-cuprous ion complex, a potent inhibitor of DNA and RNA polymerases. *Biochem. Biophys. Res. Commun.* **1978,** *80*, (4), 1025-1032.
186. Sigman, D. S.; Bruice, T. W.; Mazumder, A.; Sutton, C. L., Targeted Chemical Nucleases. *Acc. Chem. Res.* **1993,** *26*, (3), 98.
187. Chen, C.-H. B.; Sigman, D. S., Nuclease Activity of 1,10-Phenanthroline-Copper: Sequence-Specific Targeting. *Proc. Natl. Acad. Sci. U.S.A.* **1986,** *83*, 7147-7151.
188. Chen, C.-H. B.; Sigman, D. S., Chemical Conversion of a DNA-Binding Protein into a Site-Specific Nuclease. *Science* **1987,** *237*, 1197-1201.
189. Stern, A. M.; Bashkin, J. K.; Sall, E. D., Hydrolysis of RNA by Transition-Metal Complexes. *J. Am. Chem. Soc.* **1990,** *112*, 5357-5359.
190. Bashkin, J. K.; Xie, J.; Daniher, A. T.; Sampath, U. S.; Kao, J. L.-F., Building Blocks for Ribozyme Mimics: Conjugates of Terpyridine and Bipyridine with Nucleosides. *J. Org. Chem.* **1996,** *61*, 2314-2321.
191. Bashkin, J. K.; Frolova, E. I.; Sampath, U. S., Sequence-Specific Cleavage of HIV mRNA by a Ribozyme Mimic. *J. Am. Chem. Soc.* **1994,** *116*, 5981-5982.
192. Inoue, H.; Furukawa, T.; Shimizu, M.; Tamura, T.; Matsui, M.; Ohtsuka, E., Efficient Site-Specific Cleavage of RNA using a Terpyridine-Copper(II) Complex joined to a 2'-*O*-Methyloligonucleotide by a Non-Flexible Linker. *Chem. Comm.* **1998**, (1), 45-46.

193. Inoue, H.; Furukawa, T.; Tamura, T.; Kamada, A.; Ohtsuka, E., Rapid RNA Cleavage Using an Antisense System with two Terpyridine-Cu(II) Complexes. *Nucl. Nucleot. Nucl. Acids* **2001,** *20*, (4-7), 833-835.

194. Sakamoto, S.; Tamura, T.; Furukawa, T.; Komatsu, Y.; Ohtsuka, E.; Kitamura, M.; Inoue, H., Highly efficient catalytic RNA cleavage by the cooperative action of two Cu(II) complexes embodied within an antisense oligonucleotide. *Nucl. Acids Res.* **2003,** *31*, (5), 1416-1425.

195. van Staveren, D. R.; Bothe, E.; Weyhermüller, T.; Metzler-Nolte, N., Spectroscopic Properties, Electrochemistry, and Reactivity of Mo^0, Mo^I, and Mo^{II} Complexes with the $[Mo(bpa)(CO)_3]$ Unit [bpa = bis(2-picolyl)amine] and Their Application for the Labelling of Peptides. *Eur. J. Inorg. Chem.* **2002**, 1518-1529.

196. Carraway, R. E.; Mitra, S. P.; Spaulding, G., The Neurobiology of Neurotensin. Proceedings of 2nd International Conference on Neurotensin. *Ann. N.Y. Acad. Sci.* **1991,** *668*.

197. Gordon, C. J.; McMahon, B.; Richelson, E.; Padnos, B.; Katz, L., Neurotensin analog NT77 induces regulated hypothermia in the rat. *Life Sci.* **2003,** *73*, (20), 2611-2623.

198. Vincent, J. P.; Mazella, J.; Kitabgi, P., Neurotensin and neurotensin receptors. *Trends Pharmacol. Sci* **1999,** *20*, (7), 302-309.

199. Benzing, W. C.; Mufson, E. J.; Jennes, L.; Armstrong, D. M., Reduction of neurotensin immunoreactivity in the amygdala in Alzheimer's disease. *Brain Res.* **1990,** *537*, (1-2), 298-302.

200. Boules, M.; Warrington, L.; Fauq, A.; McCormick, D.; Richelson, E., Antiparkinson-like effects of a novel neurotensin analog in unilaterally 6-hydroxydopamine lesioned rats. *Eur. J. Pharmacol.* **2001,** *428*, (2), 227-233.

201. Binder, E. B.; Kinkead, B.; Owens, M. J.; Nemeroff, C. B., The role of neurotensin in the pathophysiology of schizophrenia and the mechanism of action of antipsychotic drugs. *Biol. Psychiatry* **2001,** *50*, (11), 856-872.

202. García Garayoa, E.; Bläuenstein, P.; Brühlmeier, M.; Blanc, A.; Iterbecke, K.; Conrath, P.; Schubiger, P. A., Preclinical evaluation of a new, stabilized neurotensin(8-13) pseudopeptide radiolabelled with 99mTc. *J. Nucl. Med.* **2002,** *43*, (3), 374-383.

203. Bläuenstein, P.; García Garayoa, E.; Rüegg, D.; Blanc, A.; Tourwé, D.; Beck-Sickinger, A.; Schubiger, P. A., Improving the tumour uptake of 99mTc-labelled neuropeptides using stabilised peptide analogues. *Cancer Biother. Radiopharm.* **2004,** *19*, (2), 181-188.

204. Hong, F.; Zaidi, J.; Cusack, B.; Richelson, E., Synthesis and biological studies of novel neurotensin(8-13) mimetics. *Bioorg. Med. Chem.* **2002,** *10*, (12), 3849-3858.

205. Pang, Y. P.; Cusack, B.; Groshan, K.; Richelson, E., Proposed ligand binding site of the transmembrane receptor for neurotensin(8-13). *J. Biol. Chem.* **1996,** *271*, (25), 15060-15068.

206. Ito, N.; Phillips, S. E. V.; Stevens, C.; Ogel, Z. B.; McPherson, M. J.; Keen, J. N.; Yadav, K. D. S.; Knowles, P. F., Novel thioether bond revealed by a 1.7 Å crystal structure of galactose oxidase. *Nature* **1991,** *350*, (6313), 87-90.

207. Ito, N.; Phillips, S. E.; Yadav, K. D.; Knowles, P. F., Crystal structure of a free radical enzyme, galactose oxidase. *J. Mol. Biol.* **1994,** *238*, (5), 794-814.

208. Gacheru, S. N.; Trackman, P. C.; Shah, M. A.; O'Gara, C. Y.; Spacciapoli, P.; Greenaway, F. T.; Kagan, H. M., Structural and catalytic properties of copper in lysyl oxidase. *J. Biol. Chem.* **1990,** *265*, (31), 19022-19027.

209. Wang, S. X.; Mure, M.; Medzihradszky, K. F.; Burlingame, A. L.; Brown, D. E.; Dooley, D. M.; Smith, A. J.; Kagan, H. M.; Klinman, J. P., A Crosslinked Cofactor in Lysyl Oxidase: Redox Function for Amino Acid Side Chains. *Science* **1996,** *273*, (5278), 1078-1084.

210. Trackman, P. C.; Pratt, A. M.; Wolanski, A.; Tang, S. S.; Offner, G. D.; Troxler, R. F.; Kagan, H. M., Cloning of rat aorta lysyl oxidase cDNA: complete codons and predicted amino acid sequence. *Biochemistry* **1990,** *29*, 4863 - 4870.

211. Phillips, S. E., http://www.astbury.leeds.ac.uk/Report/2000/Phillips.6.html. **2000**.

212. Drew, M. G. B.; J., H.; Iveson, P. B.; Russell, M. L.; Liljenzin, J.-O.; Skålberg, M.; Spjuth, L.; Madic, C., Theoretical and experimental studies of the protonated terpyridine cation. *Ab initio* quantum mechanics calculations, and crystal structures of two different ion pairs formed between protonated terpyridine cations and nitratolanthanate(III) anions. *J. Chem. Soc., Dalton Trans.* **1998**, 2973-2980.

213. Fallahpour, R.-A., 2,2':6',2"-Terpyridines and their Metal Complexes, Ph. D. Thesis. **2003**.

214. Morgan, G. T.; Burstall, F. H., Dehydrogenation of pyridine by anhydrous ferric chloride. *J. Chem. Soc.* **1932,** *20-30*.

215. Burstall, F. H., Researches on the polypyridyls. *J. Chem. Soc.* **1938**, 1662-1672.

216. Sanna, G.; Pilo, M. I.; Minghetti, G.; Cinellu, M. A.; Spano, N.; Seeber, R., Electrochemical properties of gold(III) complexes with 2,2′-bipyridine and oxygen ligands. *Inorg. Chim. Acta* **2000,** *310*, (1), 34-40.

217. Huynh, M. H. V.; White, P. S.; Meyer, T. J., Mechanistic Control of Product Selectivity. Reactions between cis-/trans-$[Os^{VI}(tpy)(Cl)_2(N)]^+$ and Triphenylphosphine Sulfide. *Inorg. Chem.* **2000,** *39*, (13), 2825-2830.

218. Huynh, M. H. V.; El-Samanody, E.-S.; Demadis, K. D.; White, P. S.; Meyer, T. J., Mechanism and Molecular-Electronic Structure Correlations in a Novel Series of Osmium(V) Hydrazido Complexes. *Inorg. Chem.* **2000,** *39*, (14), 3075-3085.

219. Priimov, G. U.; Moore, P.; Maritim, P. K.; Butalanyi, P. K.; Alcock, N. W., Synthesis of two covalently linked bis(2,2':6',2"-terpyridine) (terpy) chelating ligands with different length spacers, comparison of the crystal structures of their mononuclear nickel(II) complexes, and kinetic and mechanistic studies of the reaction of one ligand with $[Fe(terpy)_2]_2$. *J. Chem. Soc., Dalton Trans.* **2000**, 445-450.

220. Priimov, G. U.; Moore, P.; Helm, L.; Merbach, A. E., Kinetic and Mechanistic Studies of Substitution Reactions of Solvated Cobalt(II), Nickel(II), Copper(II) and Zinc(II) Ions with 2,2':6',2"-Terpyridine and Several 2,2':6',2"-Terpyridine Derivatives. Evidence for the Formation of Intermediates. *Inorg. React. Mech.* **2001,** *3*, 1-12.

221. Dobrawa, R.; Würthner, F., Photoluminescent Supreamolecular Polymers: Metal-Ion Directed Polymerization of Terpyridine-Functionalized Perylene Bisimide Dyes. *Chem. Comm.* **2002**, (17), 1878-1879.

222. Reinen, D.; Friebel, C., Cu^{2+} in 5-Coordination: A Case of a Second-Order Jahn-Teller Effect. 2. $CuCl_5^{3-}$ and Other $Cu^{II}L_5$ Complexes: Trigonal Bipyramid or Square Pyramid? *Inorg. Chem.* **1984,** *23*, (7), 791-798.

223. Arriortua, M. I.; Mesa, J. L.; Rojo, T.; Debaerdemaeker, T.; Beltrán-Porter, D.; Stratemeier, H.; Reinen, D., $Cu(terpy)X_2$ ($X = Br^-, NCS^-$): Complexes with an Unusual Five-Coordination. Structural and Spectroscopic Investigation. *Inorg. Chem.* **1987,** *27*, (17), 2976-2981.

224. Palaniandavar, M.; Mahadevan, S.; Köckerling, M.; Henkel, G., The Structural Pathways of (dipicolylamine)dinitratocopper(II): An Example of the Uncommon see-saw sterochemistry. *J. Chem. Soc., Dalton Trans.* **2000**, (7), 1151-1154.

225. Ugozzoli, F.; Massera, C.; Lanfredi, A. M. M.; Marsich, N.; Camus, A., $[Cu(phdpa)Cl]^+$ (phdpa=bis(2-pyridylmethyl)aniline): a moiety of unusual stability in some 1:1 Cu(II) complexes of phdpa. Synthesis and X-ray crystal structures of $[Cu(phdpa)Cl_2]$ and $[Cu_2(phdpa)_2Cl_3]PF_6 \cdot 0.5MeOH$. *Inorg. Chim. Acta* **2002,** *340*, 97-104.

226. Egholm, M.; Buchardt, O.; Nielsen, P. E.; Berg, R. H., Peptide nucleic acids (PNA). Oligonucleotide analogs with an achiral peptide backbone. *Journal of the American Chemical Society* **1992,** *114*, (5), 1895-7.

227. Egholm, M.; Nielsen, P. E.; Buchardt, O.; Berg, R. H., Recognition of guanine and adenine in DNA by cytosine and thymine containing peptide nucleic acids (PNA). *Journal of the American Chemical Society* **1992,** *114*, (24), 9677-8.

228. Breipohl, G.; Will, D. W.; Peyman, A.; Uhlmann, E., Novel synthetic routes to PNA monomers and PNA-DNA linker molecules. *Tetrahedron* **1997,** *53*, (43), 14671-14686.

229. Uhlmann, E.; Will, D. W.; Breipohl, G.; Peyman, A.; Langner, D.; Knolle, J.; O'Malley, G., Synthesis of polyamide nucleic acids (PNAs), PNA/DNA-chimeras and phosphonic ester nucleic acids (PHONAs). *Nucleosides & Nucleotides* **1997,** *16*, (5 & 6), 603-608.

230. Capasso, D.; De Napoli, L.; Di Fabio, G.; Messere, A.; Montesarchio, D.; Pedone, C.; Piccialli, G.; Saviano, M., Solid phase synthesis of DNA-3'-PNA chimeras by using Bhoc/Fmoc PNA monomers. *Tetrahedron* **2001,** *57*, (46), 9481-9486.

231. Goodnow, R. A., Jr.; Richou, A.-R.; Tam, S., Synthesis of thymine, cytosine, adenine, and guanine containing N-Fmoc protected amino acids: building blocks for construction of novel oligonucleotide backbone analogs. *Tetrahedron Letters* **1997,** *38*, (18), 3195-3198.

232. Bergmann, F.; Bannwarth, W.; Tam, S., Solid phase synthesis of directly linked PNA-DNA-hybrids. *Tetrahedron Letters* **1995,** *36*, (38), 6823-6.

233. Timar, Z.; Kovacs, L.; Kovacs, G.; Schmel, Z., Fmoc/Acyl protecting groups in the synthesis of polyamide (peptide) nucleic acid monomers. *Perkin 1* **2000**, (1), 19-26.

234. Zou, R.; Robins, M. J., Nucleic acid related compounds. 52. High-yield regioselective synthesis of 9-glycosylguanine nucleosides and analogs via coupling with 2-N-acetyl-6-O-diphenylcarbamoylguanine. *Canadian Journal of Chemistry* **1987,** *65*, (6), 1436-7.

235. Maurer, A.; Metzler-Nolte, N., *Unpublished Results*.

236. Rapp Polymers, I., http://www.rapp-polymere.com/. **2004**.

237. Wei, Y.; Marino, M.; Thompson, B.; Girard, J. E., High-Performance Liquid Chromatography Separation Methods fo the Analysis of Peptide Nucleic Acids. *J. Chromatogr. A* **1999,** *864*, 49-57.

238. Butler, J. M.; Jiang-Baucom, P.; Huang, M.; Belgrader, P.; Girard, J. E., Peptide Nucleic Acid Characterization by MALDI-TOF Mass Spectrometry. *Anal. Chem.* **1996,** *68*, 3283-3287.

239. Colleaux, L., Recognition and cleavage site of the intron-encoded omega transposase. *Proc. Natl. Acad. Sci. U.S.A.* **1988,** *85*, 6022-6026.

240. Monteheit, C., Purification and characterization of the in vitro activity of I-Sce I, a novel and highly specific endonuclease encoded by a group I intron. *Nucl. Acids Res.* **1990,** *18*, 1407-1413.

241. Jasin, M., Genetic manipulation of genomes with rare-cutting endonucleases. *Trends in Genetics* **1996,** *12*, 224-228.

242. Guhan, N.; Muniyappa, K., Structural and Functional Characteristics of Homing Endonucleases. *Crit. Rev. Biochem. Mol. Biol.* **2003,** *38*, (3), 199-248.

243. Gruen, M.; Chang, K.; Serbanescu, I.; Liu, D. R., An in vivo selection system for Homing Endonuclease Activity. *Nucleic Acids Res.* **2002,** *30*, (7), e29.

244. Belfort, M.; Roberts, R. J., Homing endonucleases: keeping the house in order. *Nucleic Acids Res.* **1997,** *25*, 3379-3388.

245. Chevalier, B. S.; Stoddard, B. L., Homing endonucleases: Structural and functional insight into the catalysis of intron/intein mobility. *Nucleic Acids Res.* **2001,** *29*, 3757-3774.

246. Liu, Q.; Segal, D. J.; Ghiara, J. B.; Barbas, C. F., Design of polydactyl zinc-finger proteins for unique addressing within complex genomes. *Proc. Natl. Acad. Sci. U.S.A.* **1997,** *94*, (11), 5525-5530.

247. Gildea, B. D.; Casey, S.; MacNeill, S.; Perry-O'Keefe, H.; Sørensen, D.; Coull, J. M., PNA Solubility Enhancers. *Tetrahedron Letters* **1998,** *39*, 7255-7258.

248. Hess, A.; Sigel, R. K. O.; Metzler-Nolte, N., Base Pairing Properties of Novel Transition Metal PNA Conjugates. *J. Inorg. Biochem.* **1999,** *74*, 161.

249. Herschlag, D.; Cech, T. R., Catalysis of RNA cleavage by the Tetrahymena thermophila ribozyme. 2. Kinetic description of the reaction of an RNA substrate that forms a mismatch at the active site. *Biochemistry* **1990,** *29*, (44), 10172 - 10180.

250. Kolasa, K. A.; Morrow, J. R.; Sharma, A. P., Trivalent lanthanide ions do not cleave RNA in DNA-RNA hybrids. *Inorg. Chem.* **1993,** *32*, (19), 3983 - 3984.

251. Hall, J.; Hüsken, D.; Häner, R., Towards Artificial Ribonucleases: The Sequence-Specific Cleavage of RNA in a Duplex. *Nucl. Acids Res.* **1996,** *24*, (18), 3522-3526.

252. Hüsken, D.; Goodall, G.; Blommers, M. J. J.; Jahnke, W.; Hall, J.; Häner, R.; Moser, H. E., Creating RNA Bulges: Cleavage of RNA/DNA Duplexes by Metal Ion Catalysis. *Biochemistry* **1996,** *35*, 16591-16600.

253. Popescu, D.-L.; Parolin, T.; Achim, C., Metal Ion Incorporation in PNA Duplexes. *J. Am. Chem. Soc.* **2003,** *125*, (21), 6354-6355.

254. Maiorana, S.; Licandro, E.; Perdicchia, D.; Baldoli, C.; Vandoni, B.; Giannini, C.; Salmain, M., Synthesis of the first chiral PNA monomer labelled with a Fischer-type carbene complex. *J. Mol. Catal. A* **2003,** *204-205*, 165-175.

255. Baldoli, C.; Maiorana, S.; Licandro, E.; Zinzalla, G.; Perdicchia, D., Synthesis of Chiral Chromium Tricarbonyl Labeled Thymine PNA Monomers via the Ugi Reaction. *Org. Lett.* **2002,** *4*, (24), 4341-4344.

256. Hamzavi, R.; Dolle, F.; Tavitian, B.; Dahl, O.; Nielsen, P. E., Modulation of the Pharmacokinetic Properties of PNA: Preparation of Galactosyl, Mannosyl, Fucosyl, *N*-Acetylgalactosaminyl, and *N*-Acetylglucosaminyl Derivatives of Aminoethylglycine Peptide Nucleic Acid Monomers and Their Incorporation into PNA Oligomers. *Bioconj. Chem.* **2003,** *14*, (5), 941-954.

257. Hudson, R. H. E.; Viire, R. D.; McCourt, N.; Tse, J., Nucleobase Modified Peptide Nucleic Acid. *Nucleosides, Nucleotides & Nucleic Acids* **2003,** *5-8*, 1029-1033.

258. Hudson, R. H. E.; Viire, R. D.; Liu, Y. H.; Wojciechowski, F.; Dambenieks, A. K., Chemistry for the Synthesis of Nucleobase-Modified Peptide Nucleic Acid. *Pure Appl. Chem.* **2004,** *78*, (7-8), 1591-1598.

259. Hudson, R. H. E.; Li, G.; Tse, J., The Use of Sonogashira Coupling for the Synthesis of Modified Uracil Peptide Nucleic Acid. *Tetrahedron Letters* **2002,** *43*, 1381-1386.

260. Pooga, M.; Soomets, U.; Hällbrink, M.; Valkna, A.; Saar, K.; Rezaei, K., Cell Penetrating PNA Constructs Regulate Galanin Receptor Levels and Modify Pain Transmission *in vivo*. *Nat. Biotechnol.* **1998,** *16*, 857-861.

261. Aldrian-Herrada, G.; Desarménien, M. G.; Orcel, H.; Boissin-Agasse, L.; Méry, J.; Brugidou, J.; Rabié, A., A Peptide Nucleic Acid (PNA) is more rapidly internalized in Cultured Neurons when coupled to a *Retro-Inverso* Delivery Peptide. The Antisense Activity depresses the Target mRNA and Protein in Magnocellular Oxytocin Neurons. *Nucleic Acids Res.* **1998,** *26*, 4910-4916.

262. Cutrona, G.; Carpaneto, E. M.; Ulivi, M.; Roncella, S.; Landt, O.; Ferrarini, M., Effects in Live Cells of a c-myc anti-gene PNA linked to a Nuclear Localization Signal. *Nat. Biotechnol.* **2000,** *18*, 300-303.

263. Good, L.; Awasthi, S. K.; Dryselius, R.; Larsson, O.; Nielsen, P. E., Bactericidal Antisense Effects of Peptide-PNA Conjugates. *Nature Biotechnol.* **2001,** *19*, 360-364.

264. Mier, W.; Eritja, R.; Mohammed, A.; Haberkorn, U.; Eisenhut, M., Peptide-PNA Conjugates: Targeted Transport of Antisense Therapeutics into Tumors. *Angew. Chem. Int. Ed.* **2003,** *42*, (17), 1968-1971.

265. Goodwin, T. E.; Holland, R. D.; Lay, J. O.; Raney, K. D., A Simple Procedure for Solid-Phase Synthesis of Peptide Nucleic Acids with *N*-Terminal Cysteine. *Bioorg. Med. Chem. Lett.* **1998,** *8*, 2231-2234.

266. Mier, W.; Eritja, R.; Mohammed, A.; Haberkorn, U.; Eisenhut, M., Preparation and Evaluation of Tumor-Targeting Peptide-Oligonucleotide Conjugates. *Bioconj. Chem.* **2000,** *11*, 855-860.

267. Millo, E.; Nicolai, R.; Scarfi, S.; Scapolla, C.; Biasotti, B.; Benatti, U.; Damonte, G., Optimised Solid Phase Synthesis of a Cystine-Linkes Peptide-PNA Chimera. *Tetrahedron Letters* **2002,** *43*, 3057-3059.

268. deKoning, M. C.; Filippov, D. V.; Meeuwenoord, N.; Overhand, M.; van der Marel, G. A.; van Boom, J. H., Synthesis of a PNA-Peptide Conjugate by Chemical Ligation. *Synlett* **2001,** *10*, 1516-1518.

269. Garner, P.; Yoo, J. U., Peptide-Based Nucleic Acid Surrogates Incorporating Ser[CH_2B]-Gly Subunits. *Tetrahedron Letters* **1993,** *34*, (8), 1275-1278.

270. Lewis, I., Peptide Analogues of DNA Incorporating Nucleobase-Ala-Pro Subunits. *Tetrahedron Letters* **1993,** *34*, (36), 5697-5700.

271. Ganesh, K.; Nielsen, P. E., Peptide Nucleic Acids: Analogs and Derivatives. *Curr. Org. Chem.* **2000,** *4*, 931-943.

272. Almarsson, Ö.; Bruice, T. C.; Kerr, J.; Zuckermann, R. N., Molecular Mechanics Calculations of the Structures of Polyamide Nucleic Acid Duplexes and Triple Helical Hybrids. *Proc. Natl. Acad. Sci. U.S.A.* **1993,** *90*, 7518-7522.

273. Lowe, G.; Vilaivan, T., Amino Acids Bearing Nucleobases for the Synthesis of Novel Peptide Nucleic Acids. *J. Chem. Soc., Perkin Trans. 1* **1997**, 539-546.

274. Lowe, G.; Vilaivan, T., Dipeptides Bearing Nucleobases for the Synthesis of Novel Peptide Nucleic Acids. *J. Chem. Soc., Perkin Trans. 1* **1997**, 547-554.

275. Lowe, G.; Vilaivan, T., Solid-Phase Synthesis of Novel Peptide Nucleic Acids. *J. Chem. Soc., Perkin Trans. 1* **1997**, 555-560.

276. Lenzi, A.; Reginato, G.; Taddei, M.; Trifilieff, E., Solid Phase Synthesis of a Self Complementary (Antiparallel) Chiral Peptide Nucleic Acid Strand. *Tetrahedron Letters* **1995,** *36*, (10), 1717-1718.

277. Mattes, A.; Seitz, O., Sequence Fidelity of a PNA-based Ligation Reaction. *Chem. Comm.* **2001**, (20), 2050-2051.

278. Mattes, A.; Seitz, O., Mass-spectrometrical Monitoring of a PNA-based Ligation Reaction for the Multiplex Detection of DNA Single Base Mutations. *Angew. Chem. Int. Ed.* **2001,** *40*, (17), 3178-3181.

279. Ficht, S.; Mattes, A.; Seitz, O., Single-Nucleotide-Specific PNA-Peptide Ligation on Synthetic and PCR DNA Templates. *J. Am. Chem. Soc.* **2004,** *126*, (32), 9970-9981.

280. Puglisi, J. D.; Tinoco, J. I., Absorbance Melting Curves of RNA. *Meth. Enzym.* **1989,** *180*, 304-325.

281. Turner, D. H., Thermodynamics of Base-Pairing. *Curr. Opin. Struct. Biol.* **1996,** *6*, 299-304.

282. Marky, L. A.; Breslauer, K. J., Calculating Thermodynamical Data for Transitions of any Molecularity from Equilibrium Melting Curves. *Biopolymers* **1987,** *26*, 1601-1620.

283. Eriksson, M.; Nielsen, P. E., PNA-Nucleic Acid Complexes. Structure, Stability and Dynamics. *Quart. Rev. Biophys.* **1996,** *29*, 369-394.

284. Ratilainen, T.; Holmén, A.; Tuite, E.; Haaima, G.; Christensen, L.; Nielsen, P. E.; Nordén, B., Hybridization of Peptide Nucleic Acid. *Biochemistry* **1998,** *37*, (12331-12342).

285. Wittung, P.; Nielsen, P. E.; Buchardt, O.; Egholm, M.; Nordén, B., DNA Double Helix formed by Peptide Nucleic Acid. *Nature* **1994,** *368*, 561-563.

286. Rasmussen, H.; Kastrup, J. S.; Nielsen, J. N.; Nielsen, J. M.; Nielsen, P. E., Crystal structure of a peptide nucleic acid (PNA) duplex at 1.7 A resolution. *Nat. Struct. Biol.* **1997,** *4*, (2), 98-101.

287. Wang, J.; Nielsen, P. E.; Jiang, M.; Cai, X.; Fernandes, J. R.; Grant, D. H.; Ozsoz, M.; Beglieter, A.; Mowat, M., Mismatch-Sensitive Hybridization Detection by Peptide Nucleic Acids Immobilized on a Quartz Crystal Microbalance. *Anal. Chem.* **1997,** *69*, (24), 5200-5202.

288. Egholm, M.; Nielsen, P. E.; Buchardt, O.; Berg, R. H., Recognition of Guanine and Adenine in DNA by Cytosine and Thymine Containing Peptide Nucleic Acids (PNA). *J. Am. Chem. Soc.* **1992,** *114*, 9677-9678.

289. Nielsen, P. E., *Peptide Nucleic Acids - Methods and Protocols*. Humana Press Inc.: 2002; 'Vol.' 208.

290. Noble, S. A.; Bonham, M. A.; Bisi, J. E.; Bruckenstein, D. A.; Brown, P. H.; Brown, S. C., Impact of Biophysical Parameters on the Biological Assessment of Peptide Nucleic Acids, Antisense Inhibitors of Gene-Expression. *Drug Dev. Res.* **1995,** *34*, 184-195.

291. Woolf, T. M., To cleave or not to cleave: ribozymes and antisense. *Antisense Res Dev.* **1995,** *5*, (3), 227-232.

292. Jennette, K. W.; Lippard, S. J.; Vassiliades, G. A.; Bauer, W. R., Metallointercalation reagents. 2-hydroxyethanethiolato(2,2',2'-terpyridine)-platinum(II) monocation binds strongly to DNA by intercalation. *Proc. Natl. Acad. Sci. U.S.A.* **1974,** *71*, (10), 3839-3843.

293. Erkkila, K. E.; Odom, D. T.; Barton, J. K., Recognition and Reaction of Metallointercalators with DNA. *Chem. Rev.* **1999,** *99*, (9), 2777-2795.

294. Patel, K. K.; Plummer, E. A.; Darwish, M.; Rodger, A.; Hannon, M. J., Aryl substituted ruthenium bis-terpyridine complexes: intercalation and groove binding with DNA. *J. Inorg. Biochem.* **2002,** *91*, (1), 220-229.

Appendix

Sequences – Overview

Reaction No.	Name	Sequence	M_{calc}	M_{found}
NMN-TK-135-02	^{Ac}**8**^{K}	Ac-tgttatcc-Lys	2321.0	2323.0
NMN-TK-143-02	^{Ac}**9**^{K}	Ac-tgttatccc-Lys	2572.1	2573.2
NMN-TK-138-02	^{Ac}**10**^{K}	Ac-tgttatccct-Lys	2838.2	2839.7
NMN-TK-134-03	^{tpy}**8**^{K}	tpy*-tgttatcc-Lys	2624.1	2626.2
NMN-TK-143-03	^{tpy}**9**^{K}	tpy*-tgttatccc-Lys	2875.2	2876.3
NMN-TK-138-03	^{tpy}**10**^{K}	tpy*-tgttatccct-Lys	3141.3	3143.5
NMN-SK-115	$^{bpa'}$**8**^{K}	bpa*Ahx-tgttatcc-Lys	2707.2	2709.0
NMN-TK-124-01	^{Ac}**4-c-4**^{K}	Ac-taccctgtt-Lys	2572.1	2573.1
NMN-TK-140-01	^{Ac}**5-c-5**^{K}	Ac-ttaccctgtta-Lys	3113.3	3115.1
NMN-TK-157-01	^{Ac}**6-c-6**^{K}	Ac-attaccctgttat-Lys	3655.5	3654.9
NMN-TK-154-01	^{Ac}**4-4**^{K}	Ac-tacctgtt-Lys	2321.0	3221.7
NMN-TK-155-01	^{Ac}**5-5**^{K}	Ac-ttacctgtta-Lys	2862.2	2863.1
NMN-TK-156-01	^{Ac}**6-6**^{K}	Ac-attacctgttat-Lys	3404.4	3404.5
NMN-TK-136-01	^{Ac}**4-GF-4**^{K}	Ac-tacc-GlyPhe-tgtt-Lys	2525.0	2526.7
NMN-TK-144-01	^{Ac}**5-GF-5**^{K}	Ac-ttacc-GlyPhe-tgtta-Lys	3066.3	3067.6
NMN-TK-150-01	^{Ac}**6-GF-6**^{K}	Ac-attacc-GlyPhe-tgttat-Lys	3608.5	3608.3
NMN-TK-151-01	^{Ac}**g$_1$-GF-g$_2$**^{K}	Ac-gggtt-GlyPhe-aaggg-Lys	3221.3	3221.3
NMN-TK-152-01	^{Ac}**g$_3$-GF-g$_4$**^{K}	Ac-ggagg-GlyPhe-ggtgg-Lys	3262.3	3263.0
NMN-TK-127-11	^{Ac}**4-GF^{tpy}-4**^{K}	Ac-tacc-GlyPhe(tpy*)-tgtt-Lys	2885.2	2886.2
NMN-TK-137-04	^{Ac}**5-GF^{tpy}-5**^{K}	Ac-ttacc-GlyPhe(tpy*)-tgtta-Lys	3426.4	3428.6
NMN-TK-158-04	^{Ac}**6-GF^{tpy}-6**^{K}	Ac-attacc-GlyPhe(tpy*)-tgttat-Lys	3967.6	3968.8
NMN-TK-148-04	^{Ac}**4-GF^{bpa}-4**^{K}	Ac-tacc-GlyPhe(bpa*)-tgtt-Lys	2855.2	2855.1
NMN-TK-149-04	^{Ac}**5-GF^{bpa}-5**^{K}	Ac-ttacc-GlyPhe(bpa*)-tgtta-Lys	3396.4	3397.8

DNA-Sequences Purchased from IBA

#	5'	Sequenz	3'		A	G	C	T	M	ε	c
68137N	TAG GGA TAA CAG GGT AAT			$^{3'}$6-G-11$^{5'}$	7	6	1	4	6018	222.70	0.0782
68138N	TAG GGA TAA CAG GGT AAT			$^{3'}$6-G-11$^{5'}$	7	6	1	4	6018	222.70	0.0834
73329N	TAG GGA TAA CAG GGT AAT			$^{3'}$6-G-11$^{5'}$	7	6	1	4	6018	222.70	0.0952
76339N	TAG GGA TAA CAG GGT AAT			$^{3'}$6-G-11$^{5'}$	7	6	1	4	6018	222.70	0.0594
77512N	TAG GGA TAA CAG GGT AAT			$^{3'}$6-G-11$^{5'}$	7	6	1	4	6018	222.70	0.0672
77513N	TAG GGA TAA CAG GGT AAT			$^{3'}$6-G-11$^{5'}$	7	6	1	4	6018	222.70	0.0477
77514N	TAG GGA TAA CAG GGT AAT			$^{3'}$6-G-11$^{5'}$	7	6	1	4	6018	222.70	0.0890
77122N	TAG GGA TAA CAG GGT AAT			$^{3'}$6-G-11$^{5'}$	7	6	1	4	6018	222.70	0.0590
76340N	TAG GGA TAA CA		GGT AAT	$^{3'}$6-11$^{5'}$	7	5	1	4	5665	210.50	0.0847
77515N	TAG GGA TAA CA		GGT AAT	$^{3'}$6-11$^{5'}$	7	5	1	4	5665	210.50	0.0782
77516N	TAG GGA TAA CA		GGT AAT	$^{3'}$6-11$^{5'}$	7	5	1	4	5665	210.50	0.0834
77131N	TAG GGA TAA CA			$^{3'}$11$^{5'}$	5	3	1	2	3629	138.10	0.0952
77132N	GGT AAT			$^{3'}$6$^{5'}$	2	2	0	2	1952	72.40	0.0891
67230N	AAC AGG GT			$^{3'}$8$^{5'}$	3	3	1	1	2611	101.10	0.0752
68139N	TAC CCT GTT			$^{5'}$4-C-4$^{3'}$	1	1	3	4	2857	85.10	0.0845
77124N	TTA CCC TGT TA			$^{5'}$5-C-5$^{3'}$	2	1	3	5	3522	109.10	0.0860
77123N	ATT ACC CTG TTA T			$^{5'}$6-C-6$^{3'}$	3	1	3	6	4187	133.10	0.0501
77127N	TAC CTG TT			$^{5'}$4-4$^{3'}$	1	1	2	4	2544	77.50	0.0902
77126N	TTA CCT GTT A			$^{5'}$5-5$^{3'}$	2	1	2	5	3209	101.50	0.0954
77125N	ATT ACC TGT TAT			$^{5'}$6-6$^{3'}$	3	1	2	6	3874	125.50	0.0872
77130N	TGT TAT CC			$^{5'}$8$^{3'}$	1	1	2	4	2544	77.50	0.0969
77129N	TGT TAT CCC			$^{5'}$9$^{3'}$	1	1	3	4	2857	85.10	0.0966
77128N	TGT TAT CCC T			$^{5'}$10$^{3'}$	1	1	3	5	3185	93.80	0.0968

Supplementary Material

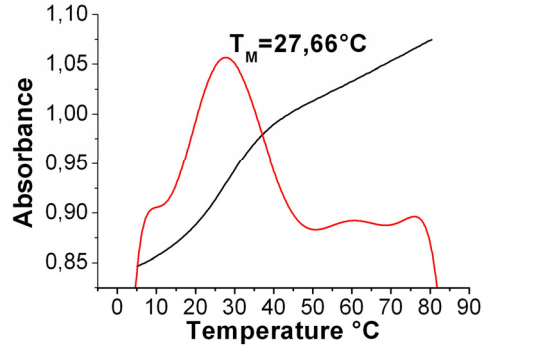

DNA $^{5'}8^{3'}$ • DNA $^{3'}$6-G-11$^{5'}$

∅=27.9±0.3°C / f_M=2.06 / 26%

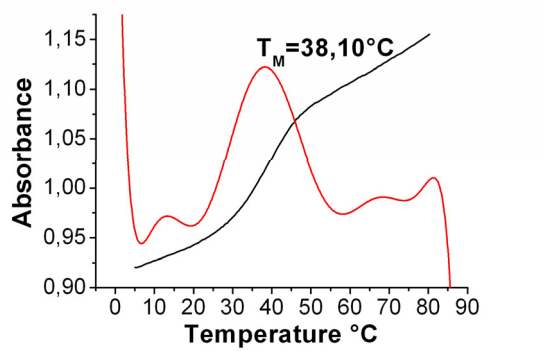

DNA $^{5'}9^{3'}$ • DNA $^{3'}$6-G-11$^{5'}$

∅=38.1±0.02°C / f_M=2.76 / 25%

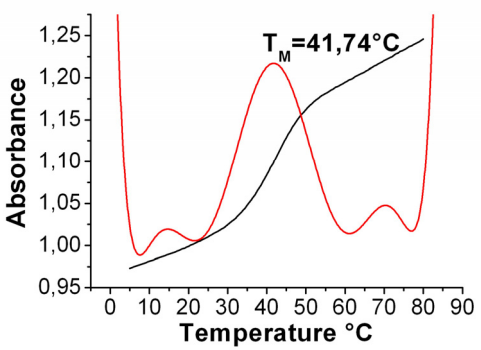

DNA $^{5'}10^{3'}$ • DNA $^{3'}$6-G-11$^{5'}$

∅=41.8±0.1°C / f_M=3.33 / 28%

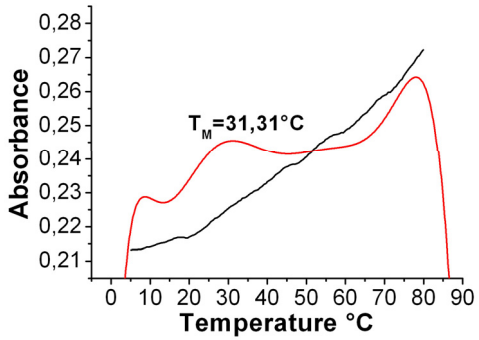

PNA $^{Ac}8^{K}$ self-melting

(T_M=31.3°C) / f_M=0.18 / 30%

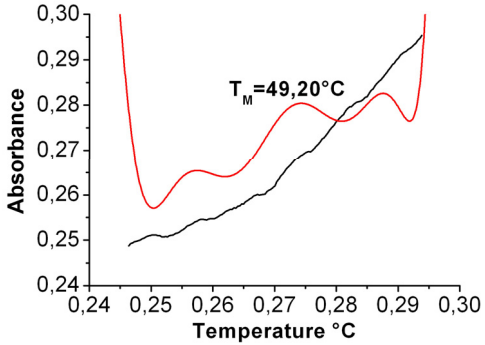

PNA $^{Ac}9^{K}$ self-melting

(T_M=49.2°C) / f_M=0.20 / 18%

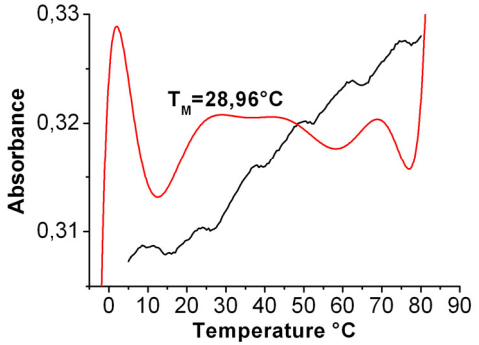

PNA $^{Ac}10^{K}$ self-melting

T_M=29.0°C / f_M=0.10 / 7%

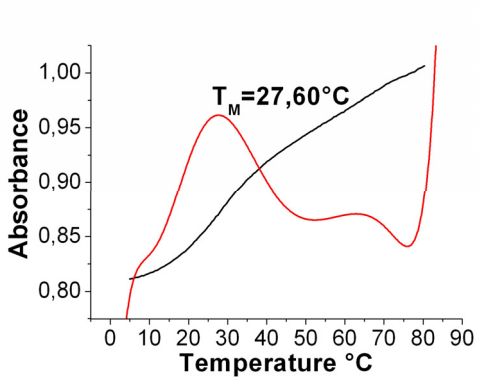

PNA $^{Ac}8^{K}$ • DNA $^{3'}$6-G-11$^{5'}$

∅=27.6±0.1°C / f_M=1.21 / 22%

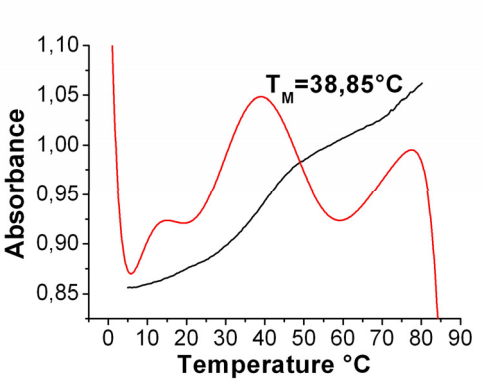

PNA $^{Ac}9^{K}$ • DNA $^{3'}$6-G-11$^{5'}$

∅=38.9±0.1°C / f_M=1.80 / 24%

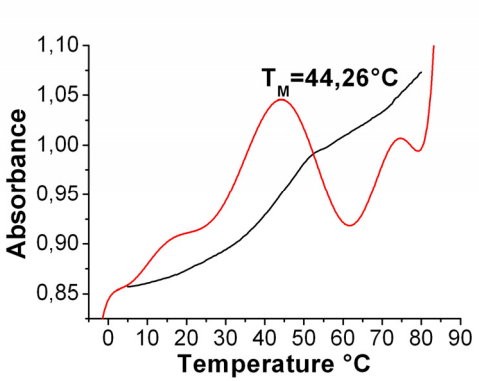

PNA $^{Ac}10^{K}$ • DNA $^{3'}$6-G-11$^{5'}$

∅=43.8±0.4°C / f_M=1.74 / 24%

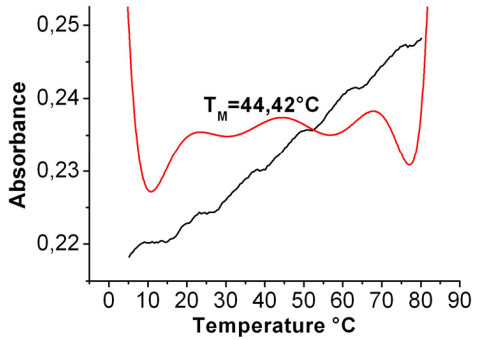

PNA $^{tpy}8^{K}$ self-melting

(T_M=44.4°C) / f_M=0.08 / 14%

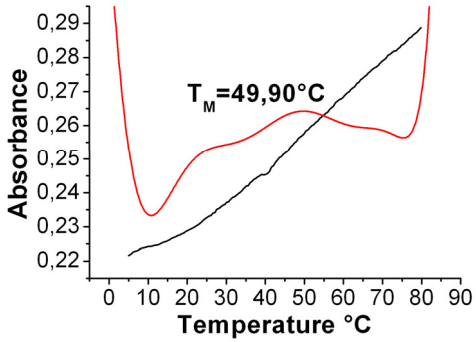

PNA $^{tpy}9^{K}$ self-melting

(T_M=49.9°C) / f_M=0.05 / 27%

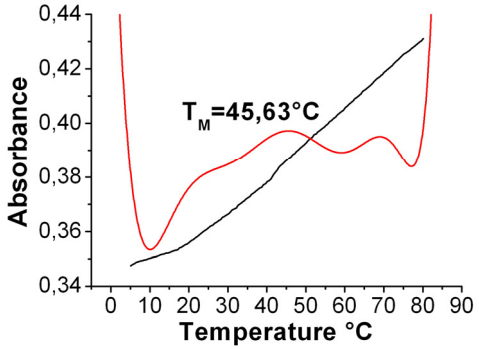

PNA $^{tpy}10^{K}$ self-melting

(T_M=45.6°C) / f_M=0.15 / 23%

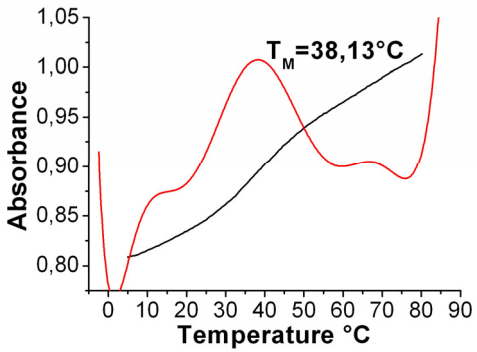

PNA $^{tpy}8^{K}$•DNA $^{3'}$6-G-11$^{5'}$

∅=38.4±0.3°C / f_M=1.01 / 23%

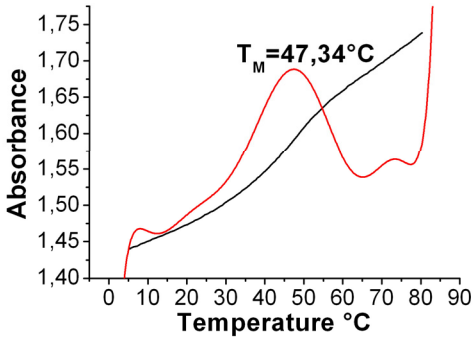

PNA $^{tpy}9^{K}$•DNA $^{3'}$6-G-11$^{5'}$

∅=46.8±0.2°C / f_M=0.73 / 20%

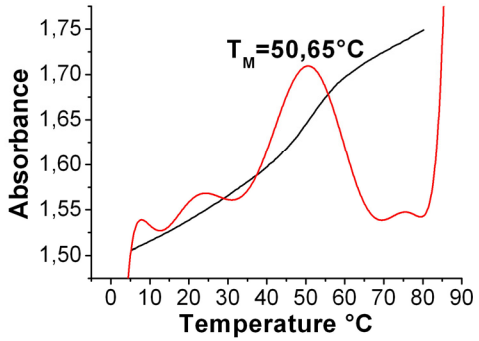

PNA $^{tpy}10^{K}$•DNA $^{3'}$6-G-11$^{5'}$

∅=50.0±0.2°C / f_M=1.76 / 15%

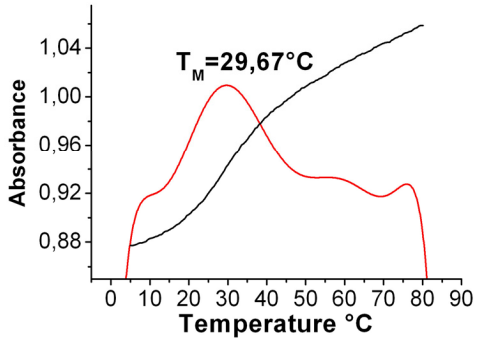

PNA $^{bpa'}8^{K}$ • DNA $^{3'}$6-G-11$^{5'}$

∅=29.7±0.3°C / f_M=1.54 / 20%

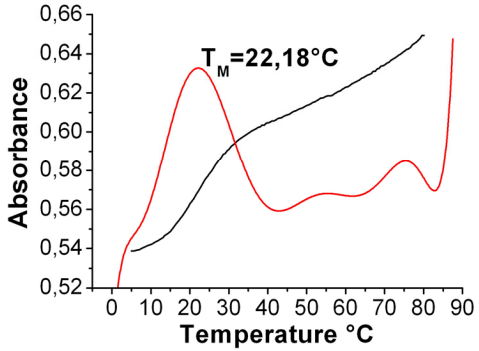

PNA $^{bpa'}8^{K}$ • DNA $^{3'}8^{5'}$

∅=22.3±0.7°C / f_M=1.38 / 20%

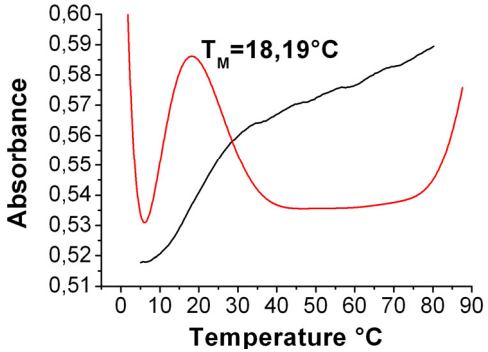

PNA $^{Ac}8^{K}$ • DNA $^{3'}8^{5'}$

∅=18.2±0.3°C / f_M=1.27 / 14%

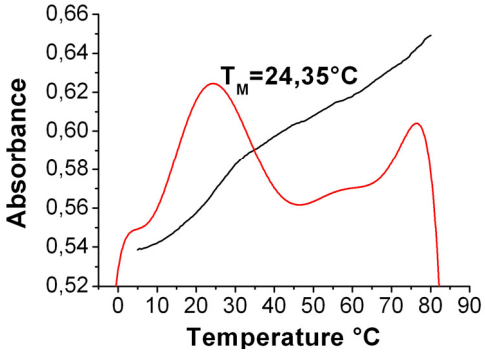

PNA $^{tpy}8^{K}$ • DNA $^{3'}8^{5'}$

∅=24.8±0.4°C / f_M=0.81 / 19%

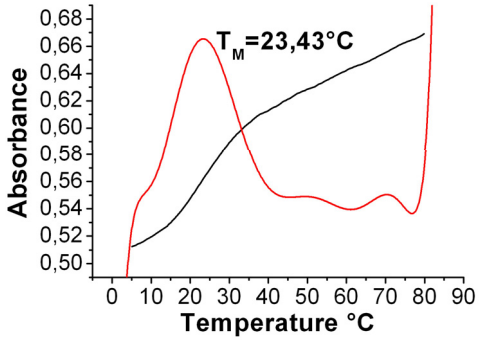

DNA $^{5'}8^{3'}$ • DNA $^{3'}8^{5'}$

∅=23.2±0.4°C / f_M=1.86 / 29%

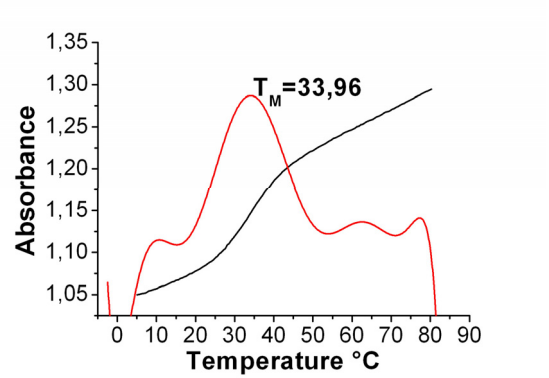

DNA $^{5'}$4-C-4$^{3'}$ • DNA $^{3'}$6-G-11$^{5'}$

∅=34.2±0.2°C / f_M=2.62 / 24%

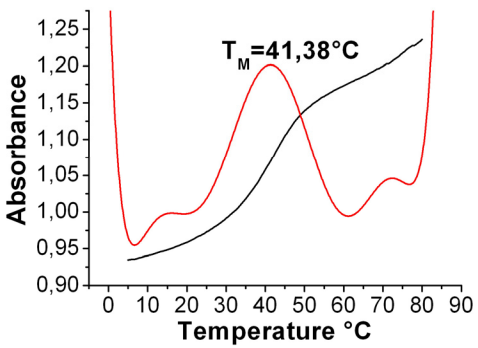

DNA $^{5'}$5-C-5$^{3'}$ • DNA $^{3'}$6-G-11$^{5'}$

∅=41.1±0.2°C / f_M=3.32 / 32%

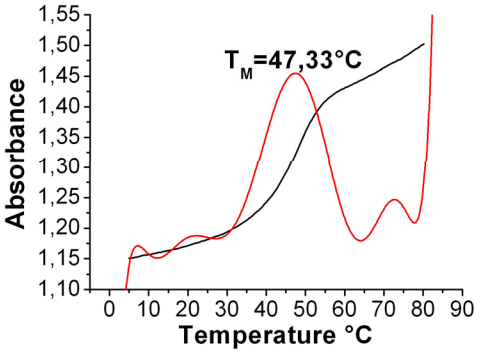

DNA $^{5'}$6-C-6$^{3'}$ • DNA $^{3'}$6-G-11$^{5'}$

∅=47.4±0.1°C / f_M=5.94 / 30%

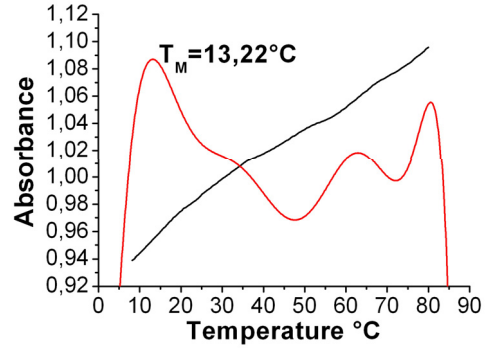

DNA $^{5'}$4-C-4$^{3'}$ • DNA $^{3'}$6-11$^{5'}$

∅=13.1±0.1°C / f_M=1.00 / 17%

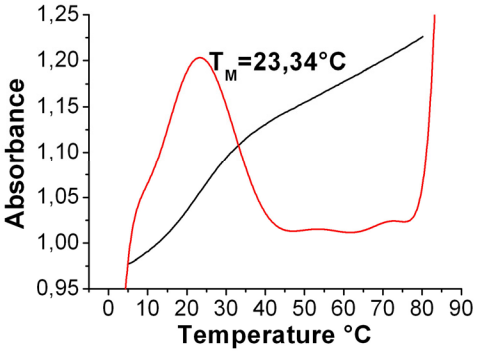

DNA $^{5'}$5-C-5$^{3'}$ • DNA $^{3'}$6-11$^{5'}$

∅=23.4±0.3°C / f_M=1.96 / 24%

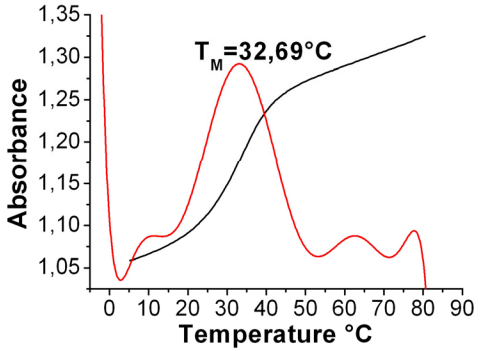

DNA $^{5'}$6-C-6$^{3'}$ • DNA $^{3'}$6-11$^{5'}$

∅=32.9±0.1°C / f_M=3.97 / 25%

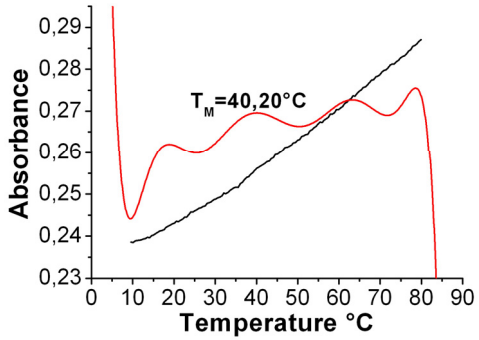

PNA ^{Ac}4-c-4^{K} self-melting

T_M=40.2°C / f_M=0.10 / 21%

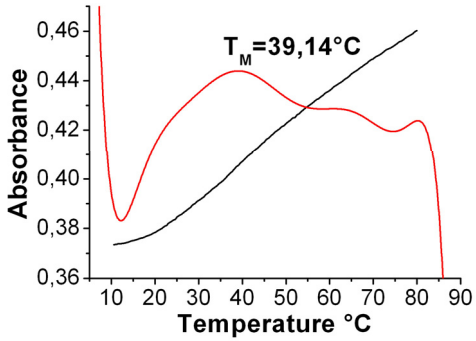

PNA ^{Ac}5-c-5^{K} self-melting

T_M=39.1°C / f_M=0.21 / 24%

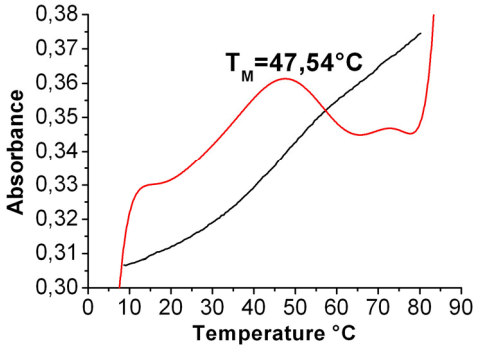

PNA ^{Ac}6-c-6^{K} self-melting

T_M=47.5°C / f_M=0.25 / 22%

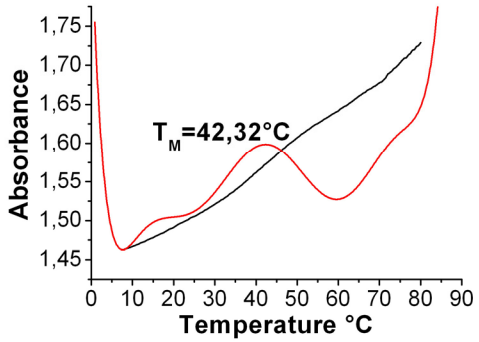

PNA ^{Ac}4-c-4^{K} • DNA $^{3'}$6-G-11$^{5'}$

∅=41.8±0.5°C / f_M=0.94 / 17%

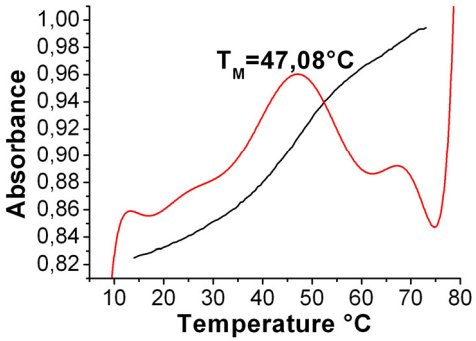

PNA ^{Ac}5-c-5^{K} • DNA $^{3'}$6-G-11$^{5'}$

∅=47.4±0.3°C / f_M=1.28 / 20%

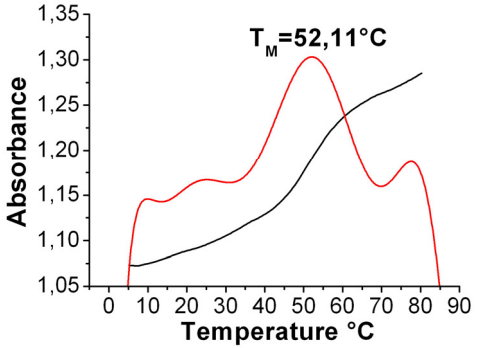

PNA ^{Ac}6-c-6^{K} • DNA $^{3'}$6-G-11$^{5'}$

∅=52.1±0.2°C / f_M=2.55 / 20%

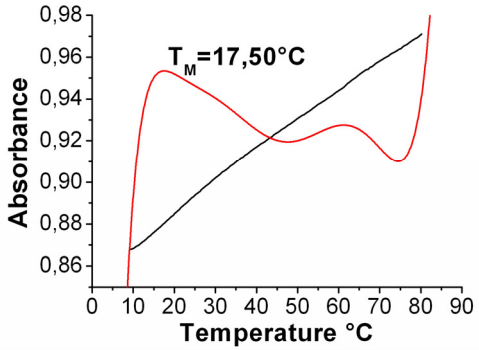

PNA ^{Ac}4-c-4^{K} • DNA $^{3'}$6-11$^{5'}$

∅=18.6±1.0°C / f_M=0.25 / 11%

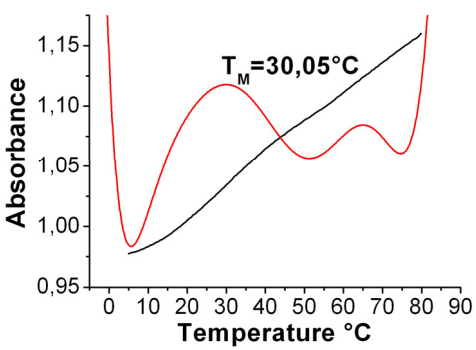

PNA ^{Ac}5-c-5^{K} • DNA $^{3'}$6-11$^{5'}$

∅=29.9±2.8°C / f_M=0.44 / 18%

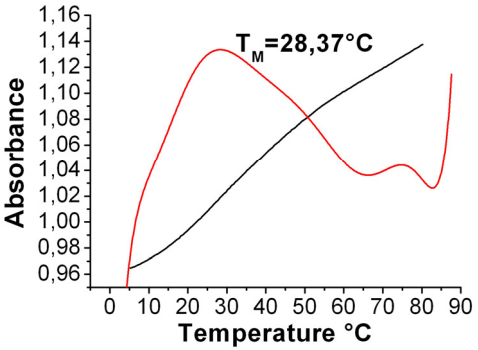

PNA ^{Ac}6-c-6^{K} • DNA $^{3'}$6-11$^{5'}$

∅=28.7±0.5°C / f_M=0.42 / 18%

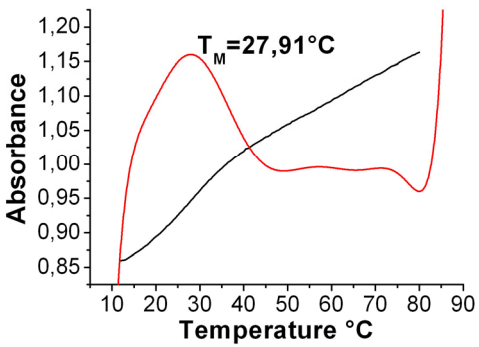

DNA $^{5'}$4-4$^{3'}$ • DNA $^{3'}$6-G-11$^{5'}$

(∅=~17°C) / f_M=1.91 / 35%

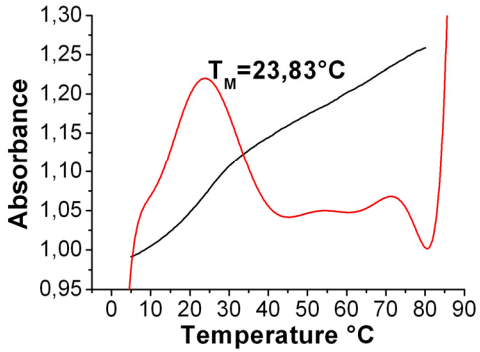

DNA $^{5'}$5-5$^{3'}$ • DNA $^{3'}$6-G-11$^{5'}$

∅=23.5±0.5°C / f_M=1.86 / 25%

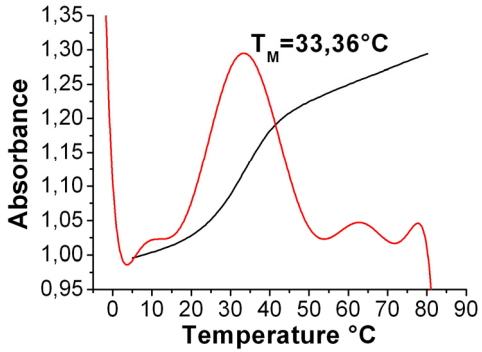

DNA $^{5'}$6-6$^{3'}$ • DNA $^{3'}$6-G-11$^{5'}$

∅=33.3±0.1°C / f_M=3.96 / 30%

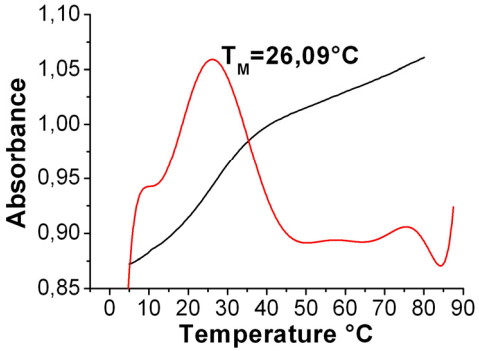

DNA $^{5'}$4-4$^{3'}$ • DNA $^{3'}$6-11$^{5'}$

∅=26.1±0.1°C / f_M=1.86 / 20%

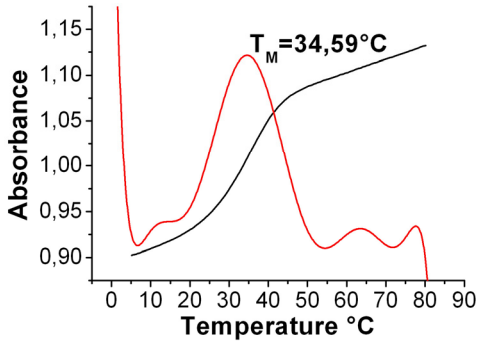

DNA $^{5'}$5-5$^{3'}$ • DNA $^{3'}$6-11$^{5'}$

∅=34.5±0.1°C / f_M=3.45 / 24%

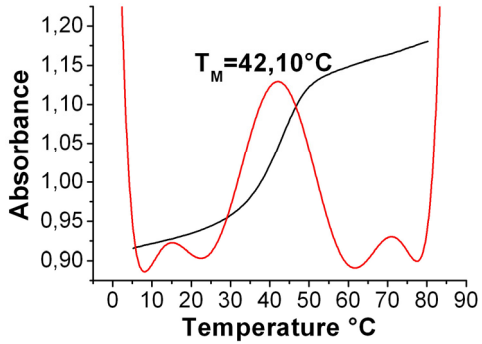

DNA $^{5'}$6-6$^{3'}$ • DNA $^{3'}$6-11$^{5'}$

∅=42.2±0.1°C / f_M=4.88 / 28%

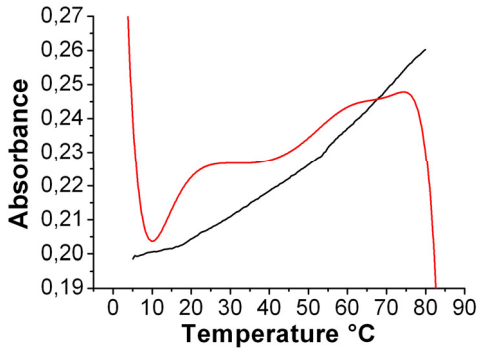

PNA ^{Ac}4-4^{K} self-melting

30%

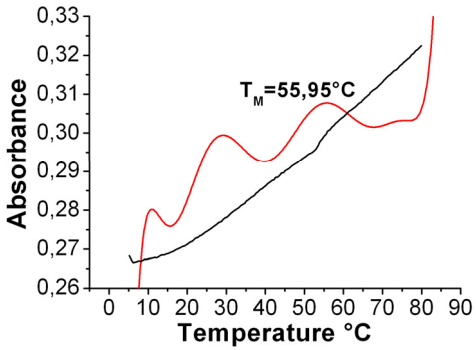

PNA ^{Ac}5-5^{K} self-melting

T_M=56.0 / f_M= 0.15 / 22%

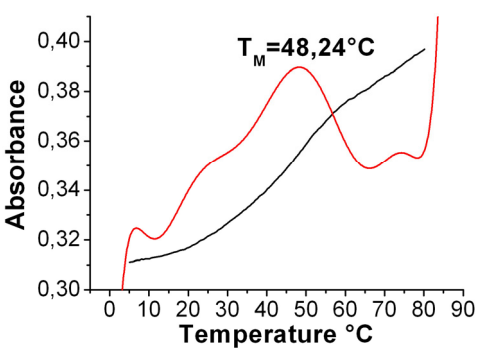

PNA ^{Ac}6-6^{K} self-melting

T_M=48.2°C / f_M=0.53 / 27%

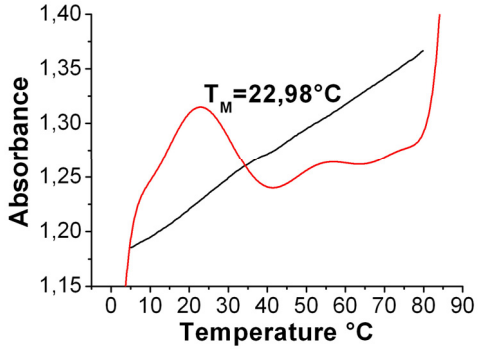

PNA ^{Ac}4-4^{K} • DNA $^{3'}$6-G-11$^{5'}$

∅=24.3±1.6°C / f_M=0.54 / 15%

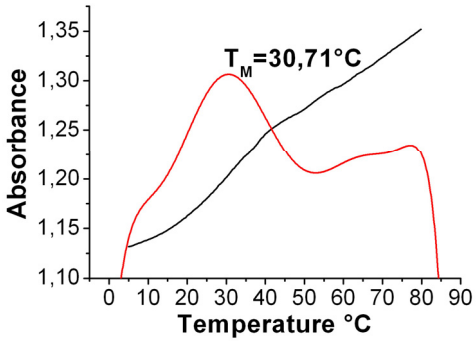

PNA ^{Ac}5-5^{K} • DNA $^{3'}$6-G-11$^{5'}$

∅=29.4±1.6°C / f_M=1.11 / 18%

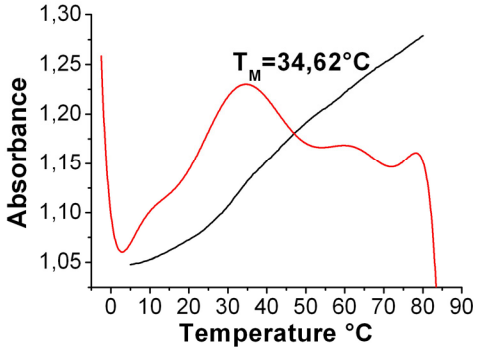

PNA ^{Ac}6-6^{K} • DNA $^{3'}$6-G-11$^{5'}$

∅=35.0±0.7°C / f_M=0.99 / 21%

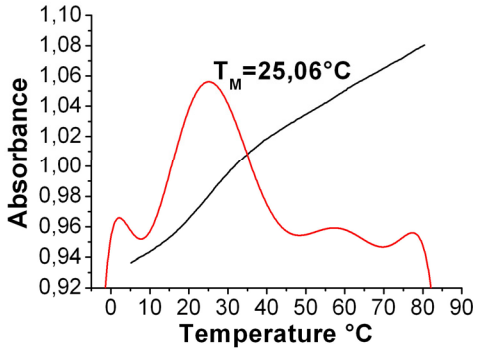

PNA ^{Ac}4-4^{K} • DNA $^{3'}$6-11$^{5'}$

∅=25.1±0.02°C / f_M=0.81 / 15%

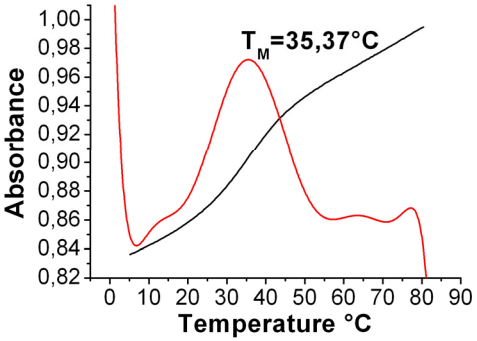

PNA ^{Ac}5-5^{K} • DNA $^{3'}$6-11$^{5'}$

∅=35.3±0.1°C / f_M=1.07 / 18%

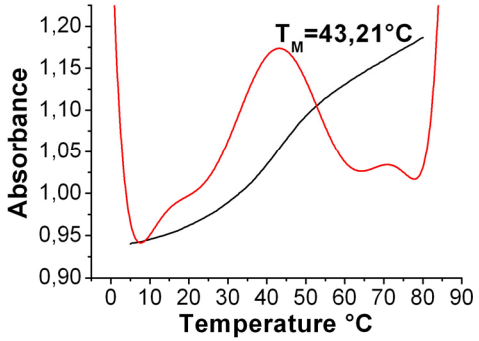

PNA ^{Ac}6-6^{K} • DNA $^{3'}$6-11$^{5'}$

∅=43.2±0.2°C / f_M=1.59 / 26%

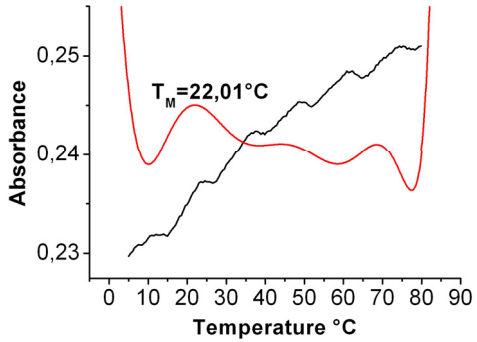

PNA ^{Ac}4-GF-4^{K} self-melting

T_M=22.0°C / f_M=0.21 / 21%

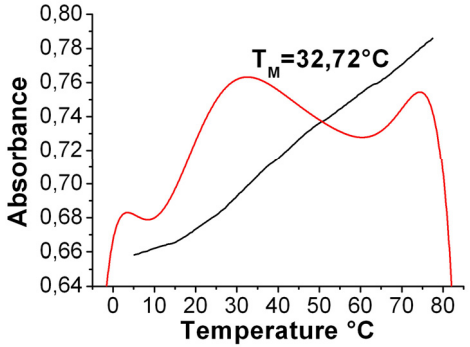

PNA ^{Ac}5-GF-5^{K} self-melting

T_M=23.7°C / f_M=0.35 / 18%

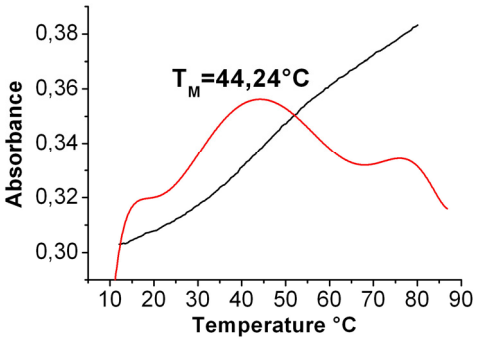

PNA ^{Ac}6-GF-6^{K} self-melting

T_M=44.2°C / f_M=0.29 / 26%

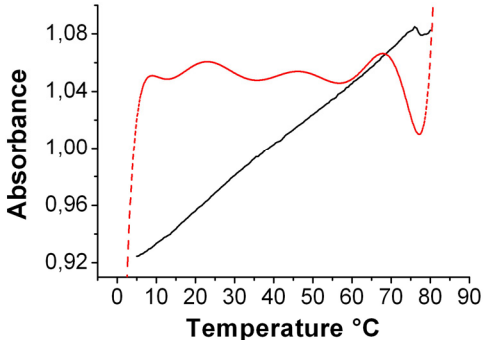

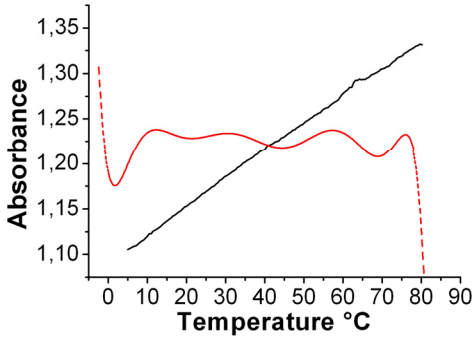

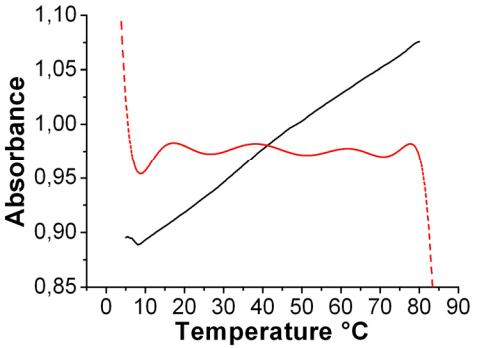

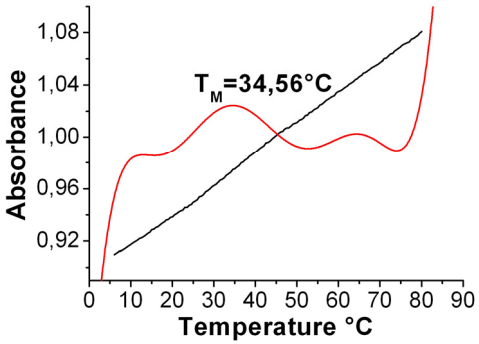

PNA ^{Ac}4-GF-4^{K} • DNA $^{3'}$6-G-11$^{5'}$

(∅=~31°C) / f_M=0.29 / 19%

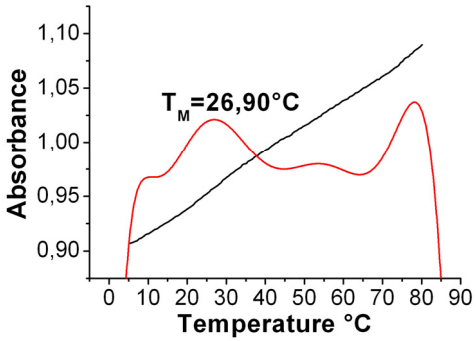

PNA ^{Ac}5-GF-5^{K} • DNA $^{3'}$6-G-11$^{5'}$

(∅=~26.5°C) / f_M=0.47 / 20%

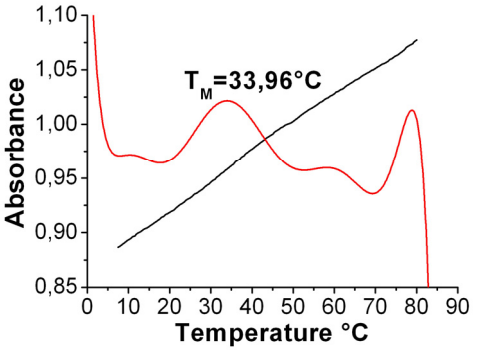

PNA ^{Ac}6-GF-6^{K} • DNA $^{3'}$6-G-11$^{5'}$

(∅=~33.3°C) / f_M=0.40 / 22%

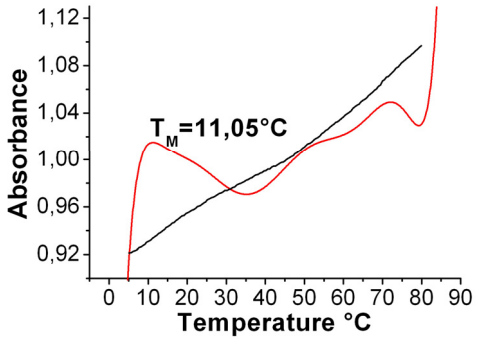

PNA ^{Ac}4-GF-4^{K} • DNA $^{3'}$6-11$^{5'}$

∅=11.0±0.1°C / f_M=0.59 / 18%

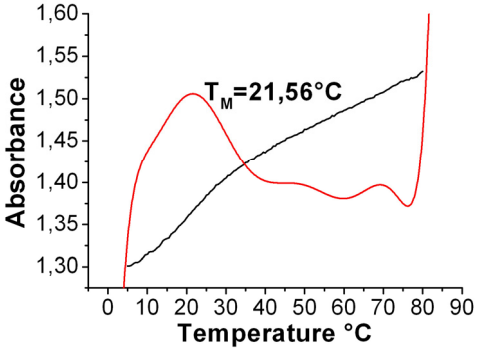

PNA ^{Ac}5-GF-5^{K} • DNA $^{3'}$6-11$^{5'}$

∅=21.5±0.1°C / f_M=1.41 / 17%

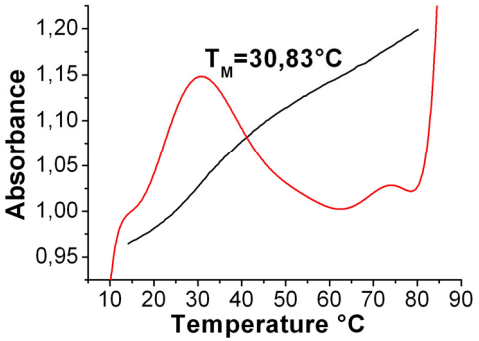

PNA ^{Ac}6-GF-6^{K} • DNA $^{3'}$6-11$^{5'}$

∅=30.7±0.2°C / f_M=1.50 / 23%

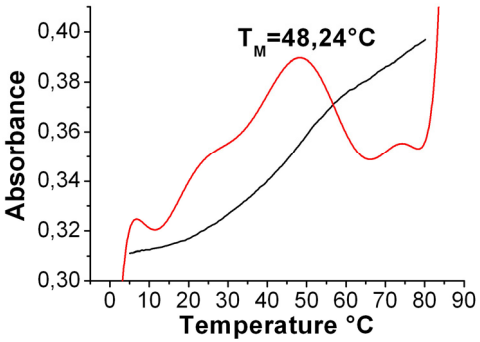

PNA ^{Ac}6-6^{K} self-melting

T_M=48.2°C / f_M=0.53 / 27%

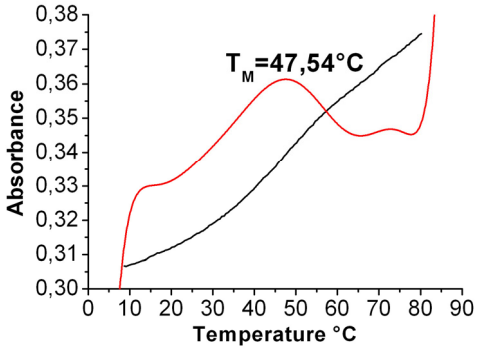

PNA ^{Ac}6-c-6^{K} self-melting

T_M=47.5°C / f_M=0.25 / 22%

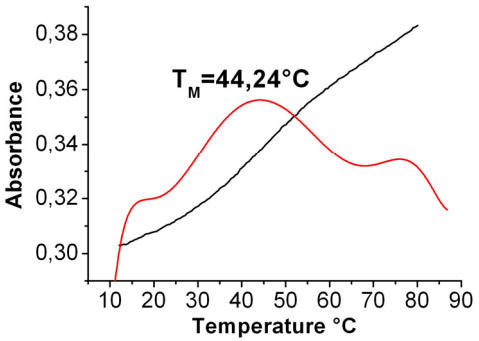

PNA ^{Ac}6-GF-6^{K} self-melting

T_M=44.2°C / f_M=0.29 / 26%

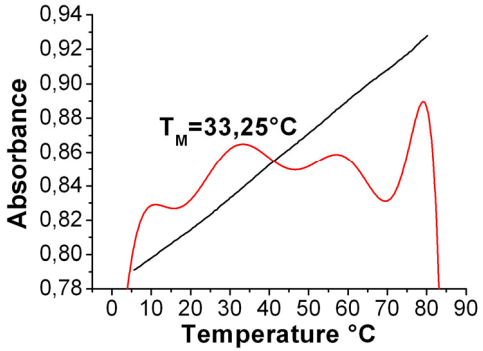

DNA $^{5'}$6-6$^{3'}$ • DNA $^{3'}$11$^{5'}$

(T_M=33.3°C) / f_M=0.14 / 18%

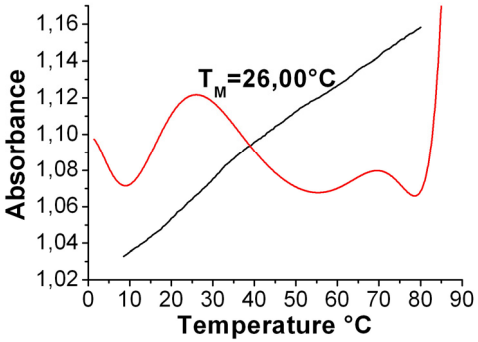

DNA $^{5'}$6-C-6$^{3'}$ • DNA $^{3'}$11$^{5'}$

(T_M=26.0°C) / f_M=0.36 / 12%

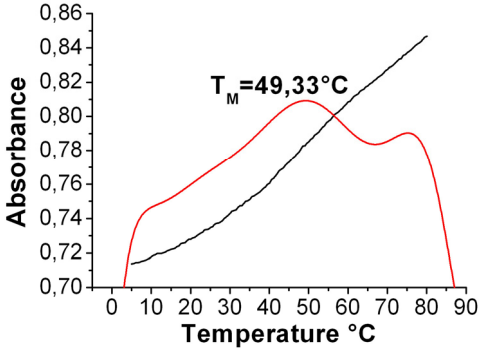

PNA ^{Ac}6-6^{K} • DNA $^{3'}$11$^{5'}$

∅=48.2±1.3°C / f_M=0.32 / 19%

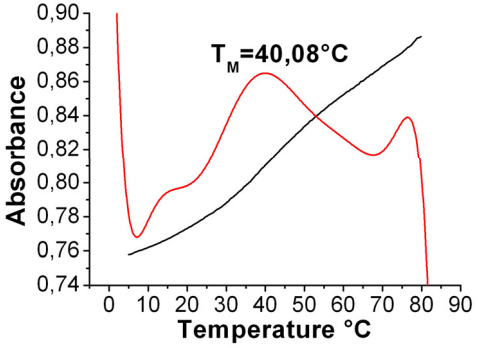

PNA ^{Ac}6-c-6^{K} • DNA $^{3'}$11$^{5'}$

∅=44.3±2.6°C / f_M=0.40 / 17%

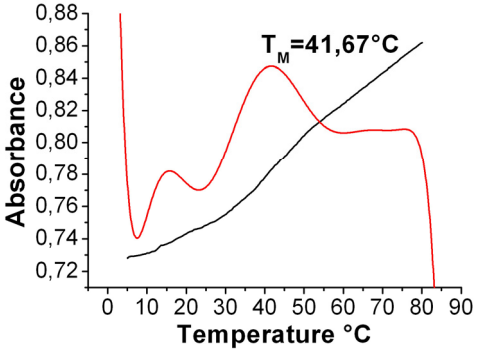

PNA ^{Ac}6-GF-6^{K} • DNA $^{3'}$11$^{5'}$

∅=41.2±1.1°C / f_M=0.68 / 18%

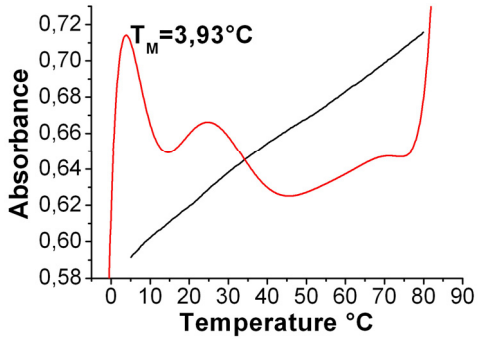

DNA $^{5'}$6-6$^{3'}$ • DNA $^{3'}$6$^{5'}$

(T_M=3.9°C) / f_M= / 21%

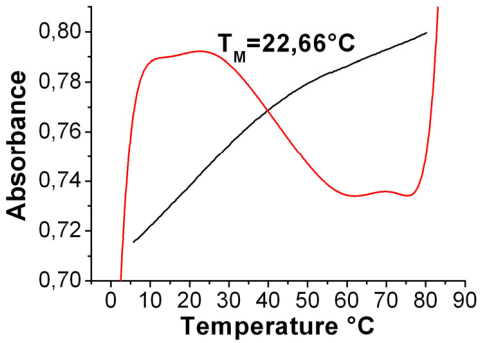

DNA $^{5'}$6-C-6$^{3'}$ • DNA $^{3'}$6$^{5'}$

(T_M=22.7°C) / f_M=0.29 / 12%

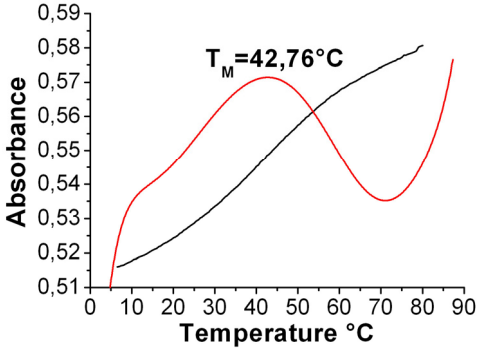

PNA ^{Ac}6-6^{K} • DNA $^{3'}$6$^{5'}$

∅=44.0±1.0°C / f_M=0.20 / 13%

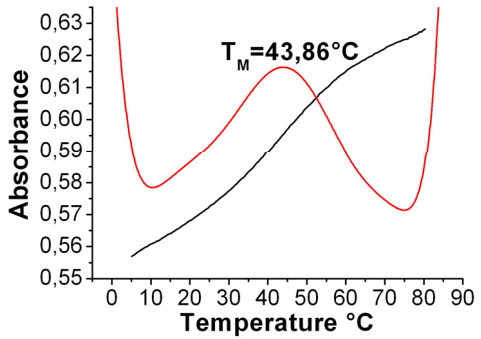

PNA ^{Ac}6-c-6^{K} • DNA $^{3'}$6$^{5'}$

∅=44.0±0.1°C / f_M=0.28 / 13%

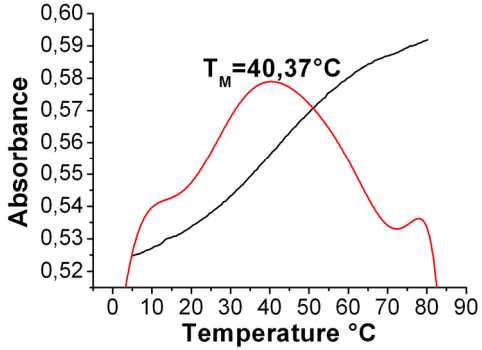

PNA ^{Ac}6-GF-6^{K} • DNA $^{3'}$6$^{5'}$

∅=40.4±0.1°C / f_M=0.26 / 13%